Department of Applied Geology

Setting and Timing of Gold Mineralization in the Jiaodong and Liaodong Peninsulas, North China Craton

Xiao'ou Zhang

This thesis is presented as part of the requirements for
the award of the Degree of Doctor of Philosophy
of Curtin University of Technology

February 2002

TABLE OF CONTENTS

ACKNOWLEDGEMENTS

This thesis could not have been completed without the encouragement and support of the following individuals and organisations.

I would like to sincerely thank Associate Professor Peter A. Cawood. As my supervisor, he gave me academic enlightenment and technical advice. I greatly appreciated his comments made directly on electronic copy of my thesis.

I would like to express my gratitude to Professor Simon A. Wilde. As one of my associate supervisors, he has contributed immense supervision, advice and training during the course of my studies. We often sit together and discuss geological problems raised during the preparation of my thesis. I like his smile and laugh and realize that it is enjoyable for me to discuss these matters with him.

I am grateful to Professor Ruqi Liu. As another of my associate supervisors, he organized my field trip in the Liaodong Peninsula in China, and accompanied and instructed me during my field work. I also thank my father, Mr. Zhimin Zhang, a local senior geologist. He organized my field trip in the Jiaodong Peninsula in China and triggered my imagination on the genesis for the Jiaodong gold deposits.

Drs. Yumin Qiu, Zhengxiang Li and Peter D. Kinny are thanked for their helpful discussions. I am indebted to Simon Bodorkos who has tirelessly helped me with computer related problems. I would like to thank Dr. Alexander A. Nemchin for help with the performance of SHRIMP, Mr. Brian Cikara for patient instructions on zircon separation, and Mr. Peter Glover and Garrie Meddings for assistance with thin section preparation.

Among my colleagues in China, Mr. Pengcheng Zhang and Lijun Dai are thanked for their accompany during my field trip in the Liaodong Peninsula. There are too many local Chinese geologists from the various gold mines examined to be listed. However, I would like to mention Hailin Song, Wen Li, Yi Han, Rifu Liu, Zhifu Sun, Yongtang Liu, Weihua Hu, Daling Li, Rongguang Lu, Xueliang Lu, Feng Liu, Hu Yu, Chunfu Yang, Junpeng Huang, Fuchun Wang, and Runyou Wu.

Thanks also due to my friends Zhongrong Zhu, Guochun Zhao, Tingguang Song, Sheng He, Min Xu, Wanwu Guo, Marcus Sweetapple, Edward Oldmeadow,

Akhilesh Singh, Shahram Sharafi and Khalid Youssef. These friends have energized me during my period at Curtin, and the good memory of them will always remain in my heart.

This thesis was sponsored by a grant from the Western Australian-China Economic and Technical Research Fund to Prof. Simon A. Wide and Associate Prof. Peter A Cawood, and was also financially supported by Placer Dome Inc. Exploration (Asia-Pacific) with special thanks to Greg Hall, who has an ongoing interest in the gold mineralization of China. I thank the Department of Employment, Education and Training of Australia for awarding me an International Postgraduate Research Scholarship (IPRS) and Curtin University of Technology for awarding me a Curtin University Postgraduate Scholarship (CUPS).

Finally, I am indebted to my wife, Cuiling Liu, who has provided invaluable support, encouragement and patience during the entire period of my PhD study. Also, I am grateful to my parents for their understanding and love.

ABSTRACT

The primary objective of this thesis was to date the age of gold mineralization in the Jiaodong and Liaodong Peninsulas, northeast China. Based on SHRIMP U-Pb zircon ages of dykes and host rocks at 13 gold deposits in the two peninsulas and the ^{40}Ar-^{39}Ar dating of sericite at the Cangshang deposit in the Jiaodong Peninsula, a single gold mineralization event at ca. 122 - 119 Ma has been identified.

Ten gold deposits in the Jiaodong Peninsula and three gold deposits in the Liaodong Peninsula were examined. Gold mineralization can be divided into the disseminated-and-veinlet type (Jiaojia-style) and vein type (Linglong-style) and all these deposits are strongly controlled by faults. The most common host rocks are granitoids, with a SHRIMP $^{206}Pb/^{238}U$ age of 150 - 165 Ma. The youngest host rocks in the Jiaodong Peninsula are granodiorite, with an age of ca. 128 Ma. The oldest dated host rock in the Jiaodong Peninsula is amphibolite with a metamorphic zircon age of 1852 ± 37 Ma; in the Liaodong Peninsula, the oldest host rock is metasandstone with the youngest detrital zircon giving an age of 1886 ± 16 Ma. The Jiaodong and Liaodong Peninsulas are underlain by Precambrian basement with components up to ca. 3.7 Ga old and these are reflected in the zircon population. There are three main peaks of inherited zircons, which yield Late Archaean (ca. 2500 Ma), Palaeoproterozoic (1800-2200 Ma) and Early Mesozoic (ca. 200-250 Ma) ages.

The close spatial and temporal relationships between dykes and gold mineralization has only recently been recognized in China. Based on the cross-cutting relationship between dykes and gold lodes (and the alteration style of dykes), three types of dykes are recognized: pre-, syn- and post-mineralization dykes. Pre-mineralization dykes yield an age of ca. 124 Ma; syn-mineralization dykes give an age of ca. 122-119 Ma, which can also be interpreted as the time of gold mineralization; further work is needed to date post-mineralization dykes, since no suitable samples were identified during this study.

^{40}Ar-^{39}Ar dating of sericite has been used to determine the timing of gold mineralization at the Cangshang Gold Deposit. It gives a well-defined ^{40}Ar-^{39}Ar age of 121.3 ± 0.2 Ma.

The second objective of this thesis was to understand why the tectonic setting of the Jiaodong and Liaodong Peninsulas is favourable for gold formation and what is a

sound genetic model for these gold deposits. Based on this study, it is interpreted that multiple orogenic events created a favourable tectonic environment for the Jiaodong and Liaodong gold deposits. It is suggested that delamination related to orogenic events occurred beneath the Jiaodong and Liaodong Peninsulas. The substantial heat and fluid transfer caused by delamination allowed mantle-derived magma and auriferous fluids to be channelled along deep faults to favourable structures within the crust. This probably explains why the dykes and gold lodes are closely associated in both time and space.

CHAPTER 1: INTRODUCTION

1.1 Background

China has become a major gold producer and one of the most prospective areas for gold exploration in the world. Its gold production has increased substantially, from about 2 tonnes in 1980 to approximately 180 tonnes in 1998 (Zhou and Lü, 2000). Its gold reserves were estimated at ~4,000 tonnes in 1998, with potential resources of about 10,000 tonnes (Zhou, 1998).

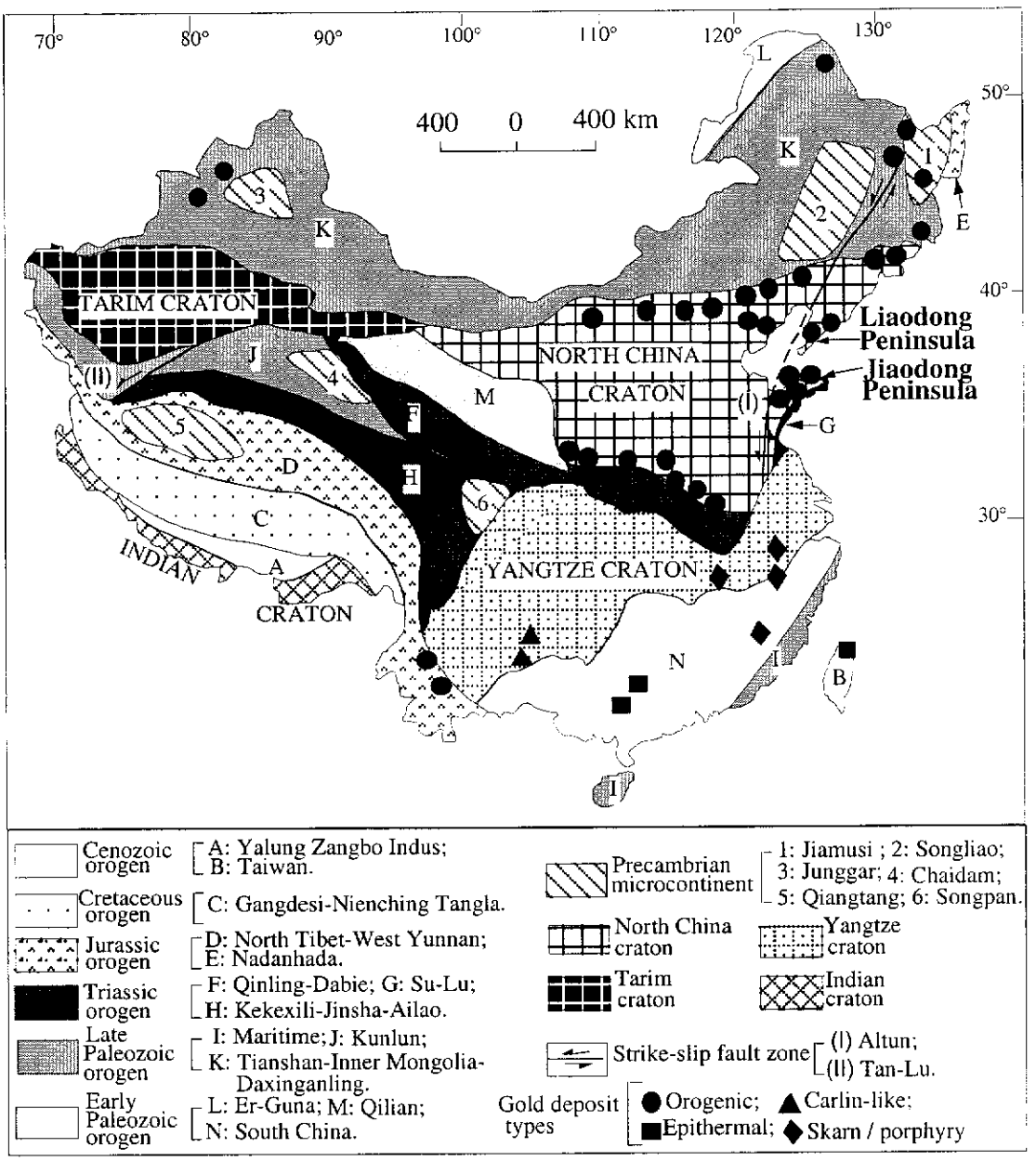

Fig. 1.1: Sketch map of main tectonic units of China, showing the overall distribution of gold deposits in China (modified after Zhang et al., 1984 and Nie, 1997a)

The gold deposits in China can be divided into 4 classes based on size: superlarge (>50 tonnes); large (50-20 tonnes); medium (20-5 tonnes) and small (<5 tonnes). This is the Chinese size classification for gold deposits and is used throughout this thesis. About 72% of Chinese gold deposits are small and these account for ca. 25% of the total proven reserves (Nie, 1997a). In western terminology, the gold deposits in China can be classified as: orogenic, epithermal, Carlin-like and skarn / porphyry gold deposits. Among them, the orogenic type is dominant (Fig. 1.1). Drilling in most existing gold deposits is generally in the upper 200-400 m of crust, indicating a large potential for further gold production from depth (Cun et al., 1995). More than 3,000 gold deposits have been reported in various parts of China (Yang, 1996), but they are predominantly distributed along the borders of the North China Craton (Fig. 1.1) (Yang, 1996; Nie, 1997b; Miller et al., 1998). In this thesis, two major gold producing areas of the North China Craton are investigated in detail: the Jiaodong and Liaodong Peninsulas (Fig. 1.1).

1.1.1 Jiaodong Peninsula

The Jiaodong Peninsula (Fig. 1.1) is situated along the southeastern margin of the North China Craton. It constitutes the most important gold province in China, referred to as the Jiaodong Gold Province (Qiu et al., 2002). This gold province comprises a number of lode-gold deposits containing 25% of China's gold reserves, and is the major gold producer in China, with approximately 1 million oz of bullion produced annually (Zhou and Lü, 2000).

Gold mineralization within the Jiaodong Gold Province is strongly controlled by fault zones (Liu, 1987). Several of the Jiaodong gold deposits are hosted by Mesozoic granitoids or Archaean metamorphic rocks, whereas others are developed at lithologic contacts along fault zones rather than within single rock units. One common character of these gold deposits is that they are all closely associated with dykes. Jiaodong gold deposits are either of disseminated-and-veinlet type or of vein type. The former, which is locally termed Jiaojia-style mineralization, is associated with the regional NNE- to NE-trending fault zones. Commonly, the gold reserves of this type of deposit are large, from tens to more than one hundred tonnes, with grades of 4-5 grams per tonne. The orebodies lack sharp contacts with the host rock and they are only distinguished by grade analysis. Lode-gold deposits with vein-type mineralization are locally termed Linglong-style. They are located in secondary structures associated with the regional fault zones. The gold reserves associated with this type of deposit are usually not large, with an average of a few tonnes, but the ore grade is much higher,

with an average of more than 10 grams per tonne. The boundary between the orebody and host rock is distinct and can be easily identified in the field. The two types of gold deposits, however, probably developed simultaneously and their occurrence depends on structural environment. The Linglong-style gold deposits occur where auriferous fluids filled large fractures developed in competent host rock, whereas Jiaojia-style deposits occur where auriferous fluid replaces rocks along regional fracture zones and, more importantly, fills the rocks in the form of quartz or sulphide veinlets. The more veinlets the ore has, the higher the grade (Zhang and Wen, 1983; Bai, 1993). Alteration assemblages associated with both styles of mineralization include sulphidation, silicification, sericitization and K-feldspar alteration.

Many studies have been carried out on the Jiaodong gold deposits by Chinese researchers (e.g. Zhang et al., 1973; Zhang and Wen, 1983; Liu et al., 1984; Liu, 1987; Luo and Wu, 1987; Xu et al., 1989; Yao et al., 1990; Zhang, 1990; Lü and Kong, 1993; Yang et al., 1993; Zhang et al., 1994; Yang and Lü, 1996; Shen et al., 1998; Xie et al., 1999; Li, 2000; Sun et al., 2000), but they are little known internationally (Wang et al., 1998; Zhou and Lü, 2000). These studies have produced different results regarding the age, tectonic setting and genesis of the Jiaodong gold deposits and the granitoids hosting many of them. For example, the age of the host granitoids is considered to vary from Early Proterozoic to Late Cretaceous, based on various radiogenic isotope dating methods (e.g. Wen, 1985; Hu et al., 1987; Xu et al., 1989). The timing of gold mineralization has been inferred to be Proterozoic (e.g. Yang and Lü, 1996), Mesozoic (e.g. Luo and Wu, 1987; Wang et al., 1998; Zhai et al., 1998) and Cenozoic (e.g. Zhang et al., 1994).

There is also no consensus as to the genesis of the Jiaodong deposits. Traditionally, many genetic models have involved partial melting of the Archaean metamorphic basement rocks to generate the granitoids, with subsequent derivation of gold mineralising fluids from these granitoids (e.g. Zhang and Wen, 1983; Lü and Kong, 1993). Xu et al. (1989) highlighted that although some granitoids are closely related to the gold mineralization in time and space they have no genetic relationship, and the granitoids just act as a heat source for enhancing hydrothermal circulation. The tectonic setting of the Jiaodong gold deposits is also controversial. Wang et al. (1998) suggested that these gold deposits formed >100 m.y. after the collision between the North China and Yangtze Cratons and were related to subduction of the Palaeo-Pacific Plate underneath the Eurasia Continent during the Cretaceous Period. In contrast, Zhou and Lü (2000) propose that the Jiaodong deposits formed as the result of collision and suturing of the North China and Yangtze Cratons during the Triassic to Jurassic.

1.1.2 Liaodong Peninsula

The Liaodong Peninsula (Fig. 1.1) is also located along the southeastern margin of the North China Craton, and contains numerous gold deposits and occurrences, with total gold reserves of several tens of tonnes (Ren, 1988). Because the tectonic setting of the Liaodong Peninsula is similar to that of the Jiaodong Peninsula, the Liaodong gold deposits are also similar in many aspects.

There are few studies on the Liaodong gold deposits by Chinese researchers (e.g. Li et al., 1987; Peng et al., 1988; Ren, 1988; Yao et al., 1988; Yang, 1997; Yang et al., 1997; Liu and Ai, 1999), and very few good-quality geochronological data on gold mineralization and host rocks are available. The origin of the Liaodong gold deposits remains controversial. For example, Ren (1988) and Yao et al. (1988) considered that ore fluid and gold of all Liaodong gold deposits were derived from the magmatic intrusions commonly associated with the gold deposits. However, Peng et al. (1988) thought that circulating metamorphic fluids extracted gold from metamorphic rocks hosting the gold deposits. Generally speaking, the Liaodong Peninsula has a great potential to become another important gold producing area in China, but this requires a much larger research effort than has been undertaken to date.

1.2 Objectives

The primary objective of this thesis is to determine the age of gold mineralization in the Jiaodong and Liaodong Peninsulas. This will be achieved primarily by SHRIMP U-Pb zircon dating and along with Ar-Ar dating of sericite associated with mineralization.

The second objective of this thesis is to understand why the tectonic setting of the Jiaodong and Liaodong Peninsulas is favourable for gold formation and what are the controls on gold mineralization. This will be accomplished by synthesis of the new research results and an evaluation of data from the Chinese literature.

The primary objective will be achieved by determining:

- the age of the host rocks (especially granitoids) by SHRIMP U-Pb zircon studies. This not only helps understand the geological evolution of the Jiaodong and Liaodong Peninsulas, but also provides constraints on the timing of gold mineralization in both areas.

- the age of dykes using SHRIMP U-Pb zircon dating. This can assist in understanding the close spatial and temporal relationship between dykes and gold mineralization and to constrain the age of gold mineralization in the Jiaodong and Liaodong Peninsulas.
- the age of certain gold-bearing shear zones, as determined by SHRIMP U-Pb zircon analysis. This can be used to establish the characteristics of auriferous shear zones in the Jiaodong and Liaodong Peninsulas and assist in further gold exploration in these areas.

The above work on gold deposits of the Jiaodong and Liaodong Peninsulas will be described for a number of individual deposits that were examined in the course of these studies.

1.3 Research methods

This thesis is based on extensive field and laboratory studies.

1.3.1 Field-based studies

A total of five months was spent working in the field in both the Jiaodong and Liaodong Peninsulas during 1997 and 1998. Ten gold deposits in the Jiaodong Peninsula and three gold deposits in the Liaodong Peninsula were examined in detail, and another 6 deposits in Jiaodong and 4 deposits in Liaodong were selected for reconnaissance study. Detailed mapping was carried out on several open pits and local details from underground working were also recorded. A total of 221 samples were collected from host rocks, orebodies and dykes at individual gold deposits, as well as from regional granitoid intrusions. These samples were located either on local mine maps, such as level plans, or by using a hand-held Garmin Global Positioning System (G .P. S). The weight of the samples collected was commonly 3-5 kilograms, which usually ensures that sufficient zircons can be separated for SHRIMP U-Pb analysis.

1.3.2 Laboratory-based studies

The laboratory work included thin section examination, ^{40}Ar-^{39}Ar sericite dating, cathodoluminescence (CL) images and SHRIMP U-Pb zircon geochronological studies.

One hundred and fifty-two samples were thin sectioned from the Jiaodong and Liaodong Peninsulas and examined using a Nikon transmitted light microscope at Curtin University.

Sericite separates of one ore sample from the Cangshang gold deposit in the Jiaodong Peninsula were dated by ^{40}Ar-^{39}Ar analysis technique. These sericites were irradiated in the TRIGA research reactor at the U.S. Geological Survey in Denver, and the $^{40}Ar/^{39}Ar$ isotope measurements were carried out at the U.S. Geological Survey Argon Laboratory in Denver on a Mass Analyser Products 215 rare gas mass spectrometer by Dr. Lawrence W. Snee.

In order to determine the internal structures of zircons, CL images were obtained using a Philips XL30 scanning electron microprobe with CL attachment located at Curtin University.

SHRIMP U-Pb zircon studies were the major part of this research and were carried out on twenty-three samples from 12 gold deposits in the Jiaodong and Liaodong Peninsulas. U-Th-Pb analyses were made using the WA consortium SHRIMP II (Sensitive High Resolution Ion Microprobe) located at Curtin University. Sample preparation and SHRIMP analytical techniques were as follows:

Sample preparation: Rock samples, weighting 3-5 kg, were crushed in a Sturtevant Engineering roll jaw crusher, then ground to < 1mm in size in a Braun plate grinder. The ground samples were washed using water and acetone, then separated in heavy liquids (Tetrabromoethane and Methylene Iodide). The heavy fraction was dried and highly magnetic particles were removed by hand magnet. The reminder was sieved into a series of size fractions i.e. <74 μm, 74 μm-105 μm, 105 μm-132 μm, and >132 μm. These fractions were passed through a Franz isodynamic separator with the magnetic current at 0.5 A and at 10° of side tilt, then with the magnetic current at 1.5 A and at progressively lower angles of side tilt (6° and 2°). All zircons analysed were extracted from the non-magnetic fractions of their respective size ranges. Commonly, under a binocular microscope, zircons from the size fractions 74 μm-105 μm and/or 105 μm-132 μm were hand-picked and mounted with the calibrated Curtin University Standard (CZ3) onto double-sided adhesive tape, then enclosed in epoxy resin discs. When dry, the discs were polished to about half their thickness to reveal a cross-section of the interior structure. Maps of the mounted crystals were made from a collage of photomicrographs taken in both reflected and transmitted light to assist in crystal location during analysis. Prior to analysis, mounts were cleaned and gold-coated.

SHRIMP techniques: The SHRIMP's operational characteristics have been reported by Kennedy and de Laeter (1994) and also briefly by Pidgeon et al. (1996). The analytical technique is described in detail by Compston et al. (1984), Williams et al. (1984), Williams and Claesson (1987), Compston et al. (1992) and Williams (1998). The Curtin SHRIMP II uses a primary beam of oxygen ions (O_2^- , at ~3 nA) focused to a spot diameter of ca. 25-30 μm and is operated at 10 kV. Positive sputtered secondary ions are extracted normal to the surface, accelerated to 11 kV, and transferred to a double-focusing mass spectrometer operated at a mass resolution of about 5000, which is sufficient to resolve interference peaks near ^{207}Pb and ^{208}Pb. The sensitivity of the ion microprobe was in the range 14 to 20 counts /second/ppm/nA for each Pb isotope during this study. Isotopic ratios were measured directly using an electron multiplier in ion-counting mode, and no correction was made for the small amount of mass-dependent mass fractionation (~2.5‰ per mass unit) that may be induced by the sputtering process and ion extraction system (Page and Sweet, 1998). Zr_2O^+, $^{204}Pb^+$, background (baseline) near $^{204}Pb^+$, $^{206}Pb^+$, $^{207}Pb^+$, $^{208}Pb^+$, $^{238}U^+$, ThO^+ and UO^+ were measured in cycles by magnetic-field switching, with seven cycles per data set. Each analysis was the mean of the seven cycles through the mass stations. The Sri Lankan gem zircon CZ3 was used as the SHRIMP standard and has been described by Pidgeon et al. (1994). The age of this zircon, determined by conventional analysis, is 564 Ma ($^{206}Pb/^{238}U = 0.0914$) and the concentration of U is 530-560 ppm.

Data quality was monitored during analysis by the lack of rejections based on counting statistics, the uncertainty on the $^{206}Pb/^{238}U$ age, concordance between $^{206}Pb/^{238}U$ and $^{208}Pb/^{238}U$ ages, and by the cumulative probability plots of data from a single population (Perkins and Kennedy, 1998). Pb/U ratios in the unknown samples were corrected using the ln(Pb/U) / ln(UO/U) relationship as measured in the standard zircon CZ3. Analytical uncertainties for isotopic ratios were governed predominantly by counting statistics and differed according to the concentrations of Pb, U, Th and common Pb in each area analysed (Page and Sweet, 1998). The common lead correction was based on the concentration of ^{204}Pb using a Broken Hill Pb composition, assuming that most of the common lead was added in the gold coat (Nelson, 1997). The SHRIMP output data for each spot analysis were reduced initially using the Krill program developed by P.D. Kinny and weighted mean $^{206}Pb/^{238}U$ age or $^{207}Pb/^{206}Pb$ ages for designated groups of analyses were calculated using the Plonk program developed by D. Nelson. Uncertainties in calculated group ages are quoted at 95% confidence limits (2σ) and analytical errors for individual analyses are quoted at the 1σ level. Ages of Neoproterozoic and Phanerozoic zircons are based on

$^{206}Pb/^{238}U$ ratios, rather than the combination of radiogenic $^{206}Pb/^{238}U$ with radiogenic $^{207}Pb/^{206}Pb$ (Compston et al. 1992). This is a consequence of the relatively low contents of ^{207}Pb in zircon of average U content and age less than ca 1.0 Ga, which gives low precision of the ^{207}Pb measurement. The $^{207}Pb/^{206}Pb$ ages are used for zircons with ages greater than ca 1.0 Ga following Perkins and Kennedy (1998). All data were corrected using ^{204}Pb, except where otherwise stated.

1.4 Organisation of the thesis

This thesis consists of seven chapters:

Chapter 1: Introduction.

Chapter 2: Regional geology of Jiaodong and Liaodong Peninsulas, North China Craton, which discusses the overall tectonic and geological setting of the Jiaodong and Liaodong Peninsulas.

Chapter 3: Gold deposits examined in the Zhao-Ye Gold Belt of the Jiaodong Peninsula were the Cangshang, Sanshandao, Jiaojia and Wangershan gold deposits, as well as the Linglong goldfield.

Chapter 4: Gold deposits examined in the Qi-Peng Gold Belt of the Jiaodong Peninsula were the Majiayao and Daliuhang gold deposits.

Chapter 5: Gold deposits examined in the Mu-Ru Gold Belt of the Jiaodong Peninsula were the Pengjiakuang, Denggezhuang and Jinqingding deposits.

Chapeter 6: Gold deposits examined in the Liaodong Peninsula were the Wulong, Sidaogou and Baiyun gold deposits.

Chapter 7: Conclusion, which synthesises the setting and timing of gold mineralization in the Jiaodong and Liaodong Peninsulas and presents a genetic model for gold mineralization that is consistent with the established tectonic setting.

CHAPTER 2: REGIONAL GEOLOGY OF THE JIAODONG AND LIAODONG PENINSULAS, NORTH CHINA CRATON

China is located in the southeastern part of the Eurasian plate, adjoining the Pacific plate in the east and the Indian plate in the southwest (Wang and Mo, 1995; Nie, 1997a). It encompasses a vast area consisting of three Precambrian cratons (i.e. North China, Yangtze and Tarim Cratons), many microcontinents, and a series of Phanerozoic orogenic belts (Fig.1.1) (Zhang et al., 1984). The tectonic framework of China is dominated by three global orogenic events, the Central-Asian or Paleo-Tethyan, the Circum-Pacific and the Tethys-Himalaya systems (Zhou et al., 2002). The Phanerozoic orogenies used in the Chinese literature include Caledonian (600-405 Ma), Variscan (405-270 Ma), Indosinian (270-208 Ma), Yanshanian (208-90 Ma) and Himalayan (<90 Ma) (Wang and Mo, 1995; Zhou et al., 2002).

2.1 North China Craton

The North China Craton, also commonly referred to as part of the Sino-Korean Craton, is triangular in shape and occupies an area of more than 1,500,000 km^2 (Fig. 1.1). To the west and north, the craton is bounded by the Early Paleozoic Qilian and Late Palaeozoic Tianshan-Inner Mongolia-Daxinganling orogens, respectively; to the south and east, it is separated from the Yangtze Craton by the Qinling-Dabie and Su-Lu orogens, respectively. Separating the craton from these younger orogenic belts is a series of major fault zones (Zhang et al., 1984).

The North China Craton comprises Early Archaean to Early Proterozoic basement rocks overlain by Middle Proterozoic to Cenozoic cover. The basement is dominated by Middle to Late Archaean rocks, represented by the Qianxi and Fuping Complexes and their equivalents. The Early Archaean rocks in the basement are only reported from the Caozhuang Complex in Eastern Hebei Province and the Anshan Complex in Central Liaoning Province, where ages of more than 3800 Ma have been recorded (Liu et al., 1992; Song et al., 1996). The Early Proterozoic rocks form a minor part of the basement, represented by the Liaohe and Fenzishan Groups in the Liaodong and Jiaodong Peninsulas, respectively. Zhao (2000) considered that the basement of the North China Craton consists of the Eastern and Western Blocks, separated by the Trans-North China Orogen; both the Eastern and Western Blocks are dominated by Late Archaean tonalitic-trondhjemitic-granodioritic gneiss domes surrounded by anastomosing networks of minor supracrustal rocks metamorphosed at ~2500 Ma. The Trans-North China Orogen is composed of reworked Late Archaean components and Early Proterozoic juvenile crustal materials that underwent deformation

and metamorphism at ~1800 Ma; the collision between the Eastern and Western Blocks resulted in the final assembly of the North China Craton at about 1800 Ma.

The North China Craton has also undergone multiple Phanerozoic tectonic events (Wang and Mo, 1995; Nie, 1997b). The collision between the North China and Yangtze Cratons during Indosinian event (270-208 Ma) resulted in formation of a suture zone comprising the Qinling-Dabie and Su-Lu orogens. The two orogens are characterised by coesite- and diamond-bearing ultra-high-pressure eclogite which indicates subduction to depths greater than ~120 km as a result of continental collision (Ames et al., 1993). Many authors have proposed that the Qinling-Dabie orogen is abruptly truncated at its eastern end and is offset a minimum of 530 km northward by the sinistral strike-slip Tan-Lu fault zone (Okay et al., 1989; Wang et al., 1992) (Fig. 1.1). It is suggested that the Su-Lu orogen is the eastern extension of the Qinling-Dabie orogen (Xü et al., 1987; Li et al., 1994). It is a widely held view that the North China Craton collided with the Yangtze Craton during the Triassic (Ames et al., 1996; Li et al., 1993; Okay and Sengör, 1992; Okay et al., 1993). Based on the similar U-Pb zircon ages obtained from eclogites from the Qinling-Dabie and Su-Lu orogens, Ames et al. (1996) suggested that the collision between the North China and Yangtze Cratons was approximately coeval along the length of the suture, which contrasts to the diachronous collision model proposed by Yin and Nie (1993).

Another important event affecting the North China Craton is the Yanshanian event (208-90 Ma). It is related to westward oblique subduction of the Paleo-Pacific Plate under the Eurasian Plate. Subduction started in the Mid-Jurassic along the entire continental margin of eastern Asia and continued well into the Late Cretaceous (Sengör et al., 1993). This event caused reactivation of the North China Craton and resulted in intensive magmatic activity in eastern China. Yanshanian granitoids are well developed and widely distributed along the circum-Pacific margin of China, including the North China Craton. The peak time for formation of the granitoids is Middle-Late Jurassic to Early Cretaceous (160-100 Ma) (Zhu, 1998). Ishihara (1984) subdivided the granitoids into 'ilmenite series' and 'magnetite series', following the criteria for the S-type and I-type granites of Chappell and White (1974). A genetic link between the Yanshanian orogeny and mineralization in east China is advocated by a number of geologists (Zhai and Deng, 1996; Pirajno et al., 1997; Zhu, 1998). Guo (1987) proposed that the Yanshanian event is the most important tectonic and metallogenic event, forming the so-called "Marginal Pacific Metallogenic Megaprovince", which extends from north to south across eastern China, and includes the Jiaodong and Liaodong Peninsulas.

2.2 Jiaodong Peninsula

2.2.1 Tectonic Setting

The Jiaodong Peninsula is situated along the southeastern margin of the North China Craton and is adjacent to the Yangtze Craton in the south (Fig. 1.1). The NNE-trending Tan-Lu Fault Zone, which is a major lithospheric fault zone that extends for about 5000 km through the eastern part of China and into Russia (Xu et al., 1987), separates the Jiaodong Peninsula from the Luxi Terrane (Fig. 2.1). The Luxi Terrane is dominated by Late Archaean Tonalite-Trondhjemite-Granodiorite (TTG) gneisses and Early Proterozoic granitoids, with minor amounts of Middle Archaean supracrustal rocks (Yang et al., 1993).

Tectonically, the Jiaodong Peninsula has been divided into two terranes—the Jiaobei Terrane and the Sulu Terrane (i.e. Su-Lu Orogen) (Zhang, 1990). The Jiaobei Terrane (Fig. 2.1), located in the northern part of the Jiaodong Peninsula, contains a high-grade metamorphic sequence dominated by orthogneiss, paragneiss, amphibolite, granulite, metaquartzite, metadolomite and mica schist, representing a part of the Precambrian basement of the North China Craton. The Sulu Terrane, situated in the southeastern part of the Jiaodong Peninsula (Fig. 2.1), consists of medium-grained, banded felsic gneiss, containing layers or lenses of eclogite, marble, and serpentinized ultramafic rocks. It has been considered to be the eastern extension of the Qinling-Dabie Orogen (Xu et al., 1987; Li et al., 1994). Traditionally, the Jiaobei and Sulu Terranes have been considered to be separated by the NE-SW trending Wulian-Rongcheng Fault Zone, consisting of the Wulian-Qingdao and Rongcheng Fault Zones (Fig. 2.1) (Cao et al., 1990). However, based on the fact that eclogites have recently been found in the Weihai area (Zhang and Cong, 1991; Wang et al., 1993; Zhang et al., 1995), Han et al.(1993) and Song et al.(1996) suggested that northern boundary is marked by the Mishan Fault Zone, not the Rongcheng Fault Zone (Fig. 2.1). The Jiaolai Basin (Fig. 2.1), located in the central part of the Jiaodong Peninsula, is dominated by Cretaceous strata which consist of terrigenous fluvio-lacustrine clastic sedimentary rocks and continental volcanic rocks (Bureau of Geology and Mineral Resources of Shandong Province (BGMRSP), 1991).

The Jiaodong Peninsula was strongly affected by two important orogenies which resulted from the collision between the North China and the Yangtze Cratons and the subduction of the Paleo-Pacific Plate beneath the Eurasian Plate (i.e. Indosinian and Yanshanian orogenies) (Wang et al., 1998; Zhou and Lü, 2000).

Gold deposits of the Jiaodong Peninsula are hosted entirely within the Jiaobei Terrane (Luo et al., 1996), which can be subdivided into three gold belts which are

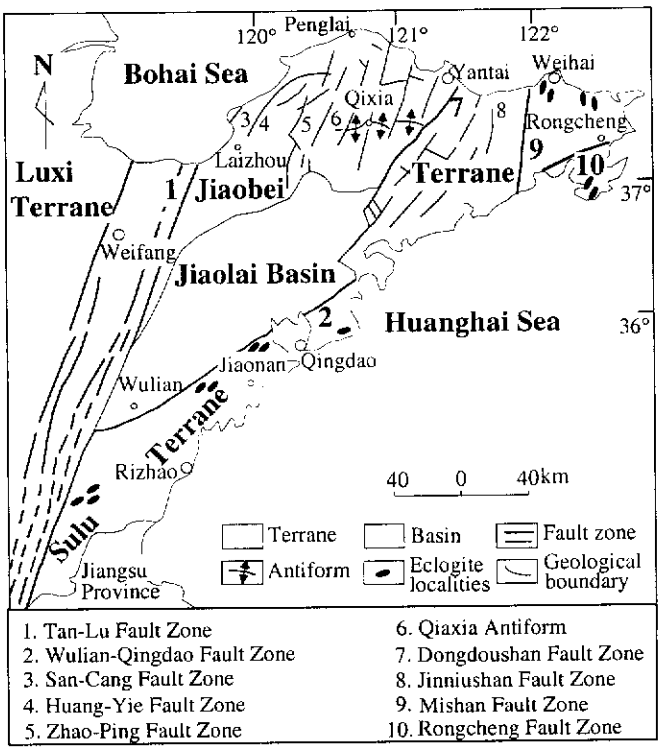

Fig. 2.1: Tectonic units of the Jiaodong Peninsula, showing major structural features (modified from Cao et al., 1990).

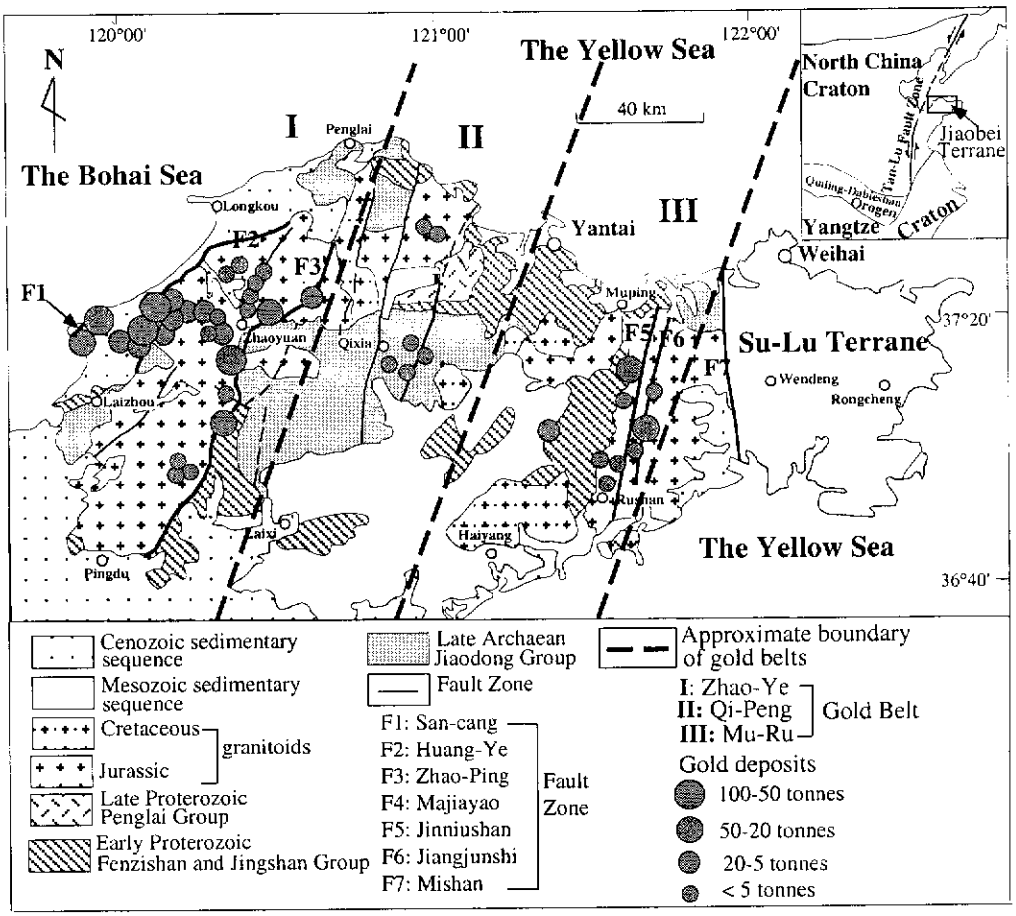

Fig. 2.2: The distribution of gold deposits within the Jiaodong Peninsula, showing Zhao-Ye, Qi-Peng and Mu-Ru Gold Belts (modified from Bureau of Geology and Mineral Resources of Shandong Province, 1992).

Zhao-Ye, Qi-Peng and Mu-Ru Gold Belts (Qiu et al., in press) (Fig. 2.2). Further details of the Jiaobei Terrane are provided below.

2.2.2 Jiaobei Terrane

2.2.2.1 Precambrian Metamorphic Rocks

Precambrian sequences in the Jiaobei Terrane consist of the Late Archaean Jiaodong Group, the Early Proterozoic Fenzishan and Jingshan Groups, and the Late Proterozoic Penglai Group (Fig. 2.3) (Li and Yang, 1993).

Jiaodong Group

The rocks of the Jiaodong Group are highly metamorphosed and strongly deformed, and are mainly composed of high-grade orthogneiss, paragneiss, amphibolite and granulite. Zhang and Wen (1983), Yang et al. (1993) and Yang and Lü (1996) considered the Jiaodong Group to be part of a granite-greenstone terrain. Wang and Yan (1992) identified some strongly deformed Archaean-Early Proterozoic Tonalite-Trondhjemite-Granodiorite (TTG) plutons, however, due to high metamorphic grade and strong deformation, primary textures and structures in the supracrustal rocks cannot be identified, so it is hard to distinguish them from strongly deformed and metamorphosed intrusive rocks. Recently, the main body of Archaean rocks in the Jiaobei Terrane have been considered to consist of TTG gneisses, with minor amount of supracrustal rocks occurring as enclaves or tectonic lenses within the gneisses (Wang and An, 1996; Zhao et al., 1998). SHRIMP U-Pb zircon results from inherited zircons in Mesozoic plutons indicate that the Jiaobei Terrane is underlain by Precambrian basement with components up to at least 3400 Ma (Wang et al., 1998). An (1990) and Zhang et al. (1994) proposed that the metamorphism of the Jiaodong Group is Late Archaean in age.

Jingshan and Fenzishan Groups

The Jingshan and Fenzishan Groups are widely considered to be the same stratigraphic unit (Ji, 1993; Zhang et al., 1994; Wang, 1995) distributed in different areas: the former in the south and the latter in the north of the Jiaobei Terrane.

The Jingshan Group consists mainly of Al-rich schist, fine-grained gneiss, marble and graphite -bearing rock. The metamorphic grade reaches amphibolite-

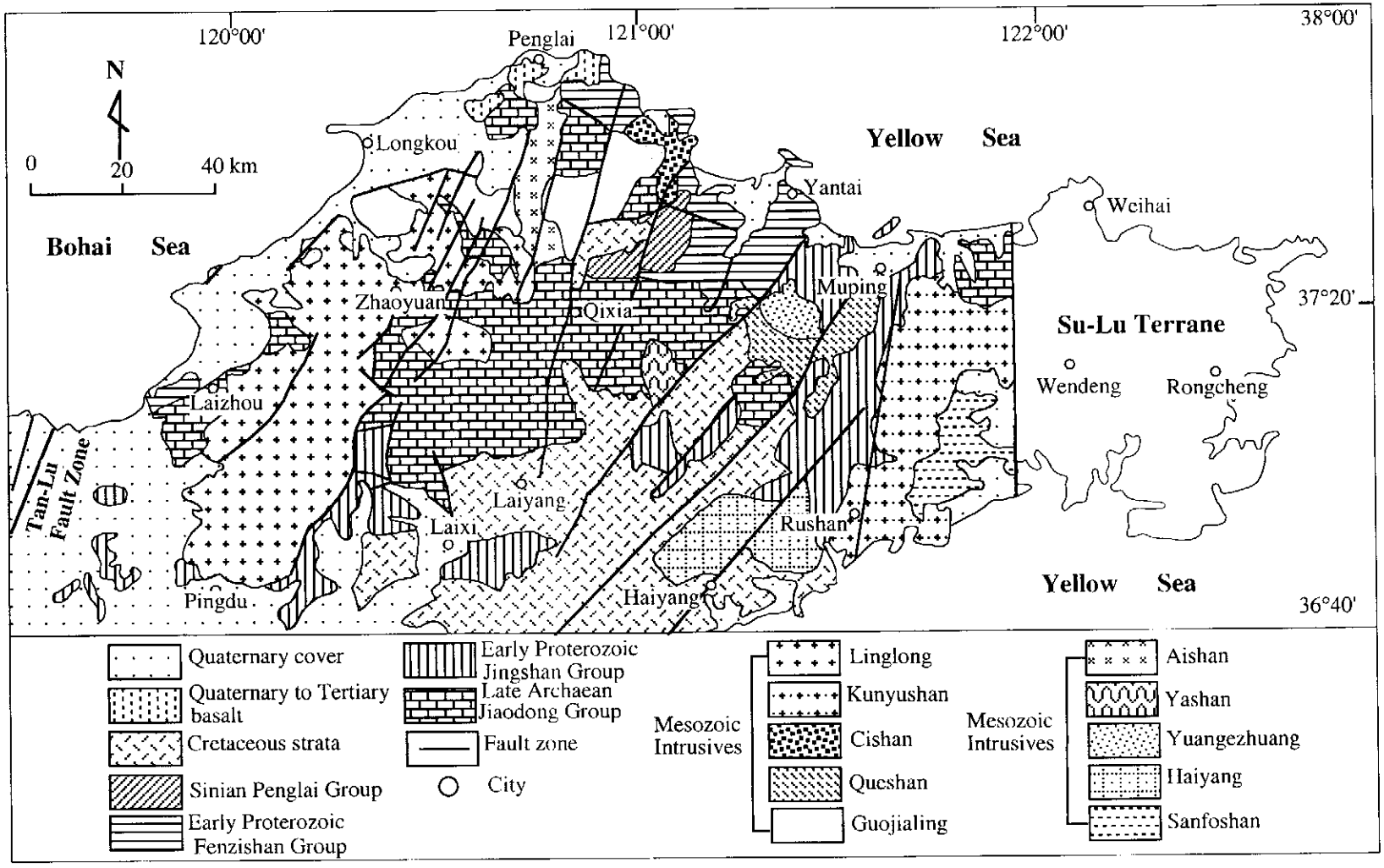

Fig. 2.3: Geological map of the Jiaobei Terrane (modified from Bureau of Geology and Mineral Resources of Shandong Province, 1991).

granulite facies. The protoliths are a suite of Al-rich, silty clastic sedimentary rocks and calcareous-magnesian carbonate rocks, intercalated with basic volcanic rocks. The contact with the underlying rocks is marked by a ductile shear zone (Zhang and Liu, 1996).

The Fenzishan Group comprises fine-grained gneiss, Al-rich schist, feldspathic quartzite, magnetite-bearing rock, marble and graphite-bearing rock. The metamorphic grade is greenschist to upper amphibolite facies. The protoliths of the Fenzishan Group were silty clastic sediments, thick-layered Mg-rich carbonates, carbonaceous clastic rocks and pelites. Contacts with underlying strata are marked by a ductile shear zone (Zhang and Liu, 1996).

Wang (1995) summarised the available age data for the Jingshan and Fenzishan Groups and inferred that 2484 to 2381 Ma represents the ages of protoliths of both groups and considered that 2224 to 1847 Ma dates one metamorphic event which coincides broadly with the Lüliang Orogeny.

Penglai Group

The Penglai Group consists of marble, slate, phyllite, quartzite and limestone, which were metamorphosed to lower greenschist facies. Its protoliths are a suite of pelitic to clastic terrigenous and carbonate sedimentary rocks (Zhang and Liu, 1996). This group unconformably overlies the Archaean rocks of the Jiaodong Group and Paleoproterozoic rocks of the Jiangshan and Fenzishan Groups. The age of the Penglai Group is controversial. According to microfossil evidence, the Penglai Group is Sinian (ca. 600-700 Ma) in age (BGMRSP, 1991; Niu et al., 1996). However, Ji (1993) reported a Rb-Sr whole-rock isochron age of 417 ± 41 Ma for the Penglai Group. Furthermore, Zhu et al. (1994) analysed two suites of whole-rock samples from the Penglai slate and obtained isochron ages of 441 ± 91 Ma and 446 ± 138 Ma, respectively. The Penglai Group thus represents the first cover sequence after cratonization of the Jiaobei Terrane and may be either Neoproterozoic or Early Phanerozoic in age.

2.2.2.2 Phanerozoic Strata

It is widely viewed that no Triassic or Jurassic rocks are present in the Jiaobei Terrane (BGMRSP, 1991; Luo et al., 1996). However, before the age of the Penlai Group is precisely determined, it is hard to say whether there are known Palaeozoic

rocks in the Jiaobei Terrane. The Cretaceous strata (Fig. 2.3), mainly comprising terrigenous fluvio-lacustrine clastic sedimentary rocks and continental volcanic rocks, unconformably overlie the earlier sequences (BGMRSP, 1991).

Some Tertiary lacustrine sediments have been identified in the Jiaobei Terrane. Quaternary strata are quite common and consist of littoral and fluvio-lacustrine sediments (BGMRSP, 1991) (Fig. 2.3). In addition, some Tertiary to Quaternary basalt (Fig. 2.3) is also present in the Jiaobei Terrane (BGMRSP, 1991).

2.2.2.3 Magmatic Rocks

Most of magmatic rocks within the Jiaobei Terrane are Mesozoic in age and comprise the Linglong, Kunyushan, Cishan, Queshan, Guojialing, Aishan, Yashan, Yuangezhuang, Haiyang and Safoshan Batholiths (Fig.2.3) (BGMRSP, 1991). The Linglong, Guojialing and Kunyushan Batholiths are considered to be spatially related to the gold deposits (e.g. Xu et al., 1989; Li, 1992; Wang et al., 1998; Qiu et al., 2002), and so they are described in more detail below.

Linglong Batholith

The Linglong Batholith occurs in the western part of the Jiaobei Terrane, and consists of the Shuangding, Yunshan, Cuizhao, Luoshan, Guojiadian, Luanjiahe, Gangshan (Biguo) and Oujiakuang Plutons (Xu et al., 1989; Yang and Lü, 1996). The batholith, with a surface area of about 3500 km^2, is the largest within the Jiaobei Terrane (Fig.2.2). The Linglong Batholith comprises two kinds of granitoids: Type I is typically light-grey in colour, fine- to medium-grained and has a gneissic fabric; Type II is characteristically grey-white in colour, medium- to coarse-grained, equigranular and has a massive fabric (Wang and Li, 1985; BGMRSP, 1991). Some authors refer to the Type II granitoids as the Luanjiahe Suite, which constitutes the Guojiadian, Luanjiahe and Gangshan (Biguo) Plutons (Luo et al., 1996; Wang et al., 1998). Type I granitoids commonly have gradational contact relationships to country rocks and contain enclaves of Precambrian metamorphic rocks. In contrast to the Type I granitoids, Type II granitoids have intrusive contacts with the Precambrian sequences and contain few enclaves of country rocks (BGMRSP, 1991). Type I granitoids are mainly composed of deformed monzogranite, with lesser amounts of quartz monzogranite, granodiorite and syenogranite; Type II granitoids are all monzogranite.

Several isotopic studies have previously been undertaken (Table 2.1), including K-Ar on biotite and K-feldspar, Rb-Sr whole-rock studies, Ar-Ar on biotite and conventional U-Pb on zircons. These have yielded a spectrum of ages ranging from Early Proterozoic (ca. 2000 Ma) to Late Mesozoic (ca. 86 Ma) (e.g Yang et al., 1984; Wen, 1985; BGMRSP, 1987; Hu et al., 1987; Yu, 1987; Xu et al., 1989; Li and Yang, 1993). However, it is considered that many of these isotopic ages may have no geological meaning (Wang et al., 1998). For example, some K-Ar and Ar-Ar dates may be unreliable due to thermal disturbances which cause excess argon or partial argon loss; Rb-Sr isochron results may not be reliable due to open system behaviour; and conventional multigrain zircon U-Pb ages may actually be "mixed" ages due to the incorporation of older zircon cores within new magmatic zircon. Recently, using SHRIMP U-Pb zircon dating, Wang et al. (1998) obtained the first precise emplacement age of 150 Ma to 160 Ma for the Linglong Batholith (Table 2.1). A few well-defined Rb-Sr and Ar-Ar ages, such as a Rb-Sr whole-rock isochron age of 156 ± 12 Ma and Ar-Ar biotite plateau age of 155 ± 2 Ma (Table 2.1), are consistent with these SHRIMP U-Pb zircon age data. New data on the Linglong Batholith are presented in this thesis and will be discussed later.

Kunyushan Batholith

The Kunyushan Batholith covers an area of about 1020 km^2 and is the second largest within the Jiaobei Terrane (Fig. 2.3). It occurs within the eastern part of the Jiaobei Terrane and comprises the Guobeishan, Hongshitou, Shaizi, Duoguding and Jiangjunshi Plutons (Xu et al., 1989; Yang and Lü, 1996). The rocks are dominantly monzogranite, with a lesser amount of syenogranite. The granitoids have gradational contacts with the Precambrian sequences and contain abundant enclaves of country rock. Adjacent to contact zones, the granites have well-developed gneissic fabrics whereas, at the inner part of the batholiths, the granitoids have medium-grained, equigranular, massive fabrics (BGMRSP, 1991).

The emplacement age of the Kunyushan Batholith is not precisely defined in the literature (Table 2.1). Ages obtained from whole rock and mineral geochronology give a range of ages from Middle Proterozoic (ca. 1500 Ma) to Late Mesozoic (ca. 120 Ma) (Xu et al., 1989; Yu, 1989; Zhang et al., 1995). This range in ages may be a reflection of the dating methods used. This research work is the first to present data on the precise emplacement age of the Kunyushan Batholith, based on SHRIMP U-Pb zircon analysis. The results will be discussed in the following chapters.

Table 2.1: Summary of previous isotopic age data for the Linglong, Kunyushan and Guojialing Batholiths within the Jiaobei Terrane, Jiaodong Peninsula

Batholith Name	Sample No.	Age (Ma)	Dated Material	Dating Method	References
Linglong	T12	125 ±5 (isochron age)	Whole rock, apatite, biotite, plagioclase	Rb-Sr	Yang et al., 1984
	III_1J-2	86	Biotite	K-Ar	Wen, 1985
	S_9W-22	115	Biotite	K-Ar	Wen, 1985
	$3T_{81}$-0002	119	K-feldspar	K-Ar	Wen, 1985
	J-06	122	Biotite	K-Ar	Wen, 1985
	Guan-1	127	Biotite	K-Ar	Wen, 1985
	J-05	129	Biotite	K-Ar	Wen, 1985
	D-9	132	K-feldspar	K-Ar	Wen, 1985
	Mo-1	135	Biotite	K-Ar	Wen, 1985
	J-26	141	Biotoite	K-Ar	Wen, 1985
	S_9W-21	144	Biotite	K-Ar	Wen, 1985
	J-04	145	Biotite	K-Ar	Wen, 1985
	Shan81J108, 3T83-03, 3T83-10, 3T83-11, 3T83-12, 3T83-19, 3T83-20.	156 ± 12 (isochron age)	Whole rock	Rb-Sr	Wen, 1985
	N/S	201 ($^{206}Pb/^{238}U$ age)	Zircon	Conventional U-Pb	BGMRSP, 1987
	N/S	1847 ($^{206}Pb/^{238}U$ age)	Zircon	Conventional U-Pb	BGMRSP, 1987
	N/S	164 ± 1 (plateau age)	Biotite	Ar-Ar	Hu et al., 1987
	ZY12-1	250 ($^{206}Pb/^{238}U$ age)	Zircon	Conventional U-Pb	Yu, 1987
	M-1	155 ± 2 (plateau age)	Biotite	Ar-Ar	Xu et al., 1989
	J87525, J87526, J87528, J87529, J87530.	217 ± 7 (isochron age)	Whole rock	Rb-Sr	Xu et al., 1989
	J86508, J86509, J86510, J86512, J86515.	297 ± 9 (isochron age)	Whole rock	Rb-Sr	Xu et al., 1989
	86R13, J86538, J86534, J86926, Shan8133, 80-31, 80-32, L-003.	2122 ± 150 (isochron age)	Whole rock	Rb-Sr	Xu et al., 1989
	N/S	110 ± 3	Whole rock	Rb-Sr	Li and Yang, 1993
	N/S	119 ± 3	Whole rock	Rb-Sr	Li and Yang, 1993
	N/S	125 ± 2	Whole rock	Rb-Sr	Li and Yang, 1993
	N/S	132 ± 1	Biotite	K-Ar	Li and Yang, 1993
	N/S	156 ± 1	Whole rock	Rb-Sr	Li and Yang, 1993
	LD-20	153 ± 4 (group age)	Zircon	SHRIMP U-Pb	Wang et al., 1998
	LX-13	157 ± 4 (group age)	Zircon	SHRIMP U-Pb	Wang et al., 1998
	JMS-1	160 ± 3 (group age)	Zircon	SHRIMP U-Pb	Wang et al., 1998
	MS-1	158 ± 3 (group age)	Zircon	SHRIMP U-Pb	Wang et al., 1998
	LJH-1	154 ± 4 (group age)	Zircon	SHRIMP U-Pb	Wang et al., 1998
	BG-1	152 ± 10 (group age)	Zircon	SHRIMP U-Pb	Wang et al., 1998

Table 2.1 (continued)

Batholith Name	Sample No.	Age (Ma)	Dating Material	Dating Method	Rereferences
Kunyushan	N/S	145 (isochron age)	K-feldspar	Rb-Sr	An et al., 1988
	N/S	146 (isochron age)	Whole rock	Rb-Sr	An et al., 1988
	N/S	164 (isochron age)	Whole rock	Rb-Sr	An et al., 1988
	N/S	165 (isochron age)	Whole rock	Rb-Sr	An et al., 1988
	N/S	698 (isochron age)	Biotite	Rb-Sr	An et al., 1988
	N/S	703 (isochron age)	Whole rock	Rb-Sr	An et al., 1988
	N/S	741 (isochron age)	Whole rock	Rb-Sr	An et al., 1988
	N/S	1518 (isochron age)	Whole rock	Rb-Sr	An et al., 1988
	TW3-1, TW3-3, TW3-5, 6, TW3-6, K839813, J86969.	521 ± 29 (isochron age)	Whole rock	Rb-Sr	Xu et al., 1989
	TW3-807, TW3-809, TW3-814, TW3-818, K836805, K8361110.	662 ± 43 (isochron age)	Whole rock	Rb-Sr	Xu et al., 1989
	83015-2	125	Biotite	K-Ar	Yu, 1989
	83055	130	Biotite	K-Ar	Yu, 1989
	83018	132	Biotite	K-Ar	Yu, 1989
	ST-1	132	Biotite	K-Ar	Yu, 1989
	D-12$^{67-5}$	172	Biotite	K-Ar	Yu, 1989
	D-12$^{67-1}$	180	Biotite	K-Ar	Yu, 1989
	21-1	120 ± 2	Biotite	K-Ar	Zhang et al., 1995
	9-1	121 ± 2	Biotite	K-Ar	Zhang et al., 1995
	23-1	124 ± 3	Biotite	K-Ar	Zhang et al., 1995
	34-4	129 ± 1	Biotite	Ar-Ar	Zhang et al., 1995
	13-1	131 ± 2	Biotite	K-Ar	Zhang et al., 1995
	4-1	147 ± 2	Biotite	K-Ar	Zhang et al., 1995
	34-4	186 ± 2	Biotite	K-Ar	Zhang et al., 1995
Guojialing	T4	127 ± 8 (isochron age)	Whole rock, apitite, biotite, plagioclase, K-feldspar	Rb-Sr	Yang et al., 1984
	N/S	129 ± 3	Amphibole	K-Ar	Hu et al., 1987
	N/S	130 ± 3	Amphibole	K-Ar	Hu et al., 1987
	N/S	132 ± 3	Amphibole	K-Ar	Hu et al., 1987
	N/S	134 ± 2	Amphibole	K-Ar	Hu et al., 1987
	N/S	135 ± 2 (plateau age)	Amphibole	Ar-Ar	Hu et al., 1987
	G-5	119 ± 1 (plateau age)	Amphibole	Ar-Ar	Xu et al., 1989
	G-5, G-6, G-7, G-9, G-10, G-13, J86540.	132 ± 9 (isochron age)	Whole rock	Rb-Sr	Xu et al., 1989
	S-1	137 ± 1 (plateau age)	Biotite	Ar-Ar	Xu et al., 1989
	N/S	118	Whole rock	K-Ar	Li and Yang, 1993
	N/S	121	Whole rock	K-Ar	Li and Yang, 1993
	N/S	127 ± 8 (isochron age)	Whole rock	Rb-Sr	Li and Yang, 1993
	N/S	132	Whole rock	K-Ar	Li and Yang, 1993
	N/S	133 ± 10	Biotite	K-Ar	Li and Yang, 1993
	JH-8	126 ± 2 (group age)	Zircon	SHRIMP U-Pb	Wang et al., 1998
	SSD-15	128 ± 2 (group age)	Zircon	SHRIMP U-Pb	Wang et al., 1998
	NM-1	128 ± 6 (group age)	Zircon	SHRIMP U-Pb	Wang et al., 1998
	MZS-1	129 ± 3 (group age)	Zircon	SHRIMP U-Pb	Wang et al., 1998
	TJ-1	130 ± 3 (group age)	Zircon	SHRIMP U-Pb	Wang et al., 1998

Guojialing Batholith

The Guojialing Batholith occupies an area of about 500 km^2 within the western part of the Jiaobei Terrane (Fig. 2.3). Xu et al. (1989) subdivided the batholith into five plutons; the Sanshandao, Shangzhuang, Beijie, Congjia and Guojialing Plutons. These intrude into both the Precambrian sequences and the Linglong granitoids (BGMRSP, 1991). The rocks are dominantly granodiorite, with some monzogranite. They have a porphyritic texture, with K-feldspar phenocrysts commonly ranging from 2 cm to 5 cm in length and rarely up to 15 cm long (Xu et al., 1989; BGMRSP, 1991).

According to previous Rb-Sr, K-Ar and Ar-Ar dates (Hu et al., 1987; Xu et al., 1989; Li and Yang, 1993), the age of the Guojialing Batholith ranges from 120 Ma to 130 Ma (Table 2.1). Wang et al. (1998) confirmed that the emplacement age of the Guojialing Batholith was between 126 Ma and 130 Ma (Table 2.1), based on precise SHRIMP U-Pb zircon dating. New geochronological data on the Guojialing Batholiths are presented in this thesis and will be discussed later.

2.2.2.4 Structure and Deformation

A series of well-developed regional NNE- to NE-trending fault zones are present within the Jiaobei Terrane (Fig. 2.1). Some of these fault zones, such as the San-Cang, Huang-Ye, Zhao-Ping, Douai, Majiayao and Jinniushan Fault Zones, are spatially closely related to the distribution of gold deposits (e.g. Zhang and Wen, 1983; Lü and Kong, 1993). Five phases of deformation were recognized in these fault zones by Luo et al. (1996). The first phase (D_1) is related to N-S and/or NNE-SSW compression, resulting in nearly EW-trending shear zones with dextral movement. The second phase (D_2) resulted from NNW-SSE compression, producing regional NNE to NE-trending shear zones with sinistral oblique reverse movement. The third phase (D_3) reflects NW-SE compression, causing brittle reactivation of D_2 shear zones. The fourth phase (D_4) is a period of NW-SE or WNW-ESE extension, resulting in further brittle reactivation of D_2 shear zones. The fifth phase (D_5) is NNW-SSE and/or ENE-WSW compression, producing ENE-striking sinistral fault zones and dextral and sinistral NW- and WNW-trending fault zones. Based on SHRIMP U-Pb zircon studies of the granitoid batholiths (Wang et al., 1998), the timing of D_2 and D_3 deformation is constrained between 165 Ma and 120 Ma. Wang et al. (1998) considered that two main phases of deformation occurred within the Jiaobei Terrane during the Mesozoic, with the first phase being NW-SE oblique compression, producing prominent NNE- to NE-

trending brittle-ductile shear zones with sinistral oblique reverse movements, followed by reactivation involving development of brittle structures, which were accompanied by hydrothermal alteration and gold mineralization.

2.2.2.5 Metamorphism

The Bureau of Geology and Mineral Resources of Shandong Province (1988) has identified four metamorphic stages (M1 to M4) within the Jiaobei Terrane. The M1 stage is represented by the mineral assemblage almandine + hornblende (brownish colour) + plagioclase (An_{37-45}) which appears in metabasic rocks, and the mineral assemblage almandine + biotite (brown colour) ± hornblende (brownish colour) + plagioclase (An_{30-37}) in metamorphosed intermediate to acid volcanic rocks. Metamorphism of this stage is at upper amphibolite facies and occurred at ca. 2500 Ma (BGMRSP, 1988). Equilibrium conditions of the M1 stage were estimated using hornblende-plagioclase thermobarometers at ~780°C and ~ 5.0 kbar (Li, 1993). The metamorphism of the M2 stage is prograde and was completed by ca. 2000 Ma (BGMRSP, 1988). Locally, the M2 metamorphism reaches granulite facies, which results in the mineral assemblage hypersthene + clinopyroxene + hornblende (brownish colour) ± biotite ± plagioclase (An_{45-60}), with the hypersthene, hornblende and plagioclase replacing almandine of the M1 stage (BGMRSP, 1988). The P-T conditions of this stage were estimated at 850-900°C and 8.0-8.5 kbar utilizing two-pyroxene, garnet-orthopyroxene and garnet- clinopyroxene thermometers and garnet-orthopyroxene-plagioclase-quartz barometers (Li, 1993). The M3 stage of metamorphism is retrograde. The mineral assemblage hornblende (greenish colour) + plagioclase (An_{30-35}) occurs in metabasic rocks and almandine + muscovite ± biotite + quartz assemblage in metamorphosed pelitic rocks. The pyroxene and hornblende (brownish colour) of the M2 stage were replaced by biotite or hornblende (greenish colour). The metamorphism is at lower amphibolite facies and was completed by ca. 1700 Ma (BGMRSP, 1988). The P-T conditions of this stage were estimated at ~650°C and ~7.0 kbar (BGMRSP, 1988). The M4 metamorphic episode is another retrograde event. It is recognized by the retrogressive mineral assemblages epidote + albite + quartz and chlorite + epidote + sericite + actinolite. Chlorite replaces biotite, hornblende and pyroxene, with epidote replacing hornblende and plagioclase. The metamorphism is at lower greenschist facies and terminated at ca. 800 Ma (BGMRSP, 1988). P-T conditions were estimated at ca. 450°C and 2-4 kbar (BGMRSP, 1988). Zhao et al (1998) concluded that the metamorphic evolution of the mafic granulites from the Jiaobei Terrane is characterized by a nearly isobaric cooling with a counterclock-wise P-T path.

2.3 Liaodong Peninsula

The Liaodong Peninsula (Fig. 1.1) is situated ca. 200 km north-east of the Jiaodong Peninsula along the southeastern margin of the North China Craton. Gold deposits were investigated to check if tectonic setting and mineralization were similar to those of the Jiaodong Peninsula.

Archaean rocks of the Liaodong Peninsula predominantly comprise TTG gneisses, granitoids and supracrustal rocks. Their ages range from Early Archaean (ca. 3800 Ma) to Late Archaean (ca. 2500 Ma) (Liu et al., 1992; Song et al., 1996). Early Proterozoic rocks in the area (Fig. 2.4), named the Liaohe Group, consist of metamorphosed sediments and volcanic rocks, with ages ranging from 2300 Ma to 1900 Ma (Zhang, 1988; Sun et al., 1993). The Paleoproterozoic tectonic setting of this area has been interpreted as a palaeorift system developed within the Archaean craton (Zhang, 1988; Sun et al., 1993), although Bai (1993) considers it was a continental margin. Together with the Archaean rocks, these Early Proterozoic rocks constitute the Precambrian basement in the Liaodong Peninsula.

Sinian, Palaeozoic and Mesozoic sequences unconformably overlie the Precambrian basement (Fig. 2.4). The Sinian strata consist of shale, sandstone, limestone and dolomite; the Cambrian strata comprise a suite of marine sedimentary rocks; and the Cretaceous strata are composed of continental sedimentary and volcanic rocks. Quaternary strata consist of fluvio-lacustrine sediments and are quite common within the Liaodong Peninsula (Fig. 2.4) (Bureau of Geology and Mineral Resources of Liaoning Province, 1989).

Mesozoic granitoids, are widely distributed in the Liaodong Peninsula and occupy an area of ca. 12,000 km^2 (Peng et al., 1988). These granitoids include both deformed and undeformed varieties (Fig. 2.4). The deformed (i.e. gneissic) granitoids are represented by the Wulong Batholith covering an area of ~1200 km^2; the undeformed granitoids are represented by the Sanguliu Pluton occupying an area of ca. 50 km^2 (Yao et al., 1988). The age of emplacement of the Mesozoic granitoids is poorly constrained. Previous studies, including K-Ar dating of biotite and conventional U-Pb dating of zircon, have yielded a spectrum of ages ranging from ca. 221 Ma to ca. 106 Ma for the deformed granitoids and from ca. 200 Ma to ca. 72 Ma for the undeformed granitoids (Table 2.2) (Li et al., 1987; Yao et al., 1988). This thesis is the first to present precise crystallisation ages for both types of Mesozoic

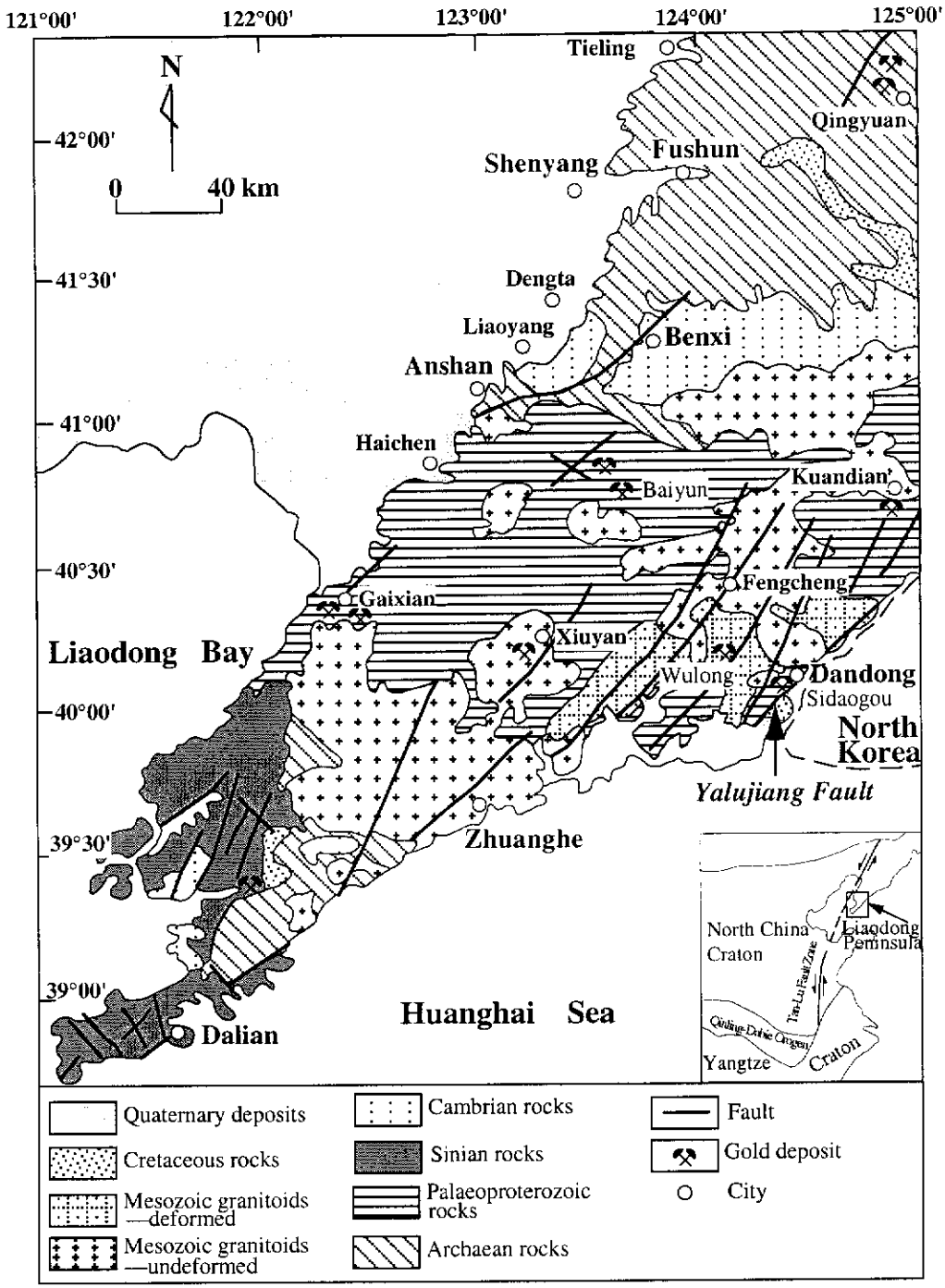

Fig. 2.4: Geological map of the Liaodong Peninsula, showing the distribution of gold deposits (modified from Bureau of Geology and Mineral Resources of Liaoning Province, 1989). Inset shows location in North China Craton.

granitoids within the Liaodong Peninsula, based on SHRIMP U-Pb zircon analysis. The results will be discussed in the following chapters.

Table 2.2: Summary of previous isotopic age data for Mesozoic granitoids within the Liaodong Peninsula

Batholith Name	Sample No.	Age (Ma)	Dated Material	Dating Method	References
Wulong (Deformed)	W35	106	Whole rock	K-Ar	Li et al., 1987
	W1	115	Whole rock	K-Ar	Li et al., 1987
	N/S	116	White mica	K-Ar	Yao et al., 1988
	N/S	125	White mica	K-Ar	Yao et al., 1988
	N/S	157	White mica	K-Ar	Yao et al., 1988
	N/S	160	Biotite	K-Ar	Yao et al., 1988
	84008	198	Zircon	Conventional U-Pb	Yao et al., 1988
	N/S	221	Biotite	K-Ar	Yao et al., 1988
Paoshouying -Baijialing (Undeformed)	N/S	72	Biotite	K-Ar	Yao et al., 1988
	DJ4	98	Zircon	Conventional U-Pb	Yao et al., 1988
	DJ3	104	Zircon	Conventional U-Pb	Yao et al., 1988
	Pao-1	114	Zircon	Conventional U-Pb	Yao et al., 1988
	N/S	182	Biotite	K-Ar	Yao et al., 1988
	N/S	200	Zircon	Conventional U-Pb	Yao et al., 1988

Northeast-Southwest trending faults, such as the Yalujiang Fault, are common in the Liaodong Peninsula (Fig. 2.4) and are considered to be spatially associated with the gold deposits (Yao et al., 1988).

CHAPTER 3: GOLD DEPOSITS EXAMINED WITHIN THE ZHAO-YE GOLD BELT OF THE JIAODONG PENINSULA

3.1 Introduction

The Zhao-Ye Gold Belt (Fig. 3.1) is located in the western part of the Jiaobei Terrane and contains 70% of the Jiaodong Peninsula's gold reserves (Luo et al., 1996). The main rock types of this area are the Linglong granitoids. Three regional

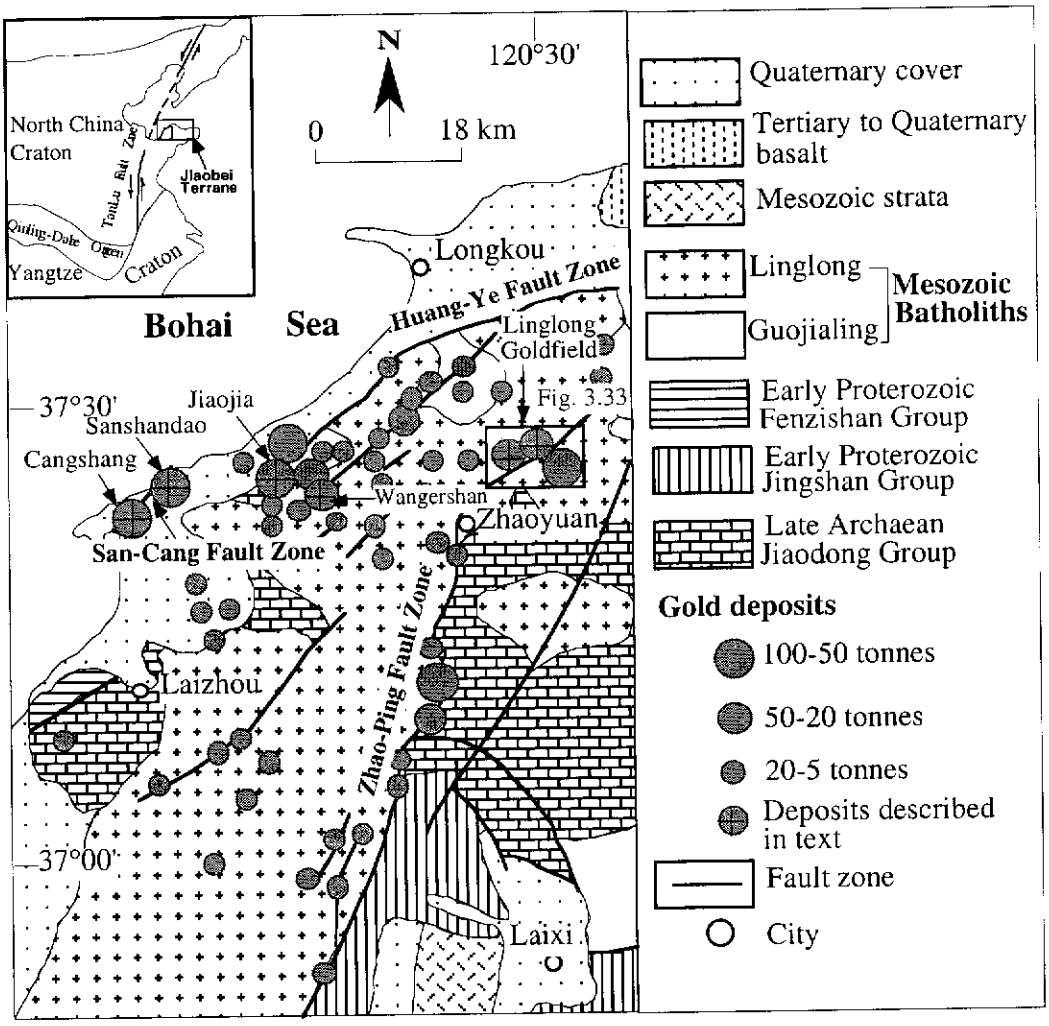

Fig. 3.1: Distribution map of gold deposits within the Zhao-Ye Gold Belt of the Jiaodong Peninsula (enlargement of black area in the insert), showing many gold deposits spatially related to the Linglong and Guojialing Batholiths and fault zones (modified from Chang, 1996).

fault zones (i.e. San-Cang, Huang-Ye and Zhao-Ping) and their secondary structures are spatially associated with gold deposits (Fig. 3.1). These gold deposits are either of the Jiaojia-style (disseminated-and-veinlet type) or Linglong-style (vein-filling type).

The former, represented by the Cangshang, Sanshandao and Jiaojia Gold Deposits, are developed at lithologic contacts along fault zones; the latter, represented by gold lodes within the Linglong Goldfield, are situated in secondary structures of the regional fault zones. The Cangshang, Sanshandao, Jiaojia and Wangershan Gold Deposits, as well as the Linglong Goldfield, are described in more detail below.

3.2 Cangshang Gold Deposit

The Cangshang Gold Deposit (lat. 37°20'58.9" to 37°21'44.0" N; long. 119°53'38" to 119°54'51.2" E) is located 18 km north of the city of Laizhou (Fig. 3.2), and occupies an area of 2.52 km^2. This deposit was discovered in 1984 by the No.6 Team of Geology and Exploration, BGMRSP, based on interpretation of geophysical data, 1:50,000 scale mapping and drilling. A total of 0.625 tonnes of gold were produced in 1990, with the known reserves estimated at 28.724 tonnes. By 1997, the known reserves were extended to 50 tonnes, and 1.875 tonnes of gold were produced in 1997, with a cut-off grade of 2.13 g/t and daily ore production of 1500 tonnes as reported in the 1997 Annual Report of the Cangshang Gold Mine. The deposit is mined from the largest open pit gold mine in China, and in 1997 the pit was 850 m in length and 390 m in width. Mining depth as of 1997 was down to the -94 m bench with a designed final mining depth of -166 m. A detailed map of the pit and the principal orebody (No.1) was prepared by the author over a two week period in 1997 and is presented as Figure 3.3. The deposit is typical of the Jiaojia-style (i.e. disseminated-and-veinlet type) gold occurrence which is characteristic of all the large scale gold deposits in the Jiaobei Terrane. Some aspects of this deposit are discussed in Zhang et al. (in press).

The deposit is located at the contact between a hanging wall sequence of Early Proterozoic Fenzishan Group to the southeast and a footwall sequence of Mesozoic Linglong granitoid to the northwest. The contact is marked by the San-Cang Fault Zone (Fig. 3.2). There is a change in trend of the fault: south of the Cangshang Deposit, it trends in a southwest direction; in the vicinity of the deposit it trends east-north-east direction; whereas north of the deposit, it trends in a north-north-east direction.

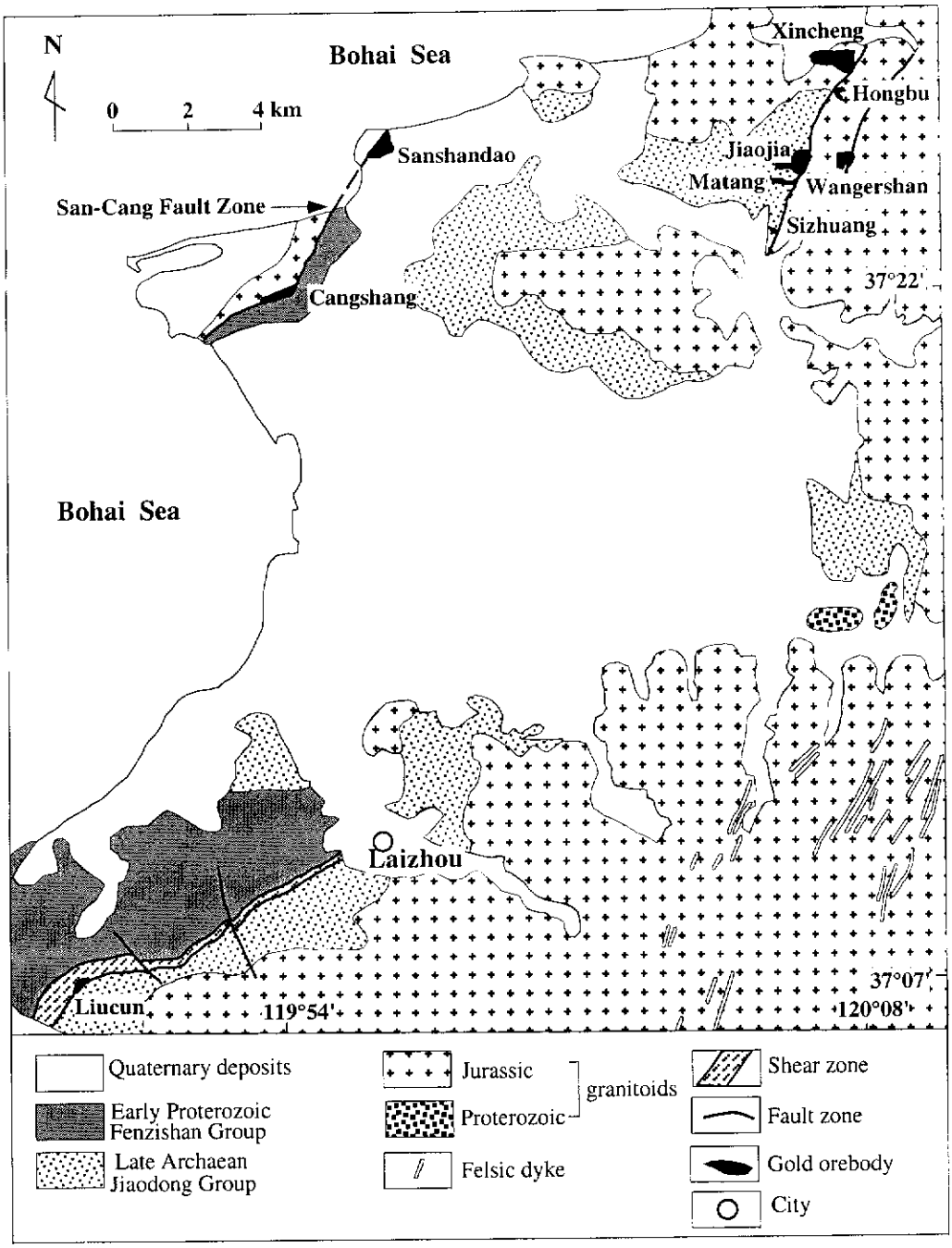

Fig. 3.2: Geological map of the Laizhou region of the Jiaobei Terrane, showing the San-Cang Fault Zone and gold deposits distributed in this area (modified after Laizhou Gold Company, 1996).

3.2.1 Lithological Units

Fenzishan Group

The Early Proterozoic Fenzishan Group makes up the hanging wall of the Cangshang Gold Deposit and in the vicinity of the No. 1 orebody comprises amphibolite, with lesser amounts of fine-grained gneiss and hornblendite. The amphibolite is fine-grained and consists of plagioclase and hornblende with rare quartz and garnet. Accessory minerals include titanite, apatite and zircon. Where fresh, the unit has a grey-green to dark green colour. The amphibolite was metamorphosed to upper amphibolite facies and the rock is strongly foliated, containing felsic segregations 2-5 mm thick of plagioclase, quartz and hornblende. Brittle fractures and joints with small amounts of quartz-carbonate infilling are common. Pronounced late crosscutting, irregular felsic pegmatites and quartz veins, typically 10-30 cm in width, can be observed in the amphibolite.

The fine-grained gneiss, which is intercalated with the amphibolite, is grey in colour and mainly composed of plagioclase, biotite and quartz. Accessory minerals include apatite and zircon. Locally, it is strongly mylonitized and crosscut by later calcite veins.

The hornblendite (>90% hornblende) is fine-grained, dark green in colour and has sharply intruded the amphibolite (Fig. 3.3). Locally, it is crosscut by irregular felsic pegmatites and quartz veins.

Linglong Granitoid

The Linglong Granitoid, which makes up the footwall of the Cangshang gold deposit, is exposed in the open pit and consists mainly of granodiorite, which is grey-white in colour and composed of plagioclase, quartz, K-feldspar and biotite. Accessory minerals include magnetite, allanite, apatite and zircon. It has a fine- to medium-grained, equigranular texture with a prominent foliation and is strongly fractured.

Late Dykes and Quaternary Units

The hanging wall sequence is cut by pegmatites. The pegmatites are flesh pink in colour and composed of K-feldspar, quartz and plagioclase, with minor biotite.They have a coarse-grained, massive structure and are unaltered, which suggests that they post-date the gold mineralization.

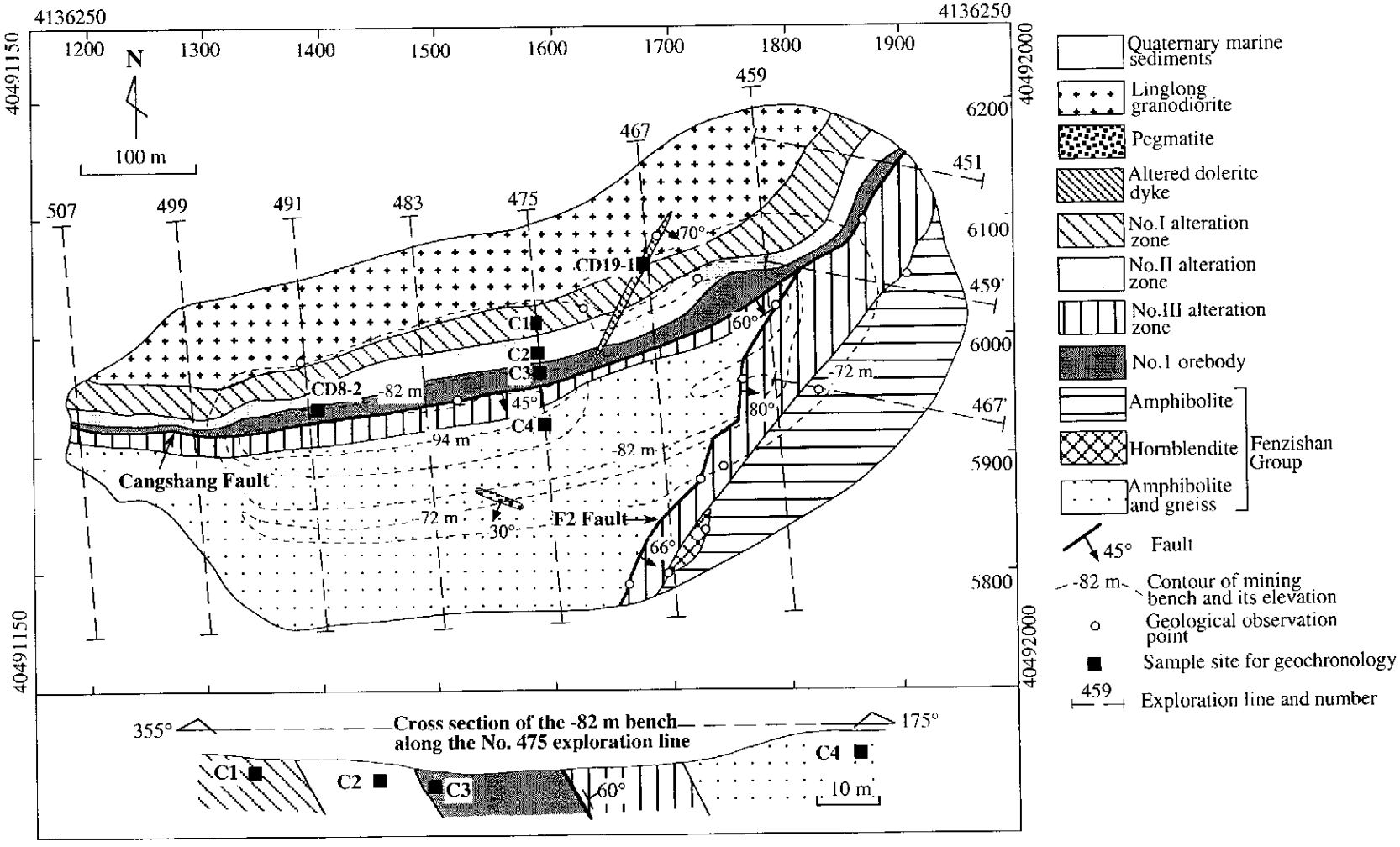

Fig. 3.3: Geology map of the open pit of the Cangshang Gold Deposit (mapped by X. Zhang, 1997).

An altered mafic dyke cross-cuts the No.1 orebody and the footwall granodiorite (Fig. 3.3). It is yellow-green in colour, and has a porphyritic texture and massive structure. Due to strong alteration, its composition could not be precisely determined in the field. Under the microscope, it consists of phenocrysts altered to chlorite, possibly after ferromagnesian minerals such as pyroxene and/or olivine; some tabular minerals in the groundmass were probably plagioclase, but are now altered to sericite. The dyke is inferred to be originally a dolerite. Based on field observations, the dyke cross-cuts the alteration zones associated with gold mineralization, but its alteration indicates that it may be affected by later remobilization of auriferous material, or that emplacement of the dyke may have been accompanied by a later, less significant phase of alteration and/or fluid movement.

Quaternary marine sediments, up to 60 m thick, cover the rocks surrounding the open pit.

3.2.2 Cangshang Fault Zone

The Cangshang Fault Zone is the southwestern segment of the San-Cang Fault Zone (Fig. 3.2). It is about 7 km long between the northeastern (No.203) and the southwestern (No.747) exploration lines (not shown on the map), and varies in width from 50 m to 200 m. This fault zone has a general trend of ~040° and dips 40°-75° SE. In detail, between the No.203 and No.459' exploration lines, it strikes 020° and dips 75°SE; between the No.459 and No.563 exploration lines, it strikes 080°-085° and dips 50°SE; and between the No.563 and No.747 exploration lines, it strikes 045° and dips 40°-50°SE. The sense of movement, deduced from the striations which plunge 45° towards 220°, is reverse and oblique. The fault zone is considered to be characteristic of compressional-shearing with dextral movement (No.6 Team of Geology and Exploration, BGMRSP, 1991). A main fault plane, marked by a grey-coloured fault gouge zone (10 to 20 cm in width), is present throughout the area.

3.2.3 Alteration

At the Cangshang Deposit (Fig. 3.3), the alteration styles are dominantly silicification, sericitization, pyritization, K-feldspar alteration, chloritization and carbonation. A large alteration halo within the Cangshang Gold Deposit is well-developed along the Cangshang Fault Zone. Within the mining area, this alteration halo is 1900 m in length, ranges from 85 m to 185 m in width, and has been explored to a depth of 640 m. Based on the type and intensity of alteration and the nature and

distribution of altered rocks, this alteration halo can be roughly divided into three sub-zones, although these change gradually and there are no clear boundaries between them. The alteration zones are the No.I, No.II and No.III zones (Fig. 3.3), respectively. The No.I alteration zone is situated below the main fault plane and adjacent to the footwall of Linglong granodiorite. This zone is characterized by K-feldspar alteration, sericitization and silicification and consists of altered Linglong granodiorite. The intensity of alteration is weaker than in the other zones, since it is farther away from the main fault plane. The closer to the main fault plane the wall rocks are, the more intensive the alteration. The No.II zone is developed below and adjacent to the main fault zone. This zone is characterized by strong pyrite alteration, sericitization and silicification and is composed mainly of pyrite-sericite-quartz rocks. The No.III alteration zone is located on the hanging wall side of the main fault plane, adjacent to the Fenzishan Group, but is terminated to the west by the F2 Fault, striking 015° and dipping 66°-80°SE. This portion of the alteration zone is wider and extends up to ca. 60 m into the hanging wall (Fig. 3.3). The No.III zone is characterized by sericitization, silicification and chloritization and consists of altered and sheared rocks of the Fenzishan Group.

3.2.4 No.1 Orebody

The No.1 orebody is predominantly controlled by the Cangshang Fault Zone (Fig.3.3) and has 98% of the proven reserves. It lies within the No.II alteration zone and is up to 50 m structurally below, and parallel to, the main fault plane (Fig. 3.3). The known length of the No.1 orebody is 1360 m between the No.449 and No.547 exploration lines, and in the open pit the orebody is mainly exposed between the No.451 and No.507 exploration lines (Fig. 3.3). The grade of the No.1 orebody changes considerably throughout the deposit (see Fig. 3.4 for vertical changes in ore grade). Its average thickness is 9.98 m, with a maximum of 43.43 m; its mean grade is 4.81 g/t, with a maximum of 24.53 g/t. In the open pit, the No.1 orebody mainly comprises pyritized, sericitized and silicified granitic rock, with different degrees of cataclasis. It lacks sharp boundaries within the No.II alteration zone and it is only distinguished by grade analysis with the cut-off taken at 2.13 g/t. The No.1 orebody pitches in a north-east direction at 35°-40°. To the north of the No.459' exploration line, the orebody strikes 021°-050° and dips 70°-88°SE; to the west of the No.459 exploration line, it strikes 080°-085° and dips 48°-60°SE. The trend and sense of movement on the mineralized fault zone indicates that the orientation of maximum compression was approximately southeast-northwest. To the west of the No.459 exploration line, there are two groups of mineralized fractures. The best developed set

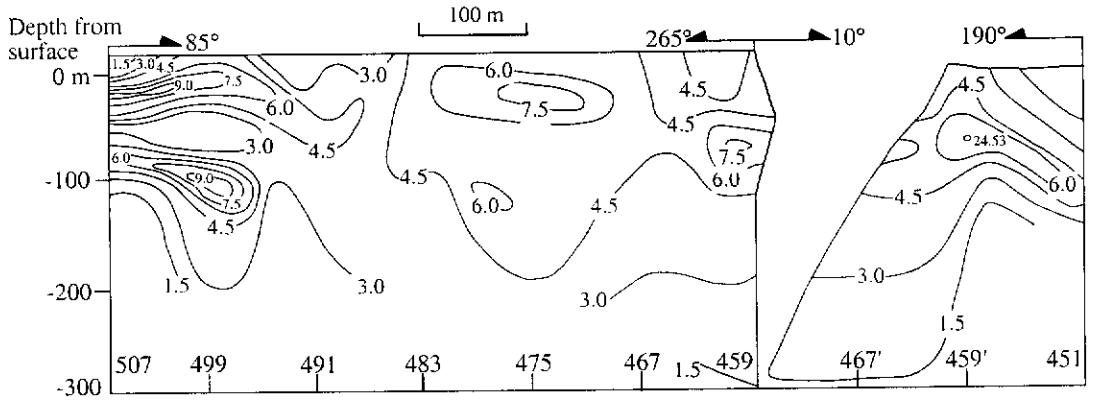

Fig. 3.4: Vertical section showing grade contours (in g/t) of the No.1 orebody (the data are from the No.6 Team of Geology and Exploration, BGMRSP, 1991).

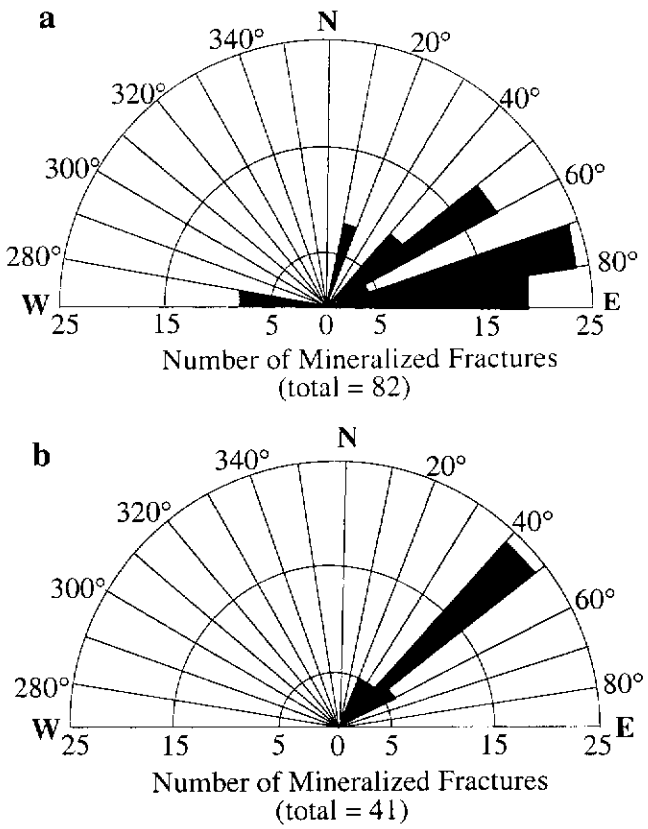

Fig. 3.5: Rose diagrams of orientations of mineralized fractures in the open pit of the Cangshang Gold Deposit (a) To the west of No.459 exploration line, (b) To the north of No.459' exploration line (the data from the No.6 Team of Geology and Exploration, BGMRSP, 1991).

strike 070°-090° and dip 40°-60°SE, which is essentially concordant with the orebody. A second set strikes 040°-060° and dips 50°-70°SE (Fig. 3.5a). To the north of the No.459' exploration line, there only exists one set of mineralized fractures, which strike 040°-050° and dip 45°-65°SE (Fig. 3.5b).

3.2.5 Ore Mineralogy and Paragenesis

Ore minerals include mainly pyrite, sphalerite, galena, chalcopyrite and arsenopyrite. Among them, pyrite is the most abundant and the main Au-bearing mineral within the deposit. Gangue minerals dominantly comprise quartz, sericite, feldspar, calcite, barite and chlorite. Gold minerals are dominantly electrum with trace amounts of native gold. Based on the mineralogical, textural, and cross-cutting relationships observed in the field (Fig. 3.6), four stages of hydrothermal mineral formation have been identified (Fig. 3.7). From the oldest to the youngest these stages are: stage 1: pyrite-quartz; stage 2: gold-quartz-pyrite; stage 3: quartz-multiple metal sulphides; and stage 4: quartz-carbonate. Fluid inclusion studies suggest temperatures associated with stages 1 to 4 are 330-300°C, 300-250°C, 250-200°C and 200-80°C, respectively (The No.6 Team of Geology and Exploration, BGMRSP, 1991).

Stage 1

In this stage, the ore mineral assemblage occurs as disseminated grains and veinlets and mainly consists of coarse-grained pyrite and quartz, with minor arsenopyrite. The pyrite is light yellow-white in colour and has a strong metallic lustre. It generally forms euhedral cubes and ranges from 0.5 mm to 3.5 mm in diameter. Fractures are well-developed in the pyrite, and many other metal sulphides, such as chalcopyrite and galena, occur as infillings. The quartz is milk-white in colour with a greasy lustre and is coarse-grained with a subhedral habit.

Stage 2

The mineral assemblage of this stage is dominantly pyrite, quartz, arsenopyrite, electrum and native gold, and forms veinlet and disseminated mineralization. The pyrite is light yellow in colour with a weak metallic lustre. It generally forms euhedral cubes and is fine- to medium-grained (0.08 mm to 0.36 mm in diameter). The quartz is fine-grained and granular, with a light grey colour and vitreous lustre.

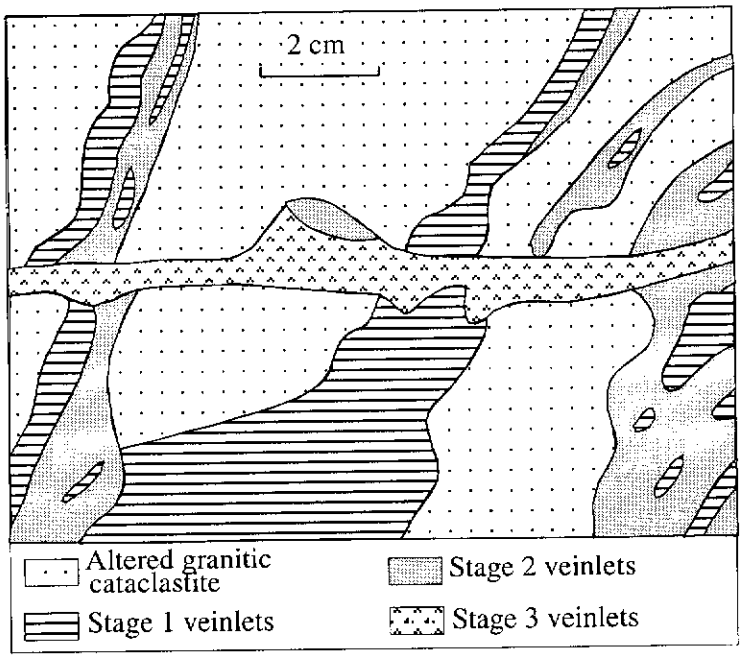

Fig. 3.6: A field sketch showing the crosscutting relationships amongst three stages of veining at the Cangshang Gold Deposit (after the No.6 Team of Geology and Exploration, BGMRSP, 1991).

Minerals	Stage 1	Stage 2	Stage 3	Stage 4
Arsenopyrite				
Pyrite				
Quartz				
Gold				
Electrum				
Siderite				
Ankerite				
Pyrrhotite				
Sphalerite				
Chalcopyrite				
Galena				
Freibergite				
Sericite				
Feldspar				
Calcite				
Barite				
Chlorite				
Temperature	330-300℃	300-250℃	250-200℃	200-80℃

Fig. 3.7: Paragenetic sequence of hydrothermal minerals of the Cangshang Gold Deposit (after the No.6 Team of Geology and Exploration, BGMRSP, 1991).

Stage 3

In this stage, the mineral assemblage is complex and characterised by multiple metal sulphides, dominantly composed of pyrite, chalcopyrite, galena, sphalerite and electrum. This paragenesis forms veinlet and disseminated mineralization. The pyrite has a dark yellow colour and dull lustre and is very fine-grained (0.012 mm to 0.048 mm in diameter). The quartz is also very fine-grained, smoke-grey in colour with a vitreous lustre.

Stage 4

The mineral assemblage in this stage mainly consists of calcite, quartz, barite and chlorite, occurring as veinlets filling in fractures within the rock units. The calcite is typically anhedral with well-developed twins. Fine-grained subhedral quartz is distributed in the calcite aggregates. This stage post-dates the gold mineralization, since it cross-cuts the mineralized veins.

3.2.6 SHRIMP Geochronological Data

In order to provide constraints on the timing of gold mineralization, as well as to understand the geological evolution in the region, samples from the No.I alteration zone (C1), the No.II alteration zone (C2), the No. 1 orebody (C3) and the hanging wall (C4) of the Cangshang Gold Deposit (Fig. 3.3) were selected for SHRIMP U-Pb zircon analysis. Unfortunately, sample C2 contained insufficient zircon for analysis. A sample from the altered dolerite dyke crosscutting the No.1 orebody (CD19-1) was also processed. However, it lacked zircons, so the minimum age of the gold mineralization at the Cangshang Gold Deposit cannot be constrained in this manner.

SHRIMP results for the samples are listed in Table 3.1 and illustrated on concordia diagrams in Figures 3.8, 3.10 and 3.12. All errors for individual analyses in Table 3.1 are given as 1σ. Group ages in concordia plots are quoted with 95% confidence error limits (2σ).

Altered granodiorite (Sample C1)

Sample C1 from the No.I alteration zone of the Cangshang Gold Deposit (Fig. 3.3) is a weakly sericitized, medium-grained granodiorite with a hypido- to

Table 3.1: SHRIMP U-Pb data for zircons from samples C1, C3 and C4 from the Cangshang Gold Deposit. Analyses are listed in order of increasing age. The following notation is used for analysed grains: 1.1=grain 1, first point analysed. Data are ^{204}Pb-corrected. Individual analyses have a 1σ error. The $^{206}Pb/^{238}U$ age is adopted for ages of less than 1.0 Ga, otherwise, the $^{207}Pb/^{206}Pb$ age is used.

spot	U (ppm)	Th (ppm)	Th/U	Total Pb (ppm)	$\frac{^{204}Pb}{^{206}Pb}$	f206 (%)	$\frac{^{207}Pb}{^{206}Pb}$	$\frac{^{206}Pb}{^{238}U}$	$\frac{^{207}Pb}{^{235}U}$	$\frac{^{206}Pb}{^{238}U}$ Age	$\frac{^{207}Pb}{^{206}Pb}$ Age
Sample C1 (altered granodiorite)											
23.1	58	32	0.56	2	0.00762	0.122	0.027±322	0.0251±11	0.09±11	160±7	
15.1	104	92	0.89	3	0.00112	0.018	0.057±148	0.0255±7	0.20±5	162±5	
16.1	365	347	0.95	11	0.00000	0	0.054±12	0.0257±5	0.19±1	163±3	
9.1	138	100	0.72	4	0.00138	0.022	0.043±97	0.0257±7	0.15±4	164±4	
21.1	141	126	0.89	4	0.00167	0.027	0.037±91	0.0258±6	0.13±3	164±4	
11.1	119	41	0.34	3	0.00178	0.029	0.047±114	0.0261±7	0.17±4	166±4	
27.1	112	106	0.96	4	0.00138	0.022	0.048±115	0.0263±7	0.17±4	167±4	
5.1	95	95	1.00	3	0.00298	0.048	0.025±44	0.0263±8	0.09±5	167±5	
6.1	193	118	0.61	6	0.00042	0.007	0.051±49	0.0267±6	0.19±2	170±4	
2.1	119	7	0.06	3	0.00209	0.033	0.041±107	0.0280±7	0.16±4	178±5	
12.1	70	15	0.21	2	0.00061	0.01	0.064±148	0.0285±9	0.25±6	181±5	
7.1	469	641	1.37	17	0.00031	0.005	0.061±30	0.0296±6	0.25±1	188±4	
25.1	162	55	0.34	5	0.00085	0.014	0.048±61	0.0319±7	0.21±3	202±5	
26.1	761	18	0.02	26	0.00019	0.003	0.050±15	0.0366±7	0.25±1	232±5	
17.1	81	4	0.05	3	0.00099	0.016	0.047±108	0.0381±10	0.25±6	241±6	
13.1	99	10	0.10	4	0.00091	0.015	0.049±77	0.0383±10	0.26±4	242±6	
1.1	150	7	0.05	6	0.00041	0.007	0.051±64	0.0398±9	0.28±4	251±6	
20.1	2225	38	0.02	81	0.00007	0.001	0.050±6	0.0401±8	0.28±1	254±5	
18.1	39	1	0.02	2	0.00210	0.034	0.048±200	0.0403±14	0.26±11	254±9	
33.1	230	163	0.71	16	0.00045	0.007	0.055±27	0.0604±13	0.45±3	378±8	

Table 3.1 (continued)

spot	U (ppm)	Th (ppm)	Th/U	Total Pb (ppm)	$\frac{^{204}Pb}{^{206}Pb}$	f206 (%)	$\frac{^{207}Pb}{^{206}Pb}$	$\frac{^{206}Pb}{^{238}U}$	$\frac{^{207}Pb}{^{235}U}$	$\frac{^{206}Pb}{^{238}U}$ Age	$\frac{^{207}Pb}{^{206}Pb}$ Age
24.1	198	152	0.77	17	0.00050	0.008	0.060±29	0.0683±14	0.56±3	426±9	
29.1	131	81	0.62	13	0.00041	0.007	0.064±28	0.0914±20	0.81±4	564±12	
8.1	149	203	1.36	26	0.00054	0.009	0.062±21	0.1330±28	1.14±5	805±16	
28.1	552	235	0.43	143	0.00006	0.001	0.112±5	0.2579±51	3.97±8		1825±9
4.1	562	246	0.44	213	0.00003	0	0.113±4	0.3553±70	5.52±11		1843±7
4.2	591	123	0.21	211	0.00003	0	0.114±4	0.3529±70	5.55±11		1865±7
32.1	907	167	0.18	326	0.00002	0	0.117±3	0.3565±70	5.74±12		1906±5
14.1	170	57	0.34	66	0.00008	0.001	0.118±10	0.3638±75	5.93±14		1928±15
22.1	704	108	0.15	261	0.00003	0	0.123±4	0.3666±73	6.20±13		1996±7
31.1	270	73	0.27	95	0.00001	0	0.123±7	0.3369±68	5.71±12		1998±10
19.1	233	65	0.28	92	0.00000	0	0.125±7	0.3782±76	6.53±14		2033±10
30.1	283	160	0.56	125	0.00003	0	0.130±7	0.3974±80	7.12±15		2098±9
3.1	76	75	0.99	36	0.00008	0.001	0.131±15	0.4069±88	7.32±19		2105±20
10.1	204	144	0.70	120	0.00004	0.001	0.168±8	0.4990±101	11.58±25		2542±8
Sample C3 (orebody)											
4.2	96	93	0.97	4	0.00246	0.173	0.072±27	0.0227±8	0.23±9	145±5	
2.1	137	49	0.36	4	0.00252	0.04	0.056±12	0.0234±5	0.18±4	149±3	
6.2	255	40	0.16	6	0.00182	0.022	0.056±7	0.0239±4	0.18±2	152±3	
5.1	1060	168	0.16	25	0.00173	0.003	0.050±2	0.0245±3	0.17±1	156±2	
6.1	131	27	0.2	3	0.00018	0.007	0.075±103	0.0245±6	0.25±4	156±4	
4.1	85	91	1.06	3	0.00042	0.028	0.057±14	0.0249±6	0.19±5	158±4	
10.1	302	66	0.22	15	0.00137	0.022	0.059±4	0.0462±7	0.37±2	291±4	
1.1	41	26	0.61	5	0.00022	0.039	0.054±10	0.0972±21	0.72±13	598±13	
7.1	389	531	1.36	64	0.00048	0.004	0.066±1	0.1271±17	1.16±2	771±10	
3.1	112	63	0.56	22	0.00009	0.029	0.135±5	0.1414±23	2.62±11		2158±61
8.1	77	55	0.72	34	0.01084	0.008	0.145±2	0.3728±56	7.47±15		2292±21
9.1	187	55	0.29	95	0.00136	0.001	0.166±8	0.4715±64	10.79±16		2517±8

Table 3.1 (continued)

spot	U (ppm)	Th (ppm)	Th/U	Total Pb (ppm)	$\frac{204Pb}{206Pb}$	f206 (%)	$\frac{207Pb}{206Pb}$	$\frac{206Pb}{238U}$	$\frac{207Pb}{235U}$	$\frac{207Pb}{206Pb}$ Age
Sample C4 (amphibolite)										
7.1	3	0	0.01	1	0.00677	0.108	0.077±41	0.3348±208	3.56±195	1125±809
2.1	5	1	0.23	2	0.00577	0.092	0.086±27	0.3493±162	4.14±133	1336±638
6.1	15	1	0.04	5	0.00133	0.021	0.110±7	0.3368±85	5.1±38	1796±123
14.1	4	0	0.01	1	0.00321	0.051	0.110±23	0.3319±144	5.04±111	1801±393
27.1	44	1	0.02	14	0.00117	0.019	0.111±5	0.3175±64	4.86±24	1815±76
3.1	54	1	0.02	18	0.00026	0.004	0.114±2	0.3357±64	5.28±16	1865±37
16.1	15	0	0.02	5	0.00184	0.03	0.114±9	0.3334±86	5.25±46	1868±145
13.1	88	14	0.16	30	0.00008	0.001	0.121±2	0.3413±61	5.71±13	1975±22
15.1	3	0	0.04	1	0.00571	0.091	0.124±33	0.3477±187	5.94±166	2013±491
23.1	5	3	0.48	3	0.00509	0.081	0.127±32	0.3229±166	5.63±147	2050±453
8.1	4	1	0.12	2	0.00472	0.075	0.134±25	0.3838±176	7.06±142	2144±339
20.1	16	1	0.04	9	0.00869	0.139	0.134±17	0.36±111	6.64±89	2147±222
22.1	50	5	0.11	20	0.00099	0.016	0.134±4	0.3721±71	6.88±24	2151±48
26.1	67	30	0.45	31	0.00141	0.022	0.142±4	0.39±75	7.61±29	2246±53
10.1	2	0	0.01	2	0.00269	0.043	0.148±25	0.4655±264	9.49±175	2321±293
1.1	670	226	0.34	307	0.00003	0	0.154±4	0.426±71	9.04±16	2391±5
9.1	358	159	0.44	171	0.00009	0.001	0.158±1	0.4317±73	9.42±17	2437±7
18.1	58	10	0.17	34	0.00086	0.014	0.158±3	0.5235±99	11.43±30	2438±26
4.1	96	26	0.27	49	0.00015	0.002	0.159±1	0.4785±86	10.46±22	2440±14
17.1	10	1	0.12	4	0.00429	0.069	0.161±20	0.3412±140	7.59±104	2470±215
24.1	41	16	0.39	21	0.00061	0.01	0.163±4	0.4456±89	9.99±33	2482±40
12.1	42	15	0.36	23	0.00039	0.006	0.163±2	0.4912±96	11.05±28	2488±24
5.1	36	10	0.28	18	0.00043	0.007	0.166±3	0.4632±92	10.61±29	2518±28
21.1	186	175	0.94	115	0.00021	0.003	0.167±1	0.491±77	11.3±20	2528±10
11.1	83	37	0.44	43	0.00023	0.004	0.167±1	0.4632±82	10.67±22	2528±14
25.1	186	149	0.8	102	0.00011	0.002	0.168±1	0.4554±72	10.57±19	2541±12
19.1	94	42	0.44	51	0.00028	0.005	0.170±2	0.4783±80	11.18±23	2553±17

allotriomophic equigranular texture. It comprises plagioclase (50%), quartz (30%), potassic feldspar (18%), muscovite (2%), biotite (mostly replaced by muscovite, 1%), and minor calcite, apatite and zircon. Zircons are usually enclosed in quartz and range in colour from colourless to pale purple with most having a pale brown colour. The selected zircons vary in size from 132 μm to 74 μm and most are euhedral, with pyramidal terminations. The average elongation ratio is about 2:1, with a maximum of 4:1.

Thirty four analyses were made on 33 zircon grains (Table 3.1 and Fig. 3.8), and ages range from 2542 ± 8 Ma to 160 ± 7 Ma.

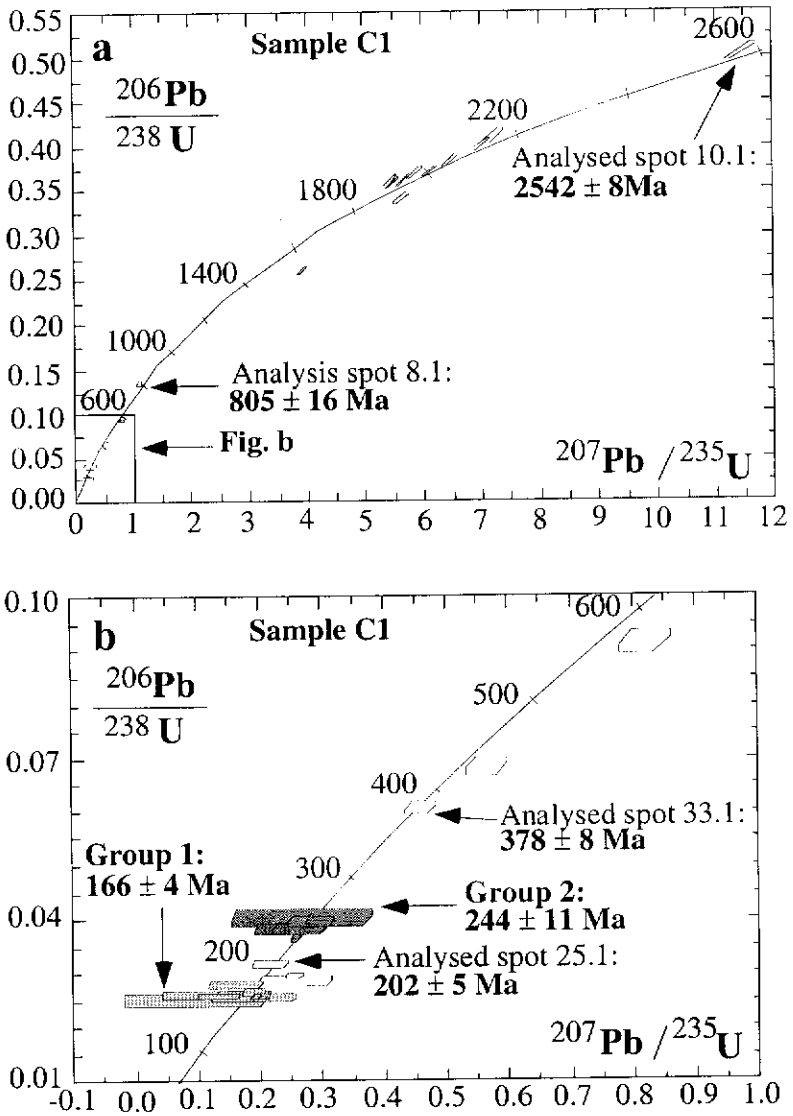

Fig. 3.8: U-Pb concordia diagrams showing (a) total SHRIMP data for Sample C1 (weakly altered granite) from the Cangshang Gold Deposit and (b) enlargement detailing younger zircon populations.

Ten analyses of the youngest 10 grains from the sample form a coherent group (Group 1 in Fig. 3.8b) with a weighted mean $^{206}Pb/^{238}U$ age of 166 ± 4 Ma and a chi-square value of 1.06. The U and Th contents of these 10 spots range from 58 ppm to 365 ppm and 7 ppm to 347 ppm, respectively. The Th/U ratios vary from 0.06 to 1.00. Cathodoluminescence images of Group 1 crystals indicate all are from grains with well developed oscillatory zoning which either constitutes the entire grain (Fig. 3.9a) or forms a broad rim around a core (Fig. 3.9b). This growth pattern is indicative of crystallization from a melt (Vavra, 1990) and the age of 166 ± 4 Ma is taken as the age of igneous crystallization of the footwall granodiorite.

The remaining zircons in the sample are considered to be inherited. These include a second relatively homogeneous group (Group 2 in Fig. 3.8b) of 6 analyses of 6 zircons. The U content of spot 20.1 is very large (2225 ppm), whereas the U contents of the other 5 spots range from 39 ppm to 761 ppm. The Th contents of 6 spots range from 1 ppm to 38 ppm, with Th/U ratios of 0.02 to 0.1. Cathodoluminescence imaging revealed Group 2 analyses are all from oscillatory zoned zircons with some evidence of possible internal recrystalisation (Fig. 3.9c). These give an age of 244 ± 11 Ma with a chi-square value of 2.41. This is coincident with the age of ca. 210-250 Ma for inherited zircons in the Linglong granitoid reported by Wang et al. (1998).

Analyses of spots 25.1 of grain 25 and 33.1 of grain 33 give concordant $^{206}Pb/^{238}U$ ages of 202 ± 5 Ma (1σ) and 378 ± 8 Ma (1σ) (Fig. 3.8b), respectively. Since grains 25 and 33 are euhedral, the two ages may represent two igneous events in the basement or disturbance of older grains by the youngest event. Analysis of spot 8.1 of grain 8 yields a near-concordant $^{206}Pb/^{238}U$ age of 805 ± 16 Ma (1σ) (Fig. 3.8a). A further concentration of analyses from inherited zircons occurs between 1800 Ma and 2200 Ma but no statistical group could be defined (Fig. 3.8a). The oldest near-concordant $^{207}Pb/^{206}Pb$ age of 2542 ± 8 Ma (1σ) was obtained from the inherited core of spot 10.1 (Fig. 3.8a).

Orebody (Sample C3)

Sample C3 was taken from a strongly altered granitic cataclasite within the No.1 orebody of the Cangshang Gold Deposit (Fig. 3.3). The rock has undergone extensive silicification, along with pyrite and sericite alteration. The rock is now composed largely of quartz (80%) together with sericite (18%) and opaque minerals (2%). The zircons are contained mainly in sericite aggregates and also within quartz.

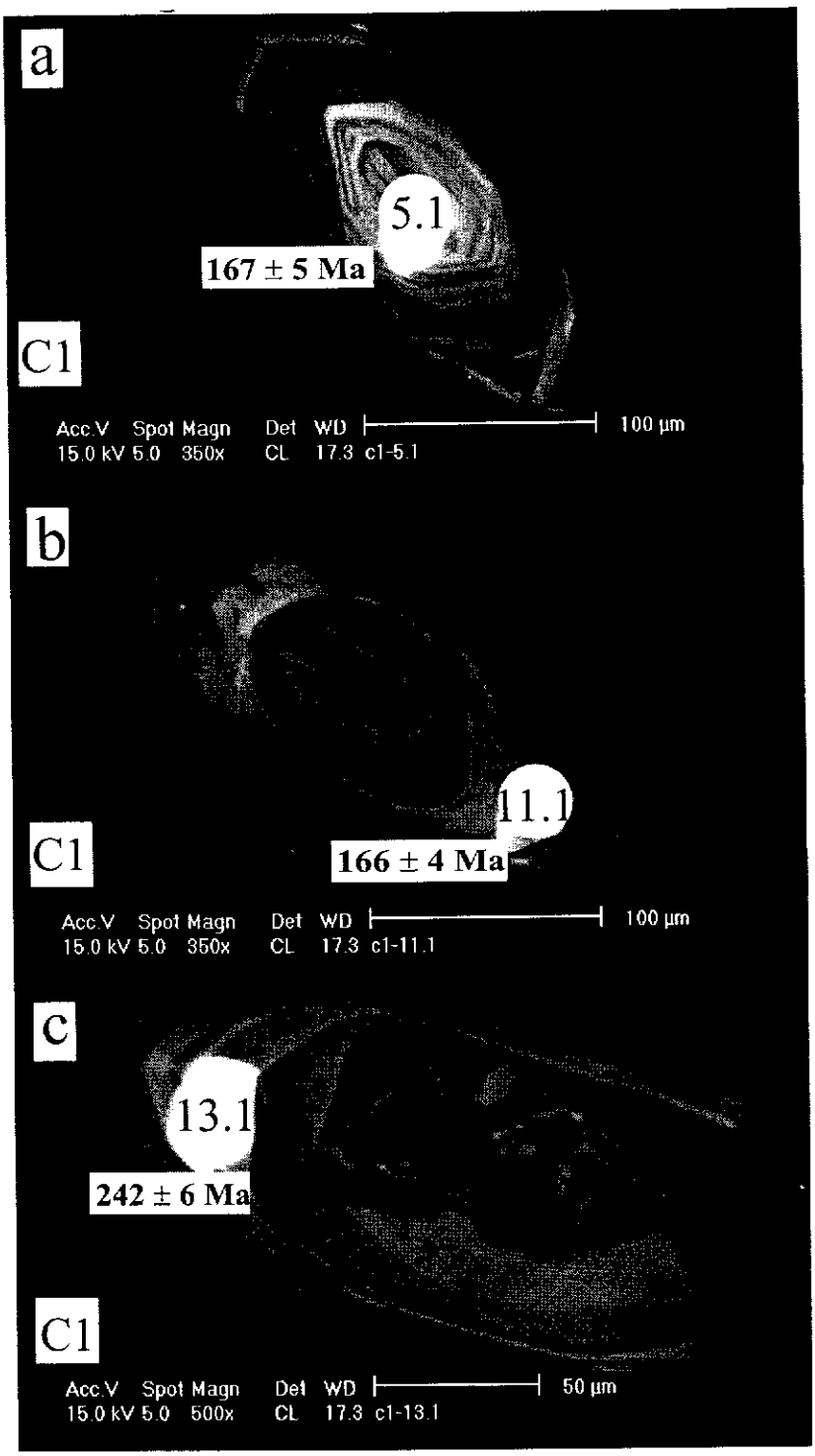

Fig. 3.9: A selection of cathodoluminescence (CL) images of zircons extracted from Sample C1 from the Cangshang Gold Deposit. The white circles are the SHRIMP ion-probe analysis spots. (a) Zircon grain 5 of sample C1, showing very distinct magmatic oscillatory zonation throughout the crystal. The $^{206}Pb/^{238}U$ age of spot 5.1 is 167 ± 5 Ma. (b) Zircon grain 11 of Sample C1, showing distinct core overgrown by younger rim. The $^{206}Pb/^{238}U$ age of spot 11.1 is 166 ± 4 Ma. (c) Zircon grain 13 of Sample C1, showing oscillator zonation with some evidence of possible internal recrystalisation. Spot 13.1 is located in the oscillatory zoned portion and its $^{206}Pb/^{238}U$ age is 242 ± 6 Ma.

Zircons range in size from 105 μm to -74 μm and are colourless. They vary in shape from rounded to euhedral and the average elongation ratio is about 2:1.

A total of 12 analyses were carried out on 10 zircon grains, with ages ranging from 2517 ± 8 Ma to 145 ± 5 Ma (Table 3.1 and Fig. 3.10).

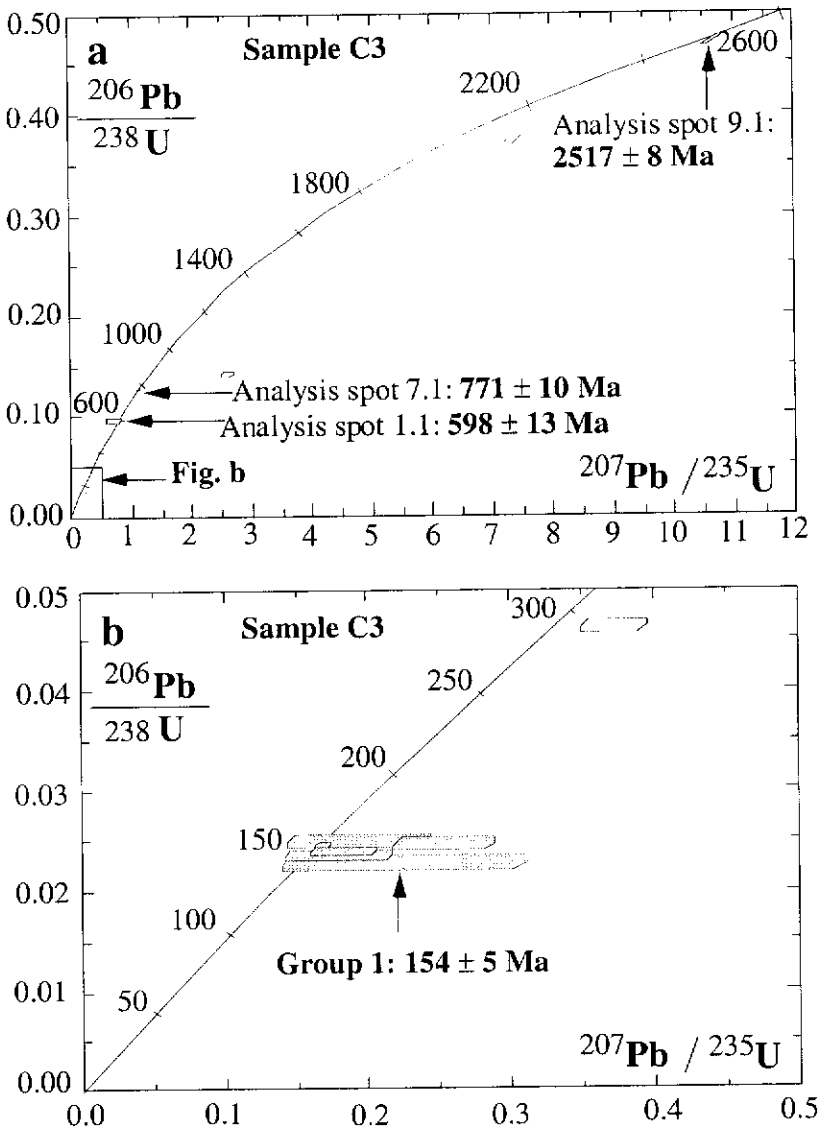

Fig. 3.10: U-Pb concordia diagrams showing (a) total SHRIMP data for Sample C3 (orebody) from the Cangshang Gold Deposit and (b) enlargement detailing younger zircon population.

The main population consists of 6 analyses of 4 grains, which form a coherent group (Group 1 in Fig. 3.10b) having a weighted mean $^{206}Pb/^{238}U$ age of 154 ± 5 Ma with a chi-square value of 1.59. The U content of spot 5.1 is high (1060 ppm), whilst the U contents of the other 5 spots range from 85 ppm to 302 ppm. The Th contents of

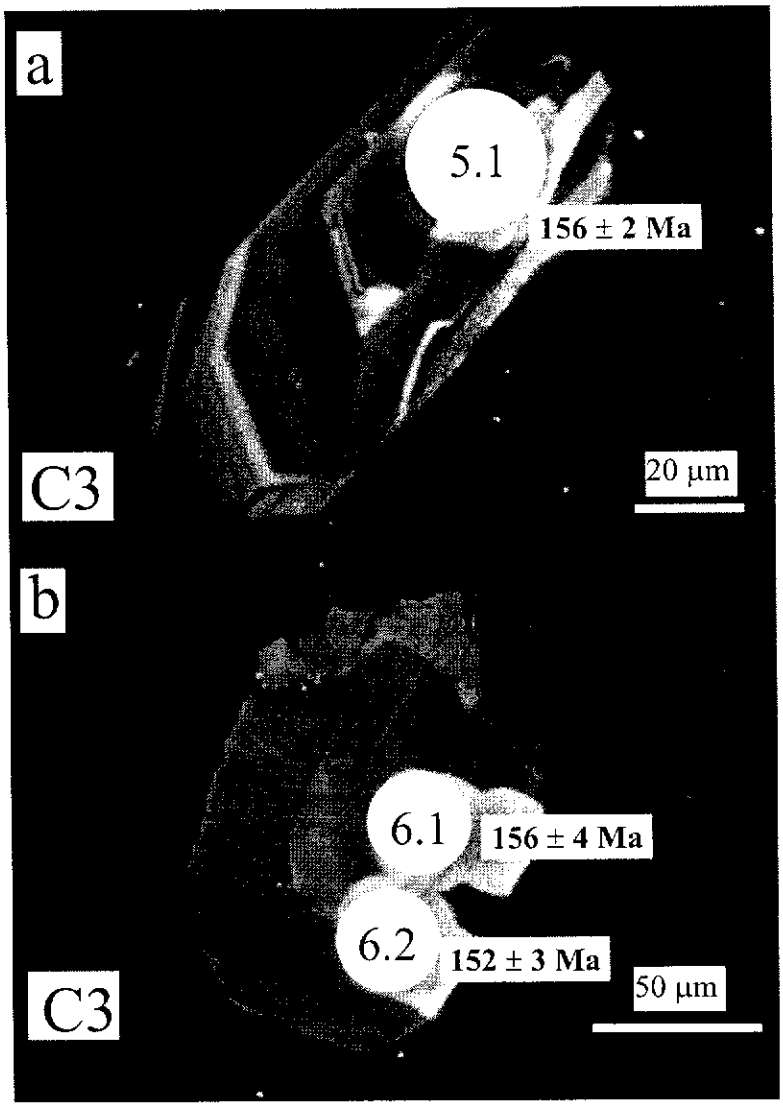

Fig. 3.11: A selection of cathodoluminescence (CL) images of zircons extracted from Sample C3 from the Cangshang Gold Deposit. The white circles are the SHRIMP ion-probe analysis spots. (a) Zircon grain 5 of Sample C3, showing igneous oscillatory growth zones. The $^{206}Pb/^{238}U$ age of spot 5.1 is 156 ± 2 Ma. (b) Zircon grain 6 of Sample C3, also showing magmatic growth zoning. The $^{206}Pb/^{238}$ ages of spot 6.1 and 6.2 are 156 ± 4 Ma and 152 ± 3 Ma, respectively.

the 6 spots range from 27 ppm to 168 ppm, with Th/U ratios of 0.2 to 1.06. Cathodoluminescence images show oscillatory zonation patterns (Fig. 3.11a and b), which suggests that these grains are magmatic in origin and 154 ± 5 Ma is interpreted as the age of the host to the orebody. The age of 154 ± 5 Ma may represent a felsic dyke emplaced along the ore zone after intrusion of the footwall granodiorite at 166 ± 4 Ma. It thus provides the maximum age of gold-related alteration at the Cangshang Gold Deposit.

Spots 1.1 and 7.1 give concordant ages of 598 ± 13 Ma (1σ) and 771 ± 10 Ma (1σ) (Fig. 3.10a), respectively, which probably represent two igneous events in the basement, but up to date no detailed research work has been done to prove this proposition. Analysis spot 9.1 yields the oldest inherited concordant $^{207}Pb/^{206}Pb$ age of 2517 ± 8 Ma (1σ) (Fig. 3.10a), which coincides with the oldest zircon inherited age (2542 ± 8 Ma) of sample C1. Accordingly, the age of ca. 2500 Ma represents a Late Archaean igneous event in the basement of this region.

Hanging wall Amphibolite (Sample C4)

Sample C4 was obtained from the hanging wall of the No.1 orebody of the Cangshang Gold Deposit (Fig. 3.3) and is an amphibolite containing green and brown hornblende (48%), plagioclase (40%) and pyroxene (10%), as well as accessory grains of quartz. Zircons occur within the hornblende and range in size from +132 μm to -74 μm. They are pale purple to colourless, and neither optical zoning nor cores are evident.

Twenty seven analyses were completed on 27 zircon grains, and ages vary from 2553 ± 17 Ma to 1125 ± 809 Ma (Table 3.1).

Six analyses of 6 zircons define a concordant population (Group 1 in Fig. 3.12) with $^{206}Pb/^{238}U$, $^{207}Pb/^{238}U$, and $^{207}Pb/^{206}Pb$ ages of 1836 ± 48, 1845 ± 38, and 1852 ± 37 Ma, respectively. The U and Th contents of these 6 spots range from 4 ppm to 54 ppm and 0 to 3 ppm, respectively. Their Th/U ratios vary from 0.01 to 0.04, except for 0.48 for spot 23.1. Owing to their low U and Th contents, their error boxes are large and the $^{207}Pb/^{206}Pb$ age is preferred with a chi-square value of 0.14. This population of zircons is mainly pale purple in colour and "football-shaped".

Another zircon population consists of 7 analyses of 7 zircons, which form a cluster of variously discordant analyses (Group 2 in Fig. 3.12) having a weighted

mean $^{207}Pb/^{206}Pb$ age of 2530 ± 17 Ma with a chi-square value of 1.16. The U and Th contents of these 7 spots range from 36 ppm to 186 ppm and 10 ppm to 175 ppm, respectively. Their Th/U ratios vary from 0.28 to 0.94, which are characteristic of igneous zircon. The zircons of this group are mainly colourless and subhedral.

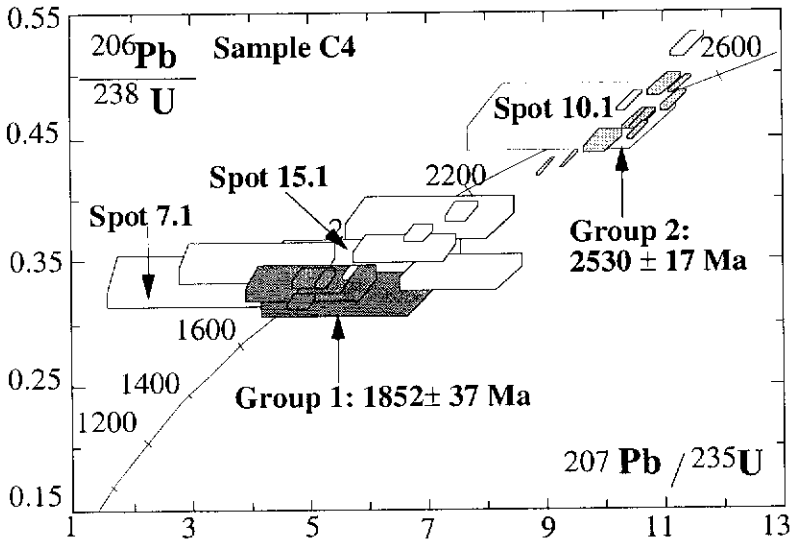

Fig. 3.12: A U-Pb concordia diagram showing SHRIMP data for the main zircon populations of Sample C4 (amphibolite) from the Cangshang Gold Deposit. Spots 7.1, 10.1 and 15.1 are excluded from the groups due to their very large errors.

Three analyses of 3 zircons (spots 7.1, 10.1 and 15.1) with extremely low U and Th contents are excluded from the above two groups due to their very large errors (Fig. 3.12). Other analyses (such as spots 1.1, 4.1, 22.1 and 26.1) are disconcordant which have resulted from subsequent disturbance or by analyzing overlapping components of zircon (Fig. 3.13b).

Under CL, the two different populations of zircons (Groups 1 and 2) exhibit distinct patterns. The younger zircon portions (Group 1) luminesce brightly, indicating low U content, and have no structural zoning (Fig. 3.13a). The older zircons (Group 2) have well-defined concentric growth zoning which is typical of magmatic zircons, and have low-U (bright) overgrowths (Fig. 3.13c). This evidence substantiates that the older zircon represents the age of the igneous protolith and that the younger zircon indicates a major metamorphic event resulting in metamorphic overgrowth of zircon rims onto pre-existing zircons and also the formation of new grains. In the protolith of the amphibolite, the hydration of clinopyroxene may lead to release of trace amounts of Zr during formation of amphibole and this could cause formation of new metamorphic

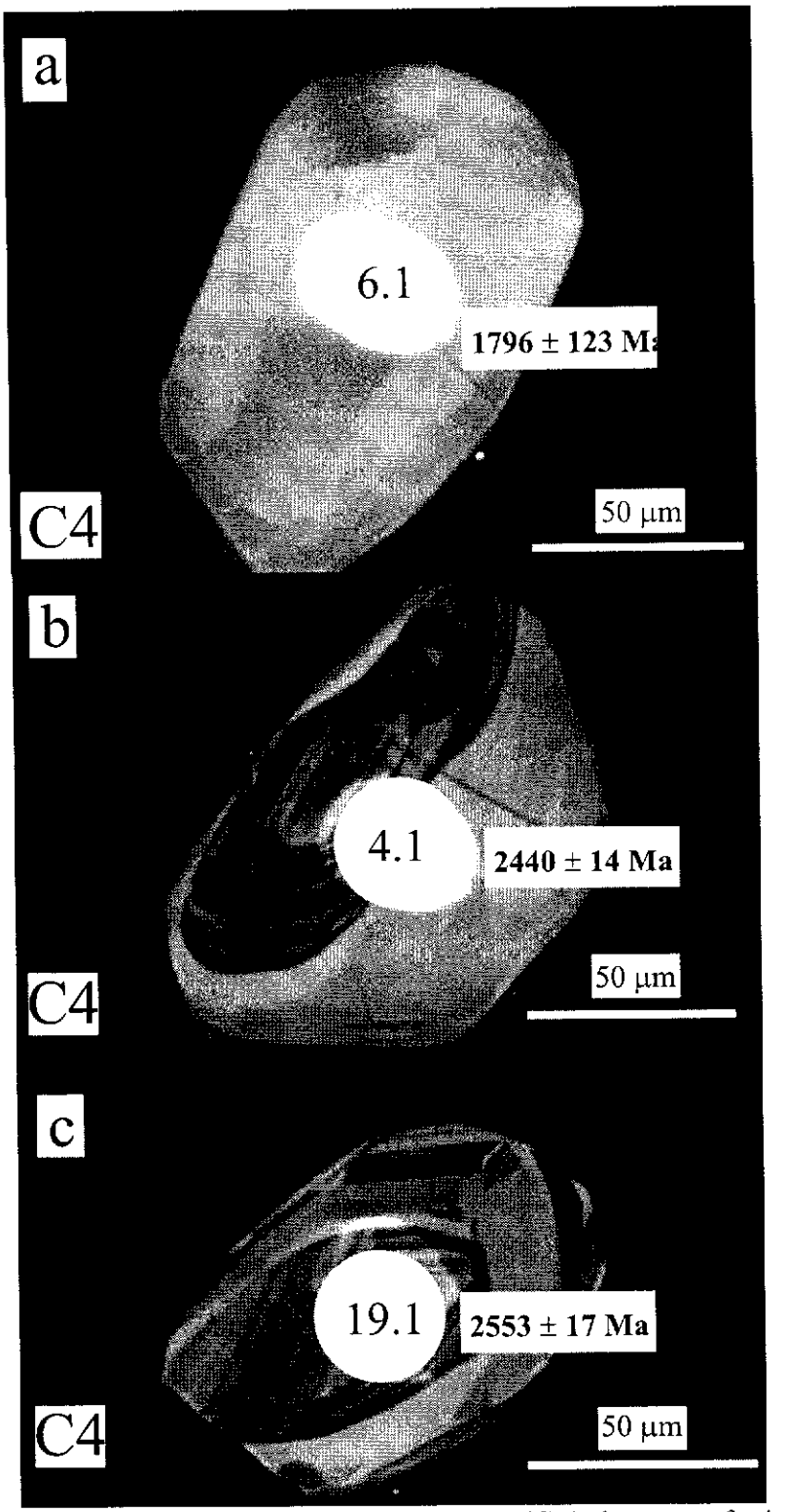

Fig. 3.13: A selection of cathodoluminescence (CL) images of zircons extracted from Sample C4 from the Cangshang Gold Deposit. The white circles are the SHRIMP ion-probe analysis spots. (a) Zircon grain 6 of Sample C4 showing no structural zoning and bright CL image. The $^{207}Pb/^{206}Pb$ age of spot 6.1 is 1796 ± 123 Ma. (b) Zircon grain 4 of Sample C4, showing clear oscillatory-zoned igneous core surrounded by low U metamorphic overgrowth. Unfortunately, the spot 4.1 straddles the boundary between the core and the younger metamorphic rim, so the $^{207}Pb/^{206}Pb$ age of spot 4.1 (2440 ± 14 Ma) is a mixed age. (c) Zircon grain 19 of Sample C4, showing concentric growth zoning which is typical of magmatic zircons, and bright low U content of metamorphic rim. The $^{207}Pb/^{206}Pb$ age of spot 19.1 is 2553 ± 17 Ma.

zircons (Heaman and Parrish, 1991). This may be the reason why many zircons were contained in the hornblende of Sample C4.

3.2.7 ^{40}Ar-^{39}Ar Results

Since white mica is a common hydrothermal mineral in gold deposits, ^{40}Ar-^{39}Ar dating of this mica is a useful technique for determining the timing of gold mineralization events. This is particularly so in regions where ambient temperatures during mineralization were below the closure temperature (350° ± 50 °C) for Ar diffusion in muscovite (McDougall and Harrison, 1988) which is the case here (see Fig. 3.7), allowing hydrothermal muscovite to cool below its closure temperature immediately after cessation of hydrothermal acitivity. Muscovite is also resistant to diffusive Ar loss when subjected to post-crystallization thermal disturbances (Dunlap et al., 1991) and rarely incorporates large amounts of excess ^{40}Ar (McDougall and Harrison, 1988).

Strict definitions of age plateaus, which assume volume diffusive behaviour during vacuum heating, have not been used for hydrous minerals such as muscovite, as they degas largely by dehydroxylation and other mechanisms (Hodges et al., 1994) rather than by volume diffusion. Instead, the age of plateau-like segments (i.e. flat portions in ^{40}Ar-^{39}Ar spectra) have been advocated (Kent and Hagemann, 1996). Ages of plateau-like segments were calculated by weighting the age and precision of each step by the amount of ^{39}Ar released. If steps are older or younger than the majority of steps in the plateau-like segment, they are not included in the final age calculation.

Based on the above views, in order to further constrain the age of gold mineralization at the Cangshang Gold Deposit, a hydrothermal muscovite from sample CD8-2 (Fig. 3.3) from the No.1 orebody of this deposit was analysed by the ^{40}Ar-^{39}Ar technique. In hand specimen, sample CD8-2 is green-grey in colour and consists of quartz, muscovite and opaque minerals. Muscovite commonly occurs as aggregate among quartz grains. In thin section, the size of individual muscovite flakes ranges from 20 to 800 μm, but is generally in the range of 150 to 350 μm. These flakes surround quartz and opaque minerals. Quartz is common and shows undulose extinction. Auriferous pyrite occurs in textural equilibrium with muscovite as euhedral crystals. The muscovite separate was prepared using standard heavy-liquid techniques (Kent and McDougall, 1995). A 79.3 mg separate with high purity was sent to the U.S. Geological Survey in Denver and was analysed by Dr. Lawrence W. Snee. A

detailed description of the ^{40}Ar-^{39}Ar analytical technique in Denver may be found in Shaw et al. (1999).

Table 3.2: ^{40}Ar-^{39}Ar release data for sericite separates from the sample CD8-2 from the Cangshang gold deposit

Temp. (°C)	Radiogenic ^{40}Ar (10^{-16} mol)	K-derived ^{39}Ar (10^{-13} mol)	F Value	Radiogenic Yield	^{39}Ar (%)	Apparent age (Ma at 1σ)
500	.31573	.02601	12.137	56.1	1.0	105.07 ± 1.06
600	.21375	.01619	13.199	87.8	.6	113.97 ± 1.55
700	.83953	.06106	13.749	94.3	2.4	118.57 ± .33
800	2.86703	.20208	14.188	97.2	7.8	122.23 ± .18
850	2.99296	.21271	14.070	97.6	8.2	121.25 ± .18
900	3.85203	.27404	14.057	97.5	10.6	121.13 ± .18
950	5.79932	.41441	13.994	98.2	16.1	120.62 ± .18
1000	7.39248	.52588	14.057	98.9	20.4	121.14 ± .29
1050	7.42284	.52608	14.110	98.7	20.4	121.58 ± .23
1100	3.22358	.22886	14.085	98.1	8.9	121.37 ± .18
1150	1.17392	.08347	14.063	96.7	3.2	121.19 ± .44
1250	.14430	.01049	13.750	88.0	.4	118.58 ± 2.28

^{40}Ar-^{39}Ar release data are presented in Table 3.2 and age spectrum and isochron diagrams for sample CD8-2 are shown in Fig. 3.14. Errors for apparent ages in Table 3.2 are given as 1σ. Plateau-like segment age and corresponding isochron age in Fig. 3.14 are quoted with 95% confidence error limits (2σ). In this study, 12 temperature steps were used. The ^{40}Ar-^{39}Ar spectrum of muscovite (Fig. 3.14a) from sample CD8-2 exhibits young ages in the early stages (steps 1, 2 and 3) and final stage (step 12) of gas release, and illustrates well-defined plateau-like segments (steps 4-11) with 95.6% of ^{39}Ar released corresponding to an age of 121.3 ± 0.2 Ma. The isochron age is 121.1 ± 0.5 Ma, which is identical within error to the age of the plateau-like segments. Since the age spectrum for sample CD8-2 reveals no indication of Ar loss sufficient to significantly lower the plateau-like segment age, the ^{40}Ar-^{39}Ar age of ca. 121 Ma obtained from muscovites is interpreted as the time of gold mineralization at the Cangshang Deposit.

3.2.8 Summary

The Cangshang Gold Deposit is characteristic of Jiaojia-style (i.e. disseminated and veinlet type) gold mineralization, which is structurally controlled within the Cangshang Fault Zone and is associated with an alteration halo up to 185 m wide. The Cangshang Fault Zone underwent several periods of structural activation, with the trend and sense of movement on the mineralized fault zone indicating that the

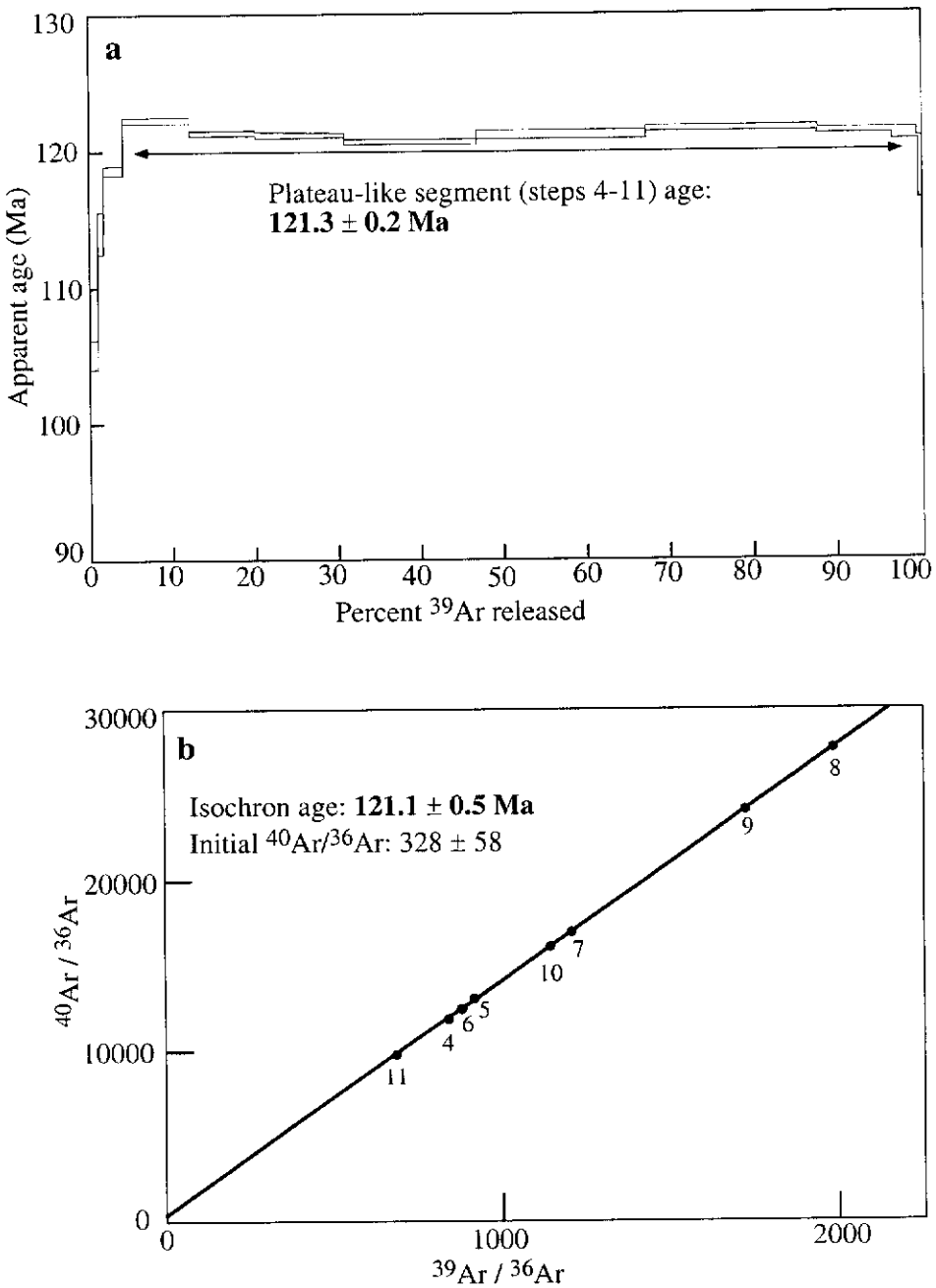

Fig. 3.14: (a) Age spectum for hydrothermal muscovites from sample CD8-2, from the Cangshang Gold Depdosit; (b) Isochron diagram related to plateau-like segments (step 4-11) in (a).

orientation of maximum extension was approximately southwest-northeast during gold mineralization.

The alteration styles at the Cangshang Gold Deposit include silicification, sericitization, pyritization, K-feldspar alteration, chloritization and carbonation, which are consistent with other gold deposits on the Jiaobei Terrane (Wang et al. 1998).

On the basis of the mineralogical, textural, and crosscutting relationships, four stages of hydrothermal mineral formation have been identified, consisting of pyrite-quartz (stage 1), gold-quartz-pyrite (stage 2), quartz-multiple metal sulphides (stage 3) and quartz-carbonate (stage 4). During stages 2 and 3, the gold mineralization is characterised by disseminated and veinlet forms, and the main orebodies were formed at this time.

The rock in the hanging wall of the No.1 orebody mainly comprises amphibolite of the Early Proterozoic Fenzishan Group. SHRIMP U-Pb isotopic dating and CL imaging indicate that the protolith of the amphibolite was a magmatic rock with a crystallization age of 2530 ± 17 Ma, and that it underwent upper amphibolite grade metamorphism at 1852 ± 37 Ma, which coincides broadly with the Lüliang Orogeny (i.e. a craton-wide tectono-thermal event within the North China Craton) (Wang et al., 1998).

The host rock in the footwall of the No.1 orebody is granodiorite with a crystallization age of 166 ± 4 Ma, obtained from whole zircon grains and zircon overgrowths. It forms part of the Linglong granitoid (with ages between 165 and 150 Ma) of Wang et al. (1998), which is related to the Yanshanian tectono-magmatic event (Xu et al. 1989). SHRIMP data and CL imaging reveal that the granodiorite has three generations of inherited zircons with Late Archaean (>2500 Ma), Palaeoproterozoic (1800-2200 Ma) and Early Mesozoic (ca. 240 Ma) ages. The inherited zircons of Precambrian age clearly indicate that the Jiaobei Terrane is underlain by Precambrian basement. The inherited zircons with an age of 244 ± 11 Ma most likely represent granitoids in the basement, intruded in response to the collision of the North China and Yangtze Cratons (F.Y. Wu, personal communication, 1999). During the collisional event, the Precambrian basement was reworked involving high grade metamorphism and partial melting (Wang et al., 1998) to produce an earlier suite of granitoids, as recorded from elsewhere in the Jiaodong Peninsula (Xu et al., 1989).

The No.1 orebody mainly consists of pyritized, sericitized and silicified granitic rock with different degree of cataclasis. The zircons obtained from it have an age of 154 ± 5 Ma and CL images reveal oscillatory zoning, suggestive of a magmatic origin. Therefore, 154 ± 5 Ma could be interpreted to indicate the age of another magmatic episode which also belongs to the Yanshanian event. During this stage, a younger granitoid dyke possibly intruded along the contact between the granodiorite (166 ± 4 Ma) and amphibolite and was strongly altered and deformed during ore formation.

To the author's knowledge, this is the first time that ^{40}Ar-^{39}Ar dating of muscovite has been used to determine the timing of gold mineralization in the Jiaodong Peninsula. The well-defined age of 121.3 ± 0.2 Ma provides the precise timing of gold mineralization at the Cangshang Deposit. This coincides with the more general age of lode-gold mineralization determined in the northwestern Jiaodong Peninsula at between 126 and 120 Ma by Wang et al. (1998).

3.3 Sanshandao Gold Deposit

The Sanshandao Gold Deposit (lat. 37°24'29.8" to 37°24'32.9"N, long. 119°56'49.5" to 119°56'43.1" E) is located 22 km north of the city of Laizhou and 4 km northeast of the Cangshang Gold Deposit (Fig. 3.1). Sanshandao was named after three hills lying adjacent to the shore of the Bohai Sea. The gold deposit, mined by means of an underground tunnel, is situated below the three hills. It was discovered in 1966 by the No.6 Team of Geology and Exploration, BGMRSP, based on regional reconnaissance mapping. In 1969, the known gold reserves were 60.2 tonnes and since then it has become the first superlarge gold deposit in China, with the known reserves extending to about 100 tonnes. The deposit is located near to, and controlled by, the San-Cang Fault Zone (Fig. 3.1). This deposit shows the characteristic Jiaojia-style of disseminated-and-veinlet gold ore.

3.3.1 Lithological Units

Apart from Mesozoic granitoids which constitute the three hills around the gold deposit, most of the mining area is covered by Quaternary marine sediments up to 50 m thick. Extensive drilling has revealed the distribution of lithological units in the region (Fig. 3.15). The basement rocks within this deposit include Archaean metamorphic rocks of the Jiaodong Group and Mesozoic granitoid, which are distributed in the southeast and northwest parts of the mining area, respectively (Fig.

3.15a). The Jiaodong Group mainly comprises amphibolite and fine-grained biotite gneiss. The Mesozoic granitoid constitutes the Sanshandao Pluton which belongs to the Guojialing suite (Xu et al., 1989). It is a porphyritic granodiorite, grey-white in colour and mainly consists of plagioclase (ca. 50%), quartz (ca. 25%, strongly deformed, with an undulose extinction), K-feldspar (ca. 20%) and biotite (ca. 5%, partly replaced by chlorite). Accessory mineral phases include magnetite, titanite, allanite, monazite, apatite and zircon. A swarm of mafic dykes, including lamprophyre and dolerite, are present at the deposit and generally cut the orebodies and are also affected by later alteration (Jia, 1995). Although lamprophyres are present, their proportion has been over-estimated by local mine geologists as a significant number are in fact dolerite dykes. The dolerite (such as the sample SD3) is melanocratic and has a porphyritic texture. Its phenocryst phase mainly comprises plagioclase and clinopyroxene, with a subophitic texture; its fine-grained groundmass dominantly consists of plagioclase and pyroxene with an intergranular texture.

3.3.2 San-Cang Fault Zone

The San-Cang Fault Zone is located in the northwestern part of the Jiaobei Terrane and is adjacent to the Bohai Sea (Fig. 3.1). It can be traced for 11 km and is 40 to 250 m wide. It strikes 035°-040° and dips 35°-40° SE. This fault zone consists of two parts: its southwestern part (called the Cangshang Fault Zone) and northeastern part (named the Sanshandao Fault Zone), which separately control the Cangshang and Sanshandao superlarge gold deposits (Fig. 3.2).

3.3.3 Alteration

The hydrothermal alteration types associated with this deposit include sericitization, silicification, pyritization and K-feldspar alteration. The main alteration zone developed along the Sanshandao Fault Zone (termed the F1 fault by local mine geologists) is over 2000 m in length and ranges in width from 8.5 to 200 m within the mining area (Fig. 3.15a). The alteration zone lies within Mesozoic granitoid. The degree of the alteration gradually decreases from the main fault plane towards the unaltered wall-rocks, although there is no distinct zonation. The most intensively-altered rock is a pyrite-sericite-quartz rock.

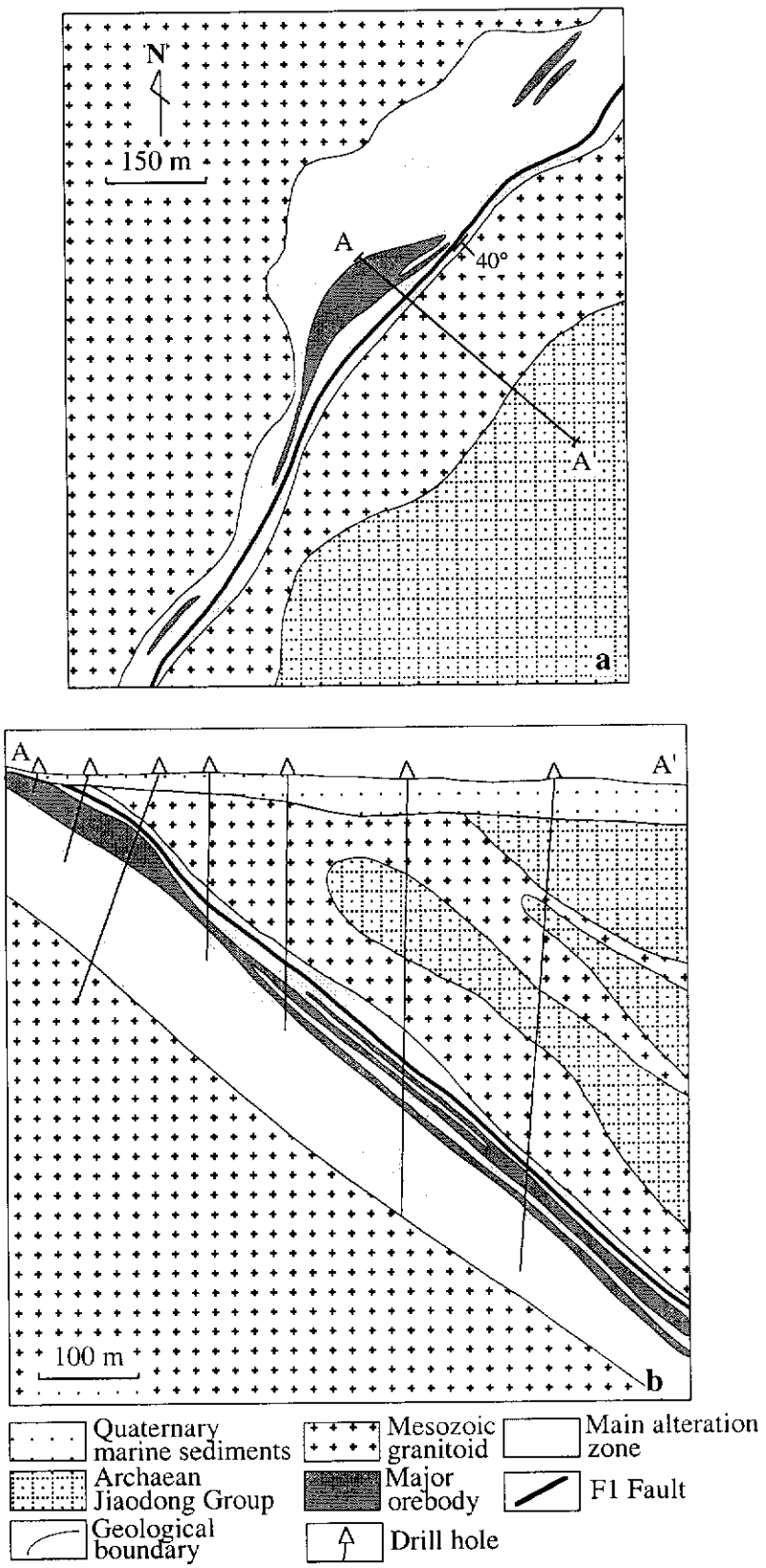

Fig. 3.15: (a) Geological plan and (b) cross-section AA' of the Sanshandao Gold Deposit (modified from Zhang and Wen, 1983). Note that Quaternary sediments have not been shown on the geological plan.

3.3.4 Orebodies

The main deposit, consisting of the No.1 and No.2 orebodies, is located within a major alteration zone and has 80% of the total reserves. The two orebodies merge in several places (Fig. 3.15b), hence they are treated as a single major orebody in this study (Fig. 3.15a and b). As described in the literature, the No.1 orebody is 1020 m in length and ranges from 0.4 to 6.2 m in thickness, with an average of around 2 m. It strikes 040° and dips 40° SE. It has been explored to a depth of more than 900 m. The gold grade varies from 3.04 to 14.50 g/t, with an average of 5.72 g/t. The No.2 orebody is 840 m in length and ranges from 0.3 to 19.9 m in thickness, with an average of 3.9 m. The depth along the dip direction is over 900 m. It strikes 040° and dips 35°-45° SE. The gold grade varies from 3.00 to 140.57 g/t, with an average of 5.13 g/t (Zhang and Wen, 1983).

3.3.5 Structural Control on Orebodies

The F1 fault controls the position of the main orebody in this deposit. The orebody is tabular to lenticular in shape and is parallel to the main fault plane (Fig. 3.15), which shows evidence for oblique slip involving reverse and dextral movement (The No.6 Team of Geology and Exploration, BGMRSP, 1969). Based on the pinch-and-swell structures of the gold lodes and alteration haloes, Luo et al (1996) concluded that the movement of the F1 fault during mineralization was dextral. Li (1996) considered that pre- to syn-mineralization, the F1 fault experienced compressional to tensional shearing.

3.3.6 Ore Mineralogy and Paragenesis

Base metal minerals include pyrite, chalcopyrite, sphalerite, galena, pyrrhotite and arsenopyrite. Pyrite is the most abundant and constitutes more than 90 percent of the metallic mineral phases. Two distinct generations of pyrite can be recognized and they occur mainly in veinlet-and-disseminated forms in the ores. The first type consists of fine to medium (1-3 mm) subhedral-euhedral grains with well-developed fractures infilled by later metal sulphides and electrum. The second generation of pyrite comprises fine (<1 mm) subhedral grains, which are usually associated with other base metal minerals such as chalcopyrite and sphalerite. The pyrite content of the orebody ranges from 5% to 25% (Jia, 1995). Gangue minerals mainly consist of quartz and sericite, with minor feldspar, calcite, dolomite and siderite. Gold minerals are predominantly composed of electrum and trace amounts of native gold. 74% of gold

minerals occur as fracture fills in pyrite. Just like the Cangshang Gold Deposit, four stages of hydrothermal mineral formation have been identified, which are, from the oldest to the youngest, stage 1: pyrite-quartz; stage 2: gold-quartz-pyrite; stage 3: quartz-base metal sulphides; and stage 4: quartz-calcite, respectively (The No.6 Team of Geology and Exploration, BGMRSP. 1969).

3.3.7 Geochronology

Wang et al (1998) dated a sample (SSD-15) of porphyritic granodiorite from the wallrock of this deposit by SHRIMP U-Pb zircon methods. The SHRIMP results are illustrated on a concordia plot in Figure 3.16. Nineteen of 24 analyses form a tight cluster (Fig. 3.16b) with a weighted mean $^{206}Pb/^{238}U$ age of 128 ± 2 Ma and a chi-square of 1.2. The age of 128 ± 2 Ma is taken as the age of crystallization of the host porphyritic granodiorite, hence providing a maximum age of gold mineralization. Of the remaining population, grain 10 has an age of 155 ± 3 Ma (1σ) (Fig. 3.16b), which is similar in age to the Linglong granitoid, and may be a zircon inherited from this source. Grain 2, which was not described by Wang et al. (1998), yields a near-concordant $^{207}Pb/^{206}Pb$ age of 1860 ± 15 Ma (1σ). Grains 5 and 6 are both slightly cloudy, euhedral, and optically homogeneous grains which are indistinguishable from the main zircon group in their morphology. However, they have concordant $^{207}Pb/^{206}Pb$ ages of 1934 ± 48 (1σ) and 2708 ± 65 Ma (1σ) (Fig. 3.16a), respectively (Wang et al., 1998). This again indicates that the Jiaobei Terrane is underlain by Precambrain basement and the zircons with mid-Archaean and Palaeoproterozoic ages were incorporated during the later magmatic event, which occurred at ca. 128 Ma.

3.3.8 Summary

The Sanshandao Gold Deposit is typical of the Jiaojia-style (i.e. disseminated-and-veinlet type) gold occurrence. The deposit is controlled by the Sanshandao Fault Zone (F1 Fault) and hosted within the Sanshandao Pluton, part of the Guojialing Suite. The No.1 and No.2 orebodies are located within the main alteration zone which is characterised by sericitization, silicification, pyritization and K-feldspar alteration.

Using SHRIMP U-Pb zircon techniques, the crystallization age of the host rock was dated at 128 ± 2 Ma, which constrains the maximum age of gold mineralization at this deposit (Wang et al., 1998). Since the Sanshandao and Cangshang Gold Deposits are both controlled by the San-Cang Fault Zone and are just ca. 4 km apart, they are considered to be formed during the same gold mineralization

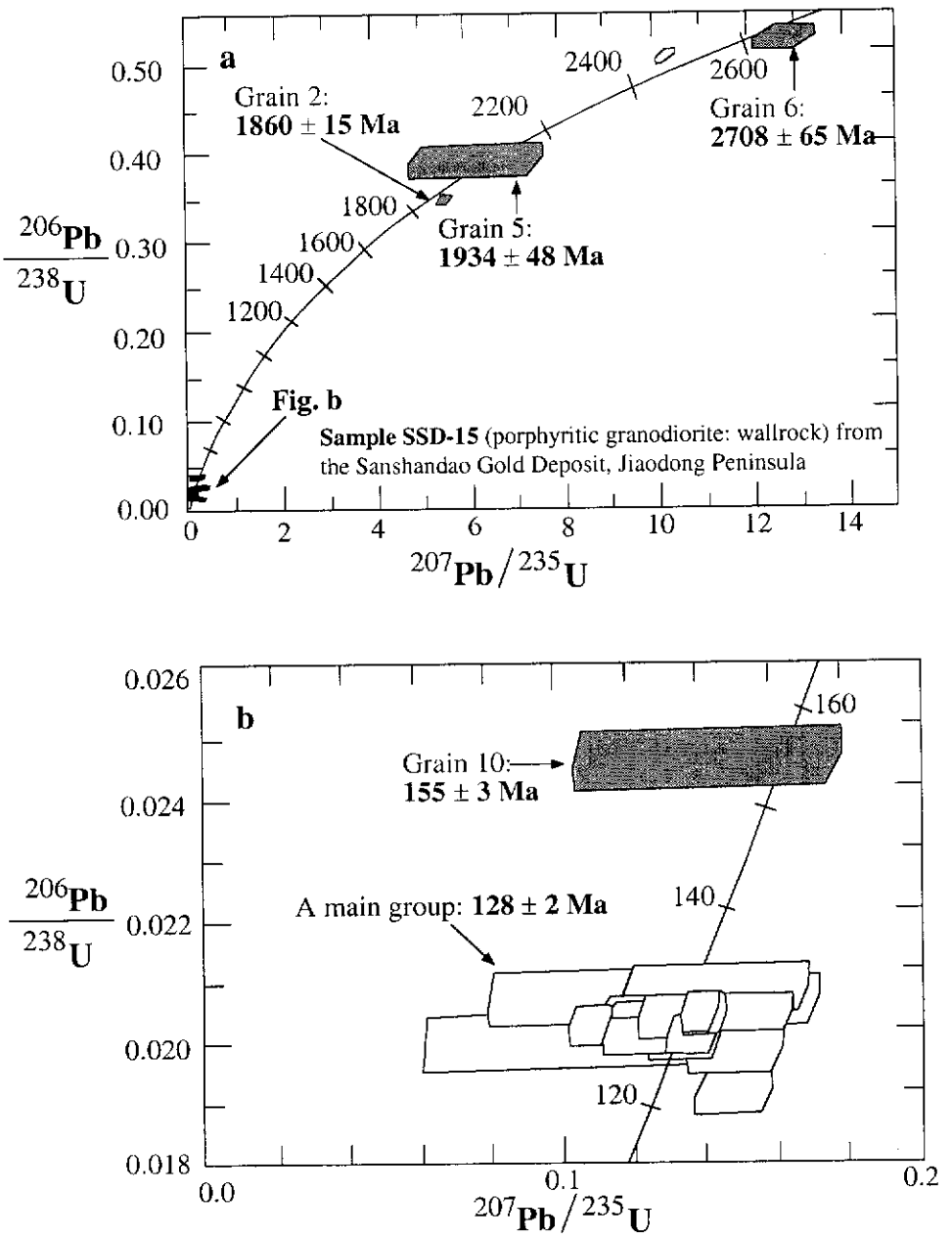

Fig. 3.16: U-Pb concordia plots showing (a) total SHRIMP analytical results for sample SSD-15 and (b) enlargement detailing younger zircon populations (modified from Wang et al., 1998).

event. Therefore, the age of 121 Ma for the gold mineralization of the Cangshang Deposit can be taken to also date the Sanshandao Deposit, since it must be younger than 128 ± 2 Ma, the age of the wallrock granitoid.

3.4 Jiaojia Gold Deposit

The Jiaojia Gold Deposit (E120°7'43", N37°24'5") is located about 30 km north-east of the city of Laizhou (Fig. 3.1). It was discovered in 1966 by the No.6 Team of Geology and Exploration, BGMRSP, based on regional reconnaissance. It is one of the largest gold deposits in China, with reported gold reserves of about 100 tonnes. The deposit is controlled by the Jiaojia-Xincheng Fault Zone and is situated at the contact between a hanging wall sequence of Archaean Jiaodong Group metamorphic rocks to the northwest and a footwall sequence of Jurassic Linglong granitoid to the southeast (Fig. 3.17). It is characterized by disseminated-and-veinlet gold ore (the disseminations are sulphides; the veinlets consist of quartz and/or sulphides), which was named the 'Jiaojia style' after this deposit.

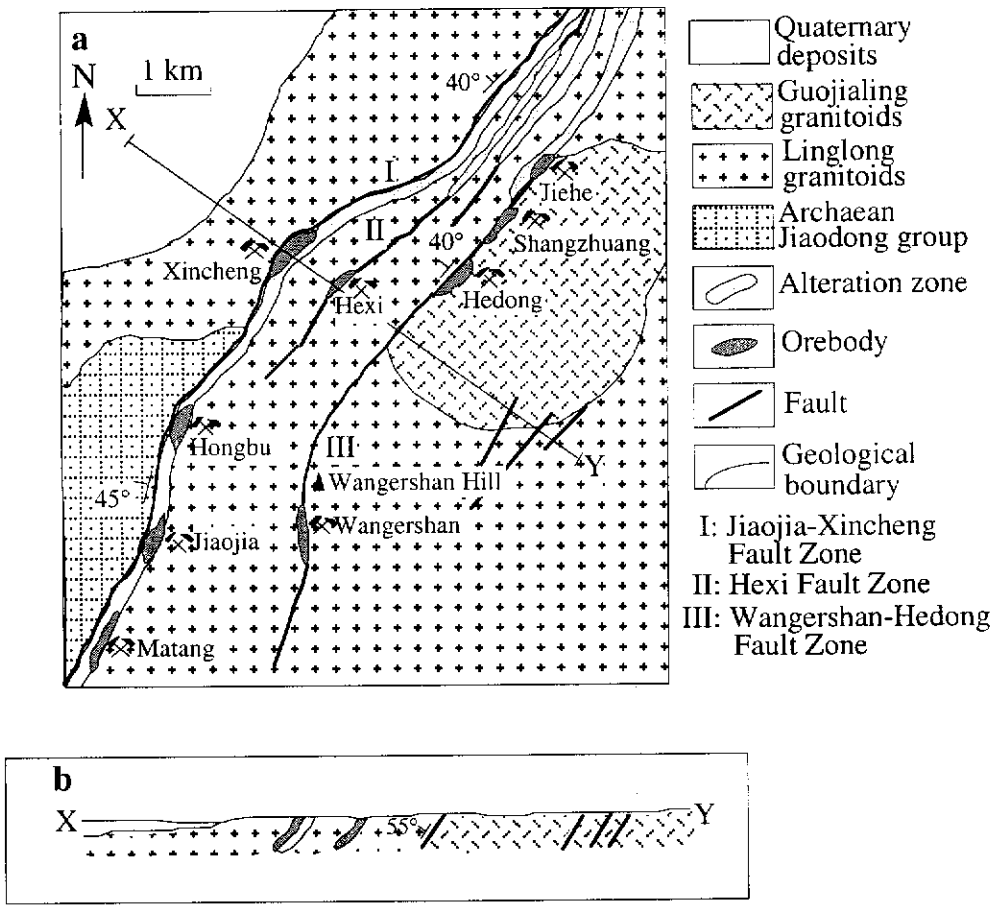

Fig. 3.17: (a) Geological map of the Jiaojia-Xincheng goldfield showing the major gold deposits and their spatial relationships with granitoids and faults. X-Y line is a profile line across the Jiaojia Gold Deposit and (b) Profile along X-Y line (modified from Wang et al., 1998).

3.4.1 Lithological Units

The Jiaodong Group makes up the hanging wall of the Jiaojia Gold Deposit and comprises amphibolite in the mining area. The amphibolite is fine- to medium-grained and grey-green in colour, and consists of plagioclase and hornblende with minor biotite and quartz. Accessory minerals include magnetite, apatite and zircon. The Linglong granitoids, which constitute the footwall of the Jiaojia Gold Deposit, consist of medium-grained, leucocratic monzogranite that is composed of K-feldspar, plagioclase, quartz and biotite. Accessory minerals include zircon, monazite, allanite, garnet, apatite and magnetite. A swarm of intermediate to mafic dykes, including microdiorite and lamprophyre, are present at the deposit (Zhang and Chen, 1997).

3.4.2 Jiaojia-Xincheng Fault Zone

The Jiaojia-Xincheng Fault Zone is the southwestern section of the first-order, regional-scale, arc-shaped Huang-Ye Fault Zone which extends for about 70 km. The strike of the Huang-Ye Fault Zone is variable, swinging from 080° in the northeast to 025° in the southwest (Fig. 3.1). The Jiaojia-Xincheng Fault Zone is 12 km in length (Fig. 3.17) and varies from 50 to 300 m in width. It strikes 010°-040° and dips 30°-45° NW. The main fault plane is well-developed, marked by a fault gauge zone ranging from 10 to 30 cm in thickness. The sense of movement, deduced from the steps and lineations on slickensides, is reverse and oblique. The regional stress field of the fault zone is inferred to have changed from compression to tension and back to compression during pre-, syn- and post-mineralization stages, respectively (Lu et al., 1988).

3.4.3 Alteration

Hydrothermal alteration associated with this deposit includes sericitization, silicification, pyritization, K-feldspar alteration, carbonation and chloritization. A large alteration halo within the Jiaojia Deposit is well-developed along the Jiaojia-Xincheng Fault Zone. The halo is 1900 m in length and ranges from 70 to 250 m in width (with an average of 148 m). The width tends to increase with depth, for example, near the surface (+ 20 m) its average width is 91 m and at the -200 m and -400 levels its average width is 165 m and 228 m, respectively (Luo et al., 1996). Based on the type and intensity of alteration and the nature and distribution of altered rocks, this alteration halo can be roughly divided into three sub-zones (Nos. I. II and III), although these change gradually and there are no clear boundaries between them (Figs. 3.18 and 3.19). The No.I alteration zone is located below the main fault plane and adjacent to

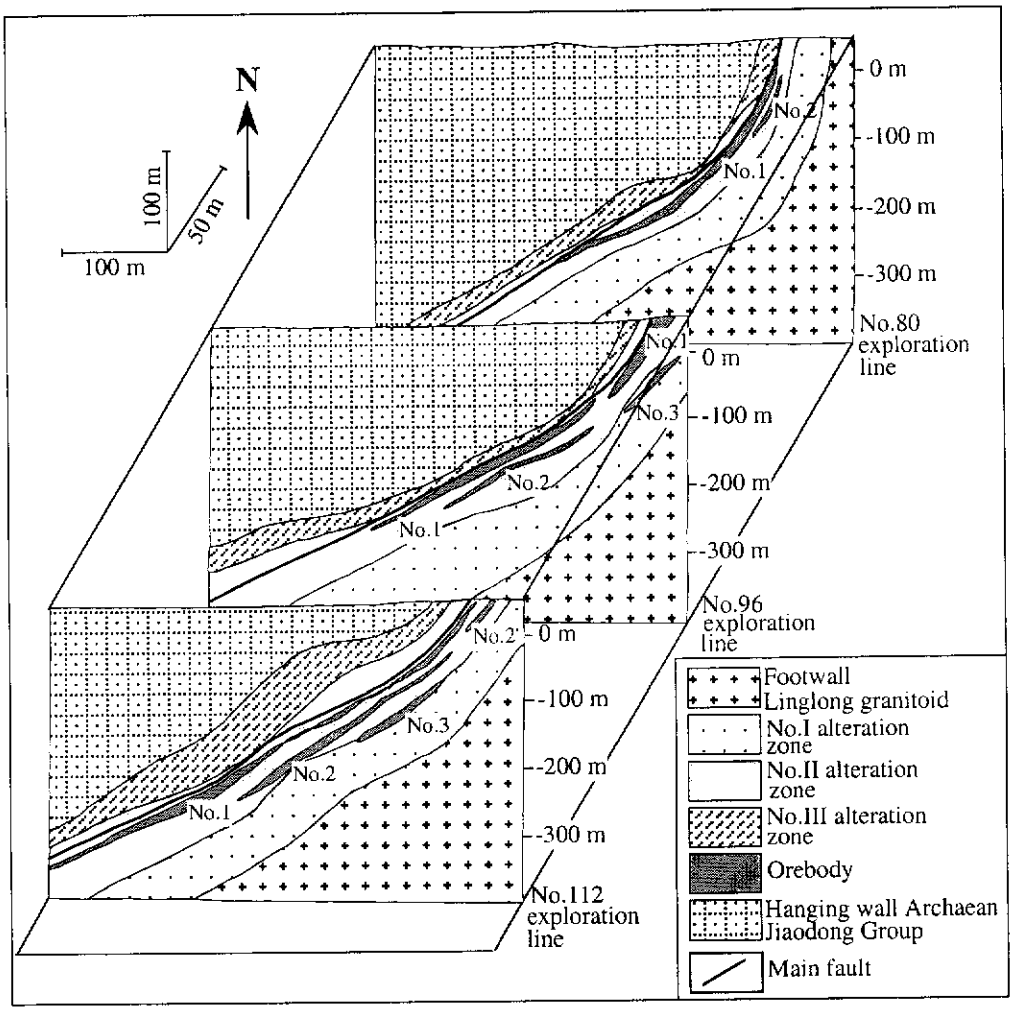

Fig. 3.18: Cross sections along No.80, No.96 and No.112 exploration lines in the Jiaojia Gold Deposit, showing the No.1, No.2 and No.3 orebodies (modified from the No.6 Team of Geology and Exploration, 1977).

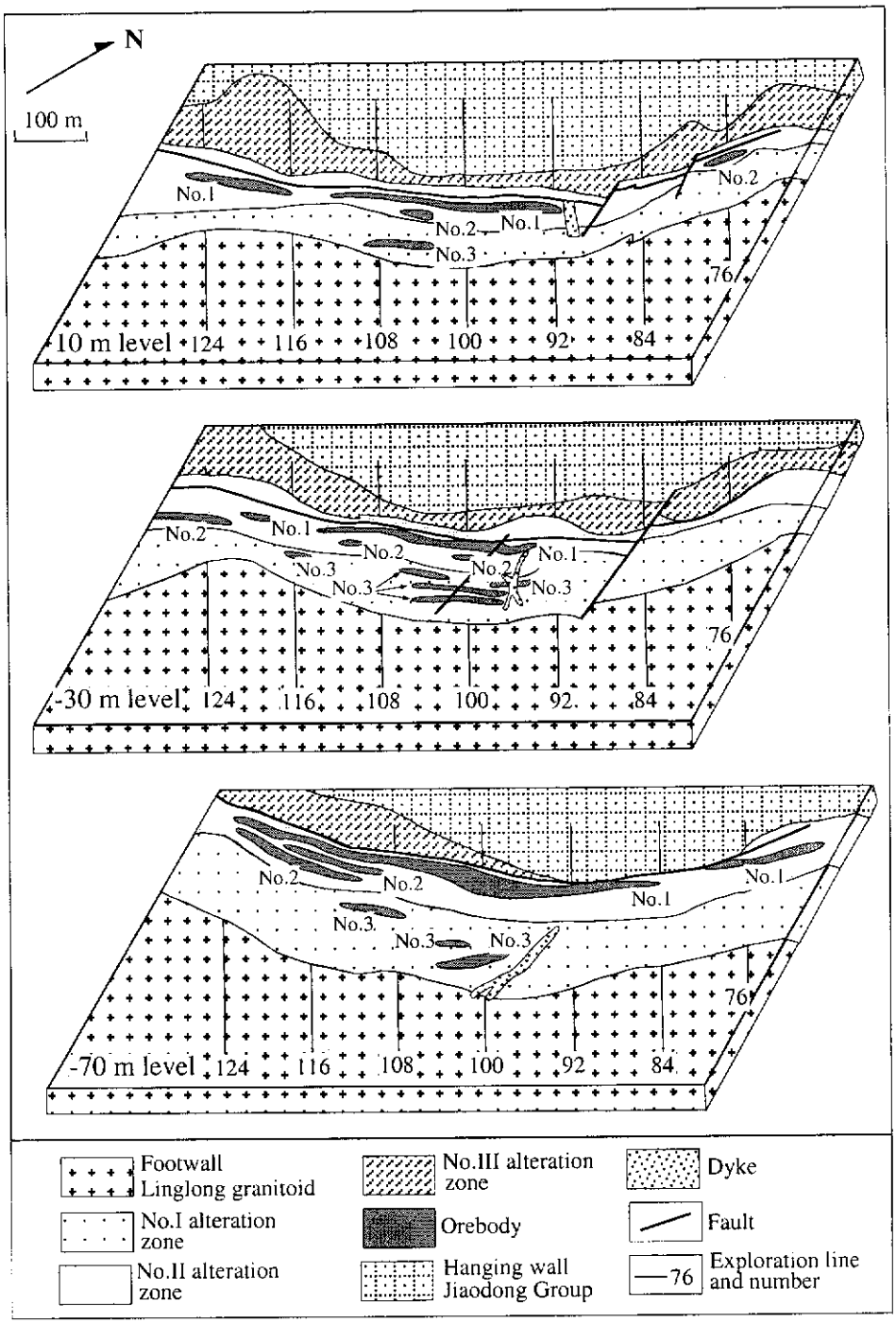

Fig. 3.19: Simplified geological plans of 10 m, -30 m and -70 m levels, showing the No.1, No.2 and No.3 orebodies in the Jiaojia Gold Deposit (modified from Yang et al., 1984).

the footwall of the Linglong granitoid. It is characterized by K-feldspar alteration, sericitization and silicification and consists of cataclastic Linglong granitoid. The degree of alteration is less than that for the other two zones reflecting its greater distance from the main fault plane; the closer to the main fault plane the wall rocks are, the more intensive the alteration. The No.II alteration zone is developed adjacent to the main fault zone and is characterized by strong pyrite alteration, sericitization and silicification. It is composed mainly of sericite-quartz-pyrite rocks which comprises sericite (30-70%), quartz (20-60%) and pyrite (5-10%). The No.III alteration zone is situated on the hanging wall side of the main fault plane and adjacent to the Jiaodong Group. This zone shows sericitization, silicification and chloritization and consists of cataclastic rocks of the Jiaodong group.

3.4.4 Orebodies

Orebodies within the deposit, including the No.1, No.2 and No.3 orebodies, are located in the No.I and No.II alteration zones (Figs. 3.18 and 3.19).

The No.1 orebody is hosted by the No.II alteration zone and is situated 0 to 43 m below the main fault plane and located mainly between the No. 92 and No. 124 exploration lines (Fig. 3.19). It is the largest orebody in the deposit, containing 85% of the total gold reserves. It strikes 010°-033° and dips 40°-50°NW, with the dip angle decreasing with depth down-dip. The No.1 orebody is 1200 m in length and varies from 0.3 m to 15.4 m (average of 3.8 m) in thickness, with a local maximum of 30 m. It extends for a depth of 500-670 m down-dip, with a maximum recorded depth of 925 m. This orebody is tabular in shape and is broadly parallel to the main fault zone and pitches in a southwest direction at 70°. In general, the gold grade ranges from 3.07 g/t to 52.59 g/t (average of 13.23 g/t), but locally reaches a maximum of 253.88 g/t (BGMRSP, 1989). However, Zhang and Chen (1997) reported the mean grade of the No.1 orebody as 4.43 g/t.

The No.2 orebody is also hosted by the No.II alteration zone and is below and parallel to the No.1 orebody, and located mainly between the No.100 and No.124 exploration lines (Fig. 3.19). This orebody strikes 007°-030°, dips 41°-63°NW and is 860 m in length along strike, ranging from 0.3 m to 7.3 m in thickness, with an average of 1.6 m. It extends for a depth of over 850 m down-dip, pitching to the southwest at 30°-45°. In general, the gold grade varies from 3.06 g/t to 80.69 g/t, but locally reaches a maximum of 145.5 g/t (BGMRSP, 1989). Zhang and Chen (1997) reported the mean grade of the No.2 orebody as 5.13 g/t.

The No.3 orebody is hosted by the No.I alteration zone and is situated mainly between the No.92 and No.116 exploration lines (Fig. 3.19). This orebody is discountinous and strikes 010°-030° and is roughly parallel to the No.2 and No.3 orebodies. However, it dips with a high angle of 70°-90° in a south-east direction, which is opposite to the No.2 and No.3 orebodies. No detailed information is available on the No.3 orebody, such as its scale and range of gold grades, but the grade of this orebody is higher than that of the No.1 and No.2 orebodies because it contains more auriferous pyrite-quartz veinlets which fill the cleavages or fractures developed within the rocks of the No.I alteration zone (Yang et al., 1984; Zhang and Chen, 1997). The average grade of the No.3 orebody is 5.22 g/t (Zhang and Chen, 1997).

The alteration is closely related to mineralization, but the orebodies do not coincide with areas of intense alteration. The gold grade of the orebodies chiefly depends on the amount of gold-bearing sulphide (dominantly pyrite)-quartz veinlets filling in the ore; the more abundant, the higher the gold grade. This view is substantiated by the No.3 orebody which occurs in a weak alteration zone (No.I) but is of higher grade. At the -70 m level along the No.100 exploration, the ore is weakly altered granitoid, but its micro-fractures are filled by auriferous sulphide-quartz veinlets, hence the average of the ore grade is high at 5.5 g/t (Bai, 1993).

3.4.5 Structural Control on Orebodies

The Jiaojia-Xincheng Fault Zone controls the distribution of orebodies within the Jiaojia Deposit. These orebodies are broadly parallel to the main fault plane and located in its footwall (Figs. 3.18 and 3.19). Along the strike or dip direction, orebodies can swell or pinch-out, locally branching or converging (Zhang and Wen, 1983). Two sets of conjugate fractures are well-developed in the orebodies; one strikes 040°-060° and dips 50-70°SE, another strikes 160°-190° and dips 40°-60°NE (The No.6 Team of Geology and Exploration, BGMRSP, 1977). Both control the distribution of gold-bearing sulphide-quartz veinlets (Fig. 3.20) which is the key factor for determining richness of the ore.

3.4.6 Ore Mineralogy and Paragenesis

Base metal minerals include pyrite, chalcopyrite, galena, sphalerite, pyrrhotite, tetrahedrite and chalcocite. Pyrite is the most abundant and makes up over 90 percent of the metallic minerals. Three distinct generations of pyrite can be recognized and they

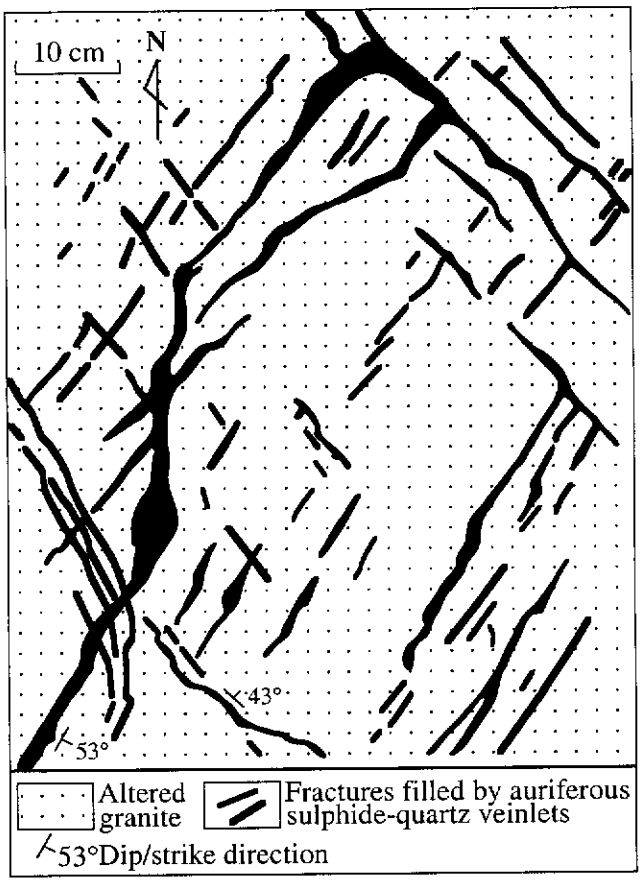

Fig. 3.20: Geological sketch of the south wall of the drive along the No.100 exploration line of the No.3 orebody, -70 m level, Jiaojia Gold Deposit, showing two sets of conjugate fractures controlling the distribution of auriferous sulphide-quartz veinlets (modified from the No.6 Team of Geology and Exploration, 1977).

mainly occur in veinlet-and-disseminated forms in the ores. The first type consists of coarse (2-5 mm) subhedral-euhedral grains. Fractures are well-developed in this kind of pyrite, and later metal sulphides and electrum occur as infillings. The second generation of pyrite comprises medium (0.5-2 mm) subhedral grains, and the third is composed of fine (0.05-0.3 mm) euhedral grains. Gangue minerals mainly consist of quartz and sericite, with minor feldspar, calcite, dolomite and chlorite. Gold minerals are dominantly electrum and trace amounts of native gold, which occur as small enclaves and infillings carried chiefly by pyrite, chalcopyrite and quartz.

Based on mineralogical, textural, and crosscutting relationships observed in the field, four stages of hydrothermal mineral formation have been identified (BGMRSP, 1989). From the oldest to the youngest these stages are: stage 1: pyrite-quartz, with the mineral assemblage consisting mainly of milk-white quartz and a small amount of coarse pyrite; stage 2: gold-quartz-pyrite, with the mineral assemblage mainly composed of smoke-grey coloured quartz and medium-grained pyrite; stage 3: gold-quartz-base metal sulphides, with the mineral paragenesis dominantly of grey quartz, fine-grained pyrite and other base metal sulphides such as chalcopyrite and galena; stage 4: quartz-carbonate, where the mineral paragenesis consists mainly of quartz and calcite.

3.4.7 Geochronology

Although the close spatial and temporal relationships between dykes and gold mineralization has recently been recognized in China (Yao et al., 1990; Trumbull et al., 1996; Wang et al., 1998), there has been no attempt to constrain the age of gold mineralization by dating such dykes. Within the Jiaojia Gold Deposit, some dykes cut the orebodies (Fig. 3.21), and were altered during late of mineralization stages, hence they are considered to be temporally associated with the gold mineralization and presumably closely approximate the time of gold mineralization. Based on this argument, a whole-rock sample from one such dyke (JJ1) (Fig. 3.21) was selected for SHRIMP U-Pb zircon analysis. The SHRIMP results are listed in Table 3.3 and illustrated on a concordia plot in Figure 3.22. Following is the description of sample JJ1 and the interpretation of its SHRIMP zircon U-Pb age.

Sample JJ1

Sample JJ1 was taken from a mafic dyke which was named as lamprophyre by local geologists but which from thin section observation is actually a basaltic dyke. It is melanocratic and has a porphyritic texture. Its phenocryst phases are plagioclase

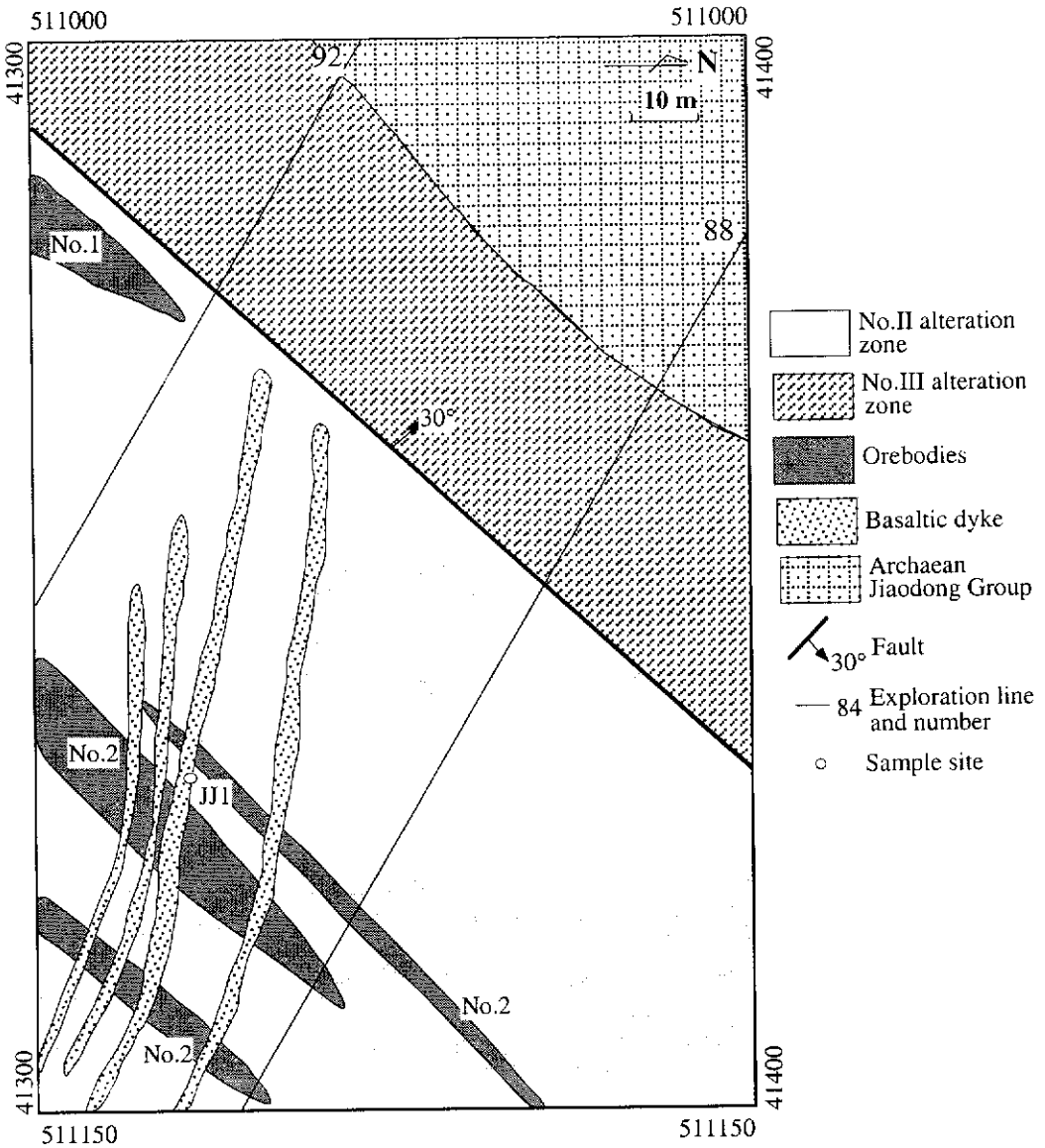

Fig. 3.21: Part of plan of -230 m level at the Jiaojia Gold Deposit, showing the distribution of dykes and sample location. Numbers refer to gold orebodies.

(euhedral, lath-shaped, multiple twin lamellae), clinopyroxene (euhedral to subhedral) and olivine (partly or wholly replaced by serpentine), which form glomeroporphyritic aggregates. The fine-grained groundmass consists mainly of plagioclase, pyroxene and olivine with an intergranular to intersertal texture. Some calcite veinlets occurred in the groundmass. Only twenty-two zircon grains were extracted from a ca. 5 kg whole-rock sample. These zircons range in size from +132 μm to -74 μm. The larger grains (+132 μm to 100 μm) are rounded and considered to be xenocrysts, so they were not analysed; the smaller ones (100 μm to -74 μm) are euhedral with well-formed prism and pyramid faces, and their average elongation ratio is about 3:1, with a maximum of 5:1. Most of these grains are colourless, with a few a pinkish colour.

A total of 8 analyses were carried out on 5 euhedral grains, and the ages range from 186 ± 4 Ma to 137 ± 3 Ma (Table 3.3 and Fig. 3.22).

Table 3.3: SHRIMP U-Pb data for zircons from sample JJ1 from the Jiaojia Gold Deposit. Analyses are listed in order of increasing age. The following notation is used for analysed grains: 1.1=grain 1, first point analysed. Data are ^{204}Pb-corrected. Individual analyses have a 1σ error. The ^{206}Pb/^{238}U age is adopted for the zircons, since the age is less than 1.0Ga.

Spot	U (ppm)	Th (ppm)	Th/U	Total Pb (ppm)	$\frac{^{204}Pb}{^{206}Pb}$	f206 (%)	$\frac{^{207}Pb}{^{206}Pb}$	$\frac{^{206}Pb}{^{238}U}$	$\frac{^{207}Pb}{^{235}U}$	$\frac{^{206}Pb}{^{238}U}$	Age
5.1	1052	618	0.59	27	0.00178	0.028	0.054±4	0.0215±5	0.16±1	137±3	
2.1	955	770	0.81	26	0.00032	0.005	0.055±2	0.0236±5	0.18±1	150±3	
1.2	352	184	0.52	9	0.00102	0.016	0.050±5	0.0241±5	0.17±2	154±3	
1.1	268	257	0.96	8	0.00074	0.012	0.060±6	0.0242±6	0.20±2	154±4	
5.2	837	307	0.37	22	0.00085	0.014	0.053±3	0.0249±5	0.18±1	158±3	
2.2	271	143	0.53	8	0.00213	0.034	0.045±6	0.0255±6	0.16±2	162±4	
4.1	479	215	0.45	13	0.00074	0.012	0.058±4	0.0254±6	0.20±1	162±4	
3.1	886	15	0.02	25	0.00080	0.013	0.056±2	0.0292±6	0.23±1	186±4	

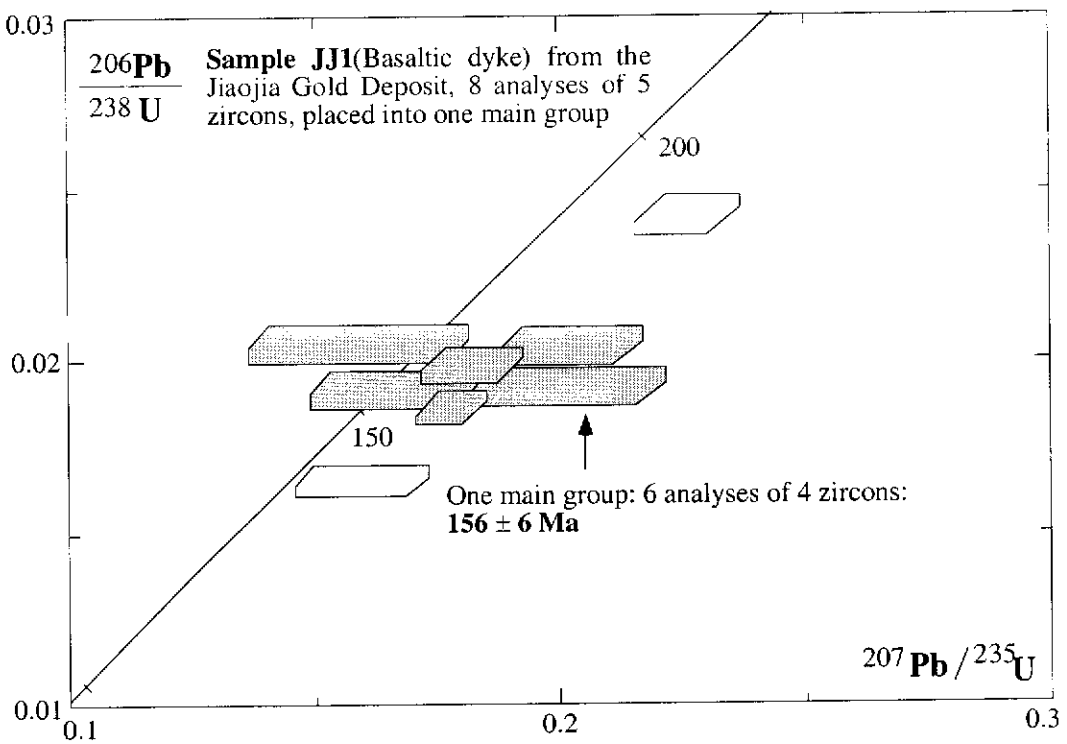

Fig. 3.22: A concordia plot showing the SHRIMP analytical results for sample JJ1, Jiaojia Gold Deposit.

One zircon population is composed of 6 analyses of 4 zircons, which form a coherent group (Fig. 3.22) having a weighted mean $^{206}Pb/^{238}U$ age of 156 ± 6 Ma with a chi-square value of 1.62. The U and Th contents of the 6 spots vary from 268 ppm to 955 ppm and 143 ppm to 770 ppm, respectively. The U/Th ratios range from 0.37 to 0.96.

The remaining 2 spots (3.1 and 5.1) from two separate zircon grains do not yield concordant ages, so may have no real geological meaning.

The group age of 156 ± 6 Ma for the mafic dyke coincides with the age of the host Linglong granitoid (165 to 150 Ma) (Wang et al., 1998), which makes its geochronological interpretation more complicated. Normally, the age of euhedral zircon grains of an igneous origin records the timing of igneous crystallization of rock, however, it is impossible for the age of 156 ± 6 Ma to represent the timing of intrusion of the mafic dyke since it is the same age as the host granitoid. Lanyon et al. (1993) reported that characteristic morphologies of zircons separated from different mafic dykes varied considerably. It is difficult to tell the origin of these euhedral zircons from sample JJ1 but there are two possibilities. One is that they were entrapped from the host granitoid by ascending mafic magma; another is that they were derived from the deep source of gabbro that was crystallising as the phenocryst phase now caught up in the dyke and carried upward. No matter which explanation, the deep gabbro and host granitoid pluton were formed during the same event, and the basaltic dyke can be taken as a syn-plutonic dyke (Pitcher, 1993). The intrusion of the basaltic dykes are associated with the gold mineralization in time and space, and its age must be younger than the age of the host Linglong granitoid. However, this study has proved that the mafic magma rapidly ascended and no zircons crystallized during the process, hence no reliable ages recording the intrusive age of the dyke were obtained by SHRIMP zircon U-Pb analysis. Furthermore, these zircons were most likely inherited from host granitoid or a deep gabbroic source.

Using the Rb-Sr isochron method to date hydrothermal muscovites from ores, Luo and Wu (1987) concluded that there are two gold mineralization events in the Jiaojia Deposit, which occurred at 105 ± 7 Ma and 88.1 ± 0.1 Ma. Although it is hard to justify the reliability of these data, it is believed that there may exist multiple stages of hydrothermal activity in the region which may be closely related to the dyke activity (Yao et al., 1990).

3.4.8 Summary

The Jiaojia Gold Deposit is located at the contact between a hanging wall of Archaean Jiaodong Group amphibolite to the northwest and a footwall of Jurassic Linglong monzogranite to the southeast. The contact is marked by the Jiaojia-Xincheng Fault Zone. Based on the features of alteration (sericitization, silicification, pyritization, K-feldspar alteration, carbonation and chloritization), three alteration zones (No.I, No.II and No.III) are identified within this deposit. The No.1 and No.2 orebodies are in the No.II alteration zone, and the No.3 orebody is located in the No.I alteration zone. These orebodies are broadly parallel to the main fault plane of the Jiaojia-Xincheng Fault and located in its footwall. Two sets of conjugate fractures are well-developed in the orebodies and control the distribution of the gold-bearing sulphide-quartz veinlets, the density of which is the important factor for determining richness of the ore.

Within the Jiaojia Gold Deposit, intermediate to mafic dykes occur widely and are considered to be closely related to gold mineralization in space and time. Based on this view, one sample of mafic dyke was dated by SHRIMP U-Pb zircon analysis in order to constrain the age of gold mineralization at the Jiaojia Deposit. The obtained weighted mean $^{206}Pb/^{238}U$ age is 156 ± 6 Ma, which cannot represent the age of intrusion of this dyke, since it is as the same age as the host Linglong monogranite. The dated euhedral zircons are interpreted to be entrapped from the host granitoid by ascending magma or derived from a deep source of syn-plutonic gabbro. Hence no reliable intrusive age for the dyke was obtained by SHRIMP zircon U-Pb dating. Furthermore, dating this dyke cannot provide constraints on the timing of gold mineralization at this deposit. Although some authors consider that there may exist two stages of gold-related hydrothermal activity (at ca. 105 Ma and 88 Ma), this cannot be established from the available geochronological evidence.

3.5 Wangershan Gold Deposit

The Wangershan Gold Deposit is located about 30 km north-east of the city of Laizhou (Fig. 3.1). It was discovered in the 1960s by the No.6 Team of Geology and Exploration, BGMRSP, based on 1: 2,000 scale mapping, drilling and prospecting trenches. In 1985, the known gold reserves were 10.7 tonnes with an average gold grade of 10.93 g/t. A new shaft, with designed depth of 700 m, is being built and the known reserves have been extended to 50 tonnes, with the gold deposit becoming one of the superlarge deposits of the Jiaodong Terrane. The deposit is hosted by the Linglong granitoid and controlled by the Wangershan-Hedong Fault Zone (Fig. 3.17).

Gold mineralization includes Jiaojia-style (i.e. disseminated-and-veinlet type) and Linglong-style (i.e. vein type). The grade of the ore of the Linglong-style is higher, ranging from 15 to 29.82 g/t but with a localized maximum of 114.77 g/t; the grade of the ore of the Jiaojia-style is lower, varying from 3 to 15 g/t.

3.5.1 Lithologic Units

The host of the Wangershan Gold Deposit is dominantly granitoid of the Linglong Suite, which consist of monzogranite within the mining area. This is grey-white in colour, has a fine- to medium-grained equigranular texture with a weak foliation and is mainly composed of K-feldspar, plagioclase, quartz and biotite. Accessory minerals include hornblende, epidote, titanite, allanite, rutile, apatite and zircon.

3.5.2 Wangershan-Hedong Fault Zone

The Wangershan-Hedong Fault Zone is about 10 km in length (Fig. 3.17) and, ranges from 2 to 200 m in width, averaging 25 m. Its strike changes considerably: to the north of Wangershan Hill, it strikes 030°-045° and dips 45°-60° NW; to the south of Wangershan Hill, it strikes from 0°-015° to 350°-360° and correspondingly dips 36°-45° NW or SW. The sense of movement, deduced from the steps on slickensides, is strike-slip, with both sinistral and dextral offsets. Close to the main fault plane, a fault gouge zone with a thickness ranging from 5 to 15 cm is discontinuously developed. There are smaller branch faults which are parallel to, or intersect, the main fault zone and occur along both sides. Four main sets of fractures are well-developed within the deposit (Fig. 3.23) with strikes of 10°-20°, 30°-40°, 280°-290° and 300°-310° (data from the No.6 Team of Geology and Exploration, BGMRSP, 1985).

3.5.3 Alteration

The common wall-rock alteration types of the Wangershan Deposit include sericitization, silicification, sulphidation, K-feldspar alteration and carbonation. The largest alteration zone within the deposit is called the No.AI and it is controlled by the Wangershan-Hedong Fault Zone. This alteration zone is 1800 m in length and ranges from 2 m to 50 m in width. To the north of the No. 22 exploration line (Fig. 3.24), the alteration zone strikes 005°-015° and dips 45°-62°NW; to the south of the No. 22 exploration line, it trends ca. 002° and dips 36°-45°SW. The degree of sericitization,

silicification and sulphidation which are associated with gold mineralization increase towards the orebodies, although there is no distinct zonation.

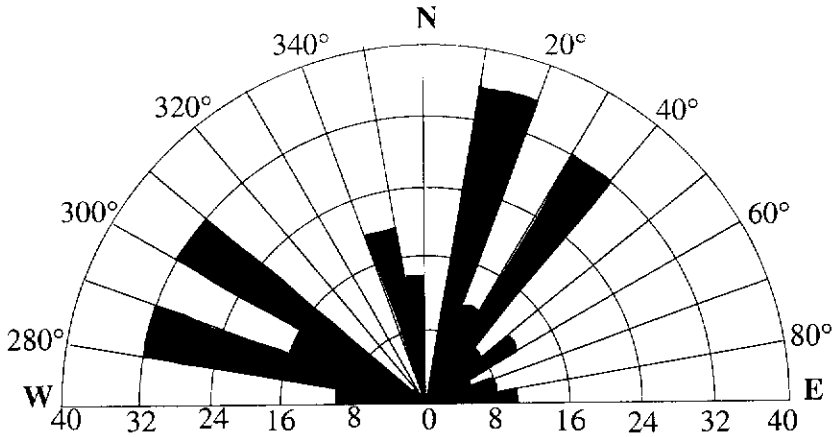

Fig. 3.23: Rose diagram of orientations of fractures within the Wangershan Gold Deposit (the data from the No.6 Team of Geology and Exploration, BGMRSP, 1985).

3.5.4 Orebodies

Orebodies within the deposit consist of auriferous pyrite-quartz veins and disseminated sericite-quartz rocks. The latter show different degrees of alteration and cataclasis and consist dominantly of sericite (40-55%), quartz (40-50%) and minor pyrite. Most of the orebodies, including the No. 1, No. 2 and No. 3 orebodies, are located in the No.AI alteration zone (Figs. 3.24 and 3.25).

The No. 1 orebody, located between the No. 14 and No. 42 exploration lines (Fig. 3.24), is the largest one in the deposit, with gold reserves of 6.5 tonnes. It strikes 005°-015° and dips 45°-53° NW and is 600 m in length, reaching 12.7 m in width, with an average of 3.8 m. It extends to a depth of over 500 m down-dip. The gold grade ranges from 2 to 28 g/t, with a local maximum of 120.76 g/t. Both Jiaojia and Linglong types of gold ore are found in the No. 1 orebody (The No.6 Team of Geology and Exploration, BGMRSP, 1985).

The No. 2 orebody, with gold reserves of 2 tonnes, is situated between the No. 22 and No. 34 exploration lines (Fig. 3.24). It also strikes 005°-015°, parallel to the No. 1 orebody, and dips 45°-55° NW. The No. 2 orebody is 240 m along strike and up to 9.5 m in width, with an average of 3.2 m. It extends to a depth of about 150 m down-dip. The gold grade ranges from 2 to 18 g/t (average of 9.23 g/t), with a local

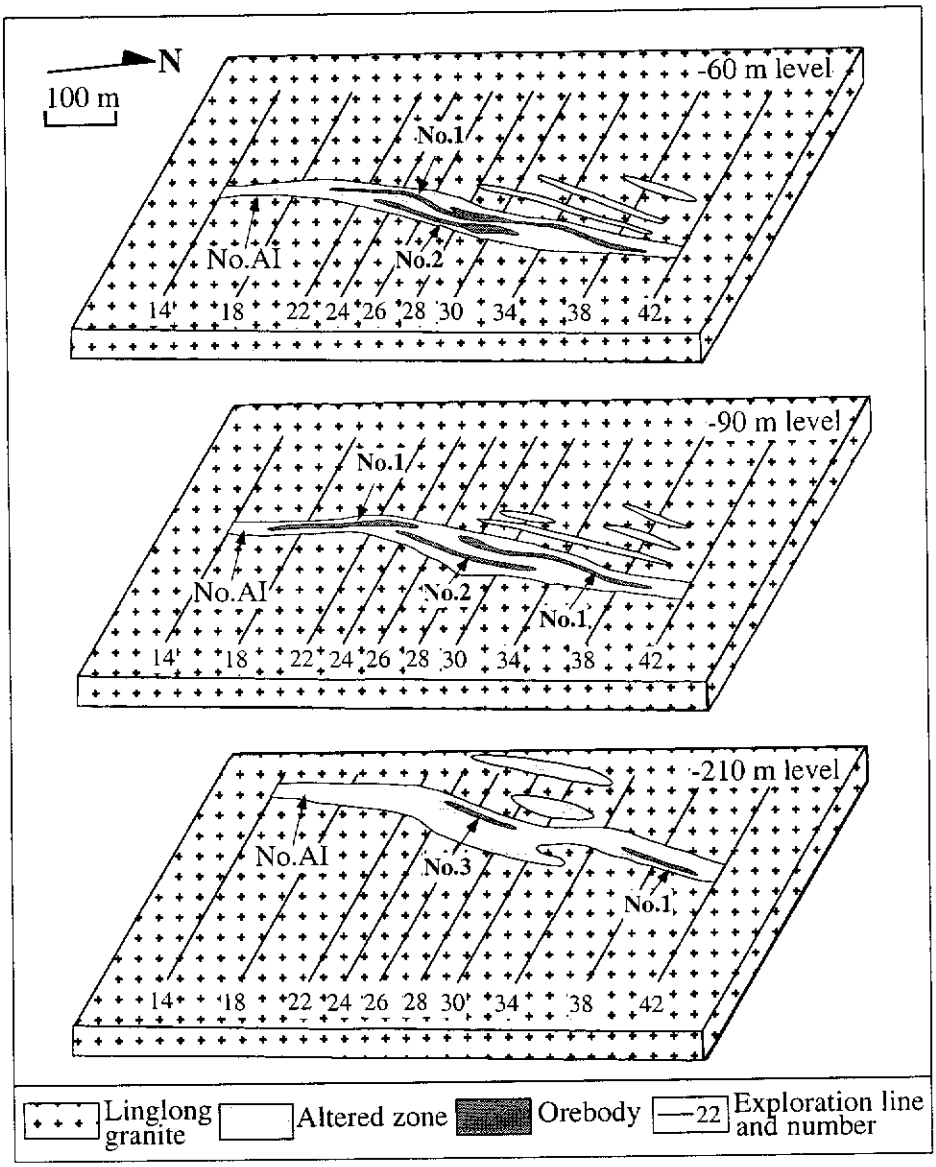

Fig. 3.24: Simplified geological plans of -60 m, -90 m and -210 m levels of the Wangershan Gold Deposit showing the No.AI alteration zone and No.1, No.2 and No.3 orebodies (The No.6 Team of Geology and Exploration, BGMRSP, 1985).

maximum of 92.7 g/t (The No.6 Team of Geology and Exploration, BGMRSP, 1985).

The No. 3 orebody, with gold reserves of 0.5 tonnes, is located between the No. 22 and No. 30 exploration lines (Fig. 3.24). It also trends 005°-015° and dips 55°-63° NW. The length of this orebody is 300 m and its width is up to 2.1 m, with an average of 1.4 m. It extends to a depth of over 310 m down-dip and its average gold grade is 10.43 g/t, with a maximum of 88.06 g/t (The No.6 Team of Geology and Exploration, BGMRSP, 1985).

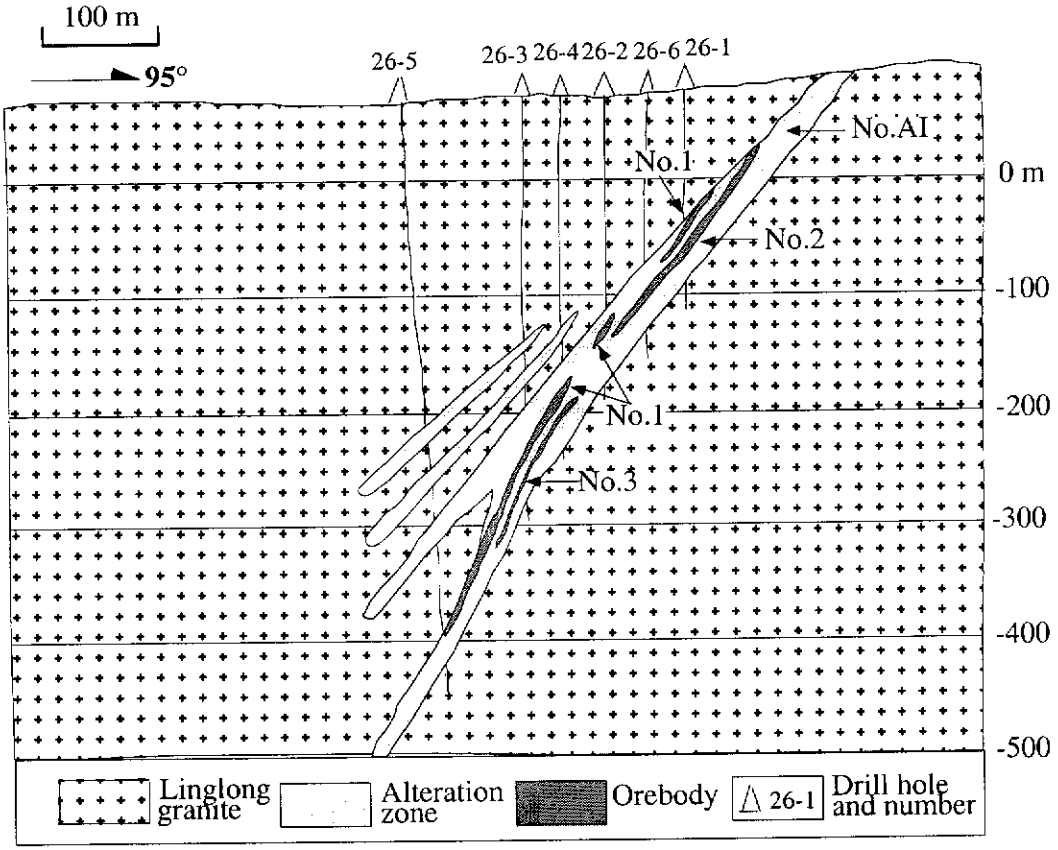

Fig. 3.25: Part of vertical section along the No.26 exploration line at the Wangershan Gold Deposit, showing the No.AI alteration zone and the No.1, No.2 and No.3 orebodies (the No.6 Team of Geology and Exploration, BGMSP, 1985).

3.5.5 Structural Control on Orebodies

Structure is the most important control on orebodies within this deposit. Compressional or tensional tectonic environments occur at the jogs or bends in the Wangershan-Hedong fault zone and at intersections of this fault zone with branch faults. In compressional environments, auriferous fluid disseminates within the host

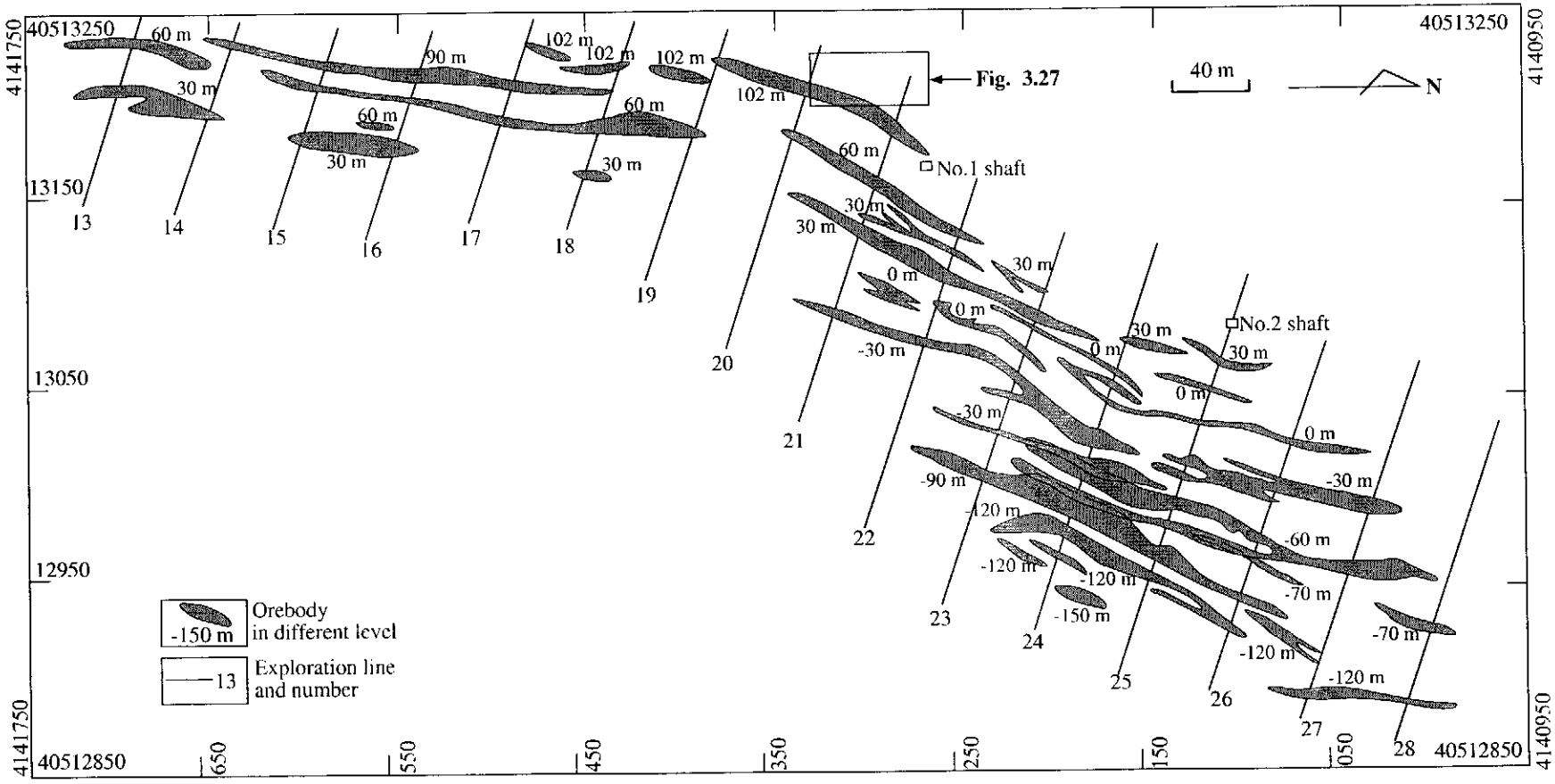

Fig. 3.26: Part of the No.1 orebody within the Wangershan Gold Deposit distributed in different levels, showing NE-SW en-echelon array (the data from the No.6 Team of Geology and Exploration, BGMRSP, 1985).

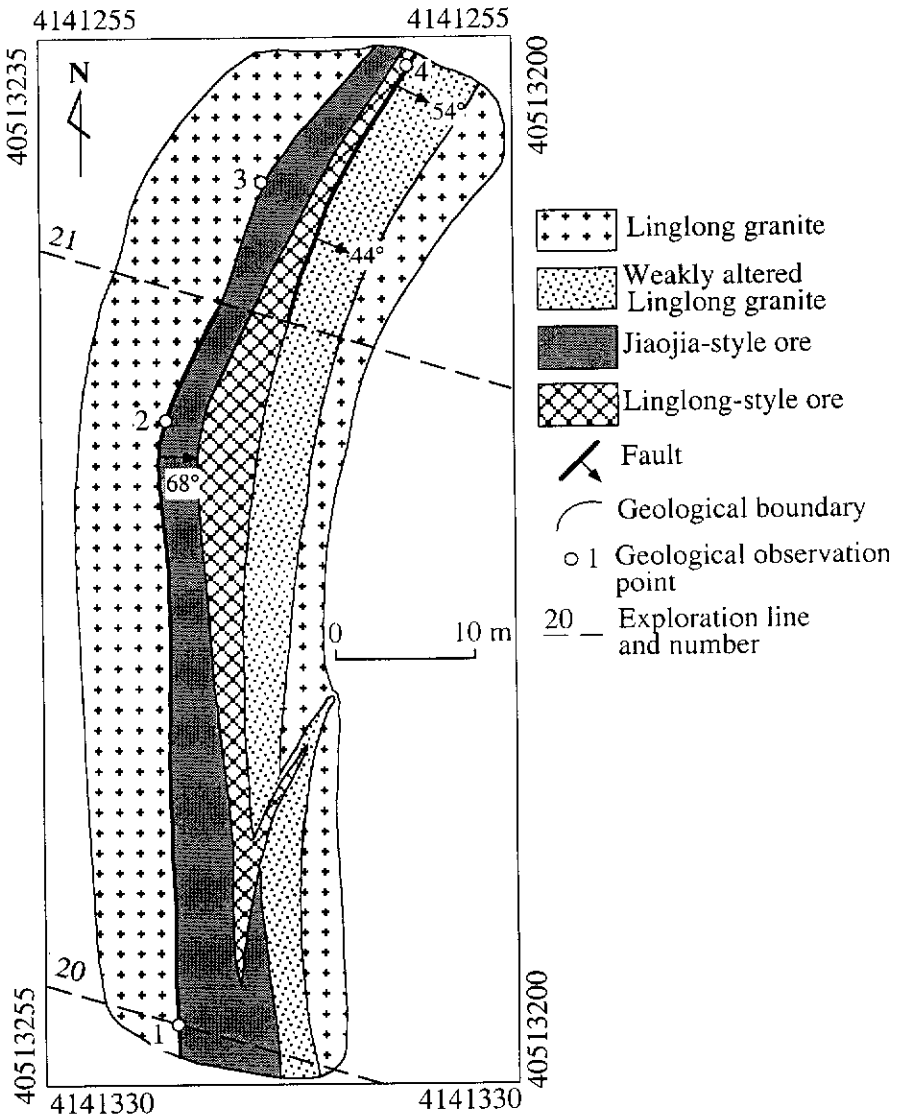

Fig. 3.27: Geological map of an abandoned open pit of the Wangershan Gold Deposit, showing that the Jiaojia-style and Linglong-style ores occur together (mapped by X. Zhang, 1997).

rock and fills microfractures in the wallrock as veinlets, which result in Jiaojia-style ore; in tensional settings, auriferous fluid fills fractures to form the Linglong-style ore. Liu (1997) pointed out that some fractures with NNE, NE, WNW and NW strikes are filled by auriferous sulfide-quartz veinlets which extend for a maximum of 30 m along strike, with a maximum width of about 0.5 m. High-grade ore is located at the intersection of NNE- and NW-striking fractures. The No. 1 orebody is a NE-SW striking en-echelon array (Fig. 3.26). Liu (1997) considered that in the upper part of the No. 1 orebody, ore of the Linglong style developed within a tensional environment and in its lower part, ore of the Jiaojia style occurred within a compressional environment. However, based on the mapping of one abandoned open pit (Fig. 3.27), the two types of gold ore are found to coexist at the same level, and they probably developed at different stages in the gold mineralization event, corresponding to different stress environments. Actually, the two styles of gold ore usually occur together, depending on local structural environment.

3.5.6 Ore Mineralogy and Paragenesis

Metallic minerals include pyrite and chalcopyrite, with minor chalcocite, galena, sphalerite and pyrrhotite; pyrite is the most abundant. Two distinct generations of pyrite can be recognized. The first consists of fine to medium (0.1-2 mm) subhedral-euhedral grains which occur in veinlets and aggregates through altered rocks. The second generation of pyrite comprises fine (<0.1 mm) euhedral grains which form aggregates within the altered rocks. Gangue minerals are mainly feldspar, quartz, sericite, calcite, ankerite and chlorite. Gold minerals are dominantly electrum and trace amounts of native gold, which occurs as small inclusions carried by pyrite, chalcopyrite and quartz (No.6 Team of Geology and Exploration, BGMRSP, 1985).

Based on mineralogical, textural, and crosscutting relationships observed in the field and in hand specimens, four stages of hydrothermal mineral formation have been distinguished (Fig. 3.28). From the oldest to the youngest these stages are: stage 1-quartz; stage 2-quartz-pyrite; stage3-quartz-polysulphide; stage 4-quartz-calcite.

3.5.7 Geochronology

In order to constrain the timing of gold mineralization at the Wangershan Gold Deposit, as well as the age of emplacement of the host granite, whole-rock samples from the wall rock (W1), from the No. 1 orebody (W2) and from a narrow zone of host cataclastic granite (W4) (Fig. 3.29) were selected for SHRIMP analysis.

Minerals	Stage 1	Stage 2	Stage 3	Stage 4
Quartz				
Sericite				
K-feldspar				
Dolomite				
Calcite				
Pyrite				
Ankerite				
Ferrocalcite				
Sphalerite				
Chalcopyrite				
Pyrrhotite				
Galena				
Electrum				

Fig. 3.28: Paragenetic sequence of hydrothermal and ore minerals at the Wangershan Gold Deposit. Thickness is proportional to relative abundance of each mineral (after the No.6 Team of Geology and Exploration, BGMRSP, 1985).

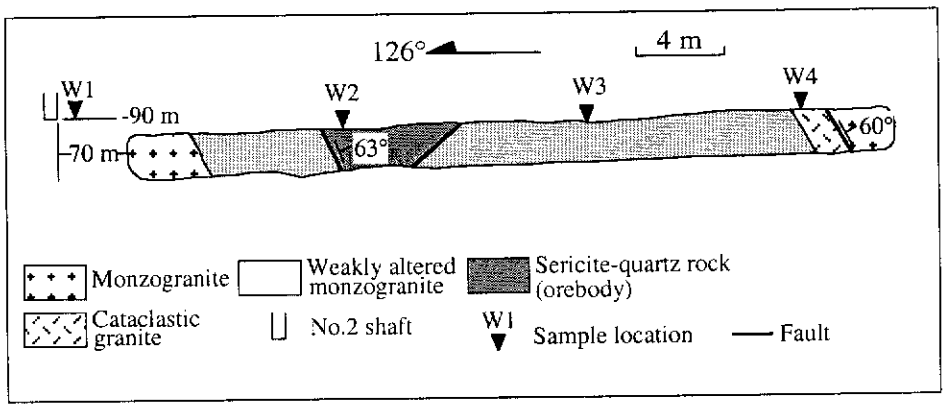

Fig. 3.29: Geological sketch of the south wall of the No.7 drive of the No.1 orebody, -120 m level, Wangershan Gold Deposit, showing the location of the geochronology samples.

SHRIMP results are listed in Table 3.4 and illustrated on concordia diagrams in Figures 3.30, 3.31 and 3.32. Outlined below is the description of samples W1, W2 and W4, and the interpretation of their SHRIMP zircon U-Pb ages.

Sample W1

Sample W1 was collected from the host Linglong granitoid and is a leucocratic, medium-grained monzogranite with a weakly foliation. The mineralogical composition of the monzogranite is 45 percent K-feldspar (subhedral, microperthitic, biotite and quartz inclusions), 30 percent plagioclase (subhedral to euhedral, multiple twinning, myrmekite common), 20 percent quartz (strong undulose extinction, anhedral, interstitial) and 5 percent biotite (euhedral, straw to dark-green pleochroism, chloritized). Accessory minerals include titanite, allanite, rutile, apatite, zircon and epidote. Zircons selected for analysis range in colour from colourless to pale purple with most having a brownish colour. They vary in size from +132 μm to -74 μm and most of these zircons are transparent and euhedral with perfectly preserved pyramidal terminations indicating crystallization from a magma. The elongation ratio ranges from 2:1 to 3:1.

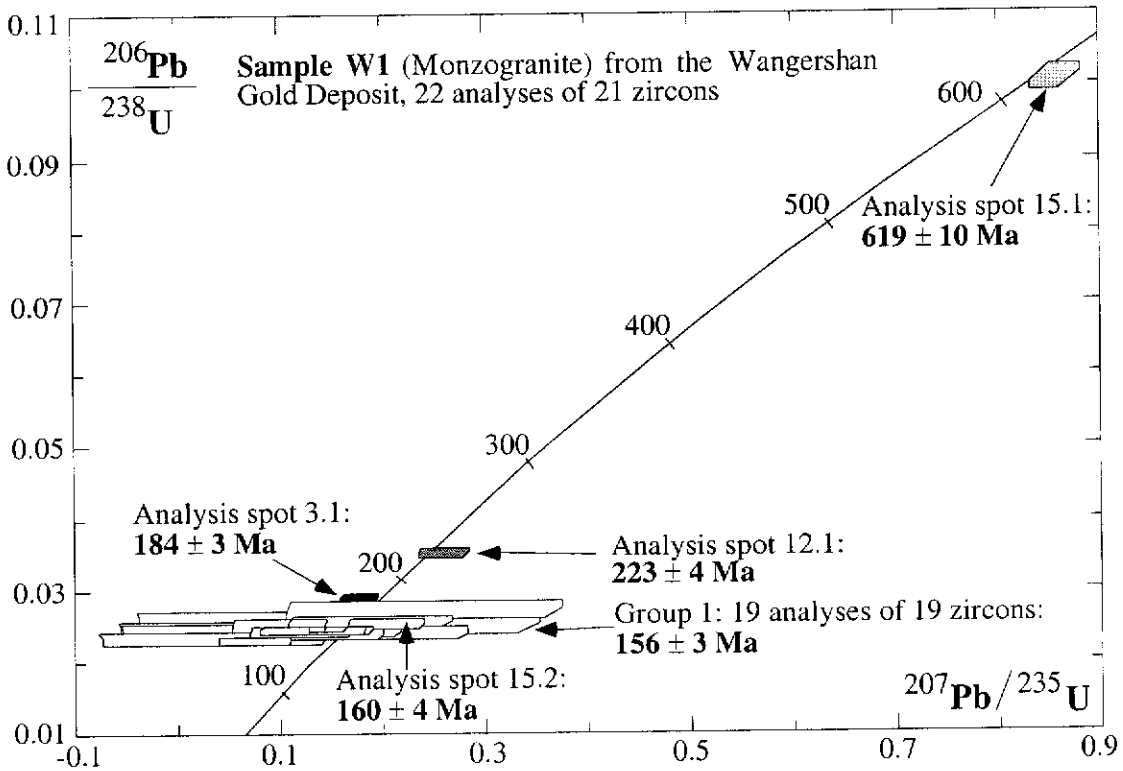

Fig. 3.30: A concordia plot showing the SHRIMP zircon analytical data from sample W1, Wangershan Gold Deposit.

Table 3.4: SHRIMP U-Pb data for zircons from samples W1, W2 and W4, from the Wangershan Gold Deposit. Analyses are listed in order of increasing age. The following notation is used for analysed grains: 1.1=grain 1, first point analysed. Data are ^{204}Pb-corrected. Individual analyses have a 1σ error. The $^{206}Pb/^{238}U$ age is adopted for zircons with an age of less than 1.0 Ga, otherwise the $^{207}Pb/^{206}Pb$ age is used.

spot	U (ppm)	Th (ppm)	Th/U	Total Pb (ppm)	$\frac{204Pb}{206Pb}$	f206 (%)	$\frac{207Pb}{206Pb}$	$\frac{206Pb}{238U}$	$\frac{207Pb}{235U}$	$\frac{206Pb}{238U}$ Age	$\frac{207Pb}{206Pb}$ Age
Sample W1											
5.1	178	215	1.21	6	0.00436	0.07	0.024±11	0.0228±5	0.08±4	145±3	
16.1	45	46	1.02	2	0.00931	0.149	0.012±34	0.0233±10	0.04±11	149±6	
13.1	110	88	0.8	4	0.00561	0.09	0.043±18	0.0238±7	0.14±6	152±4	
6.1	75	74	0.99	3	0.00807	0.129	0.061±26	0.0238±8	0.2±8	152±5	
8.1	134	136	1.01	5	0.00487	0.078	0.036±15	0.0241±6	0.12±5	153±4	
4.1	100	80	0.8	3	0.00477	0.076	0.049±17	0.024±7	0.16±6	153±4	
21.1	49	37	0.75	2	0.01066	0.171	0.019±35	0.0241±11	0.06±12	154±7	
18.1	267	172	0.64	8	0.0021	0.034	0.048±7	0.0244±5	0.16±2	155±3	
2.1	561	80	0.14	14	0.00115	0.018	0.046±3	0.0245±4	0.15±1	156±3	
20.1	211	31	0.15	6	0.00311	0.05	0.048±9	0.0245±5	0.16±3	156±3	
9.1	152	125	0.82	5	0.00487	0.078	0.038±13	0.0245±6	0.13±4	156±4	
19.1	55	29	0.53	2	0.01101	0.176	0.022±38	0.0245±11	0.07±13	156±7	
1.1	444	24	0.05	11	0.00147	0.024	0.043±5	0.0246±5	0.14±2	157±3	
11.1	67	49	0.72	3	0.00825	0.132	0.04±25	0.0249±9	0.14±9	158±5	
15.2	178	33	0.19	5	0.00316	0.051	0.059±11	0.0251±6	0.2±4	160±4	
14.1	35	23	0.66	2	0.01347	0.216	0.046±56	0.0252±16	0.16±20	161±10	
10.1	448	88	0.2	12	0.00234	0.037	0.037±5	0.0254±5	0.13±2	162±3	
7.1	81	92	1.13	3	0.00666	0.107	0.054±22	0.0254±8	0.19±8	162±5	
17.1	34	26	0.76	2	0.008	0.128	0.064±36	0.0272±12	0.24±14	173±8	
3.1	424	23	0.05	12	0.00165	0.026	0.044±4	0.029±5	0.18±2	184±3	
12.1	156	1	0.01	5	0.00141	0.023	0.054±5	0.0352±7	0.26±3	223±4	
15.1	461	425	0.92	57	0.00066	0.011	0.062±1	0.1007±17	0.86±3	619±10	

Table 3.4 (continued)

spot	U (ppm)	Th (ppm)	Th/U	Total Pb (ppm)	$\frac{^{204}Pb}{^{206}Pb}$	f206 (%)	$\frac{^{207}Pb}{^{206}Pb}$	$\frac{^{206}Pb}{^{238}U}$	$\frac{^{207}Pb}{^{235}U}$	$\frac{^{206}Pb}{^{238}U}$ Age	$\frac{^{207}Pb}{^{206}Pb}$ Age
Sample W2											
19.1	809	150	0.19	29	0.00856	0.137	0.042±11	0.0234±6	0.14±4	149±4	
7.1	612	93	0.15	14	0.00048	0.008	0.049±3	0.0238±6	0.16±1	152±3	
15.1	283	14	0.05	7	0.00199	0.032	0.073±9	0.0238±6	0.24±3	152±4	
1.1	124	18	0.15	4	0.00334	0.053	0.062±22	0.024±9	0.2±7	153±5	
14.1	193	112	0.58	6	0.00302	0.048	0.056±15	0.0243±7	0.19±5	155±5	
2.1	1210	298	0.25	30	0.00039	0.006	0.05±3	0.0246±6	0.17±1	157±3	
13.1	785	290	0.37	20	0.00064	0.01	0.055±4	0.0246±6	0.19±1	157±4	
6.1	678	93	0.14	17	0.00069	0.011	0.054±4	0.0248±6	0.19±2	158±4	
5.1	565	523	0.93	17	0.00109	0.017	0.049±4	0.025±6	0.17±2	159±4	
17.1	333	62	0.19	9	0.00121	0.019	0.048±7	0.0252±6	0.17±3	160±4	
3.1	194	52	0.27	6	0.00351	0.056	0.05±14	0.0252±7	0.17±5	161±5	
4.1	307	111	0.36	9	0.00186	0.03	0.052±7	0.0256±6	0.18±3	163±4	
9.1	219	73	0.33	6	0.00237	0.038	0.054±12	0.0257±7	0.19±4	163±4	
10.1	1005	195	0.19	32	0.00418	0.067	0.048±6	0.0261±6	0.17±2	166±4	
12.1	153	9	0.06	5	0.00393	0.063	0.058±15	0.0298±9	0.24±6	189±5	
11.1	94	50	0.53	4	0.00502	0.08	0.062±25	0.0297±11	0.25±10	189±7	
18.1	802	20	0.03	23	0.00044	0.007	0.053±3	0.0302±7	0.22±1	192±4	
8.1	250	43	0.17	9	0.00145	0.023	0.058±7	0.0342±9	0.27±4	217±5	
16.1	572	737	1.29	301	0.00004	0.001	0.162±1	0.396±87	8.86±20		2479±6

Table 3.4 (continued)

spot	U (ppm)	Th (ppm)	Th/U	Total Pb (ppm)	$\frac{^{204}Pb}{^{206}Pb}$	f206 (%)	$\frac{^{207}Pb}{^{206}Pb}$	$\frac{^{206}Pb}{^{238}U}$	$\frac{^{207}Pb}{^{235}U}$	$\frac{^{206}Pb}{^{238}U}$ Age	$\frac{^{207}Pb}{^{206}Pb}$ Age
Sample W4											
16.1	128	94	0.74	3	0.00169	0.027	0.042±12	0.0219±5	0.13±4	139±3	
8.1	180	203	1.13	5	0.00091	0.015	0.047±8	0.0239±4	0.16±3	152±3	
1.1	478	267	0.56	13	0.00061	0.01	0.044±3	0.0247±3	0.15±1	157±2	
5.1	452	220	0.49	12	0.00067	0.011	0.044±3	0.0246±3	0.15±1	157±2	
4.1	271	33	0.12	7	0.00146	0.023	0.046±8	0.0268±5	0.17±3	171±3	
2.1	972	1123	1.16	35	0.00004	0.001	0.066±1	0.0294±4	0.27±1	186±2	
14.1	200	2	0.01	7	0.00085	0.014	0.045±5	0.0347±5	0.22±2	220±3	
13.1	597	23	0.04	20	0.00015	0.002	0.051±2	0.0357±5	0.25±1	226±3	
3.1	68	6	0.09	3	0.00085	0.014	0.071±23	0.0366±12	0.36±12	232±7	
11.1	180	17	0.1	7	0.00044	0.007	0.051±6	0.0387±7	0.27±3	245±4	
6.1	248	195	0.78	15	0.00069	0.011	0.056±4	0.0521±8	0.4±3	327±5	
7.1	538	668	1.24	74	0.00015	0.002	0.064±1	0.1088±14	0.95±2	666±8	
12.1	155	119	0.77	60	0.00006	0.001	0.111±1	0.3353±44	5.13±9		1816±17
15.1	358	111	0.31	147	0.00002	0	0.146±1	0.3844±48	7.74±11		2301±7
9.1	295	37	0.13	83	0.00002	0	0.175±1	0.2695±34	6.52±9		2610±8
10.1	77	32	0.41	48	0.00027	0.004	0.202±2	0.5471±77	15.26±26		2845±12

Twenty two analyses were made on 21 zircon grains, and ages range from 619 ± 10 Ma to 145 ± 3 Ma (Table 3.4 and Fig. 3.30).

Nineteen analyses of the youngest 19 grains from the sample form a coherent group (Group 1 in Fig. 3.30) with a weighted mean $^{206}Pb/^{238}U$ age of 156 ± 3 Ma and a chi-square value of 1.39. The U and Th contents of these 19 spots range from 34 ppm to 561 ppm and 23 ppm to 215 ppm, respectively. The Th/U ratios vary from 0.05 to 1.21. Since these euhedral grains are of igneous origin, the age of 156 ± 3 Ma is taken as the age of crystallization of the host monzogranite. Spot 3.1 yields an age of 184 ± 3 Ma (1σ) (Fig. 3.30), which may indicate the resetting of U-Th-Pb systems of older inherited zircons due to the influence of the later igneous events. Spot 12.1 is situated in the core of grain 12 and gives an age of 223 ± 4 Ma (1σ) (Fig. 3.30). This age represents inheritance from a possible earlier igneous source, as identified in the Cangshang granodiorite (Table 3.1). Spot 15.1 is located in the core of grain 15 and yields an age of 619 ±10 Ma (1σ) (Fig. 3.30). This core was inherited and mantled by a rim (spot 15.2) formed during the magmatic event at 160 ± 4 Ma (1σ) (Fig. 3.30).

Sample W2

Sample W2 was taken from the No. 1 orebody and is a grey-coloured, medium-grained sericite-quartz rock. It has undergone extensive silicification, sericite and pyrite alteration, and cataclasis. The rock is now composed of 60 percent quartz (most grains are anhedral and strongly deformed with undulose extinction; others are recrystallized), 40 percent sericite (variable grain size) and minor opaque minerals. Zircons are contained mainly in sericite aggregates and also within quartz. The zircon grains selected for analysis range in size from 132 μm to 74 μm and are pale brown or transparent. Most are euhedral with well-formed prism and pyramid faces. The average elongation ratio is about 2:1, with a maximum of 4:1.

A total of 19 analyses were carried out on 19 zircon grains, and ages range from 2479 ± 6 Ma to 149 ± 4 Ma (Table 3.4 and Fig. 3.31).

One zircon population is composed of 14 analyses, which form a coherent group (Group 1 in Fig. 3.31b) having a weighted mean $^{206}Pb/^{238}U$ age of 158 ± 4 Ma with a chi-square value of 1.67. The U and Th contents of these 14 spots vary from 124 ppm to 1210 ppm and 14 ppm to 523 ppm, respectively. The Th/U ratios range from 0.05 to 0.93. Kerrich and King (1993), Yeats et al. (1996), and Nesbitt et al. (1999) reported that hydrothermal zircons which were generated during the alteration

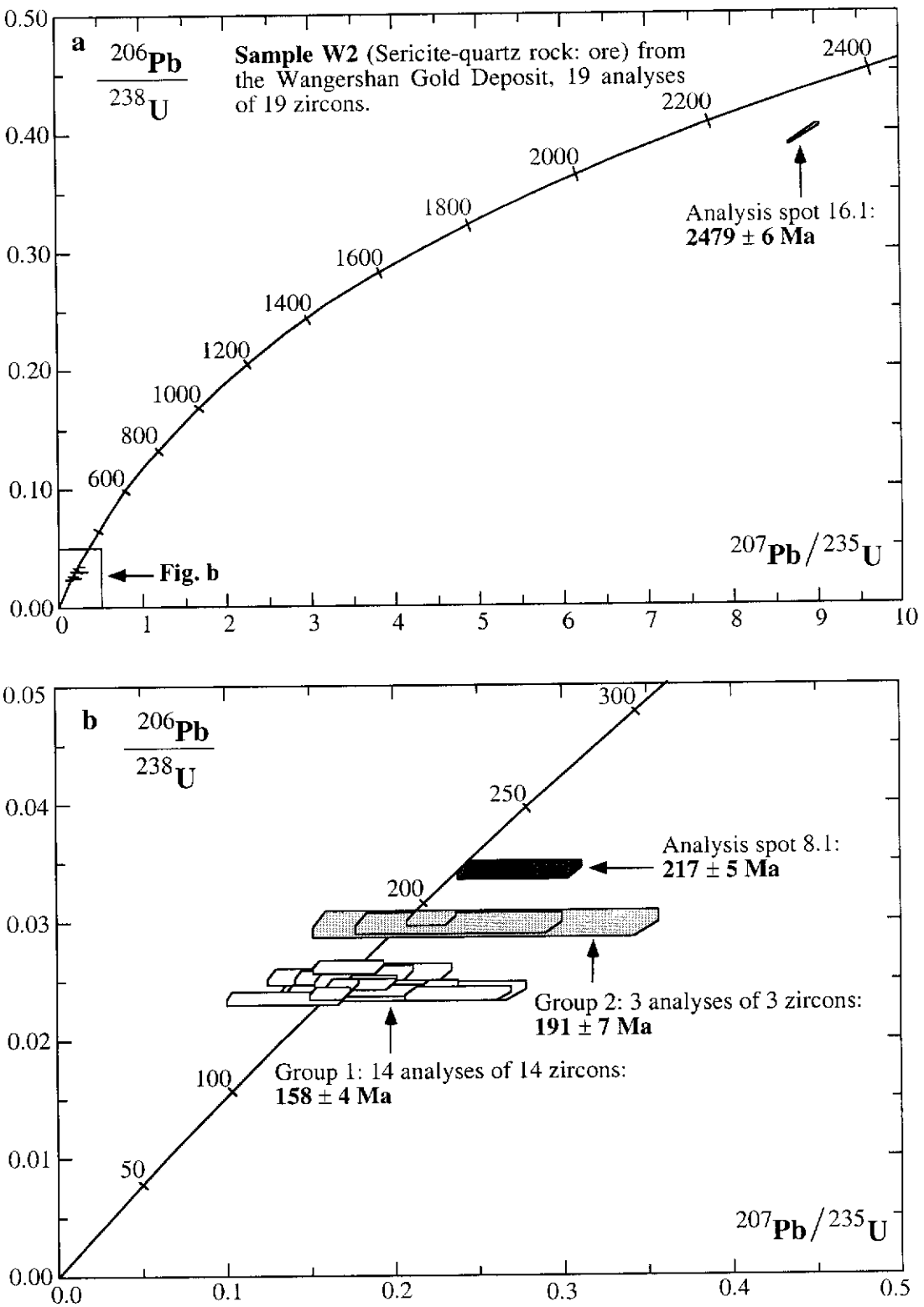

Fig. 3.31: U-Pb concordia diagrams showing (a) total SHRIMP data for Sample W2 from the Wangershan Gold Deposit and (b) enlargement detailing younger zircon populations.

process have been extracted from some ore zones. However, zircons separated from the No. 1 orebody of the Wangershan deposit are euhedral grains of an igneous origin, and the age of 158 ± 4 Ma is the same, within error, as the group age of 156 ± 3 Ma obtained from the host monzogranite, therefore, these grains were not affected by the gold-related hydrothermal event and still record the age of igneous crystallization of the host rock.

Another zircon population consists of only 3 analyses, which define a coherent group (Group 2 in Fig. 3.31b) having a weighted mean $^{206}Pb/^{238}U$ age of 191 ± 7 Ma with a chi-square value of 0.03. The U and Th contents of these 3 spots range from 94 ppm to 802 ppm and 9 ppm to 50 ppm, respectively. The Th/U ratios vary from 0.03 to 0.53. The three zircon grains are also euhedral and may have formed during an earlier igneous event at 191 ± 7 Ma, and then were incorporated by the main magmatic event at ~156 Ma.

Analysis spot 8.1 yields a near-concordant $^{206}Pb/^{238}U$ age of 217 ± 5 Ma (1σ) (Fig. 3.31b), which is coincident with the age of ca. 210-250 Ma for inherited zircons in the Cangshang granodiorite (Table 3.1) and Wangershan monzogranite (Table 3.4). Analysis spot 16.1 does not give a concordant age, but it records a $^{207}Pb/^{206}Pb$ age of 2479 ± 6 Ma (1σ) (Fig. 3.31a), indicating inheritance from Precambrian basement rocks.

Sample W4

Sample W4 was obtained from a narrow zone of cataclastic granite and is a leucocratic granitic cataclasite. Porphyroclasts are mainly composed of plagioclase (multiple twinning, sericite inclusions, myrmekitic texture) and quartz (strong deformation with undulose extinction); the matrix consists mainly of K-feldspar, quartz and plagioclase. Zircons selected for analysis range in size from +132 μm to -74 μm, and are pale brown in colour. Most grains are transluscent, and some contain inclusions. These zircons are mostly euhedral, with the elongation ratio ranging from 2:1 to 3:1; some are broken fragments.

Sixteen analyses were completed on 16 zircon grains, and ages range from 2845 ± 12 Ma to 139 ± 3 Ma (Table 3.4 and Fig. 3.32).

One zircon population is composed of 3 analyses, which form a coherent group (Group 1 in Fig. 3.32b) having a weighted mean $^{206}Pb/^{238}U$ age of 156 ± 7 Ma with a

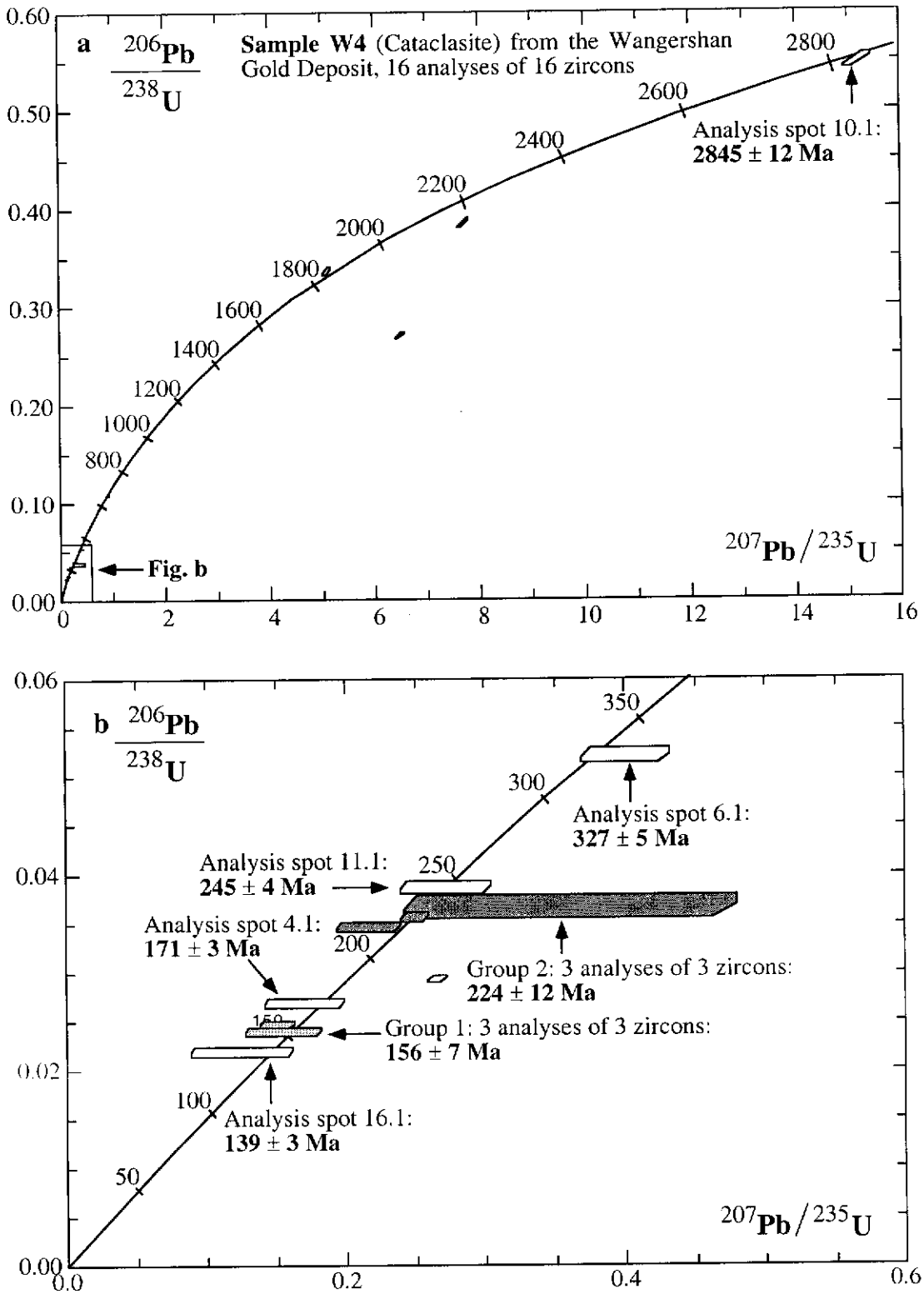

Fig. 3.32: U-Pb concordia diagrams showing (a) total SHRIMP data for Sample W4 from the Wangershan Gold Deposit and (b) enlargement detailing younger zircon populations.

chi-square value of 1.1. The U and Th contents of these 3 spots range from 180 ppm to 478 ppm and 203 ppm to 267 ppm, respectively. The Th/U ratios vary from 0.49 to 1.13. These grains are euhedral, and this group age of about 156 Ma coincides with the age of the least-deformed monzogranite (sample W1) (Fig. 3.30).

Another zircon group also comprises 3 analyses, which define a coherent group (Group 2 in Fig. 3.32b) having a weighted mean $^{206}Pb/^{238}U$ age of 224 ± 12 Ma with a chi-square value of 1.24. The U and Th contents of these 3 spots range from 68 ppm to 597 ppm and 2 ppm to 23 ppm, respectively. The Th/U ratios vary from 0.01 to 0.09. The 3 spots are all located in the centre of zircons, hence the age of 224 ± 12 Ma represents the age of the core or the whole grain which may have been generated during an earlier igneous event. This event has previously been recorded in the Cangshang granodiorite (Table 3.1).

Analysis spot 16.1 is located in the core of grain 16 and yields a concordant $^{206}Pb/^{238}U$ age of 139 ± 3 Ma (1σ) (Fig. 3.32b). The U and Th content of this spot are 128 ppm and 94 ppm, respectively. Since grain 16 is euhedral, the age of 139 ± 3 Ma (1σ) is interpreted to represent the timing of a later igneous event or disturbance of ~156 Ma population by some even younger event.

Spots 4.1, 11.1 and 6.1 give concordant $^{206}Pb/^{238}U$ ages of 171 ± 3 Ma (1σ), 245 ± 4 Ma (1σ) and 327 ± 5 Ma (1σ) (Fig. 3.32b), respectively, which may indicate the resetting of U-Th-Pb systems of older inherited zircons due to the influence of later geological events or else record a mixing age. Analysis spot 10.1 yields the oldest inherited concordant $^{207}Pb/^{206}Pb$ age of 2845 ± 12 Ma (1σ) (Fig. 3.32a), again indicating that the rocks were developed within Precambrian basement.

3.5.8 Summary

The Wangershan Gold Deposit is hosted by Linglong monzogranite. Both Jiaojia-style and Linglong-style of gold mineralization occur at this deposit, depending on structural setting. The former is associated with compression and the latter is related to tension. The No.1, No.2 and No.3 orebodies are situated in the No. AI alteration zone, which is controlled by the Wangershan-Hedong Fault Zone. The degree of sericitization, silicification and sulphidation, which are considered to be gold-related alterations, increase towards the orebodies, although no distinct zonation can be identified.

SHRIMP U-Pb zircon dating of samples from the host monzogranite, the No.1 orebody and a narrow zone of cataclastic granite was undertaken. The weighted mean $^{206}Pb/^{238}U$ age of 156 ± 3 Ma is considered to be the crystallization age of the host, which is consistent with the Jurassic age of the Linglong granitoid (165 to 150 Ma) obtained by Wang et al. (1998). Zircons from the No.1 orebody were extracted in order to test if hydrothermal zircons were formed during gold-related alteration. However, the zircons are euhedral, indicative of an igneous origin, and they yield a weighted mean $^{206}Pb/^{238}U$ age of 158 ± 4 Ma which is the same age as the host rock. The youngest concordant $^{206}Pb/^{238}U$ age of 139 ± 3 Ma was obtained from the sample from the narrow deformed zone. This age is interpreted to represent the age of a later igneous event such as dyke intrusion. In the all three samples (W1, W2 and W4) dated from this deposit, there exist inherited zircons yielding ages of ca. 210-250 Ma, which represents the timing of a significant earlier igneous event in this region. Two of the three samples also contain inherited Archaean zircon, indicating the existence of Precambrian basement rocks.

3.6 Linglong Goldfield

The Linglong Goldfield (lat. 37°25'00" to 37°35'00" N; long. 120°26'15" to 120°33'45" E) is located approximately 12 km northeast of the city of Zhaoyuan (Fig. 3.1), and encompasses an area of ca. 70 km^2. The mining history of this goldfield can be traced back to 1007 A. D., and its estimated gold production has been more than 200 tonnes (Kong, 1989). The Linglong Goldfield is hosted by the Linglong granitoids, which form an area of steep topography. The Luoshan (elevation of 758.5 m) and Shuangding (elevation of 672.6 m) are the highest and second highest mountains in the region, respectively. This goldfield is famous for vein-filling type lode gold, which was named the Linglong-style and was thought to be the only lode style in the goldfield prior to 1966. However, based on regional reconnaissance and drilling, the No.6 Team of Geology and Exploration, BGMRSP, discovered the Jiaojia-style (i.e. disseminated-and-veinlet type) lode gold along the Potouqing Fault Zone within the Linglong Goldfield (Fig. 3.33) in 1966, which indicates that both styles of gold lode can coexist in the region. It is widely held that the Linglong Goldfield is structurally controlled by the Potouqing Fault Zone (Fig. 3.33) and its branch structures (Zhang et al., 1973; Gong, 1989; Kong et al., 1991; Qiu et al., in press).

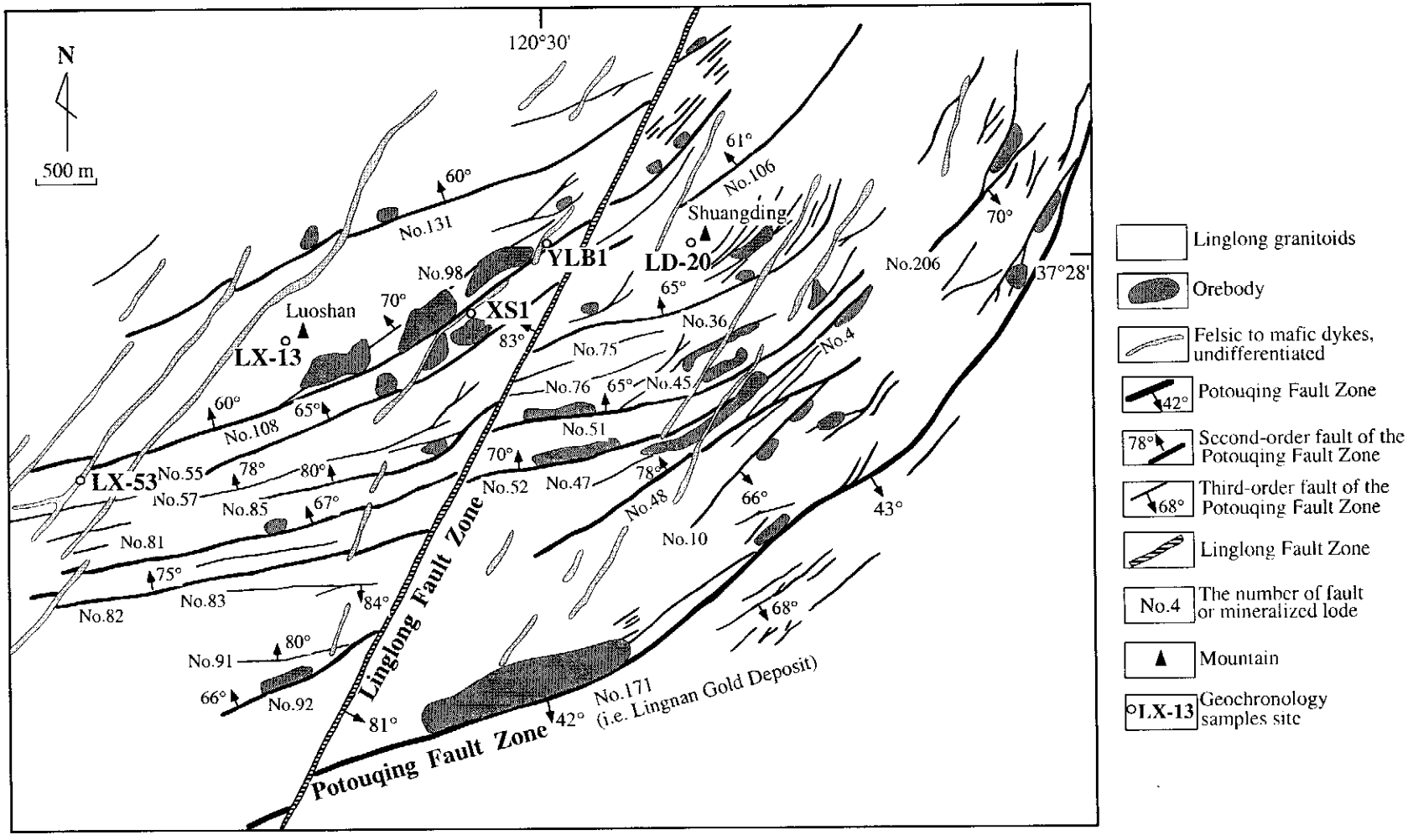

Fig. 3.33: Geological map of part of the Linglong Goldfield, showing the distribution of structural features, orebodies and dykes (modified from Zhang et al., 1973).

3.6.1 Lithological Units

The Linglong Goldfield is dominated by the Linglong granitoids (Fig. 3.33), which mainly consist of fine- to medium-grained monzogranite and granodiorite, and locally have gneissic textures. Several types of dyke are present within the goldfield (Luo et al, 1996), with intermediate and mafic dykes widely developed (Zhang et al., 1973; Kong et al., 1989).

3.6.2 Fault Zones

Potouqing Fault Zone and lower order related faults

The Potouqing Fault Zone, located in the southeast margin of the Linglong Goldfield (Fig. 3.33), is widely considered to be a first-order structure (Kong, 1989; Kong et al, 1991). It is a northern extension of the regional-scale Zhao-Ping Fault Zone which is about 200 km in length and roughly strikes 020° (Fig. 3.1) (Gong, 1989). The strike of the Potouqing Fault Zone is variable, swinging from 070° in the southwest to 010° in the northeast, and it dips ca. 40°SE (Fig. 3.33). The length of this fault zone is over 10 km and its width varies from 100 to 400 m. A wavy main fault plane, marked by a fault gouge zone with a thickness ranging from 10 to 20 cm, is well-developed. The sense of movement is reverse and oblique towards the northeast direction, with sinistral offset (Kong et al., 1991).

The second-order faults of the Potouqing Fault Zone are all situated in its footwall (Fig. 3.33). They strike 040°-080° and generally dip in a northwest direction with an angle of 50°-75°; they vary from hundreds to thousands of metres in length and from a few to tens of metres in width (Gong, 1989). Among them, the longest is the No.108 Fault (Fig. 3.33) which is 5,000 m in length, and strikes 050°-080° and dips 60°NW. The sense of movement on these faults is the same as that of the Potouqing Fault Zone, which is reverse and oblique, with sinistral offset (Kong et al., 1991).

The third-order faults of the Potouqing Fault Zone are generally the branches of the second-order faults (Fig. 3.33). They range from ca. 100 to 1000 m in length and from 0.3 to 5 m in width. One set of these faults, including the No.57, No.75, No.76 and No.83, strike 060°-080° and dip 60°-85° NW or SE; another set, including the No.10, No.45 and No.98, strike 030° to 050° and dip 60°-80° NW or SE; they intersect with the second-order faults at ca. 20° in plan (Fig. 3.33) (Zhang et al., 1973).

Linglong Fault Zone

The Linglong Fault Zone is situated in the central part of the Linglong Goldfield (Fig. 3.33). It strikes 025° and dips in a northwest or southeast direction with an angle of ca. 80°; it is about 8.000 m in length and ranges from 50 to 100 m in width. This fault cuts the Potouqing Fault Zone and its branch structures (Fig. 3.33), hence, it post-dates the formation of the Potouqing Fault System. The sense of movement is strike-slip, with sinistral offset (Kong et al., 1991).

3.6.3 Main Mineralized Lodes and Orebodies

Jiaojia-style

The typical Jiaojia-style (i.e. disseminated-and-veinlet type) occurrence is represented by the No.171 mineralized lode (Fig. 3.33) (also called the Lingnan Gold Deposit). The No.1 orebody within the No.171 lode, contains 90% of the total gold reserves (>100 tonnes), strikes 060°-070° and dips 38°-40°SE. It is 1,080 m in length along strike and varies from 0.7 m to 32.4 m (average of 8.2 m) in thickness and extends for a depth of 1,400 m down-dip. The gold grade ranges from 1.56 g/t to 12.34 g/t, with an average grade of 5.35 g/t (Guo et al., 1989).

Linglong-style

About 200 Linglong-style (i.e. vein-filling type) lodes occur throughout the Linglong Goldfield (Kong et al., 1991). Among them, the No.108 lode is the largest, with total gold reserves of more than 10 tonnes. It is about 5 km in length and ranges from 3 to 5 m in thickness. This lode includes 13 orebodies. The average grade is 20.15 g/t, with a maximum of ca. 500 g/t; the largest orebody is 320 m in length (Gong, 1989; Kong et al., 1991). The second largest mineralized lode is the No.55, with total gold reserves of ca. 5 tonnes. It is about 3 km in length and averages 2.8 m in width. This lode includes 6 orebodies. The average grade is 23.3 g/t and the largest orebody is 240 m in length (Gong, 1989; Kong et al., 1991).

3.6.4 Structural Controls on Mineralized Lodes and Orebodies

The No.171 mineralized lode within the Linglong Goldfield is controlled by the first-order Potouqing Fault Zone (Fig. 3.33), and is similar to other Jiaojia-style gold

deposits in this region, such as the Cangshang, Sanshandao and Jiaojia Deposits. The No.1 orebody of this lode is situated 5 to 25 m below the main fault plane and is broadly parallel to it (Guo et al., 1989). It is tabular in shape, and locally branches or merges along the strike and dip directions (Figs. 3.34a and 3.34b).

The Linglong-style mineralized lodes are strictly delimited by the second- and/or third-order faults of the Potouqing Fault Zone (Fig. 3.33). These lodes are given the same numbers as the faults controlling them, for example, the No.108 lode is controlled by the No.108 fault. The preferred sites of orebodies within this kind of lode include: (a) flexures of faults along strike; (b) positions where the dip angle changes; (c) fault intersections; (d) tension gashes created by fault movement (Lu and Kong, 1993; Luo et al., 1996). Since some lodes such as the No.92 experienced sinistral shearing, their orebodies exhibit left-lateral en-echelon arrays (Fig. 3.35) (Chen and Li, 1989).

3.6.5 Alteration

The most common wall-rock alteration styles of the Linglong Goldfield include silicification, sericitization, pyritization, potassic alteration and carbonation of host Linglong granitoids (Kong, 1989). Mineralized lodes, including the Linglong- and Jiaojia-style, exhibit essentially similar alteration patterns and alteration mineral assemblages, which may reflect broadly uniform wall-rock compositions, identical mineralizing fluids and similar P-T conditions of mineralization. The only difference in alteration between the Linglong- and Jiaojia-style gold occurrences is the alteration scale: the former is of a smaller scale, with alteration widths ranging from a few metres to ca. 10 m; whereas the latter are larger, with alteration widths varying from tens to hundreds of metres (Fig. 3.34) (Luo et al., 1996). Although there are no clear boundaries between different zones, wall-rock alteration is commonly zoned and is most intense near the main fault plane. Based on the alteration type and intensity, three alteration zones can be roughly identified (Fig. 3.36) (Yao et al., 1990). The most intense alteration zone (I) is characterised by strong pyritization, silicification and sericitization and consists of quartz-sericite-pyrite rock; zone II is characterised mainly by silicification and sericitization and is composed of quartz-sericite rock; the weakest alteration zone (III) is characterised by weak silicification and sericitization, and K-feldspar alteration and consists of weakly-altered Linglong granitoids. However, in some deposits, such as the No.171 mineralized lode, only two alteration zones (I and III) can be identified (Fig. 3.34a) (Wang et al., 1989).

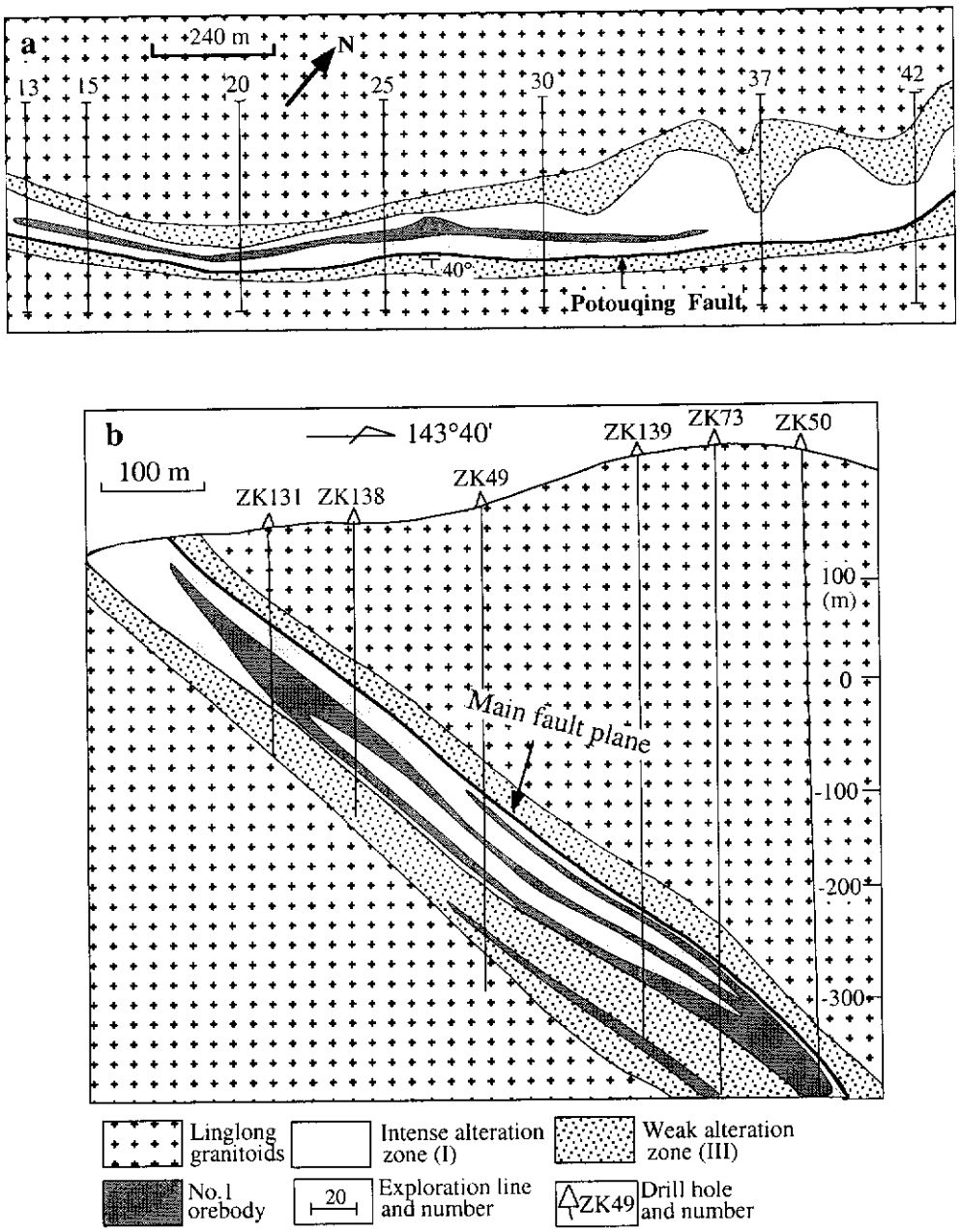

Fig. 3.34: (a) Geological plan of part of the No.171 mineralized lode in the Linglong Goldfield; (b) vertical section along part of the No.13 exploration line (modified from Wang et al., 1989).

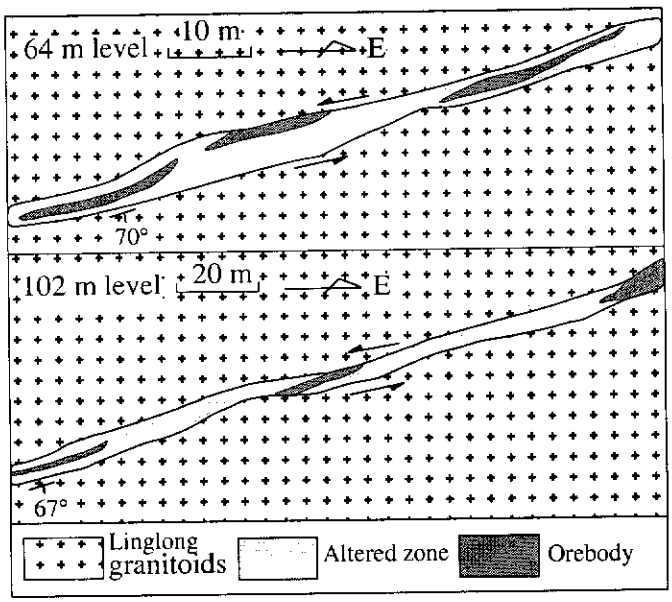

Fig. 3.35: Part of orebodies of the No.92 lode within the Linglong Goldfield, showing a sinistral en-echelon array (modified from Chen and Li, 1989).

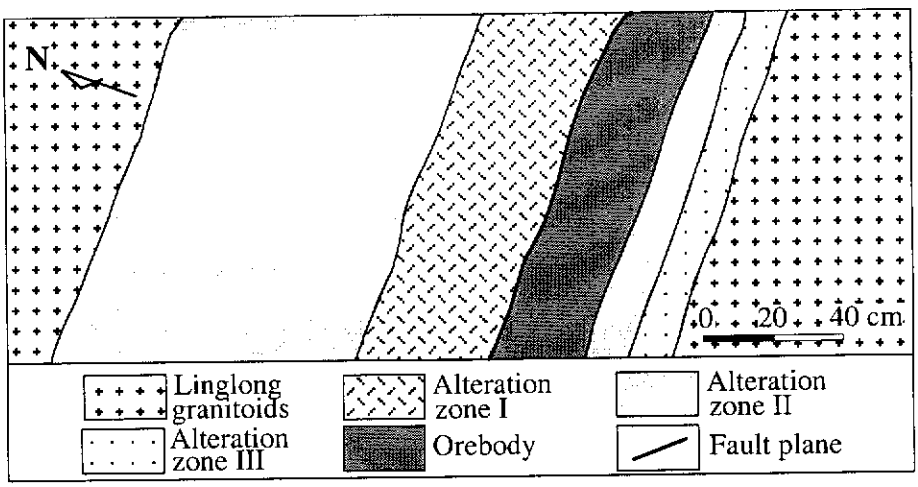

Fig. 3.36: Sketch of part of the No.108 mineralized lode at the 300 m level in the Linglong Goldfield, showing the alteration zones (Kong, 1989).

3.6.6 Ore Mineralogy and Paragenesis

Both the Jiaojia-style and Linglong-style ores have similar mineralogy and paragenesis within the Linglong Goldfield (Kong, 1989). Ore minerals include mainly pyrite, chalcopyrite, sphalerite, galena, pyrrhotite, magnetite and hematite. Among them, pyrite is the most abundant and makes up about 87% of the ore minerals. Three distinct generations of pyrite can be recognized. The first type consists of coarse (>5 mm) euhedral grains, which occur in disseminated form in the ores. The second generation of pyrite comprises medium (1-5 mm) subhedral grains which occur mainly in aggregates in the ores and form the main gold-bearing mineral. Fractures are well-developed in this kind of pyrite, and later metal sulphides and electrum occur as infillings. The third generation is composed of fine (0.1-0.5 mm) grains, which occur mainly in veinlet form in the ores. Gangue minerals consist of quartz, sericite and plagioclase, with minor biotite, carbonate and barite. Gold minerals are chiefly electrum and trace amounts of native gold, which occurs as small enclaves and infillings carried by pyrite, chalcopyrite and quartz (Kong, 1989).

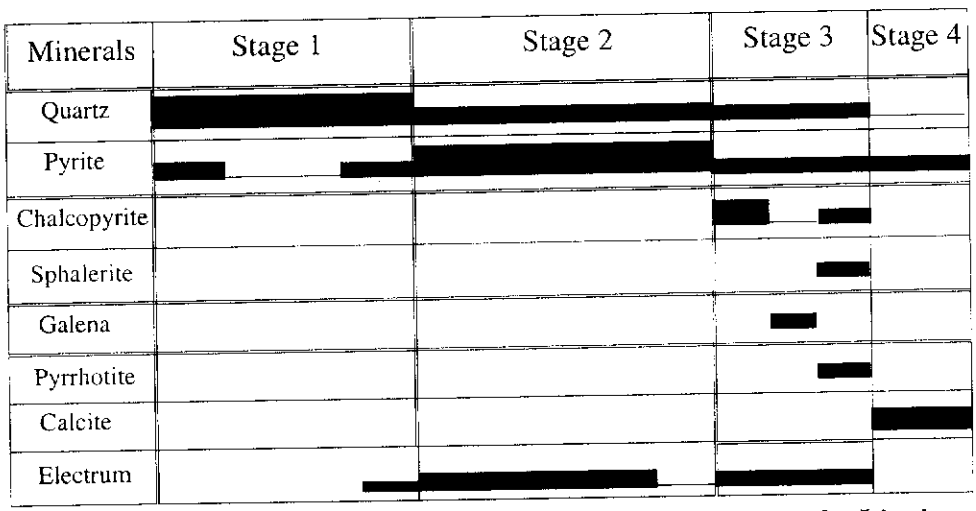

Fig. 3.37: Paragenetic sequence of hydrothermal minerals at the Linglong Goldfield. Thickness is proportional to relative abundance of each mineral phase (after Kong, 1989).

Based on mineralogical, textural, and crosscutting relationships observed in the field and hand specimens, four stages of hydrothermal mineral formation have been identified (Fig. 3.37) (Kong, 1989). From the oldest to the youngest these stages are: stage 1: pyrite-quartz, with the mineral assemblage consisting mainly of coarse, milk-white quartz and a small amount of coarse pyrite; stage 2: gold-quartz-pyrite, where the mineral assemblage is mainly composed of medium-grained pyrite and smoke-grey coloured quartz; stage 3: gold-quartz-base metal sulphides, with the mineral

paragenesis dominated by fine-grained pyrite, chalcopyrite, galena, sphalerite and quartz; stage 4: quartz-calcite, with the mineral paragenesis consisting almost entirely of calcite and quartz. Stage 2 is the main period of gold mineralization, with stage 3 also important (Kong, 1989).

3.6.7 Dykes

Dykes, including felsic, intermediate and mafic types, are widely distributed within the Linglong Goldfield (Fig. 3.33). They range from less than one metre to several kilometres in length and from a few centimetres to more than ten metres in width, with an average density of 10 dykes per square kilometre (Yao et al., 1990). The felsic dykes are mainly porphyry, the intermediate dykes consist chiefly of microdiorite, and the mafic dykes mainly comprise dolerite and lamprophyres (Yao et al., 1990).

The intermediate and mafic dykes are said to be closely related to gold mineralization in both space and time (Liu et al., 1991). Although some dykes trend 040°-080°, which is the trend of the orebodies, most of these dykes strike 010°-020° and dip 50°-70°NW. Based on the crosscutting relationship between the dykes and orebodies, and whether the dykes were affected by the late stage gold mineralization, the dykes can be subdivided into three kinds: they either predate, are synchronous with, or post-date gold mineralization (Yao et al., 1990; Liu et al., 1991 and Luo et al., 1996). Dykes which crosscut orebodies but contain the late stage gold-bearing quartz-sulphide veinlets, are considered to be emplaced during the gold mineralization (Fig. 3.38). From studies of trace elements, rare earth elements and isotopes, the magma of the intermediate and mafic dykes and auriferous ore fluid are considered to have originated from the same deep-seated source (Yao et al., 1990; Liu et al., 1991).

3.6.8 SHRIMP Zircon U-Pb Dating

Linglong Granitoids (host rock)

Wang et al (1998) dated two samples (LD-20 and LX-13 on Fig. 3.33) of Linglong granitoids from the Linglong Goldfield by SHRIMP U-Pb zircon methods. In order not to repeat work, no Linglong granitoids within this goldfield were dated as part of this investigation. Wang et al (1998) reported that nineteen analyses of magmatic zircons from sample LD-20 (porphyritic granodiorite) yielded a weighted mean $^{206}Pb/^{238}U$ age of 153 ± 4 Ma, and thirteen analyses of magmatic zircons from

sample LX-13 (medium-grained granite) gave a weighted mean $^{206}Pb/^{238}U$ age of 158 ± 4 Ma. The age of ca. 150-160 Ma is interpreted as the crystallization age of the magmatic zircon population (Wang et al., 1998).

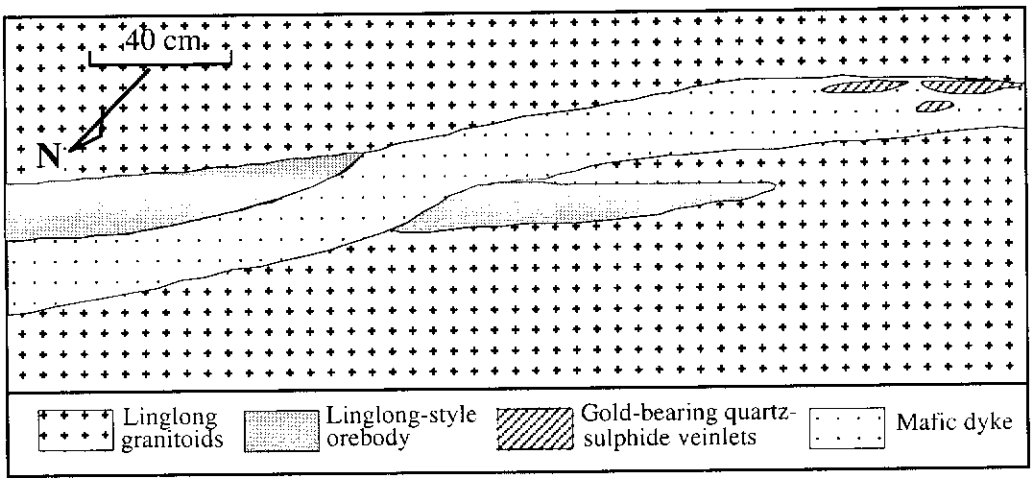

Fig. 3.38: Part of the No. 55 gold-bearing lode at the 260 m level in the Linglong Goldfield, showing a mafic dyke cutting the orebody and itself containing late-stage gold-bearing quartz-sulphide veinlets (Yao et al., 1990).

Dykes

In order to constrain the timing of mineralization, samples XS1 (Fig. 3.39) and YLB1 (Fig. 3.33) from dykes closely related to gold mineralization were selected for SHRIMP analysis in this study. SHRIMP results for the samples are listed in Table 3.5 and illustrated on concordia plots in Figures 3.40 and 3.41. Wang et al. (1998) dated a sample LX-53 (Fig. 3.33) from a post-mineralization dyke in this goldfield by SHRIMP U-Pb zircon methods, and the results are illustrated on a concordia plot (Fig. 3.42). Following are the description of my samples XS1 andYLB, as well as Wang et al.'s sample LX-53, and the interpretation of all three SHRIMP zircon U-Pb ages.

Sample XS1

Sample XS1 was taken from a mafic dyke which was exposed in an underground drive (Fig. 3.39) and was classified as lamprophyre by local geologists. Due to strong alteration, the sample cannot be identified exactly from thin section. It is considered that the dyke intruded during mineralization because it cuts the Linglong-style orebody and was itself altered. The zircon grains selected for analysis range in size from 132 μm to 74 μm and are nearly colourless. Most are euhedral with well-formed prism and pyramid faces, and the elongation ratio varies from 2:1 to 3:1; some are broken fragments.

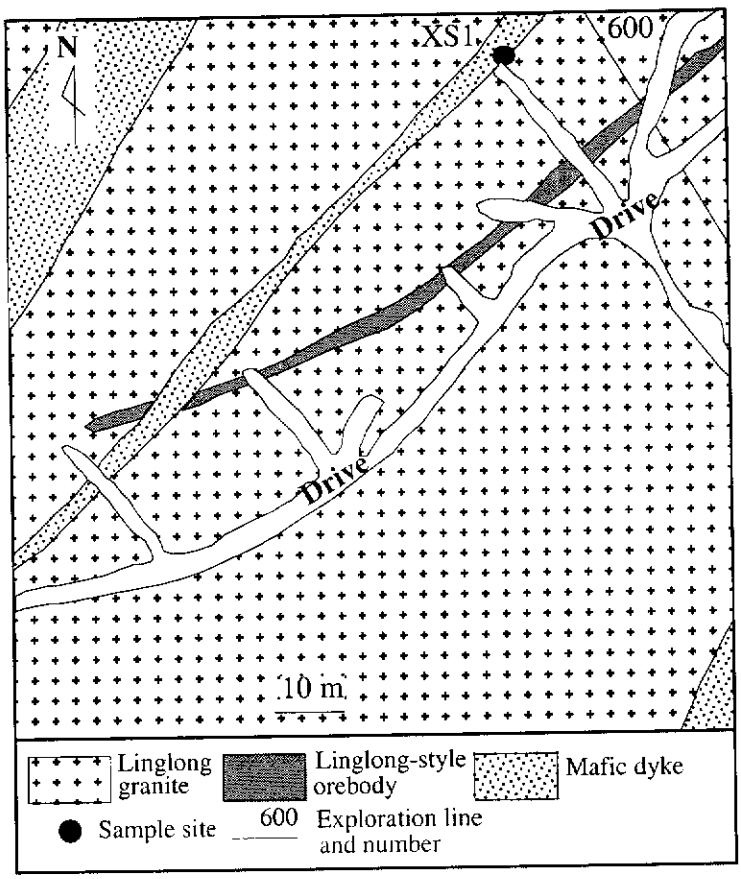

Fig. 3.39: Plan showing part of the No. 55 gold-bearing lode at the 230 m level in the Linglong Goldfield, showing a mafic dyke cutting the orebody. Also shown is the location of sample XS1.

Since only a few zircons of good quality (no inclusions and cracks) were separated, a total of only 12 analyses were carried out on 10 grains, and ages range from 2799 ± 3 Ma to 113 ± 3 Ma (Table 3.5 and Fig. 3.40). Because the zircon populations are strongly discordant, with variations in common lead indicating that the ^{204}Pb correction is not really appropriate for the sapmle, the ^{208}Pb correction was used for these data.

One zircon population (Group 1) is composed of 7 analyses, which form a coherent group (Fig. 3.40b) having a weighted mean $^{206}Pb/^{238}U$ age of 119 ± 5 Ma with a chi-square value of 2.47. The U and Th contents of these 7 spots range from 95 ppm to 968 ppm and 93 ppm to 1037 ppm, respectively. The Th/U ratios vary from 0.22 to 1.35. Since these euhedral grains with good pyramid terminations are of igneous origin, the age of 119 ± 5 Ma is taken as the intrusive age of the dyke. If the dyke did indeed accompany gold mineralization, then this might also record the timing of this event.

Table 3.5: SHRIMP U-Pb data for zircons from samples XS1 and YLB1 from the Linglong Goldfield. Analyses are listed in order of increasing age. The following notation is used for analysed grains: 1.1=grain 1, first point analysed. Data for sample XS1 are ^{208}Pb-corrected. Individual analyses have a 1σ error. The $^{206}Pb/^{238}U$ age is adopted for zircons with an age of less than 1.0 Ga, otherwise, the $^{207}Pb/^{206}Pb$ age is used.

spot	U (ppm)	Th (ppm)	Th/U	Total Pb (ppm)	$\frac{^{204}Pb}{^{206}Pb}$	f206 (%)	$\frac{^{207}Pb}{^{206}Pb}$	$\frac{^{206}Pb}{^{238}U}$	$\frac{^{207}Pb}{^{235}U}$	$\frac{^{206}Pb}{^{238}U}$ Age	$\frac{^{207}Pb}{^{206}Pb}$ Age
Sample XS1											
10.1	968	214	0.22	18	0.00085	0.014	0.046±15	0.0176±4	0.11±1	113±3	
6.1	194	185	0.95	6	0.00198	0.032	0.02±6	0.0177±4	0.05±2	113±3	
1.1	201	93	0.46	7	0.01119	0.179	0.047±64	0.0187±5	0.12±2	119±3	
10.2	95	98	1.04	3	0.00067	0.011	0.018±97	0.0188±5	0.05±3	120±3	
4.1	452	404	0.89	11	0.00063	0.01	0.047±30	0.0189±4	0.12±1	121±3	
5.1	768	1037	1.35	20	0.00043	0.007	0.045±26	0.0192±4	0.12±1	123±3	
2.1	854	742	0.87	20	0.0014	0.022	0.051±2	0.0195±1	0.14±1	124±3	
7.2	607	93	0.15	14	0.00063	0.01	0.047±19	0.0213±5	0.14±1	136±3	
7.1	956	187	0.2	22	0.00058	0.009	0.048±11	0.0228±5	0.15±1	145±3	
8.1	177	31	0.17	5	0.00146	0.023	0.045±38	0.0231±6	0.14±1	147±4	
9.1	215	79	0.37	20	0.00032	0.005	0.032±16	0.0801±18	0.36±2	497±11	
3.1	1054	14	0.01	579	0	0	0.197±4	0.5323±118	14.44±33		2799±3
Sample YLB1											
10.1	504	274	0.54	12	0.00483	0.077	0.033±10	0.0174±3	0.08±2	111±2	
9.1	396	473	1.19	15	0.0099	0.158	0.053±15	0.019±4	0.14±4	121±2	
7.1	134	157	1.17	5	0.01091	0.175	0.05±29	0.0196±7	0.14±8	125±4	
11.1	1047	240	0.23	23	0.00156	0.025	0.048±4	0.0205±2	0.13±1	131±1	
6.1	250	16	0.06	8	0.00715	0.114	0.055±16	0.0219±5	0.17±5	140±3	

Table 3.5 (continued)

spot	U (ppm)	Th (ppm)	Th/U	Total Pb (ppm)	$\frac{^{204}Pb}{^{206}Pb}$	f206 (%)	$\frac{^{207}Pb}{^{206}Pb}$	$\frac{^{206}Pb}{^{238}U}$	$\frac{^{207}Pb}{^{235}U}$	$\frac{^{206}Pb}{^{238}U}$ Age	$\frac{^{207}Pb}{^{206}Pb}$ Age
2.1	514	45	0.09	13	0.0032	0.051	0.049±7	0.0224±3	0.15±2	142±2	
5.1	159	126	0.79	7	0.00947	0.152	0.017±22	0.0247±7	0.06±7	157±4	
12.1	207	4	0.02	9	0.00711	0.114	0.046±16	0.03±6	0.19±7	191±4	
8.1	200	18	0.09	9	0.00563	0.09	0.037±12	0.0349±6	0.18±6	221±4	
1.1	73	45	0.62	4	0.00039	0.006	0.065±8	0.0491±9	0.44±5	309±5	
13.1	522	19	0.04	41	0.00108	0.017	0.06±2	0.0794±8	0.65±2	493±5	
3.1	262	467	1.79	44	0.00085	0.014	0.067±2	0.1142±13	1.05±4	697±7	
4.1	359	715	1.99	66	0.00106	0.017	0.061±2	0.1231±13	1.04±4	749±7	
14.1	422	132	0.31	136	0.00036	0.006	0.113±1	0.3022±30	4.72±6		1852±13

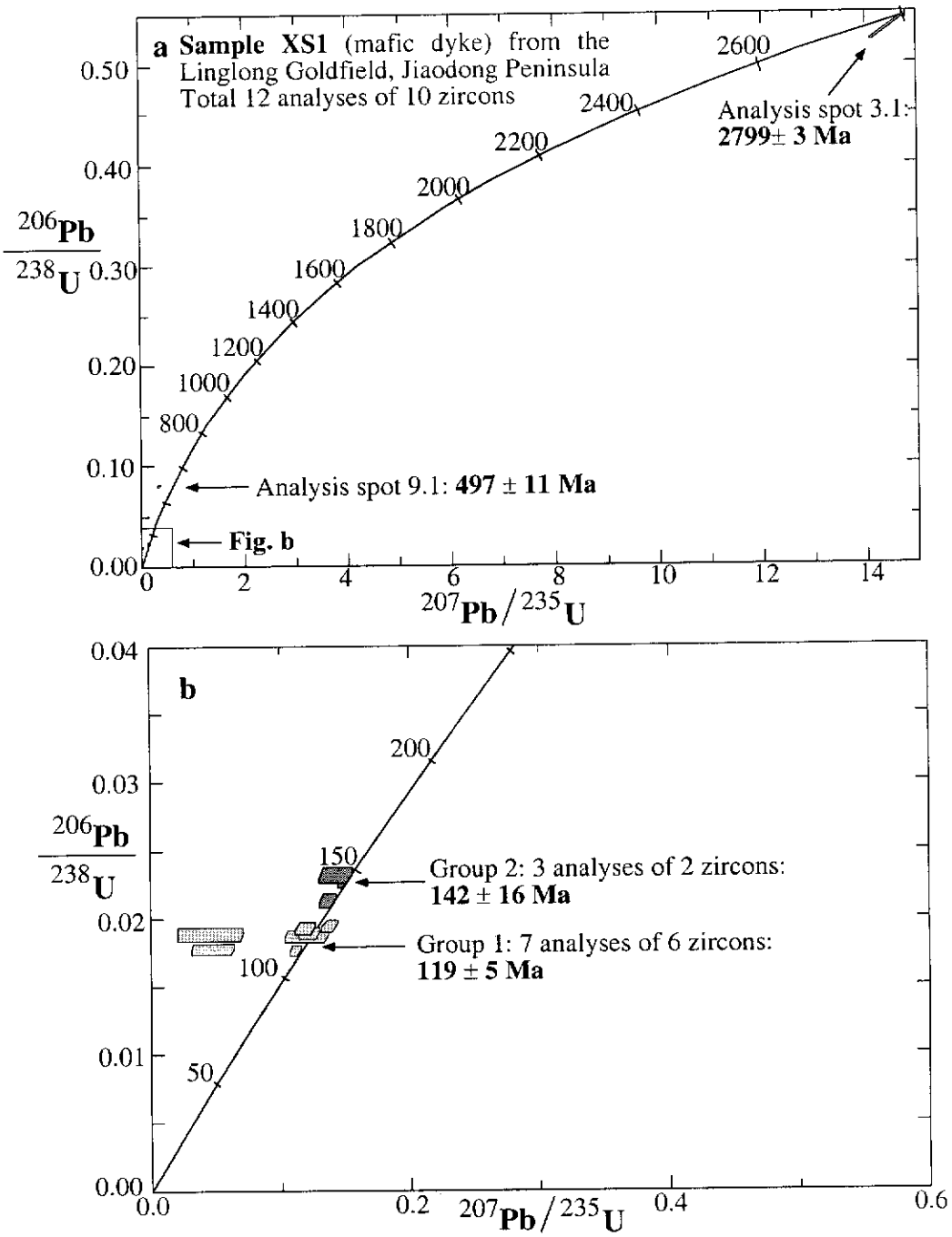

Fig. 3.40: U-Pb concordia plots showing (a) total SHRIMP zircon analytical data from sample XS1 and (b) enlargement detailing the main magmatic zircon populations (shaded areas).

Another zircon population (Group 2 in Fig. 3.40b) comprises 3 analyses of 2 zircons, which yields a weighted mean $^{206}Pb/^{238}U$ age of 142 ± 16 Ma with a chi-square value of 2.78. The U and Th contents of these 3 spots range from 177 ppm to 956 ppm and 31 ppm to 187 ppm, respectively. The Th/U ratios vary from 0.15 to 0.2. The 2 zircon grains are euhedral, and this group age of about 150 Ma coincides with the age of Linglong granitoid (150-160 Ma) (Wang et al., 1998). Accordingly, these grains have formed during an igneous event at ca. 150-160 Ma, and then were incorporated by the later dyke intrusion event at ~ 119 Ma. These grains occur as inherited cores rimmed by younger zircon overgrowths.

Of the remaining analyses, spot 9.1 of grain 9 gives a discordant $^{206}Pb/^{238}U$ age of 497 ± 11 Ma (1σ) (Fig. 3.40a). spot 3.1 of grain 3 yields a concordant $^{207}Pb/^{206}Pb$ age of 2799 ± 3 Ma (1σ) (Fig. 3.40a). It is a euhedral zircon and optically homogeneous, and is indistinguishable from the main magmatic zircon population in morphology. It indicates that this region is underlain by Precambrian basement and zircons with Archaean ages may reflect the sources of Mesozoic granitoids within the area or else were incorporated during ascent of the dyke.

Sample YLB1

Sample YLB1 (lat. 37°28'17" N; long. 120°30'21" E) was collected from an intermediate dyke (Fig. 3.33) which crops out at the surface and is strongly weathered. This dyke was classified as microdiorite by local geologists. It contains some cubic pseudomorphs of pyrite, which indicates that the dyke experienced sulphide alteration. It is considered that the dyke intruded during the mineralization, because this dyke also occupies the same space as the Linglong-style No.108 lode. The zircon grains selected for analysis range in size from 132 μm to 74 μm and are pale brown or transparent. The average elongation ration is about 3:1, with a maximum of 5:1. Some are euhedral with good crystal shapes, and some are broken fragments.

Fourteen analyses were made on 14 zircon grains. and ages range from 111 ± 2 Ma to 1852 ± 13 Ma (Table 3.5 and Fig. 3.41). The interpretation of these zircon U-Pb ages is complicated, since no single statistical group could be defined.

Analysis spot 10.1 gives a $^{206}Pb/^{238}U$ age of 111 ± 2 Ma (1σ) (Fig. 3.41b), which is interpreted to be the result of post-crystallization Pb-loss (Wang et al., 1998). Analysis spots 7.1 and 9.1 yield a weighted mean $^{206}Pb/^{238}U$ age of 122 ± 2 Ma with a chi-square value of 0.49 (Fig. 3.41b). Analysis spot 11.1 gives a concordant

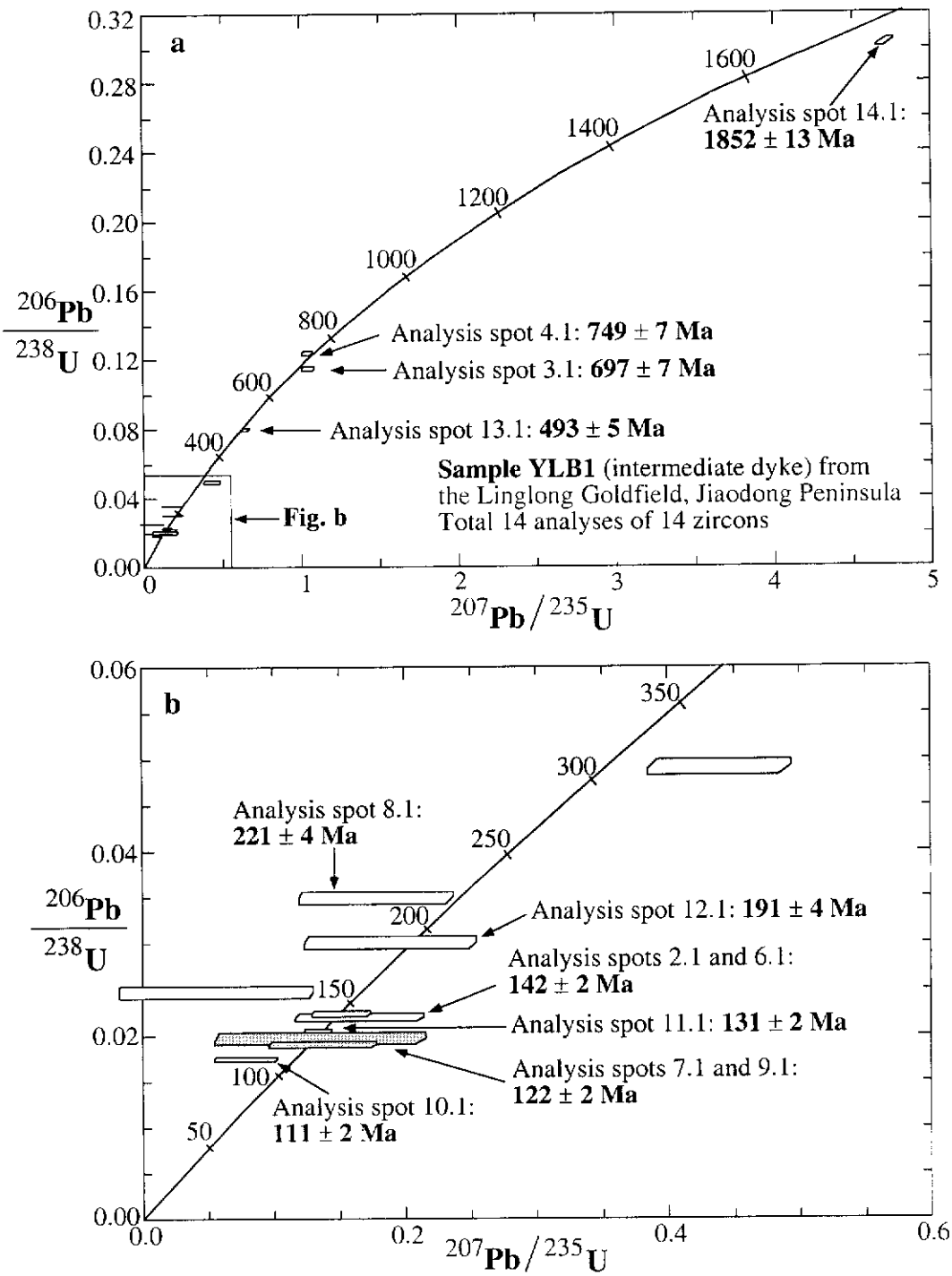

Fig. 3.41: U-Pb concordia plots showing (a) total SHRIMP zircon analytical data from sample YLB1 and (b) enlargement detailing the main magmatic zircon population (shaded areas).

$^{206}Pb/^{238}U$ age of 131 ± 4 Ma (2σ) (Fig. 3.41b). Two analyses (2.1 and 6.1) yield a weighted mean $^{206}Pb/^{238}U$ age of 142 ± 2 Ma with a chi-square value of 0.48 (Fig. 3.41b). Analysis spot 12.1 has a concordant $^{206}Pb/^{238}U$ age of 191 ± 8 Ma (2σ) (Fig. 3.41b). Analysis spots 8.1, 13.1, 3.1 and 4.1 give near-concordant $^{206}Pb/^{238}U$ ages of 221 ± 8 Ma, 493 ± 10 Ma, 697 ± 14 Ma and 749 ± 14 Ma (2σ) (Fig. 3.41b and a), respectively. Since samples YLB1 and XS1 are all from dykes temporally and spatially related to the gold mineralization within the Linglong Goldfield, the age of 122 ± 2 Ma, which is consistent with the age of 119 ± 5 Ma obtained from sample XS1, probably represents the timing of dyke intrusion. The other zircons with concordant or near-concordant ages are considered to be formed during earlier geological events and to be inherited. For example, the inherited zircon with an age of ca. 220 Ma is the same as those identified in Wangershan samples (W1, W2 and W4, in Table 3.4), therefore, this age represents an Early Mesozoic igneous event widely distributed in this region; since grain 3 is euhedral, the age of ca. 700 Ma dated from the core of grain 3 (spot 3.1) represents inheritance from a Late Proterozoic igneous source. Analysis spot 14.1 of grain 14 yields a $^{207}Pb/^{206}Pb$ age of 1852 ± 13 Ma (1σ) (Fig. 3.41a). Inherited zircons with an age of ca. 1850 Ma are considered to be generated during the Luliang Orogeny (Wang et al., 1998) and were present in the basement when the dyke was intruded.

Sample LX-53

Wang et al. (1998) reported SHRIMP zircon U-Pb results for sample LX-53 (Fig. 3.33). This sample was from an unaltered and unmineralized feldspar porphyry dyke which is a part of an extensive dyke swarm cutting and displacing some major gold lodes, such as the No.108, in the Linglong Goldfield. One main magmatic zircon population is composed of 21 analyses, having a weighted mean $^{206}Pb/^{238}U$ age of 120 ± 2 Ma (Fig. 3.42b). The age of 120 ± 2 Ma is taken as the intrusive age of the dyke (Wang et al., 1998), and provides a minimum age for gold mineralization. Two zircon grains yield discordant younger ages at ca. 110 Ma (Fig. 3.42b), which are interpreted to be the result of post-crystallization Pb-loss (Wang et al., 1998). The remaining analyses give various older ages which scatter from ca. 150 to 3100 Ma (Fig. 3.42). Among these analyses, one cluster yields an age of ca. 150-160 Ma (Fig. 3.42b) which coincides with the age of Linglong granitoid (150-160 Ma) (Wang et al., 1998); another cluster gives an age of ca. 200-250 Ma (Fig. 3.42b) which is consistent with the age of inherited zircons reported in other samples including C1 (Table 3.1), W1, W2, W4 (Table 3.4) and YLB1 (Table 3.5). Accordingly, The ages of ca. 150-160 Ma and ca. 200-250 Ma represent two earlier igneous events, during which zircons formed

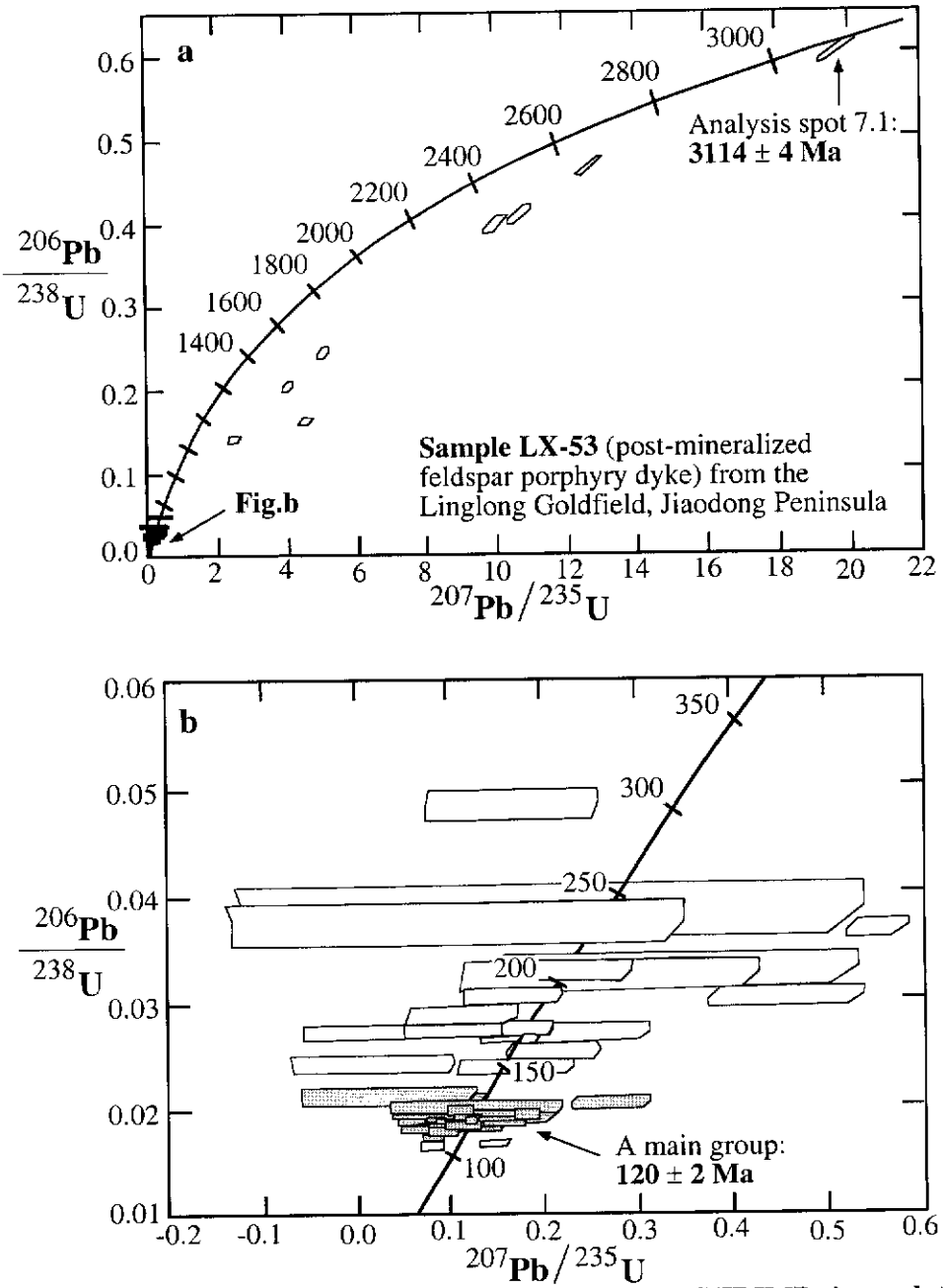

Fig. 3.42 (a,b) Concordia plot showing the SHRIMP zircon data from sample LX-53. Shaded areas are the main magmatic zircon population, and unshaded areas represent inherited zircons and zircons which have undergone Pb loss (modified from Luo et al., 1996).

and then were incorporated during dyke intrusion at ~ 120 Ma. The oldest inherited zircon of this sample yields a concordant $^{207}Pb/^{206}Pb$ age of 3114 ± 4 Ma (1σ) (Fig. 3.42a), which indicates that this region is underlain by Archaean basement.

3.6.9 Rb-Sr Isochron Age

In an attempt to constrain the timing of gold mineralization, Luo and Wu (1987) used the Rb-Sr isochron method to date hydrothermal micas (sericite and/or muscovite) from the Linglong-style ore in the Linglong Goldfield, and obtained a Rb-Sr isochron age of 112 ± 2 Ma. Zhang et al. (1994) applied the Rb-Sr whole-rock isochron method to date gold ore and hydrothermally altered whole-rock samples in the Linglong Goldfield, and Rb-Sr isochron ages of 100.7 ± 3.6 Ma (2σ) and 111.4 ± 2.8 Ma (2σ) were obtained from mineralized lodes distributed in the western and eastern parts of the Linglong Goldfield, respectively. Zhang et al. (1994) considered that the age of 100-110 Ma may represent another important gold mineralization event in the region. Alternatively, only one gold mineralization event may have occurred at ca. 120 Ma, and based on blocking temperature and the possibility of resetting, the Rb-Sr isochron age (ca. 100-110 Ma) may be interpreted to provide a minimum age for the gold mineralization in the region.

3.6.10 Summary

The Linglong Goldfield is located within the Linglong granitoids which comprise monzogranite and granodiorite. Both Jiaojia-style and Linglong-style of gold mineralization are present in this goldfield. The Jiaojia-style mineralized lode (i.e. the No. 171 lode) is controlled by the Potouqing Fault Zone. The Linglong-style mineralized lodes (such as the No. 108 lode) are associated with the second- and/or third-order faults off the Potouqing Fault Zone, and the preferred sites where orebodies are located include flexures of faults along strike, positions where the dip angle changes, fault intersections and tension gashes created by fault movement. The mineralized lodes of the Linglong- and Jiaojia-styles have the same wall-rock alteration styles, including silicification, sericitization, pyritization, potassic alteration and carbonation, but their alteration scales are different. Alteration associated with Linglong-style mineralization ranges from a few metres to ca. 10 m in width, whilst that of the Jiaojia-style varies from tens to hundreds of metres in width. Swarms of dykes varying from felsic to mafic in composition are widely present within the goldfield, with an average density of 10 dykes per square kilometre. It is recognized that the intermediate and mafic dykes are spatially and temporally associated with gold

mineralization. These dykes can be subdivided into three types which predate, are synchronous with, or post-date gold mineralization, and they are considered to have originated from the same deep-seated source as that of the auriferous ore fluid (Yao et al., 1990; Liu et al., 1991).

The crystallization age of Linglong granitoids from the Linglong Goldfield was determined at ca. 150-160 Ma by SHRIMP U-Pb zircon analysis (Wang et al., 1998). Three samples of dykes, which are considered to be closely associated with gold mineralization in space and time, were also analysed by SHRIMP and yielded ages of ca. 120-122 Ma. In the dyke samples, two generations of inherited zircons with ages of ca. 200-250 Ma and ca. 150-160 Ma are also present. Therefore, there are three significant Mesozoic magmatic events in this region. The earliest occurred at ca. 200-250 Ma which probably represents an Early Mesozoic magmatic event; the middle one occurred at ca. 150-160 Ma, during which the Linglong granitoids were intruded; the latest occurred at 120-122 Ma, during which dyke swarms were formed. Since the dykes cut orebodies and were also altered, it is considered that an important gold-forming event happened around 120-122 Ma in the region. By using the Rb-Sr isochron method to date gold ore and hydrothermally altered whole-rock samples, an age of 100-110 Ma was obtained, which may represent another important gold mineralization event or provide a minimum age for gold mineralization event (100-120 Ma) in the region.

3.7 Conclusions

Gold deposits of the Zhao-Ye Gold Belt are controlled by major regional faults, including the San-Cang, Huang-Ye and Zhao-Ping Fault Zones. The development of these fault zones is a major feature in the tectonic evolution of the region and they may represent deep ductile shear zones superimposed by later brittle components during crustal uplift caused by collision and accretion along the margins of the Eurasian and Palaeo-Pacific Plates during the Mesozoic. The ore fluid may have migrated from deep-seated sources in the lower crust and/or upper mantle to form the gold deposits (cf. Barley et al., 1989; Kerrich and Cassidy, 1994). The nearby Tan-Lu Fault Zone, which constitutes a larger-scale lithospheric fracture, has been proposed as the fluid pathway for mineralization of the Jiaobei Terrane (Cai, 1993; Zhang, 1990; Ren et al., 1997).

Gold deposits of the Zhao-Ye Gold Belt are either of the Jiaojia-style (disseminated-and-veinlet type) or Linglong-style (vein-filling type). Their features are summarized in Table 3.6.

Table 3.6: Main features of the Jiaojia- and Linglong-style gold deposits within the Zhao-Ye Gold Belt

Features	Jiaojia-style	Linglong-style
Structural control	Regional fault zones	Secondary structures off regional fault zones
Location	Lithologic contacts along regional fault zones	Single rock units
Local stress environment	Compressional	Tensional
Mechanism for forming orebodies	Auriferous fluids penetrate rocks along regional fault zones and fill the rock in the form of quartz and/or sulphide veinlets	Auriferous fluids fill large fractures developed in competent host rock
Orebodies	No sharp contacts with the host rock and they are only distinguished by grade analysis	Sharp contacts with the host rock and they can be easily identified in the field
Gold reserves	Tens to more than one hundred tonnes	An average of a few tonnes
Grade	4-5 grams per tonne	An average of more than 10 grams per tonne
Main alteration type	Silicification, sericitization, pyritization, potassic alteration and carbonation	The same as for the Jiaojia-style
Alteration scale	From tens of metres to hundreds of metres	From a few metres to ca. 10 m
Main paragenesis	Pyrite, chalcopyrite, sphalerite, galena, pyrrhotite	The same as for the Jiaojia-style
Examples	Cangshang, Sanshandao and Jiaojia Gold Deposits	The No.55 Gold Lode of the Linglong Goldfield

By using SHRIMP U-Pb zircon techniques, the Linglong granitoids which are the main rock type of this gold belt, were dated at 165-150 Ma (Wang et al., 1998). SHRIMP data and CL imaging reveal that in the Linglong granitoids there are three main generations of inherited zircons giving Late Archaean (ca. 2500 Ma), Palaeoproterozoic (1800-2200 Ma) and Early Mesozoic (ca. 200-250 Ma) ages. The Late Archaean zircons are euhedral, zoned grains of igneous origin, indicating Late Archaean magmatism in the basement rocks of the Zhao-Ye Belt, an event which is widely recognized within the North China Craton (e.g. Zhao, 2000). The Palaeoproterozoic zircons occur either as metamorphic zircon overgrowths surrounding inherited Archaean igneous cores, or as individual metamorphic zircons, and their ages coincide broadly with the Lüliang Orogeny (i.e. a craton-wide tectono-thermal event at ca. 1.8 Ga within the North China Craton). The Early Mesozoic zircons occur in three forms: inherited igneous cores surrounding by younger zircon

rims, zircon overgrowths surrounding inherited cores with Precambrian ages, and individual euhedral zircons. These Early Mesozoic inherited zircons most likely represent a magmatic event, formed in response to the collision of the North China and Yangtze Cratons. During this collisional event, the Precambrian basement was reworked by high grade metamorphism and partial melting (Wang et al., 1998) to produce an earlier suite of granitoids (ca. 200-250 Ma), as recorded in the Jiaodong Peninsula (Xu et al., 1989). In addition, a few inherited zircons yield concordant $^{206}Pb/^{238}U$ ages of ca. 750 Ma and ca. 600 Ma. These ages may represent earlier geological events in this region, however, up to date no detailed research work has been done to prove this proposition.

Dykes, including felsic, intermediate and mafic types, are widely distributed within the Zhao-Ye Gold Belt. The intermediate and mafic dykes are closely related to gold mineralization in space and time, and magma and auriferous ore fluid are considered to have originated from the same deep-seated source. These dykes can be subdivided into three kinds which either predate, are synchronous with, or post-date gold mineralization. By using SHRIMP U-Pb zircon methods, the dykes which intruded during gold mineralization were dated and yielded an age of ca. 120-122 Ma, which approximately represents the timing of the gold mineralization.

Yang et al (2000) summarized the known Rb-Sr isochron ages and K-Ar ages of gold mineralization in the Zhao-Ye Gold Belt, and concluded that the gold mineralization event occurred at ca. 100-117 Ma. In order to directly constrain the timing of gold mineralization, Ar-Ar dating of hydrothermal micas from the gold orebody of the Cangshang Gold Deposit was carried as part of this thesis. The well-defined plateau-like segment age of 121.3 ± 0.2 Ma provides the precise timing of gold mineralization in this region. In addition, the SHRIMP U-Pb ages of zircons from a dyke which is closely associated with gold mineralization in the region range between 120 Ma and 122 Ma. Therefore, it is suggested that gold mineralization occurred at ca. 121 Ma in the Zhao-Ye Gold Belt.

The gold mineralization in this region was previously considered to be closely related to the subduction of the Palaeo-Pacific Plate beneath the Eurasia Plate at 120 Ma (Sun et al., 1995). The input of heat enhanced hydrothermal circulation and resulted in the upward migration of auriferous fluids.

CHAPTER 4: GOLD DEPOSITS EXAMINED WITHIN THE QI-PENG GOLD BELT OF THE JIAODONG PENINSULA

4.1 Introduction

The Qi-Peng Gold Belt (Fig. 4.1) is situated in the central part of the Jiaobei Terrane and contains ca. 10% of the gold reserves of the Jiaodong Peninsula. Gold deposits of this belt are hosted by the Late Archaean Jiaodong Group and the Guojialing Batholith, and some are spatially associated with fault zones. These gold deposits are of the Linglong-style (vein-filling type). The Majiayao and Daliuhang Gold Deposits are documented in more detail below.

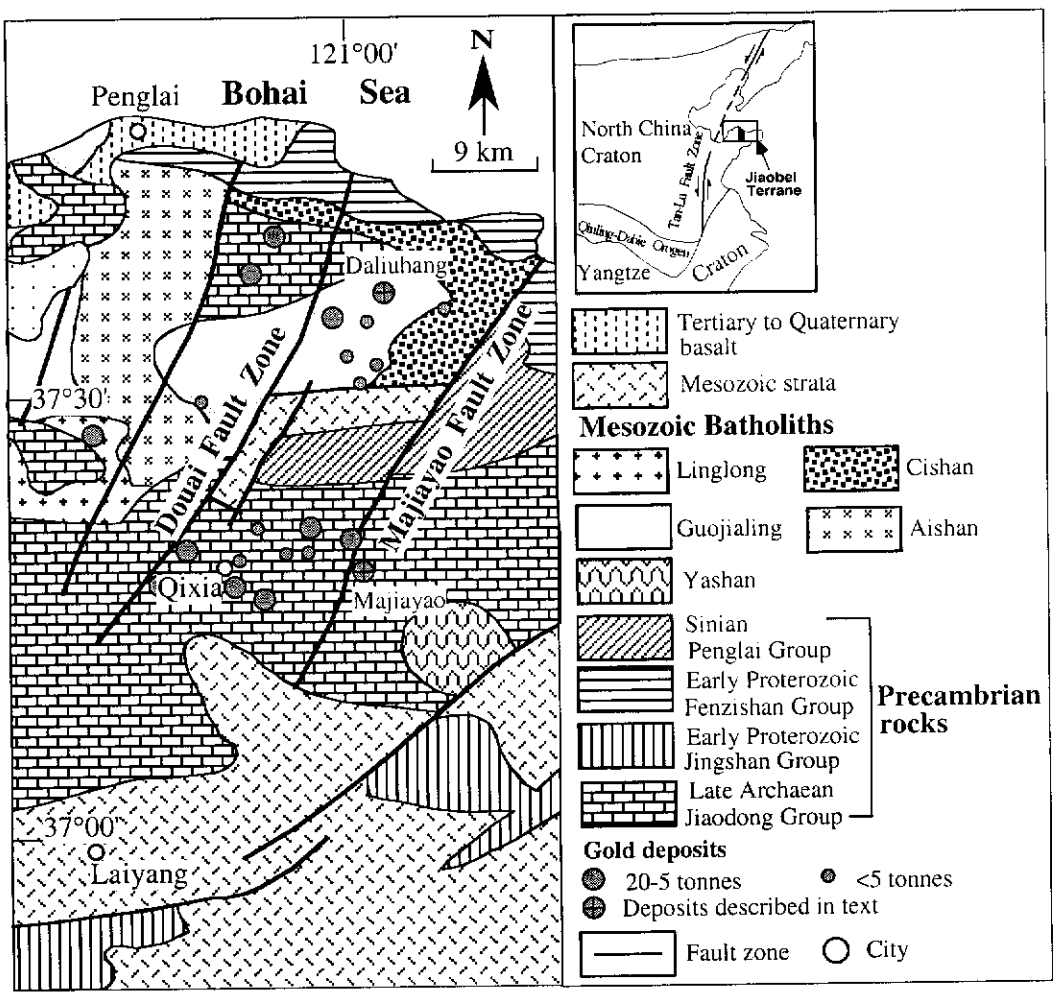

Fig. 4.1: Distribution map of gold deposits within the Qi-Peng Gold Belt of the Jiaodong Peninsula (enlargement of black area in the inset map), showing how some gold deposits are spatially associated with the Guojialing Batholith and fault zones (modified from Chang, 1996).

4.2 Majiayao Gold Deposit

The Majiayao Gold Deposit (E120°58'15", N37°17'48") is located about 12 km east of the city of Qixia (Fig. 4.1). It was discovered during 1979-1980 by the No.6 Team of Geology and Exploration, BGMRSP, based on regional reconnaissance. This deposit is located in the footwall of the Majiayao Fault which strikes 020° and dips ca. 65°NW (the No.6 Team of Geology and Exploration, BGMRSP, 1981). In sharp contrast to the Linglong Goldfield, where Mesozoic Linglong Granitoids are the host rocks for gold mineralization, this deposit is exclusively hosted within the highly metamorphosed Late Archaean Jiaodong Group (Fig. 4.1). In 1981, the reported gold reserves were about 4.5 tonnes and with subsequent drilling it has now become a medium-size (5-20 tonnes) gold deposit. The deposit is a Linglong-style (vein-filling type) ore deposit.

4.2.1 Lithological Units

The lithological unit hosting the Majiayao Gold Deposit is dominantly amphibolite of the Jiaodong Group (Fig. 4.2). The amphibolite is fine- to medium-grained and grey-green to dark green in colour. It consists of hornblende and plagioclase, with minor biotite, pyroxene, chlorite, epidote and quartz. Accessory minerals include apatite, titanite, zircon and magnetite. A swarm of felsic to mafic dykes, including microgranite, microdiorite, dolerite and lamprophyre, are present in the mining area (Fig. 4.2) (The No.6 Team of Geology and Exploration, BGMRSP, 1981).

4.2.2 Alteration

The hydrothermal alteration types associated with this deposit include sericitization, silicification and pyritization of the host Jiaodong Group amphibolite. An alteration halo occurs around the gold lodes and has a width of 1-2 m (Fig. 4.3) (The No. 6 Team of Geology and Exploration, BGMRSP, 1981).

4.2.3 Lodes

The deposit consists of the No.1 and No.2 lodes, which are believed to be controlled by branches off the Majiayao Fault Zone. The lodes strike NNW to WNW and dip 30°-50°NE (Fig. 4.2). The No.1 lode is 970 m in length and averages 0.8 m in thickness with a maximum of 2 m. This lode includes 5 orebodies which are lensoid in

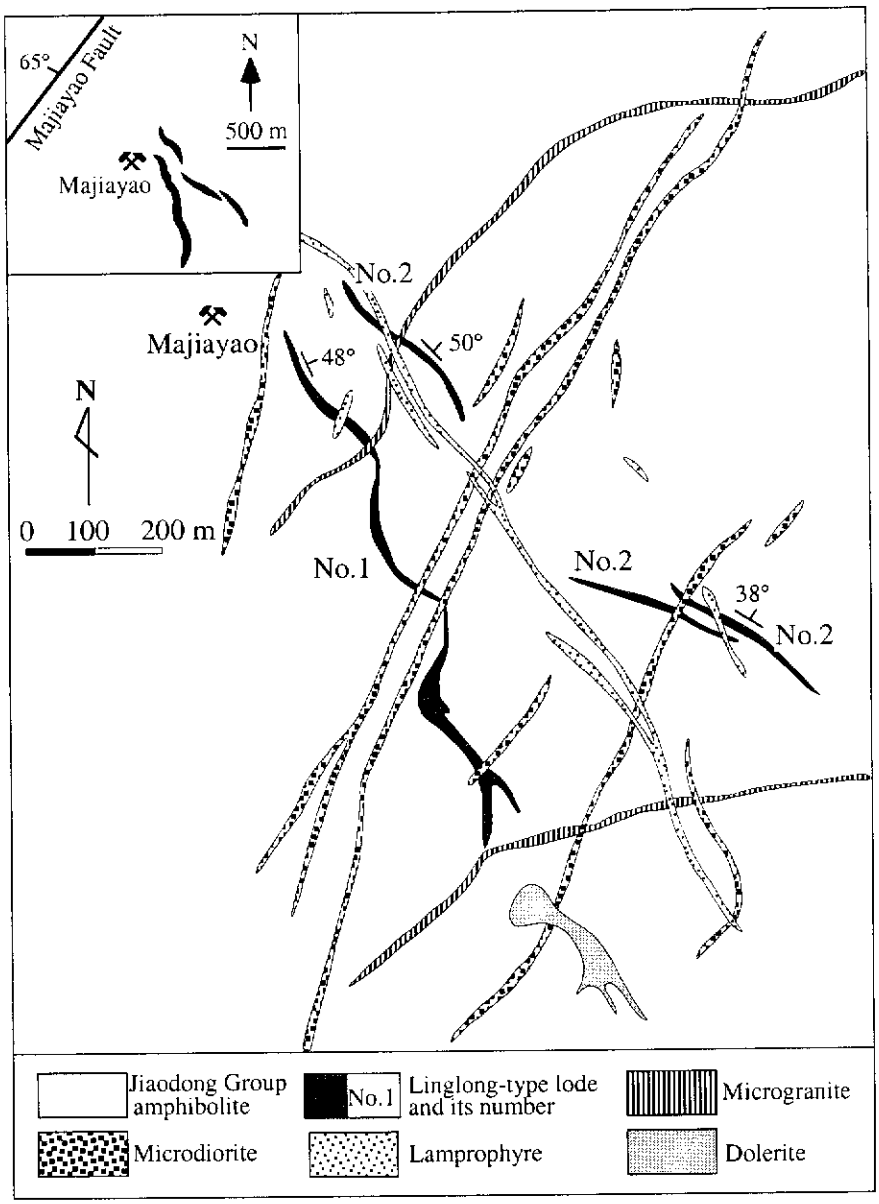

Fig. 4.2: Geological map of the Majiayao Gold Deposit, showing the distribution of lodes and dykes (modifed from BGMRSP, 1988). Inset shows position with respect to the Majiayao Fault (See also Fig. 4.1).

shape. Their average grade is 17.03 g/t, with a maximum of 176.06 g/t. The largest orebody is 367 m in length and averages 0.69 m in thickness, and its average grade is 19.96 g/t (The No.6 Team of Geology and Exploration, 1981). The No.2 lode comprises three discontinuous parts. It is 840 m in length and ranges from 0.1 to 0.5 m in thickness. Only a few small orebodies are found in this lode and their grade ranges from 4.96 to 18.81 g/t (BGMRSP, 1988).

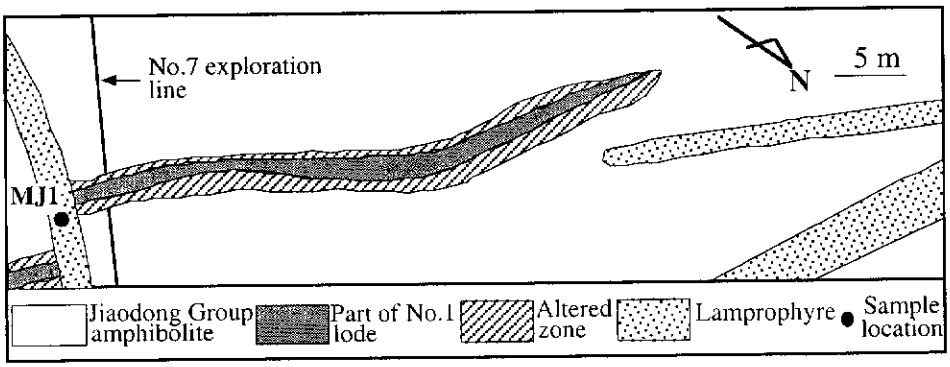

Fig. 4.3: Part of plan of 143 m level at the Majiayao Gold Deposit, showing a lamprophyre dyke cutting the No.1 gold lode. The location of geochronology sample MJ1 is also shown.

4.2.4 Ore Mineralogy and Paragenesis

Ore minerals include pyrite, chalcopyrite, galena, sphalerite and siderite. Pyrite is the most abundant and two distinct generations can be recognized. The earliest phase comprises fine to medium (0.7-2.0 mm) euhedral grains. Fractures are well-developed in this type of pyrite, and later metal sulphides and electrum occur as infillings. The second generation of pyrite consists of fine (0.02-0.4 mm) subhedral grains, which are usually associated with other base metal minerals such as chalcopyrite, galena and sphalerite. Gangue minerals consist of quartz, sericite, calcite and ankerite. Gold is predominantly present as electrum which mainly fills fractures in the pyrite of both generations (The No.6 Team of Geology and Exploration, 1981). Three stages of hydrothermal mineral formation have been identified. From the oldest to the youngest these are: stage 1: pyrite-quartz, with the mineral assemblage consisting of medium-grained quartz and pyrite; stage 2: gold-quartz-base metal sulphides, where the mineral assemblage is mainly composed of fine-grained pyrite, chalcopyrite, galena, sphalerite, electrum and fine quartz, and these ore minerals chiefly occur in the forms of veinlets and stockworks; stage 3: quartz-calcite, with the mineral paragenesis consisting mainly of calcite and quartz as well as a trace amount of ankerite. Stage 2 is the most intensive period of gold mineralization (The No.6 Team of Geology and Exploration, 1981).

Fluid inclusion studies suggest temperatures associated with stages 1 to 3 were 310-180 °C, 270-160 °C and 220-120°C, respectively (Zhai et al., 1998).

4.2.5 Geochronology

Since some dykes cut orebodies within the Majiayao deposit (Fig. 4.2 and 4.4), dating such dykes can provide the minimum age of gold mineralization. Based on this view, Sample MJ1 from a dyke cross-cutting the No.1 gold lode (Fig. 4.3) was selected for SHRIMP analysis. The SHRIMP results are listed in Table 4.1 and illustrated on a concordia plot in Figure 4.4. Following is the description of sample MJ1 and the interpretation of its SHRIMP zircon U-Pb data.

Sample MJ1

Sample MJ1 was taken from a lamprophyre dyke (Fig. 4.3) that cuts the No.1 lode. This is a melanocratic dyke and has a porphyritic texture. In thin section, the phenocryst phase is predominantly amphibole (euhedral, yellow-green colour, some replaced by chlorite); the fine-grained groundmass mainly consists of amphibole and K-feldspar. Therefore, the lamprophyre is a vogesite. The zircon grains selected for analysis vary in size from 132 μm to 74 μm and most are colourless with a few purplish in colour. Some grains are euhedral with good crystal faces, and have an elongation ratio of ca. 3:1; some are rounded and considered to be xenocrysts from the Archaean basement.

Due to only a few zircons of good quality being available (no inclusions or cracks), only 10 analyses were carried out on 10 grains (Fig. 4.4), and ages range from 2452 ± 8 Ma to 159 ± 4 Ma (Table 4.1).

Spot 10.1 of grain 10 yields a near-concordant $^{207}Pb/^{206}Pb$ age of 2452 ± 16 Ma (2σ) (Fig. 4.4a), which indicates a Palaeoproterozoic component in the basement.

One zircon population (Group 1) consists of 4 analyses, which form a coherent group (Fig. 4.4b) having a weighted mean $^{206}Pb/^{238}U$ age of 222 ± 16 Ma with a chi-square value of 3.12. The U and Th contents of these spots range from 256 ppm to 895 ppm and 138 ppm to 1035 ppm, respectively. The Th/U ratios vary from 0.54 to 1.23. The zircon grains with an age of ca. 220 Ma are widely present within the Yanshanian igneous rocks (160-70 Ma) (Wang et al., 1998), which are considered to

Table 4.1: SHRIMP U-Pb data for zircons from sample MJ1, from the Majiayao Gold Deposit. Analyses are listed in order of increasing age. The following notation is used for analysed grains: 1.1=grain 1, first point analysed. Data are ^{204}Pb-corrected. Individual analyses have a 1σ error. The $^{206}Pb/^{238}U$ age is adopted for the zircons with an age of less than 1.0 Ga, otherwise, the $^{207}Pb/^{206}Pb$ age is used.

spot	U (ppm)	Th (ppm)	Th/U	Total Pb (ppm)	$\frac{^{204}Pb}{^{206}Pb}$	f206 (%)	$\frac{^{207}Pb}{^{206}Pb}$	$\frac{^{206}Pb}{^{238}U}$	$\frac{^{207}Pb}{^{235}U}$	$\frac{^{206}Pb}{^{238}U}$ Age	$\frac{^{207}Pb}{^{206}Pb}$ Age
Sample MJ1											
1.1	918	131	0.14	22	0.00043	0.007	0.054±2	0.0249±6	0.19±1	159±4	
3.1	503	69	0.14	13	0.00033	0.005	0.062±5	0.0254±6	0.22±2	162±4	
4.1	2232	672	0.3	59	0.00041	0.007	0.055±1	0.026±6	0.2±1	166±4	
7.1	270	161	0.6	10	0.00053	0.009	0.061±6	0.033±8	0.28±3	209±5	
2.1	256	138	0.54	10	0.00047	0.007	0.07±6	0.035±8	0.34±3	221±5	
9.1	841	1035	1.23	38	0.00004	0.001	0.057±2	0.0356±8	0.28±1	225±5	
5.1	1914	37	0.02	81	0	0	0.074±0	0.0451±10	0.46±1	284±6	
8.1	895	553	0.62	36	0.00015	0.002	0.054±1	0.0368±8	0.28±1	233±5	
6.1	118	88	0.75	9	0	0	0.115±19	0.0525±43	0.83±16	330±26	
10.1	240	167	0.69	125	0.00007	0.001	0.16±1	0.4432±100	9.76±23		2452±8

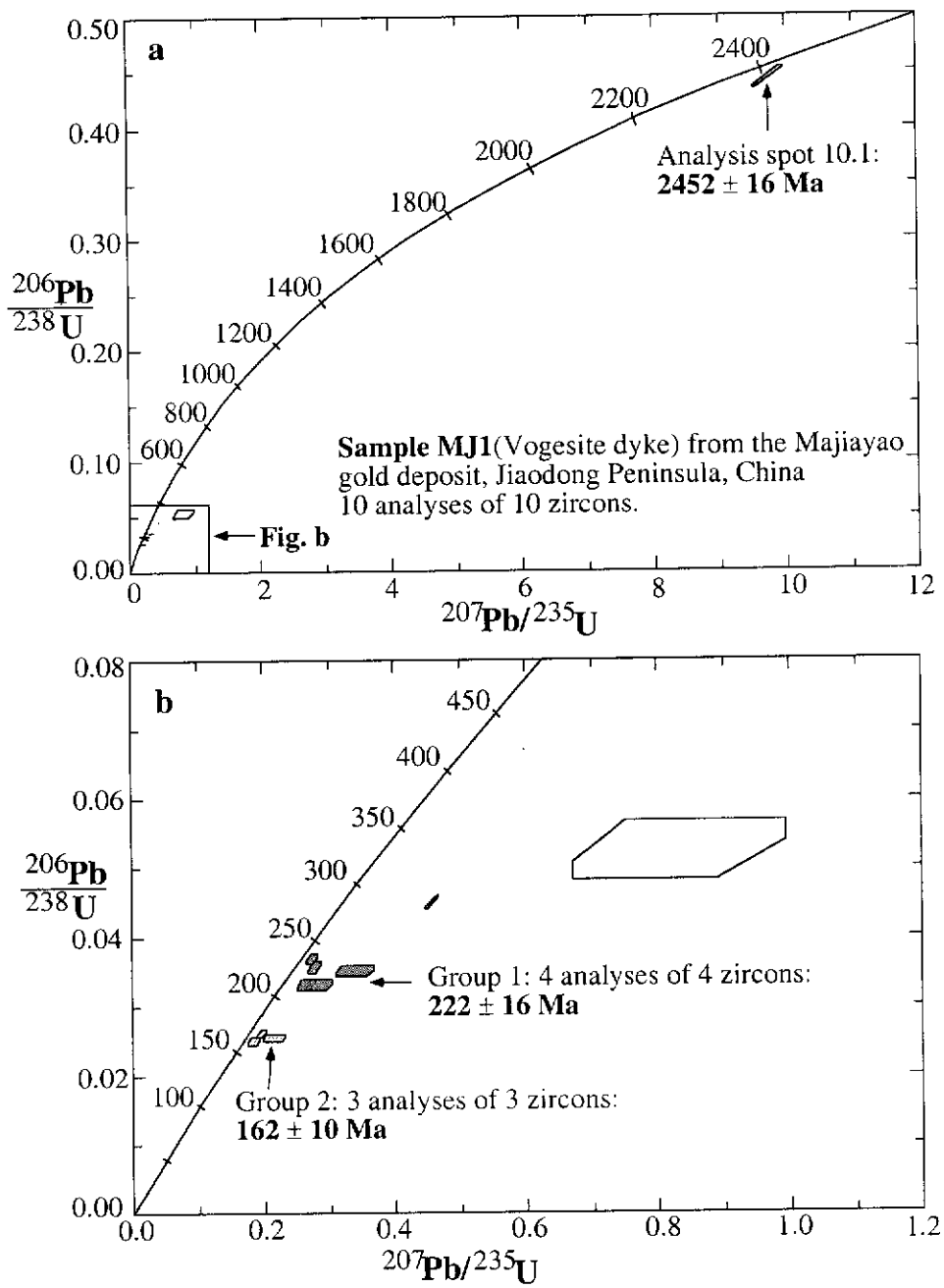

Fig. 4.4: U-Pb concordia plots showing (a) total SHRIMP zircon analytical data for sample MJ1 and (b) enlargement detailing the younger zircon populations.

be formed during an earlier geological event and to be picked up during emplacement of the dykes.

Another zircon population (Group 2) is composed of 3 analyses, which form a coherent group (Fig. 4.4b) having a weighted mean $^{206}Pb/^{238}U$ age of 162 ± 10 Ma with a chi-square value of 0.72. The U and Th contents of these 3 spots range from 503 ppm to 2232 ppm and 69 ppm to 672 ppm, respectively. The Th/U ratios vary from 0.14 to 0.3. In the previously discussed Jiaojia Gold Deposit (Chapter 3), it has been established that mafic magma rapidly ascended and that no zircon crystallized during the process, hence it is possible that there may exist a pluton within the Precambrian basement and that the three euhedral grains from sample MJ1 may be entrapped from this pluton during dyke emplacement. Alternatively, these 3 grains could have crystallised from lamprophyric magma, in which case they would date the time of dyke emplacement. Further work would be required to establish this. The group age of 162 ± 10 Ma coincides with the age of the Linglong Granitoid (165 to 150 Ma) (Chapter 3 of this thesis), widely distributed within the Jiaodong Peninsula, confirming this intepretation.

Since the intrusion age of the lamprophyre dyke cutting the No.1 lode cannot be obtained, it failed to define the minimum age of gold mineralization. Previous geochronological work determined the age of gold mineralization in this deposit as 126 ± 2 Ma (2σ) using the Rb-Sr isochron method on altered whole-rocks and sericite (Zhai et al., 1998), and as 106.1 ± 4.9 Ma employing the Rb-Sr isochron method on altered whole-rocks, chlorite and siderite (Zhang et al., 1994).

4.2.6 Summary

The Majiayao Gold Deposit is a Linglong-type gold lode, which is hosted by amphibolite of the Late Archaean Jiaodong Group and is believed to be controlled by branches off the Majiayao Fault Zone. An alteration halo, which is characterized by sericitization, silicification and pyritization, occurs around the gold lodes and has a width of 1-2 m. A swarm of felsic to mafic dykes are present within the deposit. The dykes are believed to be related to gold mineralization in the Jiaodao Peninsula (Yao et al., 1990).

SHRIMP U-Pb zircon dating of a post-mineralization dyke, however, failed to determine the intrusive age of the dyke since no zircon crystallized from the dyke. The SHRIMP geochronological data prove that there may exist a pluton within the

Precambrian basement and the age of this pluton (ca. 160 Ma) coincides with the age of Linglong Granitoids (165 to 150 Ma), widely distributed within the Jiaodong Peninsula. The age of ca.220 Ma represents an earlier igneous event, which was documented in Chapter 3. Based on the available Rb-Sr dating results, the gold mineralization at this deposit is considered to have occurred at ca.100-120 Ma, which is consistent with the timing of gold mineralization in the Zhao-Ye Gold Belt (Chapter 3).

4.3 Daliuhang Gold Deposit

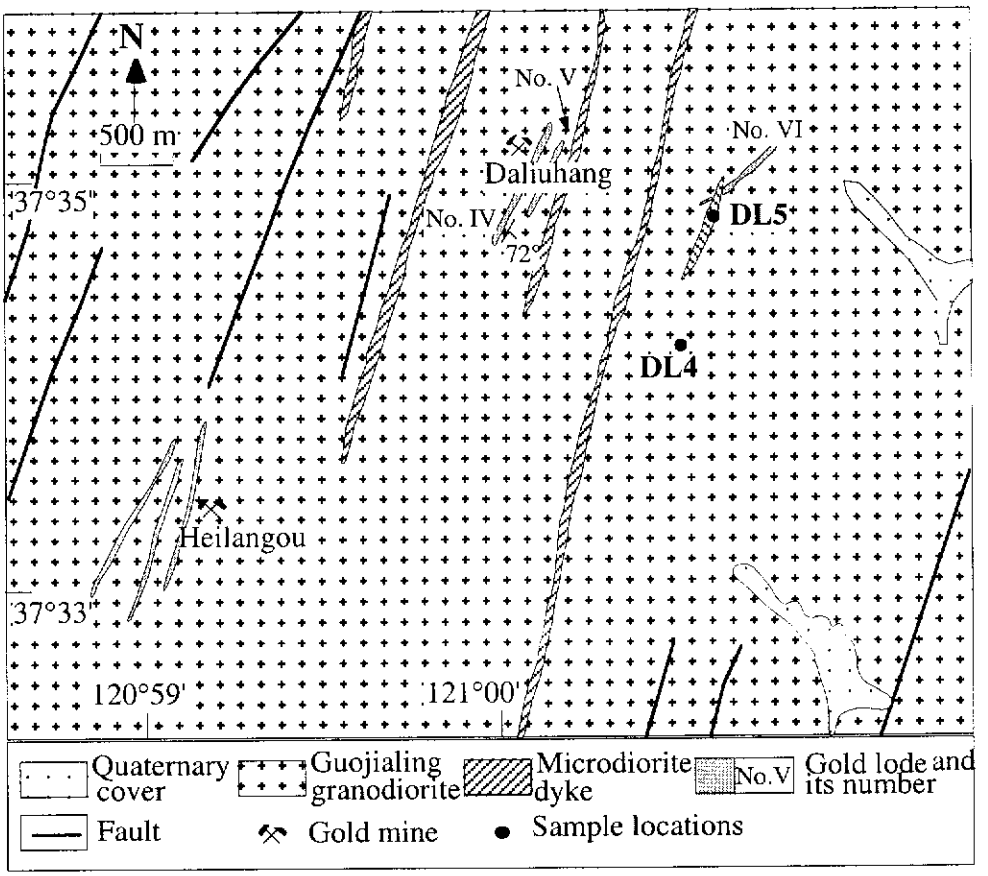

Fig. 4.5: Simplified geological map of the area around the Daliuhang Gold Deposit, showing the sample locations (modified from the No.518 Team of the No.1 Geology Exploration Company of the Metallurgical Industrial Bureau, 1989).

The Daliuhang Gold Deposit (E121°00'08", N37°35'26") is located about 27 km southeast of the city of Penglai (Fig. 4.1). It was discovered during 1987-1989 by the No.518 Team of the No.1 Geology Exploration Company of the Metallurgical Industrial Bureau, based on regional reconnaissance. The deposit is exclusively hosted within the Mesozoic Guojialing granodiorite (Figs. 4.1 and 4.5). In 1989, its reported

gold reserves were about 1.5 tonnes and by extra drilling it has now become a medium-size (5-20 tonnes) gold deposit. This deposit is a Linglong-style (vein-filling type) gold ore and is well-known in the Jiaodong Peninsula for the occurrence of visible gold.

4.3.1 Lithological Units

The Daliuhang Gold Deposit is hosted by the Guojialing granodiorite (Fig. 4.5). This granodiorite is medium- to coarse-grained and grey-white in colour. It is mainly composed of plagioclase, quartz, K-feldspar, hornblende and biotite. Accessory minerals include titanite, zircon, apatite and magnetite. A swarm of microdiorite dykes are present in the mining area (Fig. 4.5) (The No.518 Team of the No.1 Geology Exploration Company of the Metallurgical Industrial Bureau, 1989).

4.3.2 Alteration

The hydrothermal alteration types associated with this deposit include sericitization, silicification, pyritization and K-feldspar alteration of host Guojialing granodiorite, which is similar to that in other Linglong-style deposits in the Jiaodong Peninsula.

4.3.3 Lodes

The deposit is mainly hosted by the No. IV and No. V lodes (Fig. 4.5). The No. IV lode is the most important and strikes 015°-025° and dips 68°-78°SE. This lode is ca. 700 m in length and averages 0.98 m in thickness with a maximum of 2.76 m. The grade ranges from 0.53 g/t to 1217.81 g/t with an average of 14.72 g/t. The No.V lode strikes in the same direction and is 540 m in length and ranges from 0.27 to 1 m in thickness, with an average of 0.44 m. Its average grade is 4 g/t (The No.518 Team of the No.1 Geology Exploration Company of the Metallurgical Industrial Bureau. 1989).

4.3.4 Ore Mineralogy and Paragenesis

Ore minerals include pyrite, chalcopyrite, galena, sphalerite and tetrahedrite; pyrite is the most abundant. Two distinct generations of pyrite can be recognized. The first type comprises coarse euhedral to subhedral grains. The second generation of

pyrite consists of fine anhedral grains, which are usually associated with other base metal minerals, including chalcopyrite, galena and sphalerite. Gangue minerals consist of quartz, sericite, calcite, plagioclase and K-feldspar. Gold is present as electrum and native gold, which mainly fill fractures in the pyrite of both generations. Three stages of hydrothermal mineral formation in this deposit have been identified (The No.518 Team of the No.1 Geology Exploration Company of the Metallurgical Industrial Bureau, 1989). From the oldest to the youngest these are: stage 1: gold-pyrite-quartz; stage 2: gold-quartz-base metal sulphides; stage 3: quartz-calcite.

4.3.5 Geochronology

In order to constrain the timing of gold mineralization in the Daliuhang deposit, the host rock and a post-mineralization dyke were precisely dated. Samples DL4 from the host rock and DL5 from a dyke cross-cutting the No. VI gold lode (Fig. 4.5) were chosen for SHRIMP U-Pb zircon analysis. The SHRIMP results are listed in Table 4.2 and illustrated on concordia plots in Figures 4.7 and 4.8. Following are the descriptions of samples DL4 and DL5 and the interpretation of their SHRIMP zircon U-Pb ages.

Sample DL4

Sample DL4 (Fig. 4.5) is a leucocratic, hypidiomophic, medium-grained granodiorite. It locally has myrmekitic and poikilitic textures. It consists of plagioclase (45%), quartz (25%), potassic feldspar (15%), hornblende (7%) and biotite (5%), with accessory titanite, zircon, apatite and magnetite. Zircons selected for analysis vary in size from 132 μm to 74 μm and are pale brown in colour. Most grains are euhedral, with well-formed pyramidal terminations. The average elongation ratio is about 3:1, with a maximum of 5:1.

A total of 14 analyses were carried out on 13 grains (Fig. 4.6), and ages range from 2494 ± 12 Ma to 123 ± 3 Ma (Table 4.2).

Two spots (2.1 and 8.1) from two separate zircon grains do not yield concordant $^{207}Pb/^{206}Pb$ ages (Fig. 4.6a), but have values of 2494 ± 24 Ma and 1821 ± 40 Ma (2σ), respectively. These two zircons are euhedral and optically homogeneous, and are indistinguishable from the main magmatic zircon population in terms of morphology. The inherited zircons with Late Archaean (~2500 Ma) and Palaeoproterozoic (1750-2000 Ma) ages are common in Mesozoic granitoids within the

Table 4.2: SHRIMP U-Pb data for zircons from samples DL4 and DL5 from the Daliuhang Gold Deposit. Analyses are listed in order of increasing age. The following notation is used for analysed grains: 1.1=grain 1, first point analysed. Data are ^{204}Pb-corrected. Individual analyses have a 1σ error. The $^{206}Pb/^{238}U$ age is adopted for zircons with an age of less than 1.0 Ga, otherwise, the $^{207}Pb/^{206}Pb$ age is used.

spot	U (ppm)	Th (ppm)	Th/U	Total Pb (ppm)	$\frac{204Pb}{206Pb}$	f206 (%)	$\frac{207Pb}{206Pb}$	$\frac{206Pb}{238U}$	$\frac{207Pb}{235U}$	$\frac{206Pb}{238U}$ Age	$\frac{207Pb}{206Pb}$ Age
Sample DL4											
1.1	316	144	0.46	8	0.0053	0.085	0.029±11	0.0192±4	0.08±3	123±3	
3.1	311	148	0.48	8	0.00437	0.07	0.034±11	0.0196±4	0.09±3	125±3	
3.2	348	175	0.5	9	0.00357	0.057	0.039±10	0.0197±4	0.11±3	126±3	
4.1	313	147	0.47	8	0.00433	0.069	0.04±11	0.0198±4	0.11±3	126±3	
7.1	296	174	0.59	9	0.00828	0.132	0.025±15	0.0197±5	0.07±4	126±3	
13.1	258	125	0.48	6	0.00344	0.055	0.053±10	0.0197±4	0.14±3	126±3	
12.1	332	180	0.54	8	0.00347	0.055	0.035±9	0.0204±4	0.1±3	130±3	
10.1	254	139	0.55	7	0.00459	0.073	0.041±12	0.0204±5	0.11±3	130±3	
5.1	216	107	0.5	6	0.0054	0.086	0.043±14	0.0205±5	0.12±4	131±3	
9.1	325	158	0.49	9	0.00496	0.079	0.039±11	0.0207±5	0.11±3	132±3	
11.1	646	92	0.14	14	0.00129	0.021	0.048±4	0.0209±4	0.14±1	133±2	
6.1	444	190	0.43	14	0.00192	0.031	0.047±5	0.0282±5	0.18±2	179±3	
8.1	261	32	0.12	49	0.00028	0.004	0.111±1	0.1923±34	2.95±6		1821±20
2.1	200	97	0.49	91	0.00042	0.007	0.164±1	0.3968±70	8.96±18		2494±12
Sample DL5											
9.1	311	166	0.53	7	0.00195	0.031	0.052±9	0.0178±4	0.13±2	114±3	
4.1	184	96	0.52	6	0.01071	0.171	0.029±25	0.018±5	0.07±6	115±3	
8.1	395	223	0.56	8	0.00173	0.028	0.053±7	0.0181±4	0.13±2	116±3	
6.1	562	336	0.6	12	0.00042	0.007	0.057±4	0.0185±4	0.15±1	118±3	
9.2	235	117	0.5	5	0.00147	0.023	0.051±9	0.0188±5	0.13±2	120±3	

Table 4.2 (continued)

spot	U (ppm)	Th (ppm)	Th/U	Total Pb (ppm)	$\frac{^{204}Pb}{^{206}Pb}$	f206 (%)	$\frac{^{207}Pb}{^{206}Pb}$	$\frac{^{206}Pb}{^{238}U}$	$\frac{^{207}Pb}{^{235}U}$	$\frac{^{206}Pb}{^{238}U}$ Age	$\frac{^{207}Pb}{^{206}Pb}$ Age
3.1	227	151	0.67	7	0.0063	0.101	0.064±17	0.0188±4	0.17±4	120±3	
2.1	364	243	0.67	10	0.00448	0.072	0.052±10	0.019±3	0.14±3	121±2	
7.2	335	142	0.43	7	0.00093	0.015	0.061±7	0.0189±4	0.16±2	121±3	
5.1	244	130	0.53	5	0.00092	0.015	0.076±11	0.0191±5	0.2±3	122±3	
7.1	1501	1101	0.73	32	0.00011	0.002	0.052±1	0.0194±4	0.14±0	124±3	
1.1	586	490	0.84	15	0.00297	0.047	0.042±6	0.02±3	0.11±2	128±2	

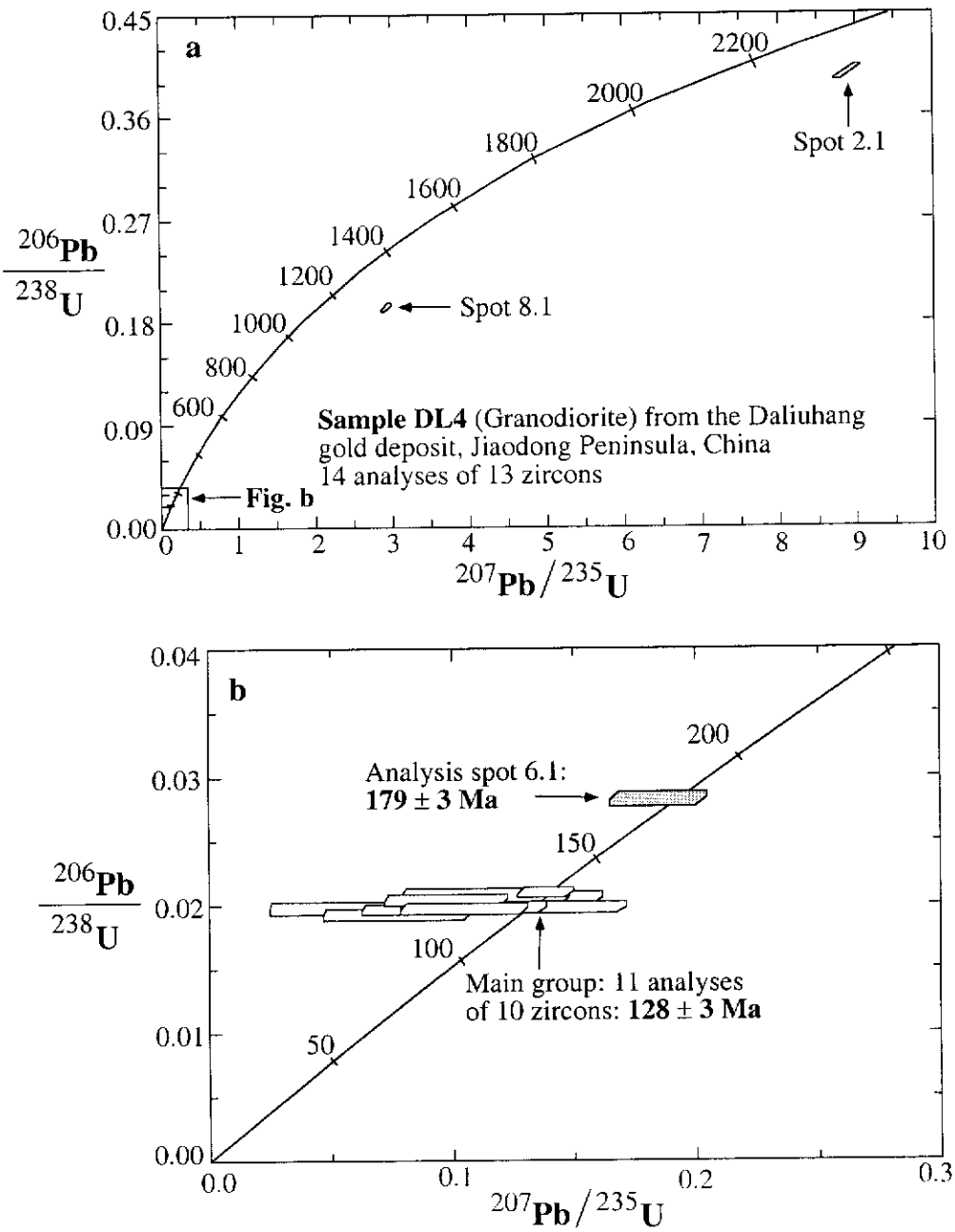

Fig. 4.6: U-Pb concordia plots showing (a) total SHRIMP zircon analytical data from sample DL4 and (b) enlargement detailing the main magmatic zircon population.

Jiaodong Peninsula (Wang et al., 1998). These Precambrian ages may date the source rocks of the Mesozoic granitoids or alternatively they may represent accidental xenocrysts incorporated during emplacement. Spot 6.1 of grain 6 yields a concordant $^{206}Pb/^{238}U$ age of 179 ± 6 Ma (2σ) (Fig. 4.6b). Grain 6 is euhedral and may have formed during an earlier igneous event at 179 ± 6 Ma, then was incorporated by the subsequent magmatic event that occurred at ca. 128 Ma (Fig. 4.6b).

The main zircon population is composed of 11 analyses on 10 euhedral grains, which form a coherent group (Fig. 4.6b) having a weighted mean $^{206}Pb/^{238}U$ age of 128 ± 3 Ma with a chi-square value of 1.49. The U and Th contents of these 11 spots range from 216 ppm to 646 ppm and 92 ppm to 180 ppm, respectively. The Th/U ratios vary from 0.14 to 0.59. The age of 128 ± 3 Ma is considered to be the crystallization age of the host Guojialing granodiorite. Based on SHRIMP zircon U-Pb analysis, Wang et al (1998) dated 5 samples from the Guojialing Suite, and their ages fall in a very restricted range between 126 Ma and 130 Ma which coincides well with the age data obtained here.

Sample DL5

Since no fresh dyke samples were available, a strongly weathered sample DL5 (Fig. 4.5) was collected from an intermediate dyke which outcrops at the surface. The dyke was classified as microdiorite by local geologists and petrographic examination confirms this. Due to the fact that it cross-cuts the No. VI gold lode, dating this dyke can constrain the minimum age of gold mineralization for the Daliuhang Deposit. Zircons selected for analysis range in size from 132 μm to 74 μm and are pale brown in colour; some contain tiny inclusions. Most grains are euhedral, with good pyramidal terminations. The average elongation ratio is about 3:1, with a maximum of 6:1.

Eleven analyses were made on 9 grains (Fig. 4.7), and ages fall in a narrow range between 128 ± 2 Ma and 114 ±3 Ma (Table 4.2).

Only one zircon population is defined and composed of 11 analyses on 9 euhedral grains, which form a coherent group (Fig. 4.7) having a weighted mean $^{206}Pb/^{238}U$ age of 121 ± 4 Ma with a chi-square value of 2.49. The U and Th contents of these 11 spots range from 184 ppm to 1501 ppm and 96 ppm to 1101 ppm, respectively. The Th/U ratios vary from 0.43 to 0.84. The age of 121 ± 4 Ma is taken as the intrusive age of the dyke.

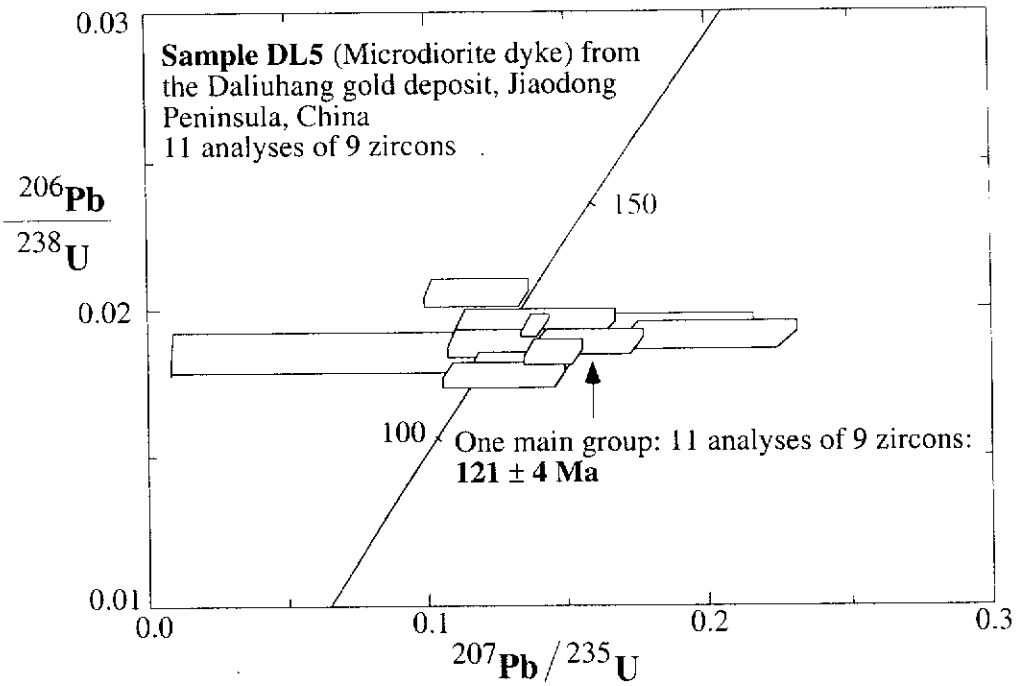

Fig. 4.7: A U-Pb concordia plot showing SHRIMP zircon analytical data from sample DL5.

4.3.6 Summary

The Daliuhang Gold Deposit is a Linglong-type gold lode and is hosted by the Guojialing granodiorite. The alteration types include sericitization, silicification, pyritization and K-feldspar alteration.

Based on the ages of the host rock and post-mineralization dyke, the timing of gold mineralization in the Daliuhang Deposit can be constrained between ca. 128 Ma and 121 Ma, which approximately coincides with the gold mineralization event (100-120 Ma) as defined within the Zhao-Ye Gold Belt by Luo and Wu (1987) and Wang et al. (1998). It is the first time, on the basis of SHRIMP zircon geochronology, that such a precise indirect age on gold mineralization in a single gold deposit within the Jiaodong Peninsula has been obtained. This is a very significant result.

4.4 Conclusion

Gold deposits of the Qi-Peng Gold Belt are related to fault zones such as the Majiayao Fault Zone, and are hosted by the Late Archaean Jiaodong Group and the Guojialing granodiorite. These gold deposits are all of the Linglong-style (vein-filling type).

By using SHRIMP U-Pb zircon analysis techniques, the Guojialing granodiorite was dated at ca. 128 Ma, which coincides well with the SHRIMP zircon results (126-130 Ma) for the Guojialing Suite obtained by Wang et al. (1998). The emplacement of the Guojialing granodiorite represents an igneous event which is later than the Linglong granitoids (150-165 Ma) which lie to the west in the Jiaodong Peninsula.

As in the Zhao-Ye Gold Belt, dykes, including felsic, intermediate and mafic types, are also widely distributed within the Qi-Peng Gold Belt. By using SHRIMP U-Pb zircon methods, a post-mineralization intermediate dyke was dated at ca. 121 Ma, which constrains the minimum age of gold mineralization. Combined with previous Rb-Sr dating data on gold mineralization in the region, it is considered that the timing of gold mineralization in the Qi-Peng Gold Belt approximately coincides with that in the Zhao-Ye Gold Belt (100-120 Ma).

CHAPTER 5: GOLD DEPOSITS EXAMINED WITHIN THE MU-RU GOLD BELT OF THE JIAODONG PENINSULA

5.1 Introduction

The Mu-Ru Gold Belt (Fig. 5.1) is located in the eastern part of the Jiaobei Terrane and contains ca. 20% of gold reserves on the Jiaodong Peninsula. Gold deposits of this belt are hosted by the Early Proterozoic Jingshan Group and the Kunyushan Batholith, and are commonly spatially controlled by fault zones (Fig. 5.1).

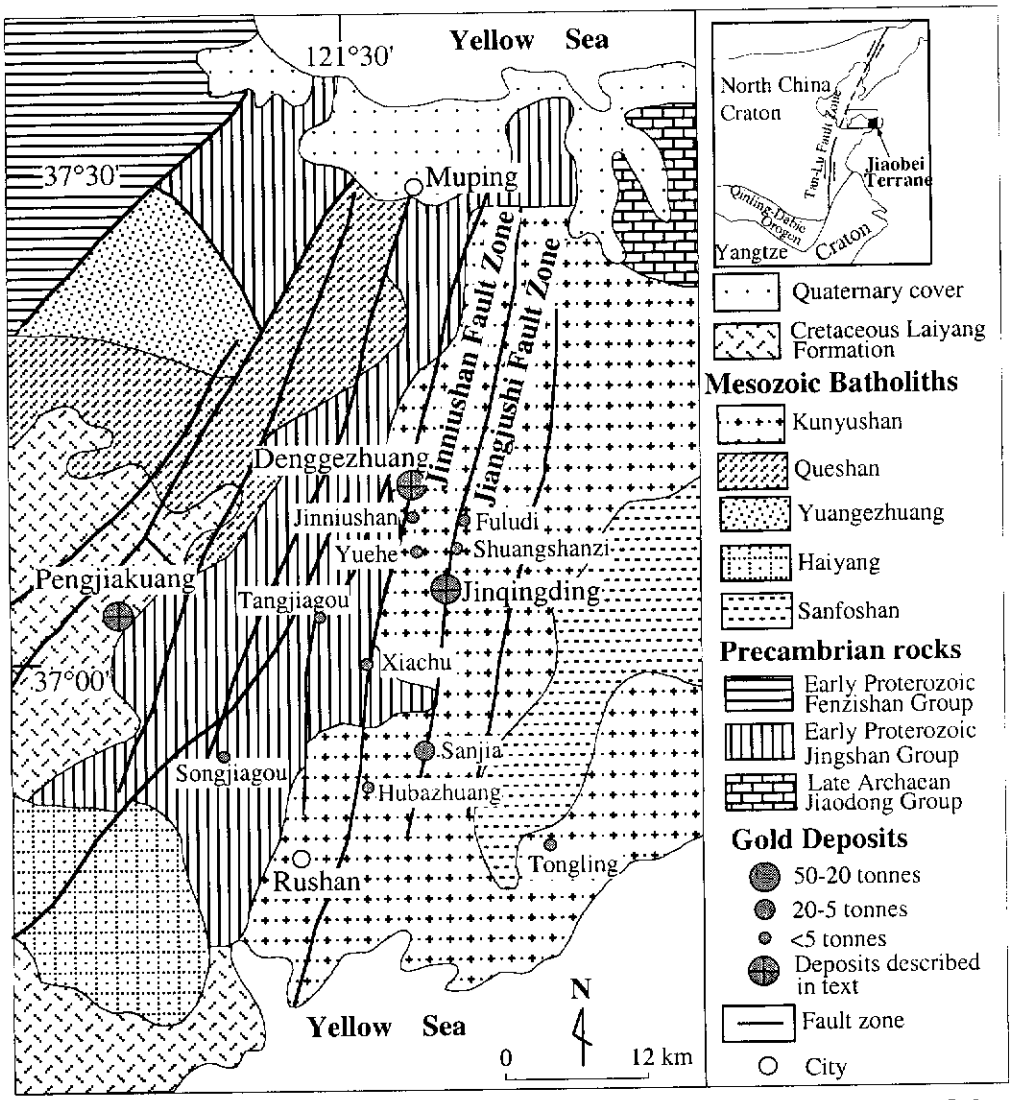

Fig. 5.1: Distribution map of gold deposits within the Mu-Ru Gold Belt of the Jiaodong Peninsula. Note that many gold deposits are spatially related to the Kunyushan Batholith and Fault Zones (modified from Gao et al., 1998).

These gold deposits are either of the Linglong-style (vein-filling type) or Jiaojia-style (disseminated-and-veinlet type). The Pengjiakuang, Denggezhuang and Jinqingding Gold Deposits are described in more detail below.

5.2 Pengjiakuang Gold Deposit

The Pengjiakuang Gold Deposit (lat. 37°04'47" to 37°05'30" N; long. 121°15'09" to 121°18'08" E) is located about 25 km northwest of the city of Rushan (Fig. 5.1), and occupies an area of 5.73 km^2. It was discovered in 1989 by the No.3 Team of Geology and Exploration, BGMRSP, based on regional reconnaissance, 1:10,000 scale mapping, trenching and drilling. The deposit is located at the contact between a hanging wall sequence of Cretaceous Laiyang Formation to the south and a footwall sequence of Early Proterozoic Jingshan Group to the north (Fig. 5.2). In 1996, its reported gold reserves were 20 tonnes.

5.2.1 Lithological Units

The Early Proterozoic Jingshan Group makes up the footwall of the Pengjiakuang Gold Deposit (Fig. 5.2a), and comprises marble and gneiss. The Cretaceous Laiyang Formation makes up the hanging wall of this deposit (Fig. 5.2a), and consists of conglomerate. Two swarms of intermediate to mafic dykes (Fig. 5.2a), which strike in nearly E-W and NE directions, respectively, are present in the mining area. Some dykes are controlled by the same structure as the orebodies (Shen et al., 1998) (Fig. 5.2a and b) which trend in an E-W direction.

5.2.2 Pengjiakuang Fault Zone

The Pengjiakuang Fault Zone is about 5 km long and varies in width from 50 m to 300 m. It generally trends in an E-W direction and dips 15°-40°S (The No.3 Team of Geology and Exploration, BGMRSP, 1994) (Fig. 5.2a and b). This fault is considered as a low-angle normal fault (Yang et al., 1999).

5.2.3 Alteration

The wall-rock alteration types associated with this deposit include sericitization, silicification, pyritization, K-feldspar alteration, carbonatization and chloritization. A large alteration halo around the deposit is well-developed along the main fault and it

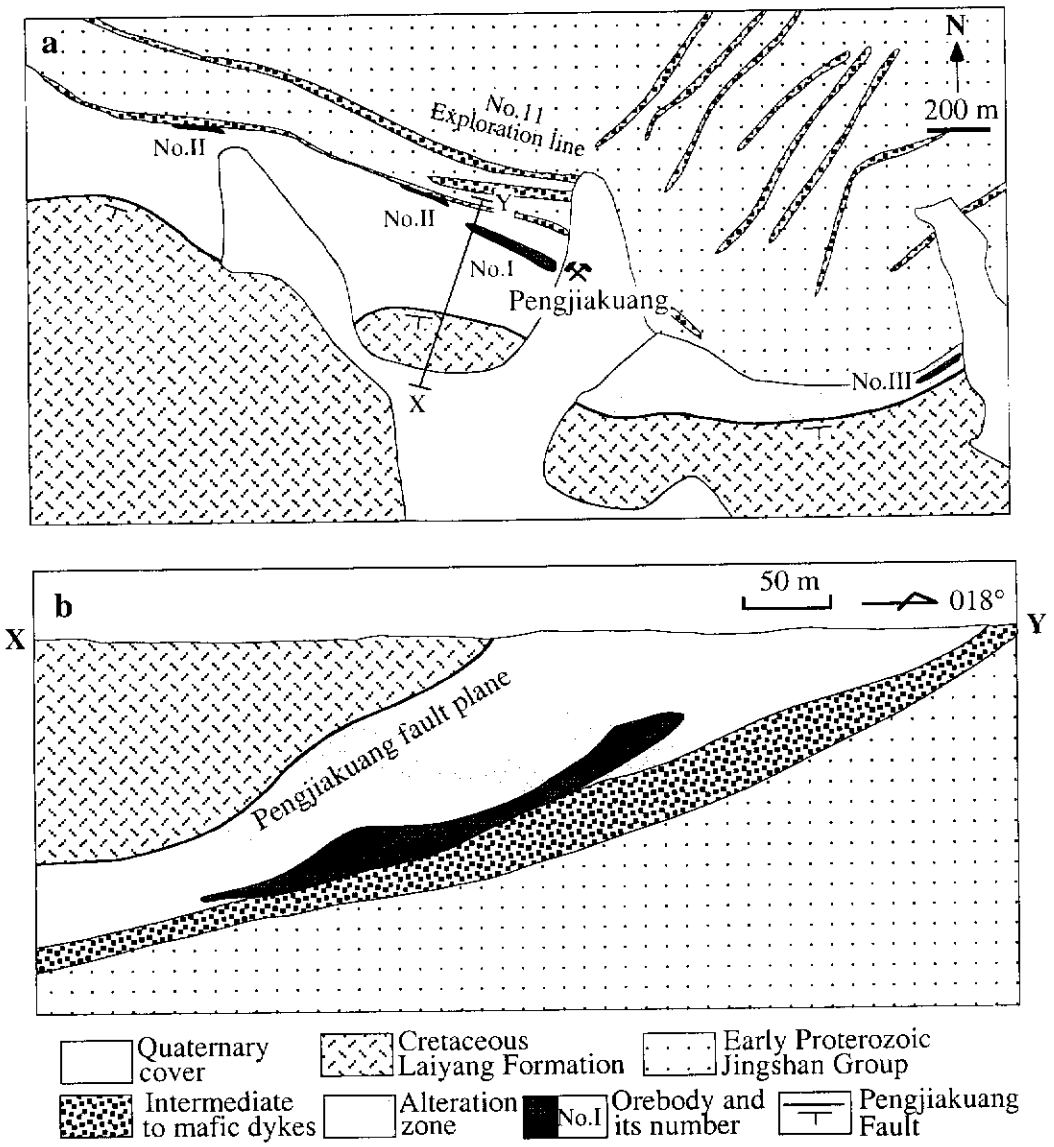

Fig. 5.2: (a) Geological plan of the Pengjiakuang Gold Deposit; (b) vertical section along part of the No.11 exploration line (modified from Shen et al, 1998).

can reach to 400 m in width (Fig. 5.2a), which is similar to Jiaojia-style deposits elsewhere in the Jiaodong Peninsula (Shen et al., 1998; Yang et al., 1999).

5.2.4 Orebodies

The deposit consists of the No.I, No.II and No.III orebodies, which are all controlled by the Pengjiakuang Fault Zone (Fig. 5.2a). The No.I orebody strikes 290° and dips 15°-40°S and is ca. 500 m in length, averaging 5.39 m in thickness with a maximum of 10.6 m. The grade averages 4.51 g/t, with a maximum of 22.42 g/t. The discontinuous No.II orebody strikes in the same direction as the No.I lode and dips 15°-30°S. It is ca. 400 m in length and ranges from 0.33 to 1.6 m in thickness, with an average of 0.75 m. The grade ranges from 2.01 g/t to 9.1 g/t. The No.III orebody strikes in a WSW direction and dips 20°S. It is ca. 300 m in length and averages 0.3 m in thickness. Its average grade is 3.45 g/t (The No.3 Team of Geology and Exploration, BGMRSP, 1994).

5.2.5 Ore Mineralogy and Paragenesis

Ore minerals include pyrite, chalcopyrite, galena and sphalerite; pyrite is the most abundant. Gangue minerals consist of quartz, sericite, calcite, plagioclase, K-feldspar and dolomite. Gold is present as electrum, carried by pyrite and quartz (Yang et al., 1999). Four stages of hydrothermal mineral formation in this deposit have been identified. From the oldest to the youngest, these stages are: stage 1: pyrite-quartz; stage 2: gold-quartz-pyrite; stage 3: gold-quartz-base metal sulphides; stage 4: quartz-carbonate (Yang et al., 1999).

5.2.6 Geochronology

Since some dykes were altered and occupy the same structure as orebodies (Figs. 5.2 and 5.3), they have been considered by some workers to be temporally associated with the gold mineralization event and presumably an approximate timing of gold mineralization can be obtained by dating these dykes. On the basis of this, sample PJ1 was selected for SHRIMP analysis. The SHRIMP results are listed in Table 5.1 and illustrated on a concordia plot in Figure 5.4. Following is the description of sample PJ1 and the interpretation of its SHRIMP zircon U-Pb age.

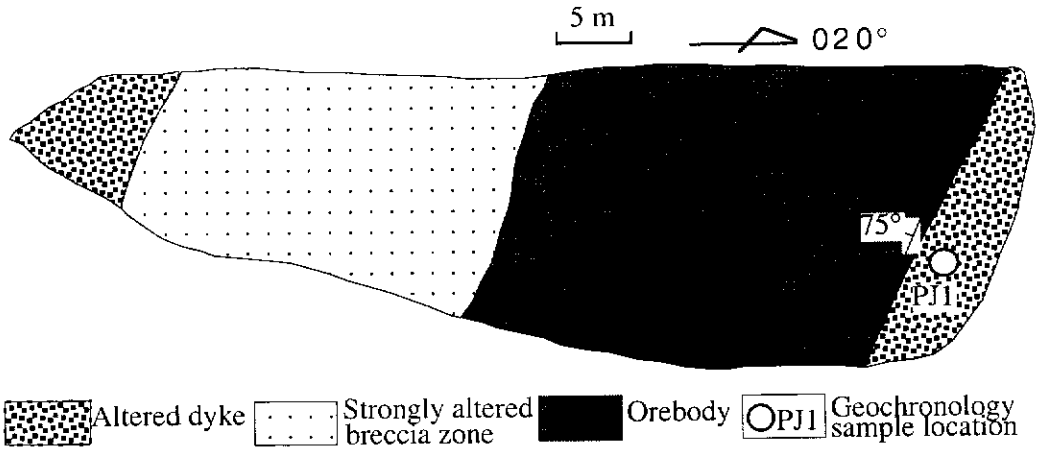

Fig. 5.3: Sketch of the northwest wall of the open pit of the Pengjiakuang Gold Deposit. Located at: lat. 37°05'8.5"N, long. 121°16'41.6"E.

Table 5.1: SHRIMP U-Pb data for zircons from sample PJ1 from the Pengjiakuang Gold Deposit. Analyses are listed in order of increasing age. The following notation is used for analysed grains: 1.1=grain 1, first point analysed. Data are ^{204}Pb-corrected. Individual analyses are shown with a 1σ error. The $^{207}Pb/^{206}Pb$ age is adopted for crystals with ages of more than 1.0 Ga.

spot	U (ppm)	Th (ppm)	Th/U	Total Pb (ppm)	$\frac{204Pb}{206Pb}$	f206 (%)	$\frac{207Pb}{206Pb}$	$\frac{206Pb}{238U}$	$\frac{207Pb}{235U}$	$\frac{207Pb}{206Pb}$ Age (Ma)
Sample PJ1										
12.1	355	99	0.28	114	0.00019	0.003	0.111±1	0.3109±54	4.75±9	1812±12
10.1	128	30	0.24	40	0.00081	0.013	0.111±2	0.2977±56	4.56±13	1816±34
1.2	405	191	0.47	139	0.0002	0.003	0.112±1	0.3169±54	4.89±9	1832±11
1.1	949	431	0.45	321	0.00007	0.001	0.113±0	0.3165±53	4.91±9	1840±6
11.1	273	77	0.28	95	0.00024	0.004	0.113±1	0.3342±58	5.22±10	1851±13
5.1	234	59	0.25	79	0.00042	0.007	0.113±1	0.325±57	5.08±11	1855±17
8.1	847	61	0.07	277	0.00011	0.002	0.114±0	0.3332±56	5.24±9	1866±6
3.1	241	83	0.34	87	0.00012	0.002	0.114±1	0.343±63	5.4±13	1866±23
2.1	453	85	0.19	144	0.00018	0.003	0.114±1	0.3148±54	4.96±9	1867±10
6.1	202	38	0.19	70	0.00043	0.007	0.114±1	0.3392±60	5.34±11	1867±18
7.1	455	128	0.28	155	0.00018	0.003	0.114±1	0.3282±56	5.18±10	1872±9
9.1	228	72	0.32	78	0.00031	0.005	0.115±2	0.3257±59	5.15±12	1876±24
4.1	812	278	0.34	276	0.00006	0.001	0.115±0	0.3248±55	5.16±9	1883±6

Sample PJ1

Sample PJ1 is an altered dyke, which was collected from the northwest wall of the open pit of this deposit (Fig. 5.3). Due to intensive alteration, petrographic

examination could not be use to precisely identify this dyke, but it was most probably of basalt-andesite composition, indicated by a large amount of altered euhedral feldspars set in a groundmass of plagioclase and altered glass. Zircons selected for analysis range in size from 132 μm to 100 μm and are pale brown in colour. Some grains are rounded and some are euhedral.

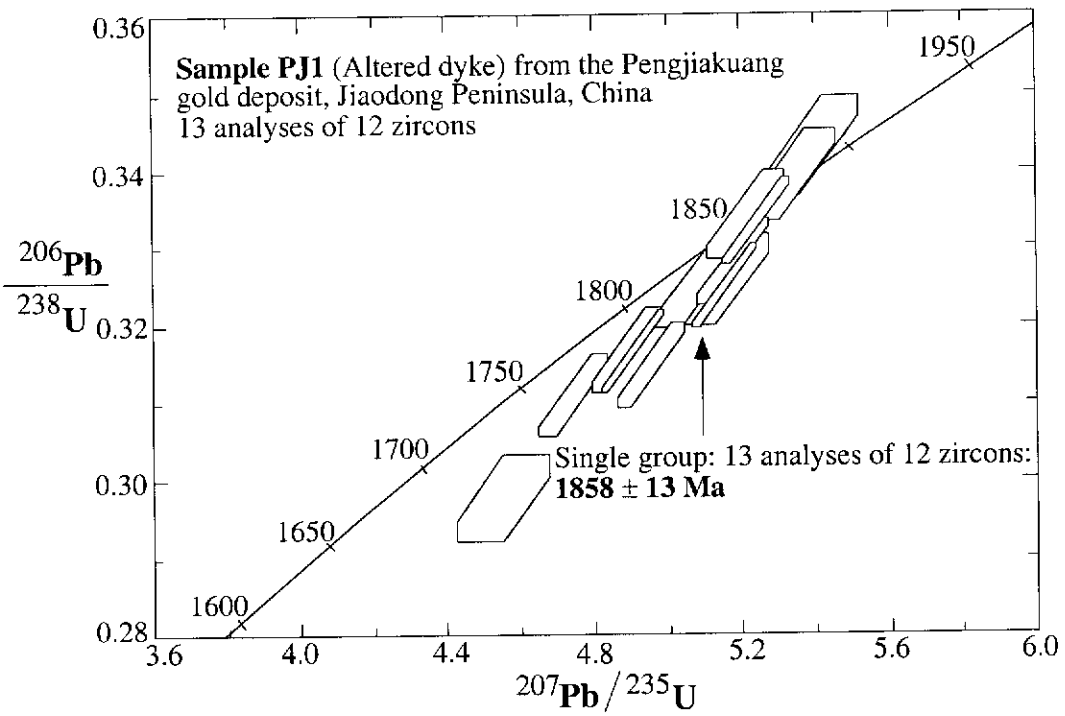

Fig. 5.4: Concordia plot showing SHRIMP U-Pb zircon analytical data for sample PJ1.

Thirteen analyses were made on 12 grains (Fig. 5.4), and ages fall in a range between 1883 ± 6 Ma and 1812 ±12 Ma (Table 5.1). These define a coherent group (Fig. 5.4) having a weighted mean $^{207}Pb/^{206}Pb$ age of 1858 ± 13 Ma with a chi-square value of 4.38. The U and Th contents of these 13 spots range from 128 ppm to 949 ppm and 30 ppm to 431 ppm, respectively. The Th/U ratios vary from 0.07 to 0.47. These zircon grains were formed during dyke intrusion and the age of 1858 ± 13 Ma. is the age of dyke emplacement. It is the first time, on the basis of SHRIMP zircon geochronology, that such an "older" dyke at 1858 ± 13 Ma has been identified within the Jiaodong Peninsula. Due to the orebodies being situated at the contact between a hanging wall sequence of Cretaceous Laiyang Formation and a footwall sequence of Early Proterozoic Jingshan Group, the timing of gold mineralization should be later than the Cretaceous period. Based on dating of sericite by the K-Ar method, Sun et al. (1995) concluded that the timing of gold mineralization in the Pengjiakuang Deposit is 100.59 ± 1.96 Ma. Therefore, the age of 1858 ± 13 Ma cannot represent the timing of

gold mineralization, although the dated dyke occupies the same structure as the orebodies.

5.2.7 Summary

The Pengjiakuang Gold Deposit is located at the contact between a hanging wall sequence (conglomerate) of Cretaceous Laiyang Formation and a footwall sequence (marble and gneiss) of Early Proterozoic Jingshan Group. This contact is marked by the Pengjiakuang Fault Zone. The wall-rock alteration types include sericitization, silicification, pyritization, K-feldspar alteration, carbonatization and chloritization. The Jiaojia-style orebodies are characterised by a large alteration halo developed along the Pengjiakung Fault Zone.

Using SHRIMP U-Pb zircon dating, a dyke, which was considered to be formed during the gold mineralization event, yields an age of ca. 1858 Ma. It represents a Palaeoproterozoic dyke event, but it cannot represent the timing of gold mineralization which should be later than the Cretaceous period (the age of the hanging wall). Sericite dating by K-Ar method indicates the timing of gold mineralization was ca.100 Ma, which is consistent with the mineralization event which occurred at ca. 100-120 Ma in the Zhao-Ye and Qi-Peng Gold Belts (Chapters 3 and 4 of this thesis).

5.3 Denggezhuang Gold Deposit

The Denggezhuang Gold Deposit (lat. 37°10' to 37°11' N; long. 121°35' to 121°36' E) is situated 25 km south of Muping (Fig. 5.1), and occupies an area of 3 km^2. It was discovered in 1958 by the No.3 Team of Geology and Exploration, BGMRSP, based on regional reconnaissance. From 1981 to 1992, further detailed exploration work, including 1:10,000 scale mapping, interpretation of geophysical and geochemical data, trenching and drilling, was carried out. The known reserves were estimated at 28.68 tonnes in 1992. This deposit is characteristic of the Linglong-style (vein-filling type) of gold occurrence. It is hosted by the Kunyushan granitoids and structurally controlled by the Jinniushan Fault Zone (Fig. 5.1).

5.3.1 Lithological Units

The unit hosting the Denggezhuang Gold Deposit is the Kunyushan granitoid, which consists of monzogranite within the mining area. It is grey in colour, has a medium- to coarse-grained equigranular texture and is mainly composed of

plagioclase, K-feldspar, quartz and biotite. Accessory minerals include titanite, apatite, pyrite and zircon. A swarm of felsic to mafic dykes, including pegmatite, microdiorite and lamprophyre, are present at the deposit and cross-cut the host monzogranite (The No.3 Team of Geology and Exploration, BGMRSP, 1992; Ying, 1994 and 1996).

5.3.2 Jinniushan Fault Zone

The Jinniushan Fault Zone is about 60 km long (Fig. 5.1) and varies in width from 5 m to 25 m. It generally strikes 010°-015° and dips 60°-82° ESE. A wavy main fault plane, marked by a grey-coloured fault gouge zone (up to 10 cm in thickness) is continuously developed. This fault zone is considered to be a first-order structure characteristic of compressional-shearing with sinistral movement (The No.3 Team of Geology and Exploration, BGMRSP, 1992). A set of second-order faults, which also strike 010°-020° and dip 50°-80° NW, are situated in the footwall of the Jinniushan Fault Zone, and host the gold lodes (Fig. 5.5) of the Denggezhuang Deposit. These are believed to be splays off the Jinniushan Fault.

5.3.3 Alteration

At the Denggezhuang Deposit, the alteration styles are dominantly sericitization, silicification, pyritization, K-feldspar alteration, carbonatization and chloritization. Alteration haloes occur along both sides of the orebodies, and range from 20 m to 40 m in width, with a maximum of 60 m. The alteration haloes mainly consist of altered monzogranite and of monzogranite cataclasite, and tend to become wider down-dip (The No.3 Team of Geology and Exploration, BGMRSP, 1992).

5.3.4 Lodes

The deposit mainly consists of the No.I, No.II and No.III lodes (Fig. 5.5), which are believed to be controlled by NNE-trending splays sub-parallel to the Jinniushan Fault Zone and are cut by a NW-trending post-mineralization fault. The No.I lode includes 7 orebodies, among which the No.$I_{1\text{-}1}$ and No.$I_{2\text{-}2}$ orebodies are the first and second largest, with known gold reserves of 12.89 and 7.17 tonnes, respectively. The No.$I_{1\text{-}1}$ orebody strikes 010°-025° and dips 60°-90° NW with an average dip angle of 81°. It is 1703 m in length and varies from 0.07 m to 4.4 m in thickness, with an average of 1.16 m. It has been explored to a depth of 554 m down-dip with, its gold grade ranging from 1.5 g/t to 52.36 g/t, with an average of 8.72 g/t.

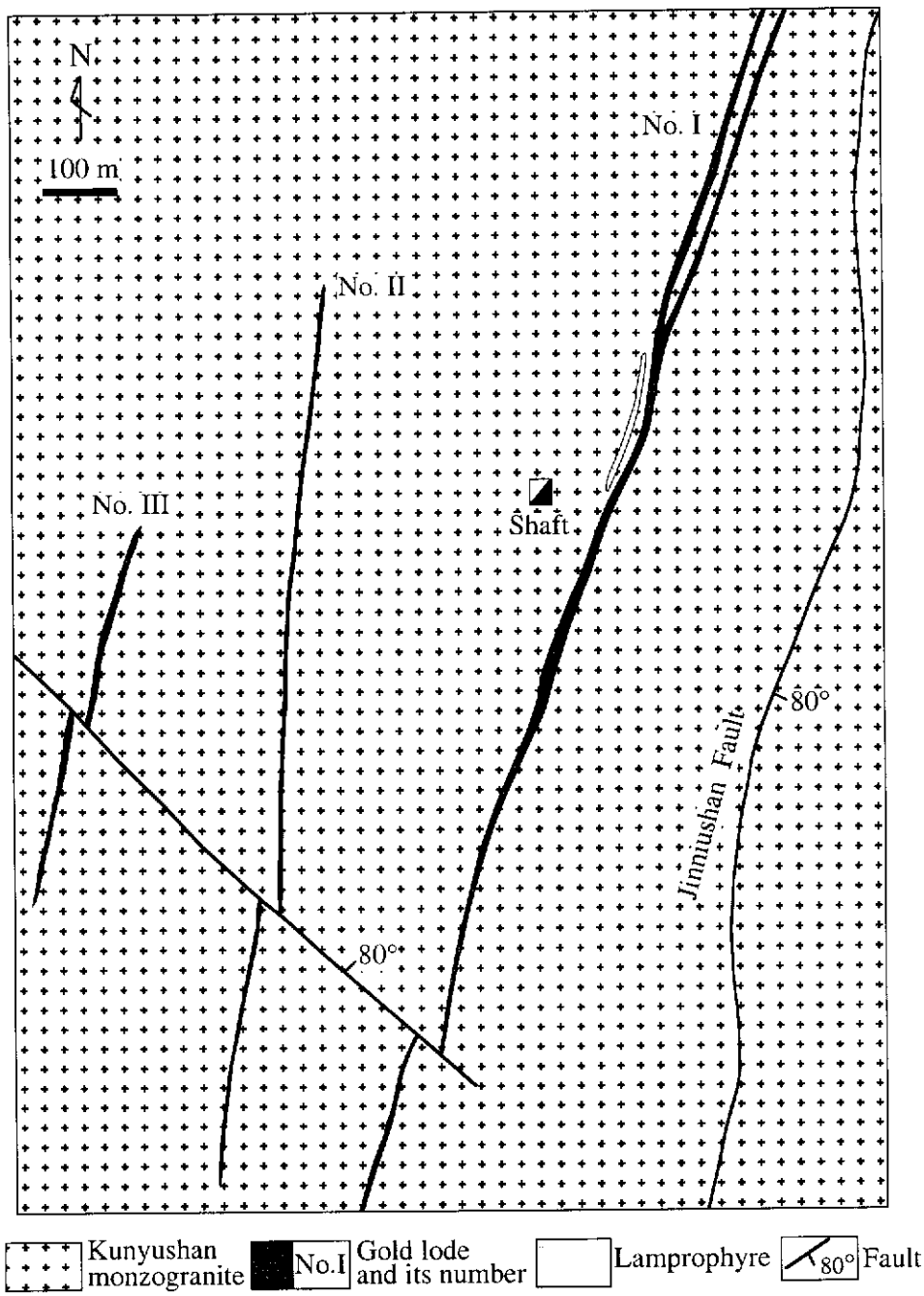

Fig. 5.5: Geological map of the Denggezhuang Gold Deposit, showing the distribution of gold lodes (labelled No. I, II and III) (modified from the No.3 Team of Geology and Exploration, BGMRSP, 1992).

The No.I2-2 orebody strikes 010°-025° and dips 22°-79° NW with an average dip angle of 53°. It is 1158 m in length and ranges from 0.16 m to 2.63 m in thickness, with an average of 0.8 m, and extends for a depth of 632 m down-dip; its gold grade ranges from 1.56 g/t to 40.24 g/t, with an average of 9.42 g/t. The No.II lode includes 6 orebodies, with known gold reserves of 7.69 tonnes. The largest orebody (No.II-1) strikes 010° and dips 60°-85° WNW with an average dip angle of 82°; it is 600 m in length and varies from 0.14 m to 3.8 m in thickness, with an average of 0.97 m. It extends for a depth of 470 m down-dip and its gold grade varies from 4.1 g/t to 77.5 g/t, with an average of 11.28 g/t. The No.III lode only comprises one small orebody (No.III-1). This orebody strikes 010°-020° and dips WNW at an average angle of 84°; it is 297 m in length and averages 0.76 m in thickness, and extends for a depth of 134 m down-dip. Its average gold grade is 6.09 g/t.

5.3.5 Ore Mineralogy and Paragenesis

Ore minerals include pyrite, siderite, hematite, magnetite, chalcopyrite, galena, sphalerite, pyrrhotite and arsenopyrite. Pyrite is the most abundant, making up 82.5% of the ore minerals, and carries about 90% of the gold (The No.3 Team of Geology and Exploration, BGMRSP, 1992). Gangue minerals are dominantly quartz, dolomite, calcite, sericite, and chlorite. Gold minerals are also present and consist mainly of electrum and trace amounts of native gold. Based on the mineralogical, textural, and crosscutting relationships observed in the field, four stages of hydrothermal mineral formation have been identified. From the oldest to the youngest these stages are: stage 1: pyrite-quartz; stage 2: gold-quartz-pyrite; stage 3: gold-quartz-multiple metal sulphides; and stage 4: quartz-carbonate. Stages 2 and 3 are closely related to gold mineralization. Fluid inclusion studies indicate temperatures associated with stages 1 to 4 are 331-270°C, 280-230°C, 240-170°C and 190-140°C, respectively (Gao et al., 1998).

Stage 1

In this stage, the mineral assemblage mainly consists of coarse-grained quartz and pyrite. The quartz is milk-white in colour and ranges from 1.5 mm to 2.5 mm in diameter, with an anhedral habit. The pyrite is generally euhedral and/or subhedral and ranges from 1.5 mm to 2.5 mm in diameter. Fractures are well-developed in the pyrite, and many other metal sulphides, such as chalcopryite and sphalerite, occur as infillings.

Stage 2

The mineral assemblage of this stage is dominantly pyrite, quartz, magnetite, pyhrrotite, electrum and native gold. The pyrite is generally euhedral and fine- to medium-grained. The quartz is fine-grained and granular, with a smoke-grey colour.

Stage 3

The mineral assemblage of this stage, which is complex and characterised by multiple metal sulphides, is dominantly composed of quartz, pyrite, chalcopyrite, galena, sphalerite and electrum. This paragenesis forms veinlet and disseminated mineralization. The quartz and pyrite are very fine-grained.

Stage 4

The mineral assemblage of this stage mainly consists of quartz, calcite and dolomite, occurring as veinlets filling in fractures within the host rocks. This stage post-dates gold mineralization, cross-cutting the mineralized veins.

5.3.6 Geochronological Data

In order to provide indirect constraints on the timing of gold mineralization in the Denggezhuang Deposit, it is necessary to reliably date the Kunyushan granitoids — the host of this deposit — and the cross-cutting dykes. Numerous previous geochronological studies, including Rb-Sr on whole rock and biotite, K-Ar on biotite, Ar-Ar on biotite and conventional U-Pb in zircon, have been carried out on the Kunyushan granitoids (An et al., 1988; Xu et al., 1989; Zhang et al., 1995). However, the ages are controversial, ranging from Palaeoproterozoic (ca. 2000 Ma) to Early Cretaceous (ca. 120 Ma). This study is the first to provide a precise SHRIMP zircon age for the Kunyushan granitoids, and sample DG5-1 (Fig. 5.6) from the wall rock of the deposit was selected for this purpose. Some dykes within the deposit were altered and occupy the same structures as the orebodies, being considered by some workers to be temporally related to the gold mineralization event. Sample DG5-3 (Fig. 5.6) from one of these dykes was selected for SHRIMP zircon dating to test this view.

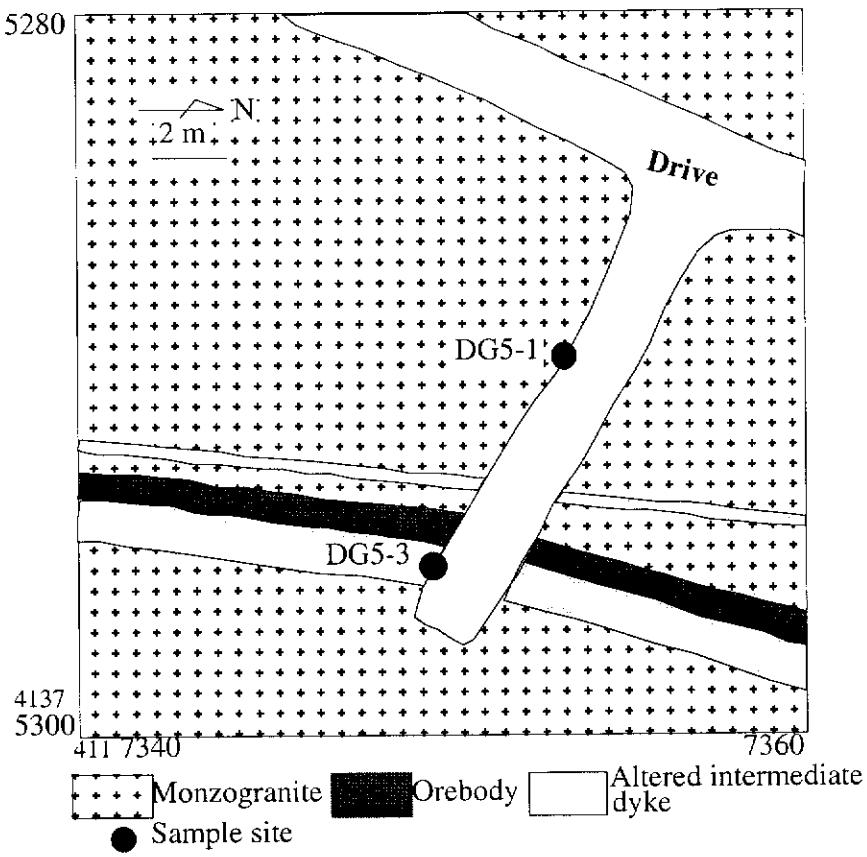

Fig. 5.6: Part of plan of level 5 at the Denggezhuang Gold Deposit, showing the location of geochronology samples.

SHRIMP results for the two samples are listed in Table 5.2 and illustrated on concordia diagrams in Figures 5.7 and 5.8. Following are the descriptions of the samples and the interpretation of their SHRIMP zircon U-Pb ages.

Sample DG5-1

Sample DG5-1 is a medium-grained monzogranite with a hypido- to allotriomophic equigranular texture. It comprises plagioclase (polysynthetic albite twins, 40%), potassic feldspar ("tartan" twins, 30%), quartz (25%), biotite (partly replaced by sericite, 3%), and minor titanite, zircon, apatite and opaque minerals. Zircons range in colour from colourless to pale brown. Most grains are euhedral, with perfect pyramidal terminations, and their elongation ratios vary from 2:1 to 4:1. Zircons selected for analysis were above 132 μm in size.

Sixteen analyses were made on 12 euhedral zircon grains (Fig. 5.7), and $^{206}Pb/^{238}U$ ages range from 134 ± 5 Ma to 758 ± 22 Ma (Table 5.2).

Table 5.2: SHRIMP U-Pb data for zircons from samples DG5-1 and DG5-3 from the Denggezhuang Gold Deposit. Analyses are listed in order of increasing age. The following notation is used for analysed grains: 1.1=grain 1, first point analysed. Data are ^{204}Pb-corrected. Individual analyses have a 1σ error. The $^{206}Pb/^{238}U$ age is adopted for zircons with an age of less than 1.0 Ga, otherwise, the $^{207}Pb/^{206}Pb$ age is used.

spot	U (ppm)	Th (ppm)	Th/U	Total Pb (ppm)	$\frac{^{204}Pb}{^{206}Pb}$	f206 (%)	$\frac{^{207}Pb}{^{206}Pb}$	$\frac{^{206}Pb}{^{238}U}$	$\frac{^{207}Pb}{^{235}U}$	$\frac{^{206}Pb}{^{238}U}$ Age	$\frac{^{207}Pb}{^{206}Pb}$ Age
Sample DG5-1											
1.1	114	60	0.53	3	0.00181	0.029	0.044±17	0.021±8	0.13±5	134±5	
6.1	358	109	0.31	9	0.00142	0.023	0.046±6	0.0235±7	0.15±2	150±4	
4.1	143	99	0.7	4	0.00358	0.057	0.032±14	0.0239±8	0.11±5	152±5	
9.1	42	21	0.5	1	0.00443	0.071	0.033±35	0.0239±12	0.11±11	152±8	
2.1	395	63	0.16	9	0.00051	0.008	0.051±4	0.0243±7	0.17±2	155±4	
11.1	50	40	0.8	2	0.00412	0.066	0.017±34	0.0244±12	0.06±11	155±8	
10.1	445	126	0.28	11	0.00052	0.008	0.051±3	0.0245±7	0.17±1	156±4	
8.1	466	110	0.24	12	0.00058	0.009	0.052±4	0.0246±7	0.18±1	157±4	
12.1	90	51	0.56	3	0.0008	0.013	0.07±16	0.0247±9	0.24±6	157±6	
7.1	297	57	0.19	7	0.00054	0.009	0.049±4	0.0248±7	0.17±2	158±5	
7.2	150	66	0.44	4	0.00272	0.043	0.034±14	0.0247±8	0.12±5	158±5	
5.1	903	585	0.65	25	0.00079	0.013	0.044±3	0.0251±7	0.15±1	160±4	
3.1	120	53	0.44	4	0.00097	0.016	0.074±7	0.0336±10	0.34±4	213±6	
5.2	191	25	0.13	9	0.00095	0.015	0.053±5	0.0434±13	0.32±3	274±8	
8.2	115	172	1.5	15	0.00029	0.005	0.066±4	0.1006±29	0.92±6	618±17	
10.2	69	103	1.51	12	0.00082	0.013	0.067±5	0.1247±38	1.16±9	758±22	
Sample DG5-3											
10.2	881	23	0.03	17	0.00032	0.005	0.047±2	0.0204±7	0.13±1	130±4	
10.1	704	21	0.03	14	0.00041	0.007	0.046±2	0.0212±7	0.13±1	135±4	
12.2	1289	31	0.02	25	0.00027	0.004	0.047±2	0.0211±7	0.14±1	135±4	

Table 5.2 (continued)

spot	U (ppm)	Th (ppm)	Th/U	Total Pb (ppm)	$\frac{^{204}Pb}{^{206}Pb}$	f206 (%)	$\frac{^{207}Pb}{^{206}Pb}$	$\frac{^{206}Pb}{^{238}U}$	$\frac{^{207}Pb}{^{235}U}$	$\frac{^{206}Pb}{^{238}U}$ Age	$\frac{^{207}Pb}{^{206}Pb}$ Age
12.1	1132	33	0.03	22	0.00019	0.003	0.049±2	0.0212±7	0.14±1	135±4	
7.1	202	131	0.65	5	0.00105	0.017	0.042±8	0.0216±8	0.12±3	138±5	
8.1	355	16	0.05	8	0.00084	0.013	0.044±6	0.0227±8	0.14±2	145±5	
9.2	763	128	0.17	17	0.00048	0.008	0.046±3	0.0231±7	0.15±1	147±5	
7.2	265	91	0.34	6	0.00064	0.01	0.044±6	0.0235±8	0.14±2	150±5	
9.1	870	158	0.18	21	0.00011	0.002	0.049±2	0.0246±8	0.17±1	157±5	
3.1	188	68	0.36	5	0.0006	0.01	0.058±8	0.0253±9	0.2±3	161±6	
8.2	405	304	0.75	12	0.00026	0.004	0.051±3	0.0267±9	0.19±1	170±5	
13.1	433	15	0.03	11	0.00034	0.005	0.048±4	0.0274±9	0.18±2	174±6	
14.1	374	5	0.01	10	0.00072	0.012	0.042±4	0.0287±9	0.17±2	183±6	
5.1	725	162	0.22	21	0.00022	0.003	0.049±2	0.0292±9	0.2±1	186±6	
15.2	1769	321	0.18	50	0.00012	0.002	0.049±1	0.0298±9	0.2±1	189±6	
1.1	1750	183	0.1	49	0.00012	0.002	0.049±1	0.03±9	0.2±1	190±6	
15.1	966	198	0.21	29	0.00031	0.005	0.046±1	0.0305±10	0.19±1	194±6	
6.1	1146	394	0.34	36	0.00027	0.004	0.048±1	0.0309±10	0.21±1	196±6	
11.1	770	238	0.31	25	0.00016	0.003	0.051±1	0.0323±10	0.23±1	205±6	
17.1	52	11	0.21	2	0.00407	0.065	0.017±19	0.035±15	0.08±9	222±9	
6.2	439	52	0.12	16	0.00005	0.001	0.052±2	0.0377±12	0.27±2	238±8	
2.1	44	27	0.61	2	0.00418	0.067	0.02±22	0.0377±16	0.11±11	238±10	
16.1	144	140	0.97	8	0.00052	0.008	0.056±5	0.0466±16	0.36±4	294±10	
4.1	425	215	0.51	120	0.00008	0.001	0.109±1	0.2591±82	3.89±13		1783±10

The concordant $^{206}Pb/^{238}U$ ages of 758 ± 22 Ma (1σ) and 274 ± 8 Ma (1σ) (Fig. 5.7) were obtained from the cores of grain 10 (spot 10.2) and grain 5 (spot 5.2), respectively. The cores were formed during earlier geological events and subsequently mantled by overgrowth rims (spots 10.1 and 5.1) yielding younger $^{206}Pb/^{238}U$ ages of 156 ± 4 Ma (1σ) and 160 ± 4 Ma (1σ), respectively (Table 5.2). The youngest concordant $^{206}Pb/^{238}U$ age of 134 ± 5 Ma (1σ) (Fig. 5.7) was obtained from the rim (spot 1.1) of grain 1, this age may represent the effect of a later magmatic event, such as dyke intrusion.

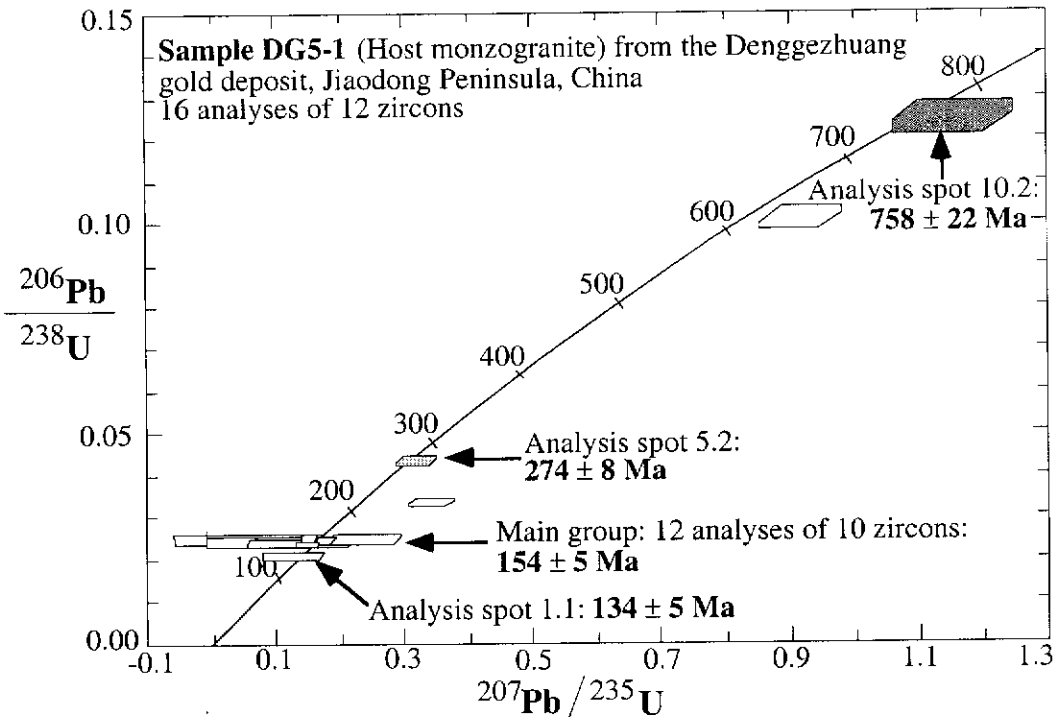

Fig. 5.7: Concordia plot showing SHRIMP U-Pb zircon analytical data for sample DG5-1.

Twelve analyses of the 10 grains from the sample form a coherent main group (Fig. 5.7) with a weighted mean $^{206}Pb/^{238}U$ age of 154 ± 5 Ma (2σ) and a chi-square value of 1.83. The U and Th contents of these 12 spots range from 42 ppm to 903 ppm and 21 ppm to 585 ppm, respectively. The Th/U ratios vary from 0.13 to 1.51. Since these euhedral grains with good pyramid terminations are considered to be of igneous origin, the weighted mean age of 154 ± 5 Ma is taken as the age of igneous crystallization of the Kunyushan monzogranite, which coincides well with the age of the Linglong granitoids (150-165 Ma) distributed within the northwestern part of the Jiaodong Peninsula (Wang et al., 1998).

Sample DG5-3

Sample DG5-3 is a mesocratic dyke with a porphyritic texture. Due to strong alteration, its primary ferromagnesian minerals are wholly replaced by chlorite. calcite and magnetite. A large amount of quartz occurs within the groundmass. Therefore, this sample seems to be an intermediate dyke, although its original nature cannot be exactly identified. Only twenty zircon grains were extracted from a ca. 5 kg sample of DG5-3, ranging in size from 132 μm to -74 μm. Most zircons are colourless and transparent. Only five grains had good crystal faces, with an average elongation ratio of about 3:1; others are rounded.

A total of 24 analyses were carried out on 17 zircon grains (Fig. 5.8), with ages ranging from 1783 ± 10 Ma to 130 ± 4 Ma (Table 5.2).

Analysis spot 4.1 yields a discordant $^{207}Pb/^{206}Pb$ age of 1783 ± 10 Ma (Fig. 5.8a). The spot 4.1 is located at the rim of grain 4, which is euhedral and is indistinguishable from the main magmatic zircon population in terms of morphology. The age of 1783 ± 10 Ma indicates Palaeoproterozoic basement in this area. Analysis spot 16.1 of rounded grain 16 yields a concordant $^{206}Pb/^{238}U$ age of 294 ± 10 Ma (1σ) (Fig. 5.8b) and is interpreted to be a xenocryst. The core (spot 6.2) and rim (spot 6.1) of grain 6 with rounded terminations give concordant $^{206}Pb/^{238}U$ ages of 238 ± 8 Ma and 196 ± 6 Ma (1σ) (Fig. 5.8b), respectively, which indicates that the core formed during an earlier geological event and was mantled by a later overgrowth rim.

The main population consists of 10 analyses of 9 grains, which form a coherent group (Group 1 on Fig. 5.8b) having a weighted mean $^{206}Pb/^{238}U$ age of 184 ± 10 Ma with a chi-square value of 4.66. If spots 3.1 and 11.1 are excluded from Group 1, the chi-square value is reduced to 2.34, but the corresponding group age of 185 ± 9 Ma is not much different from the age of 184 ± 10 Ma. Since 9 of the 10 analysis spots are from the rounded grains and the other one (spot 8.2) is located in the core of euhedral grain 8, the group age of 184 ± 10 Ma is taken to represent a real geological event, and these rounded grains and the core of grain 8 may have formed during this event. The U and Th contents of these 10 spots range from 188 ppm to 1769 ppm and 5 ppm to 394 ppm, respectively. The Th/U ratios vary from 0.01 to 0.75.

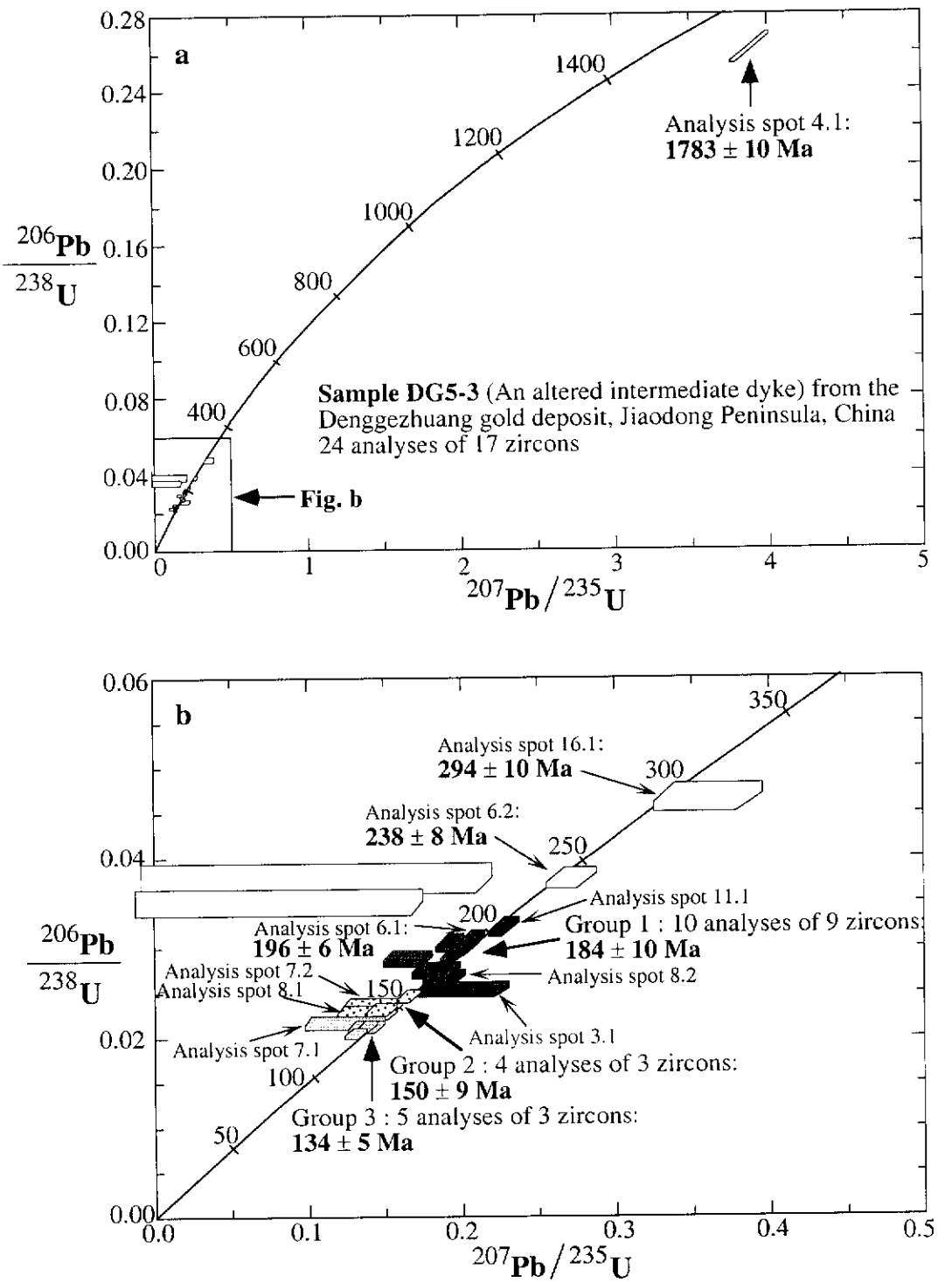

Fig. 5.8: U-Pb concordia plots showing (a) total SHRIMP zircon analytical data from sample DG5-3 and (b) enlargement detailing the young zircon populations.

The second population consists of 4 analyses of 3 zircons, which define a coherent group (Group 2 in Fig. 5.8b) having a weighted mean $^{206}Pb/^{238}U$ age of 150± 9 Ma with a chi-square value of 0.94. The three zircon grains (7, 8 and 9) are euhedral. The four analyses include spot 7.2 from the centre of grain 7, spot 8.1 from the rim of grain 8, and spots 9.1 and 9.2 from the rim and centre of grain 9, respectively. The U and Th contents of these 4 spots range from 265 ppm to 870 ppm and 16 ppm to 158 ppm, respectively. The Th/U ratios vary from 0.05 to 0.34. The group age of 150 ± 9 Ma coincides with the age of sample DG5-1 (154 ± 5 Ma) from the Kunyushan monzogranite hosting this deposit. These zircons are taken to be crystals incorporated from the host rock during emplacement of the dyke.

The third population is composed of 5 analyses of 3 zircons, which form a coherent group (Group 3 in Fig. 8.5b) having a weighted mean $^{206}Pb/^{238}U$ age of 134 ± 5 Ma with a chi-square value of 0.33. These three zircon grains (7, 10 and 12) are euhedral. The five analyses comprise spot 7.1 from the rim of grain 7, spots 10.1 and 10.2, spots 12.1 and 12.2 from the rims and centres of grains 10 and 12, respectively. The U and Th contents of these 5 spots range from 202 ppm to 1289 ppm, 21 ppm to 131 ppm, respectively. The Th/U ratios vary from 0.02 to 0.65. This group age of 134 ± 5 Ma is considered to represent the intrusive age of the intermediate dyke. This may also approximately represent the timing of gold mineralization in the area, since the dyke is associated with the mineralized fractures. When dykes intruded within this mining area, they passed through a deeper granitoid dated at 184 ± 10 Ma and host rock (Kunyushan monzogranite) with the age of 150 ± 9 Ma. Some euhedral grains such as grains 10 and 12 and some overgrowth rims such as the rim of grain 7 (spot 7.1) were formed from the dyke magma. This overgrowth rim is the same as the rim (spot 1.1) of grain 1 from sample DG5-1, which yields a concordant $^{206}Pb/^{238}U$ age of 134 ± 5 Ma (1σ) as well. Thus confirming that there was a dyke emplacement event at ca. 130 Ma in this area.

5.3.7 Summary

The Denggezhuang Gold Deposit is hosted by the Kunyushan granitoids which consist of monzogranite within the mining area. This deposit is characteristic of Linglong-style gold lodes, which are structurally controlled by NNE-trending branches off the Jinniushan Fault Zone. The alteration types includes sericitization, silicification, pyritization, K-feldspar alteration, carbonatization and chloritization. Alteration haloes occur along both margins of the orebodies.

Using SHRIMP U-Pb zircon dating, the Kunyushan monzogranite has a $^{206}Pb/^{238}U$ age of ca. 154 Ma, which coincides with the age of the Linglong granitoids (150-165 Ma). This is the first precise SHRIMP zircon age obtained for the Kunyushan granitoids. A dyke, which is considered to be associated with gold mineralization in both time and space, was also dated by SHRIMP and yielded an age of ca. 130 Ma. However, using the Rb-Sr isochron method on altered whole-rocks, the timing of gold mineralization in the Denggezhuang deposit was determined as ca. 118 Ma (Zhang et al., 1995), which coincides with the timing of gold mineralization event (100-120 Ma) elsewhere in the Zhao-Ye and Qi-Peng Gold Belts. This may suggest the dyke occurred earlier than the time of gold mineralization. The age of dyke emplacement (ca. 130 Ma) in this area is consistent with the emplacement age (126-130 Ma) of the Guojialing granodiorite distributed within the Zhao-Ye and Qi-Peng Gold Belts, but is older than the emplacement age (120-122 Ma) of many of the dykes widely distributed within the two adjacent gold belts. Whether in this area there existed another dyke emplacement event at ca. 120 Ma, which is closely associated with the timing of gold mineralization in the Zhao-Ye and Qi-Peng Gold Belts, requires further work.

5.4 Jinqingding Gold Deposit

The Jinqingding Gold Deposit (lat. 37°06' N; long. 121°38' E) is located ca. 30 km NNE of the city of Rushan (Fig. 5.1). It was discovered in 1967 by the No.3 Team of Geology and Exploration, BGMRSP, based on regional reconnaissance. From 1981 to 1989, further detailed exploration work, including 1:10,000 and 1:2,000 scale mapping, interpretation of geophysical and geochemical data, trenching and drilling, was carried out and the known reserves were estimated at 29.5 tonnes in 1989. This deposit is structurally controlled by the Jiangjunshi Fault Zone (Fig. 5.1). Just like at Denggezhuang, this deposit is also hosted by the Kunyushan granitoids and is characteristic of the Linglong-style (vein-filling type) gold occurrence.

5.4.1 Lithological Units

The lithologic unit hosting the Jinqingding Gold Deposit is the Kunyushan granitoids, which consist of biotite-monzogranite within the mining area. The granite is grey in colour, has a medium-grained equigranular texture and mainly consists of quartz, plagioclase, K-feldspar and biotite. Accessory minerals include titanite, apatite, magnetite and zircon. A swarm of felsic to more mafic dykes, including microgranite, microdiorite and lamprophyre, are present at the deposit (Fu, 1989; Xie et al., 1998).

5.4.2 Jiangjunshi Fault Zone

The Jiangjunshi Fault Zone is about 50 km long (Fig. 5.1), and varies in width from 1 m to 15 m. It generally strikes 005°-020° and dips 75°-90° ESE. This fault zone is considered to be a first-order structure characteristic of compressional-shearing with dextral movement (The No.3 Team of Geology and Exploration, BGMRSP, 1989).

5.4.3 Alteration

At the Jinqingding Deposit, the alteration styles are dominantly sericitization, silicification, pyritization, K-feldspar alteration, carbonation and chloritization. Alteration haloes occur along both margins of the orebodies, and range from 1 m to 16 m in width. Alteration increases in intensity with proximity of the orebodies. The alteration haloes mainly consist of altered monzogranite and altered cataclastic rocks derived from the granite (The No.3 Team of Geology and Exploration, BGMRSP, 1989).

5.4.4 Orebodies

The deposit is composed of 13 orebodies. The No.II orebody is the largest (Fig. 5.9), with known gold reserves of 25 tonnes, and is hosted by the Jiangjunshi Fault. This orebody is tabular in shape, strikes 035°-050°, dips 77°-90° SE and pitches in a NNE direction at about 65°. It is 365 m in length and ranges from 0.3 m to 6.96 m in thickness with an average of 2.7 m, and has been explored to a depth of 800 m down-pitch. Its gold grade varies from 1.5 g/t to 30 g/t (average of 20.1 g/t), but locally reaches a maximum of 242.38 g/t. The No.III and No. IV orebodies are the second and third largest with known gold reserves of 2.11 tonnes and 1.06 tonnes, respectively. The No.III orebody is located in the hanging wall of the No.II orebody, and the distance between them varies from 13 m to 22 m. This orebody strikes 024°-048° and dips 85° SE. It is 115 m in length and ranges from 0.6 m to 1.75 m in thickness with an average of 1.22 m. Its average gold grade is 44.14 g/t, with a maximum of 118.86 g/t. The No.IV orebody is located in the footwall of the No.II orebody, and the distance between them ranges from 10 m to 15 m. This orebody strikes 020° and dips 85°-88° SE. It is 103 m in length and ranges from 0.27 m to 3.8 m in thickness with an average of 2.41 m; its average gold grade is 15.4 g/t, with a maximum of 96.1 g/t. Both the No.III and No.IV orebodies are hidden and are not exposed at the surface.

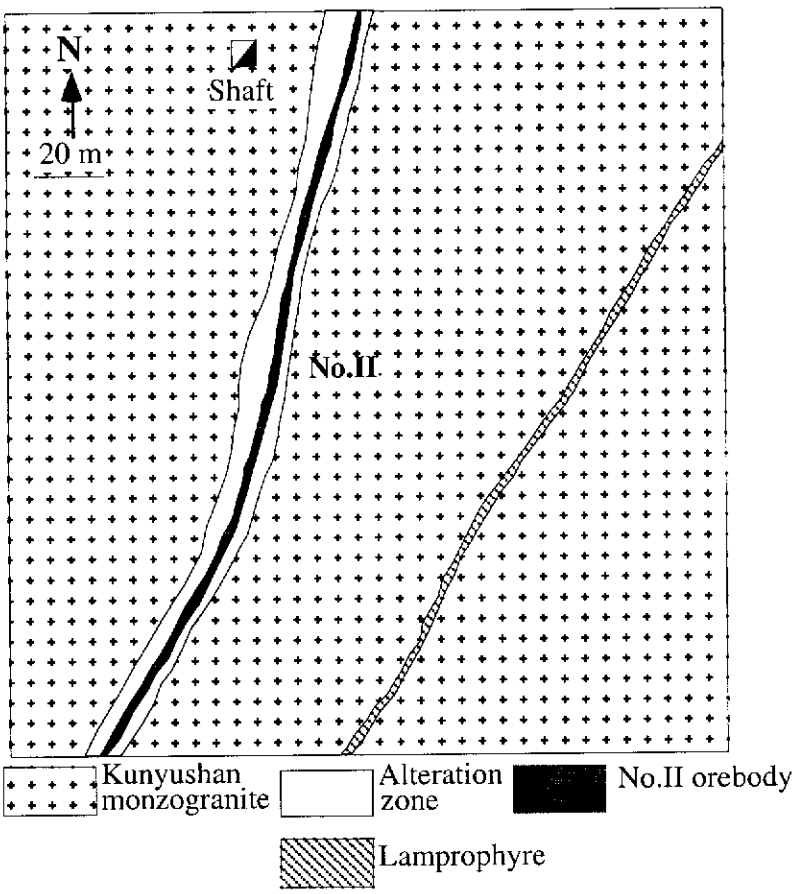

Fig. 5.9: Simplified geological map of part of the Jinqingding Gold Deposit (modified from the No.3 Team of Geology and Exploration, BGMRSP, 1989).

5.4.5 Ore Mineralogy and Paragenesis

Ore minerals include pyrite, chalcopyrite, galena, sphalerite, pyrrhotite and bornite. Among them, pyrite is the most abundant, making up about 85% of the ore minerals, and carrying about 65 % of the gold within the deposit (The No.3 Team of Geology and Exploration, BGMRSP, 1989). Gangue minerals comprise quartz, siderite, sericite, feldspar, calcite, ankerite and chlorite. Gold occurs dominantly as electrum and trace amounts of native gold. Based on the mineralogical, textural, and crosscutting relationships observed in hand specimens, four stages of hydrothermal mineral formation have been identified. From the oldest to the youngest these stages are: stage 1: pyrite-quartz, with the mineral assemblage consisting mainly of euhedral, milk-white quartz and euhedral, coarse pyrite; stage 2: gold-quartz-pyrite, with the mineral assemblage mainly composed of grey-white coloured quartz and fine-grained pyrite; stage 3: gold-quartz-multiple metal sulphides, with the mineral paragenesis

dominantly of smoke-grey coloured quartz, fine-grained pyrite and other metal minerals such as chalcopyrite, siderite and galena; stage 4: quartz-carbonate, where the mineral paragenesis consists mainly of quartz and calcite.

5.4.6 Geochronological Data

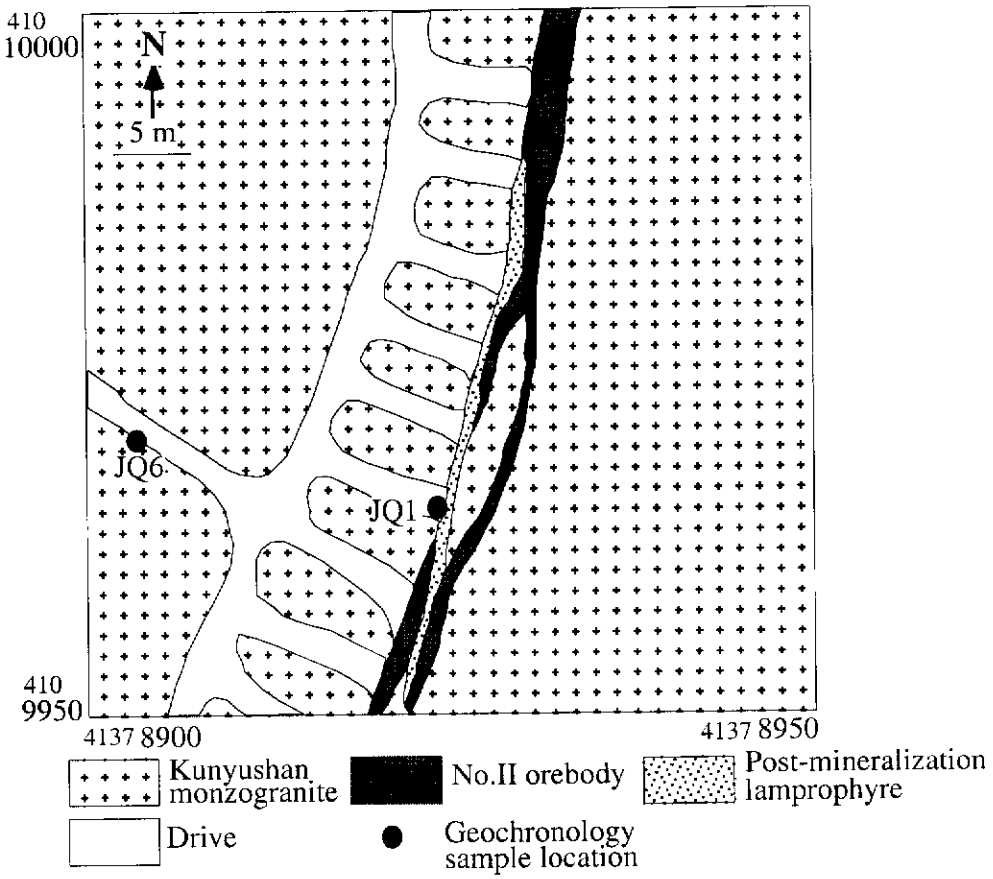

Fig. 5.10: Part of plan of Level -435 m at the Jinqingding Gold Deposit, showing the location of geochronology samples.

In order to provide indirect constraints on the timing of gold mineralization at the Jinqingding Deposit, sample JQ6 from the host rock and sample JQ1 from a post-mineralization lamprophyre dyke (Fig. 5.10) were selected for SHRIMP U-Pb zircon analysis. Unfortunately, the zircons which were extracted from sample JQ1 were insufficient for analysis, and most of them are very rounded which might mean that they are xenocrysts from the underlying basement and not formed from the dyke. Therefore, only sample JQ6 was dated by SHRIMP. The SHRIMP results are listed in Table 5.3 and illustrated on a concordia diagram in Figure 5.11. Following is the description of sample JQ6 and the interpretation of its SHRIMP zircon U-Pb age.

Sample JQ6

Sample JQ6 is a medium-grained monzogranite with a hypido- to allotriomophic equigranular texture. It comprises quartz (35%), plagioclase (polysynthetic albite twins, 35%), potassic feldspar ("tartan" twins, 20%), biotite (partly replaced by sericite, 6%), and minor titanite, zircon, apatite and opaque minerals. Zircons range from colourless to pale brown and most grains are euhedral, with well-formed pyramidal terminations, and elongation ratios varying from 2:1 to 3:1. Zircons selected for analysis were >132 μm in size.

Fifteen analyses were made on 13 euhedral zircon grains (Fig. 5.11), and ages range from 151 ± 3 Ma to 437 ± 8 Ma (Table 5.3).

Table 5.3: SHRIMP U-Pb data for zircons from sample JQ6, from the Jinqingding Gold Deposit. Analyses are listed in order of increasing age. The following notation is used for analysed grains: 1.1=grain 1, first point analysed. Data are ^{204}Pb-corrected. Individual analyses have a 1σ error. The $^{206}Pb/^{238}U$ age is adopted since all zircons are less than 1.0 Ga.

spot	U (ppm)	Th (ppm)	Th/U	Total Pb (ppm)	$\frac{204Pb}{206Pb}$	f206 (%)	$\frac{207Pb}{206Pb}$	$\frac{206Pb}{238U}$	$\frac{207Pb}{235U}$	$\frac{206Pb}{238U}$ Age (Ma)
Sample JQ6										
7.1	435	396	0.91	13	0.00248	0.04	0.041±6	0.0236±5	0.13±2	151±3
6.1	821	477	0.58	22	0.00107	0.017	0.046±3	0.0239±4	0.15±1	152±3
9.1	229	201	0.88	8	0.00466	0.075	0.029±12	0.0238±6	0.1±4	152±3
12.1	80	53	0.66	3	0.01098	0.176	0.01±31	0.024±9	0.03±10	153±6
1.1	521	413	0.79	15	0.00177	0.028	0.043±4	0.0245±5	0.14±2	156±3
5.1	1082	331	0.31	28	0.00148	0.024	0.043±3	0.0245±4	0.14±1	156±3
4.1	270	63	0.23	8	0.00375	0.06	0.045±9	0.0247±5	0.15±3	157±3
3.1	926	365	0.39	25	0.00085	0.014	0.05±3	0.025±4	0.17±1	159±3
2.1	76	30	0.39	3	0.0084	0.134	0.025±28	0.0255±10	0.09±10	162±6
13.1	2994	1058	0.35	80	0.00045	0.007	0.047±1	0.0264±4	0.17±0	168±3
1.2	161	110	0.68	6	0.00328	0.052	0.053±12	0.028±7	0.21±5	178±4
8.1	73	8	0.11	3	0.01049	0.168	0.009±29	0.0291±11	0.04±12	185±7
11.1	811	150	0.18	36	0.00069	0.011	0.054±2	0.0426±7	0.32±1	269±5
3.2	745	212	0.28	47	0.00064	0.01	0.058±2	0.0578±10	0.46±2	362±6
10.1	193	146	0.75	17	0.00202	0.032	0.056±5	0.0702±13	0.54±5	437±8

The concordant $^{206}Pb/^{238}U$ age of 437 ± 8 Ma (1σ) (Fig. 5.11) was obtained from the core (spot 10.1) of grain 10. This core is considered to have formed during an earlier geological event and is therefore inherited. Analysis spot 11.1 of euhedral

grain 11 yields a concordant $^{206}Pb/^{238}U$ age of 269 ± 5 Ma (1σ) (Fig. 5.11). This age may represent an earlier igneous event in the region. The concordant $^{206}Pb/^{238}U$ age of 178 ± 4 Ma (1σ) (Fig. 5.11) was obtained from the core (spot 1.2) of grain 1, which indicates that the core formed during an earlier igneous event and was mantled by a later overgrowth rim, represented by spot 1.1 with a $^{206}Pb/^{238}U$ age of 156 ± 3 Ma (1σ) (Table 5.3).

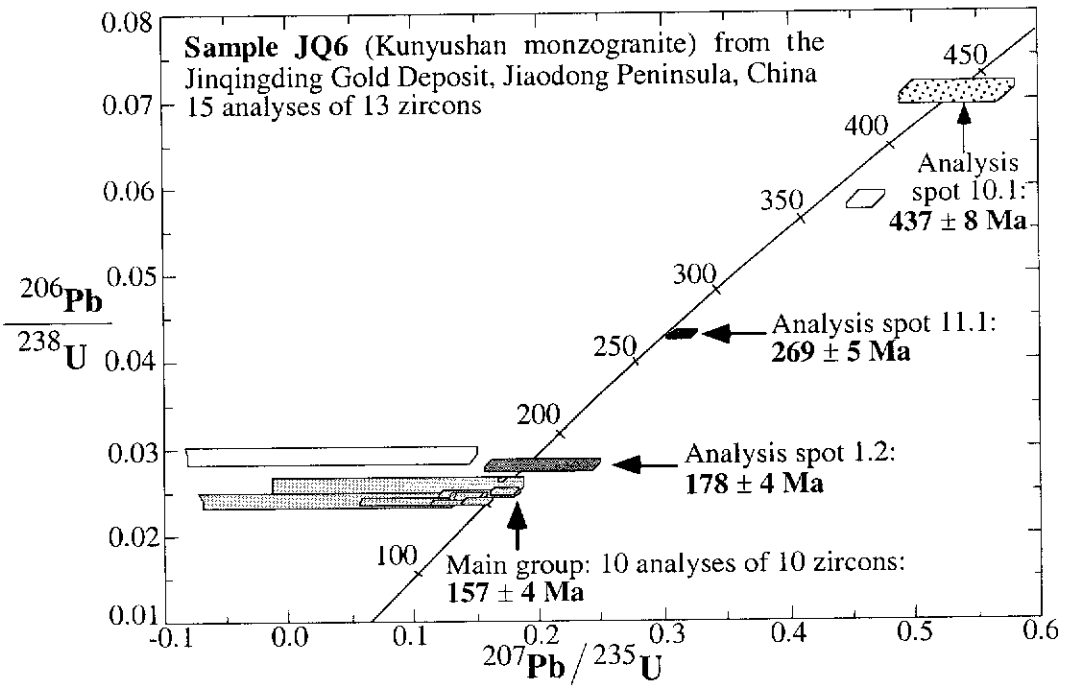

Fig. 5.11: Concordia plot showing SHRIMP U-Pb zircon analytical data from sample JQ6.

Ten analyses of the 10 grains form a coherent main population (Fig. 5.11) with a weighted mean $^{206}Pb/^{238}U$ age of 157 ± 4 Ma (2σ) and a chi-square value of 2.82. The U and Th contents of spot 13.1 are very high (2994 ppm and 1058 ppm, respectively), whilst the U and Th contents of the other 11 spots range from 73 ppm to 1082 ppm and 8 ppm to 477 ppm, respectively. The Th/U ratios vary from 0.11 to 0.91. Since these euhedral grains with good pyramid terminations are of igneous origin, the group age of 157 ± 4 Ma is taken as the age of igneous crystallization of the Kunyushan monzogranite, which coincides with the age of 154 ± 5 Ma from sample DG5-1 from the Kunyushan monzogranite at the Denggezhuang Gold Deposit. Therefore, the crystallization age of the Kunyushan granitoids is same as the age of the Linglong granitoids (150-165 Ma) within the northwestern Jiaodong Peninsula (Wang et al., 1998).

5.4.7 Summary

The Jinqingding Gold Deposit is hosted by the Kunyushan granitoids (biotite-monzogranite) and is structurally controlled by the Jiangjunshi Fault Zone. This deposit is characteristic of the Linglong-style orebodies. Alteration halos, which are characterized by sericitization, silicification, pyritization, K-feldspar alteration, carbonation and chloritization, occur along both margins of the orebodies. The closer to the orebodies the wall rocks are, the more intensive the alteration.

Using SHRIMP U-Pb zircon dating, one sample from the Kunyushan granitoids has a $^{206}Pb/^{238}U$ age of 157 ± 4 Ma, which is consistent with the age of 154 ± 5 Ma from another sample of the Kunyushan granitoids at the Denggezhuang Gold Deposit. Therefore, it is concluded that the crystallization age of the Kunyushan granitoids is the same as the age of the Linglong granitoids (150-165 Ma) within the northwestern Jiaodong Peninsula. Using the Rb-Sr isochron method on altered whole-rocks and sericite, the age of gold mineralization in this deposit was determined as 101-121 Ma (Zhang et al., 1994; Zhai et al., 1996). This age coincides reasonably well with the timing of the gold mineralization event (100-120 Ma) in the Zhao-Ye and Qi-Peng Gold Belts.

5.5 Conclusion

Gold deposits of the Mu-Ru Gold Belt are controlled by faults such as the Jinniushan and Jiangjunshi Fault Zones, and are hosted by the Early Proterozoic Jingshan Group and the Kunyushan granitoids. These gold deposits are either of the Linglong-style (vein-filling type) or Jiaojia-style (disseminated-and-veinlet type).

Using SHRIMP U-Pb zircon techniques, the Kunyushan granitoids were dated at 154 ± 7 Ma and 157 ± 4 Ma, which coincides with the emplacement age (150-165 Ma) of the Linglong granitoids. Therefore, the Kunyushan and Linglong granitoids were emplaced during the same igneous event which occurred widely within the whole of the Jiaobei Terrane.

As in the Zhao-Ye and Qi-Peng Gold Belts, dykes, including felsic, intermediate and mafic types, are also widely distributed within the Mu-Ru Gold Belt. Using SHRIMP U-Pb zircon dating, an "older" dyke emplaced at 1858 ± 13 Ma has been identified at the Pengjiakuang Deposit. In addition, one dyke spatially associated with gold mineralization yielded an age of ca. 130 Ma. This age represents the timing

of a discrete event within the Jiaobei Terrane, during which the Guojialing granodiorite was emplaced within the Zhao-Ye and Qi-Peng Gold Belts. Combined with the Rb-Sr and K-Ar data on the gold mineralization in the region, it is considered that the timing of gold mineralization event in the Mu-Ru Gold Belt is consistent with that of the Zhao-Ye and Qi-Peng Gold Belts (100-120 Ma).

CHAPTER 6: GOLD DEPOSITS EXAMINED WITHIN THE LIAODONG PENINSULA

6.1 Introduction

The Liaodong Peninsula (Fig. 1.1) is situated along the southeastern boundary of the North China Craton and contains numerous gold deposits and occurrences. The tectonic setting is similar to that of the Jiaobei Terrane which contains 25% of China's gold reserves and so this area is considered to be prospective in terms of future gold production in China (Ren, 1988). Gold deposits of the Liaodong Peninsula are hosted by Mesozoic granitoids and Palaeoproterozoic rocks and are spatially associated with fault zones (Fig. 2.4). The gold deposits are of the Linglong-style (vein-filling type). The Wulong, Sidaogou and Baiyun Gold Deposits are described in detail below.

6.2 Wulong Gold Deposit

The Wulong Gold Deposit (N40°10', E124°12') is located ca. 27 km WNW of Dandong City (Fig. 2.4), and is the deepest underground gold mine operating in China, having 13 mining levels with a maximum vertical depth of 520 m (in 1997). The deposit was discovered in the 1930s and has mineable reserves of 40 tonnes at an average grade of 7.5 g/t. It is hosted in deformed Mesozoic granite (Figs. 2.3 and 6.1). Gold mineralization is predominantly of Linglong-style (vein-filling type); the orebodies mainly occuring as gold-bearing quartz veins. There are more than 460 known auriferous quartz veins (Yang, 1997), varying from 40 m to 1100 m in length and 2 m to 17 m in width, with down-dip extensions of 250 m to 600 m (Nie, 1997b). The wall-rock alteration is weak, which indicates that gold mineralization chiefly occurs in the form of auriferous fluid filling large fractures developed within the host rock instead of replacing wall rock.

6.2.1 Structural Control of Orebodies

In the mining area, a group of faults, which extend for several kilometres along an 020° strike and dip 40°-60°W, are considered as second-order structures with respect to the Yalujiang Fault (Fig. 6.1). These faults include F1 to F7 (Yang, 1997) (Fig. 6.1). Two sets of brittle-ductile shears, controlling both orebodies and dykes, act as third-order structures of the Yalujiang Fault (Fig. 6.2a) (Yang, 1997). One set of

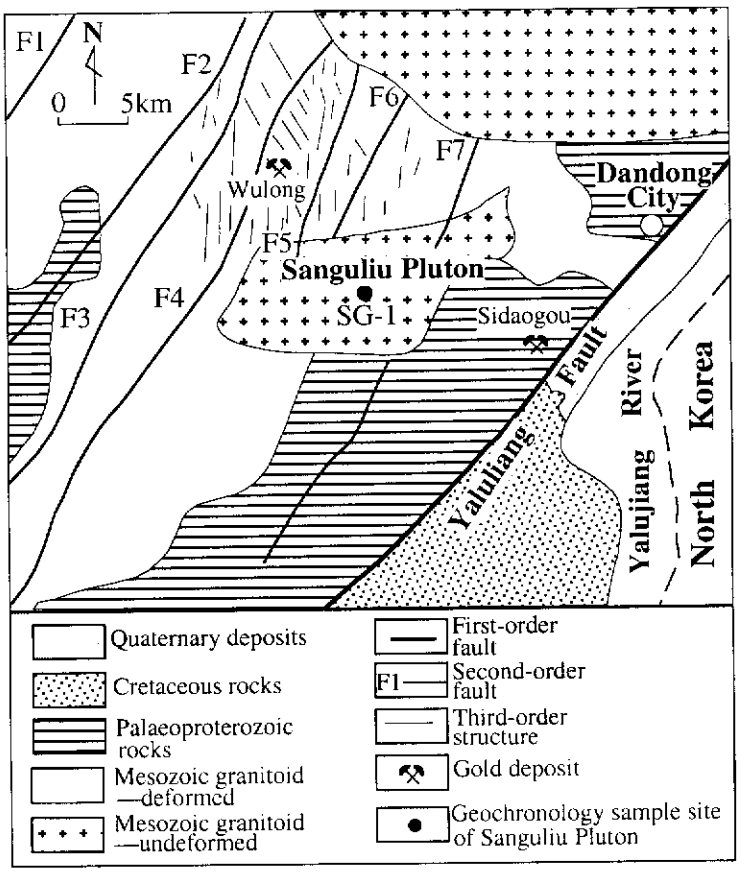

Fig. 6.1: Geological map of the Wulong Gold Deposit and environs, southeast Liaodong Peninsula (modified from Yang, 1997).

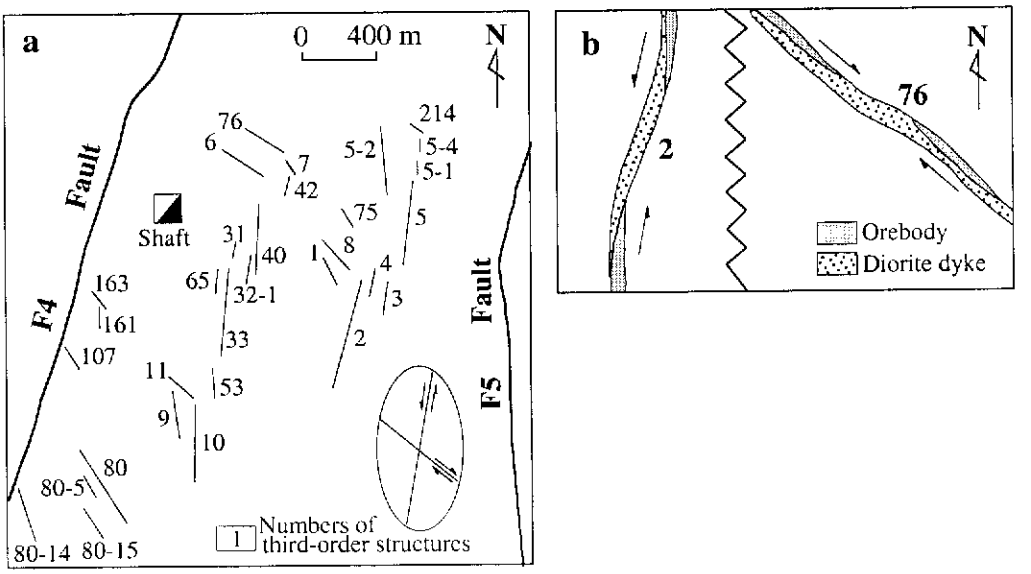

Fig. 6.2: Structural maps of the Wulong Gold Deposit showing (a) third-order structures of the Yalujiang Fault and (b) examples of orebody distribution in sinistral and dextral shears. Numbers refer to the third-order structures (modified from Yang, 1997).

shears, with sinistral motion, strikes nearly north and dips 60°- 80°W and pitches in a southerly direction; another set, with dextral sense of movement, trends northwest and dips 50°-70°SW and pitches in a southeast direction. The two sets of shears are considered to be a conjugate sets which developed approximately contemporaneously in the same stress regime and had opposite senses of movement (Yang, 1997). The orebodies in the sinistral shears occur as left-handed en-echelon arrays, whereas the orebodies in the dextral shears are arranged as right-handed en-echelon arrays (Yang, 1997) (Fig. 6.2). These orebodies can be compared to oblique shear mineralized zones as discussed by Hodgson (1989).

6.2.2 Dykes

Swarms of felsic, mafic and lamprophyric dykes are well exposed both on the surface and underground (Figs. 6.3 and 6.4). They predate, are synchronous with, or post-date gold mineralization, and some occupy the same fracture systems as the orebodies (i.e. the dykes and orebodies are controlled by the same third-order structures) (Figs. 6.2b and 6.4). The dykes are composed of foliated microdiorite, undeformed microdiorite, microgranite, lamprophyre and dolerite. The foliated microdiorite dykes are cross-cut by most other kinds of dyke and by the orebodies (Figs. 6.3 and 6.4), and fragments of them are contained in the auriferous quartz veins (Fig. 6.5), so they are regarded as the earliest dykes which predate gold mineralization. These dykes generally trend northwest and east-north-east (Figs. 6.6a and 6.6b). They are more than 100 m in length, and range from 2 m to 4 m in width. The undeformed microdiorite dykes are situated in the same structural position as the orebodies (Yang et al., 1997) (Figs. 6.4, 6.7a and 6.7b) and the majority of the dykes pervasively experienced pyritization, silicification and sericitization. The dykes thus pre-date or may possibly be synchronous with the ore formation event (Yao et al., 1990). They strike in a northwest to approximately northerly direction (Figs. 6.3, 6.6 and 6.7) and vary from ca. 100 m to ca. 2000 m in length and are commonly 2 m in width. The microgranite dykes also strike in a nearly northerly direction (Figs. 6.3, 6.6 and 6.7) and range from ca. 200 m to ca. 4000 m in length and from ca. 3 m to ca. 40 m in width. The dykes either cut or are cut by the undeformed microdiorite dykes with a northwest trend (Figs. 6.3 and 6.7a). The lamprophyre dykes cut other dykes and the orebodies (Figs. 6.3, 6.4 and 6.7b), as do dolerite dykes (Figs 6.3 and 6.6b). Therefore, the lamprophyre and dolerite dykes are the latest dykes and post-date gold mineralization. The lamprophyre dykes generally strike approximately northerly (Figs. 6.3 and 6.7b), with a maximum length of ca. 1000 m and a width of ca. 2 m. The dolerite dykes are not as widely distributed as the other dykes. They generally have in

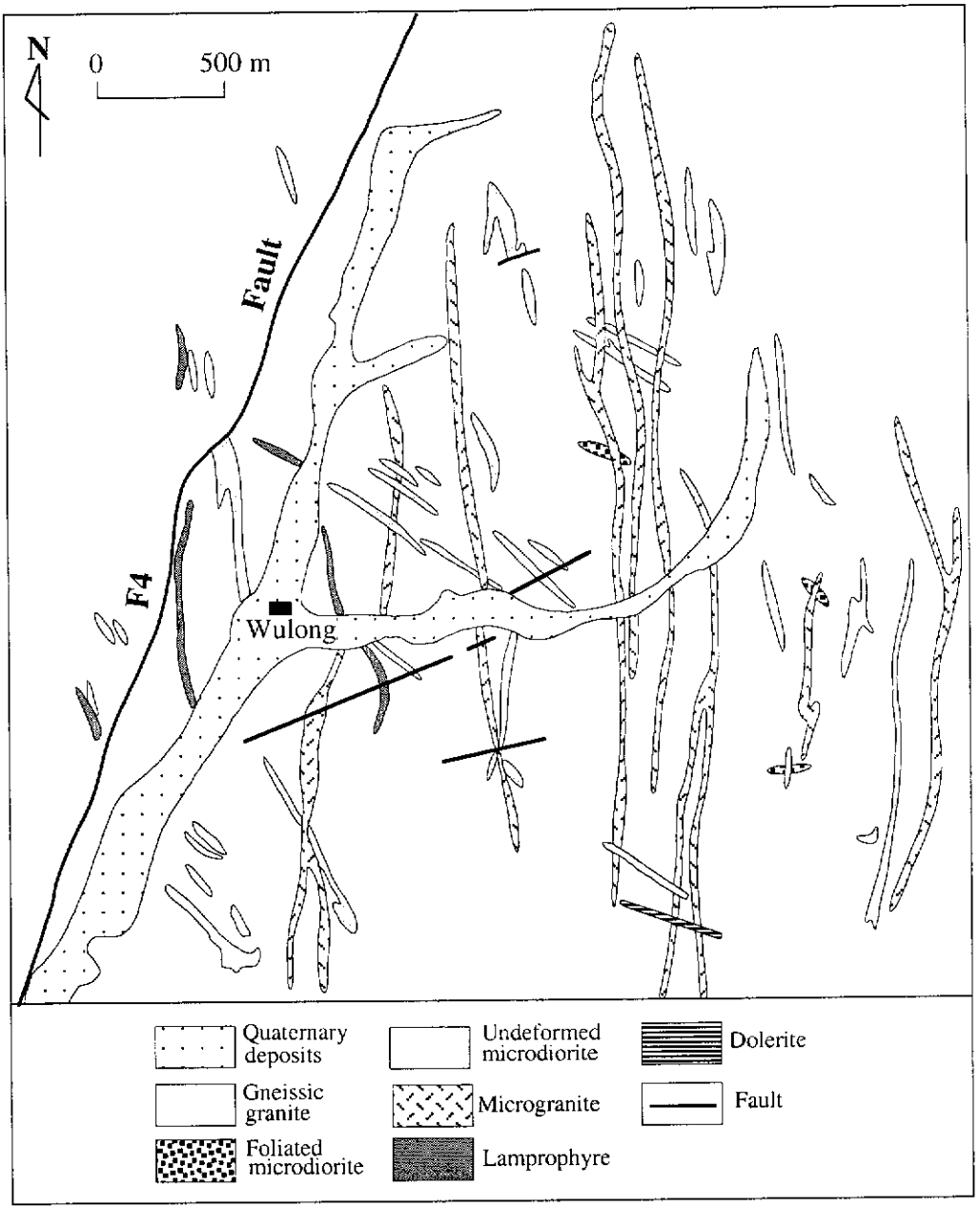

Fig. 6.3: Sketch map of main dykes exposed at the surface at the Wulong Gold Deposit (modified from Ren, 1988).

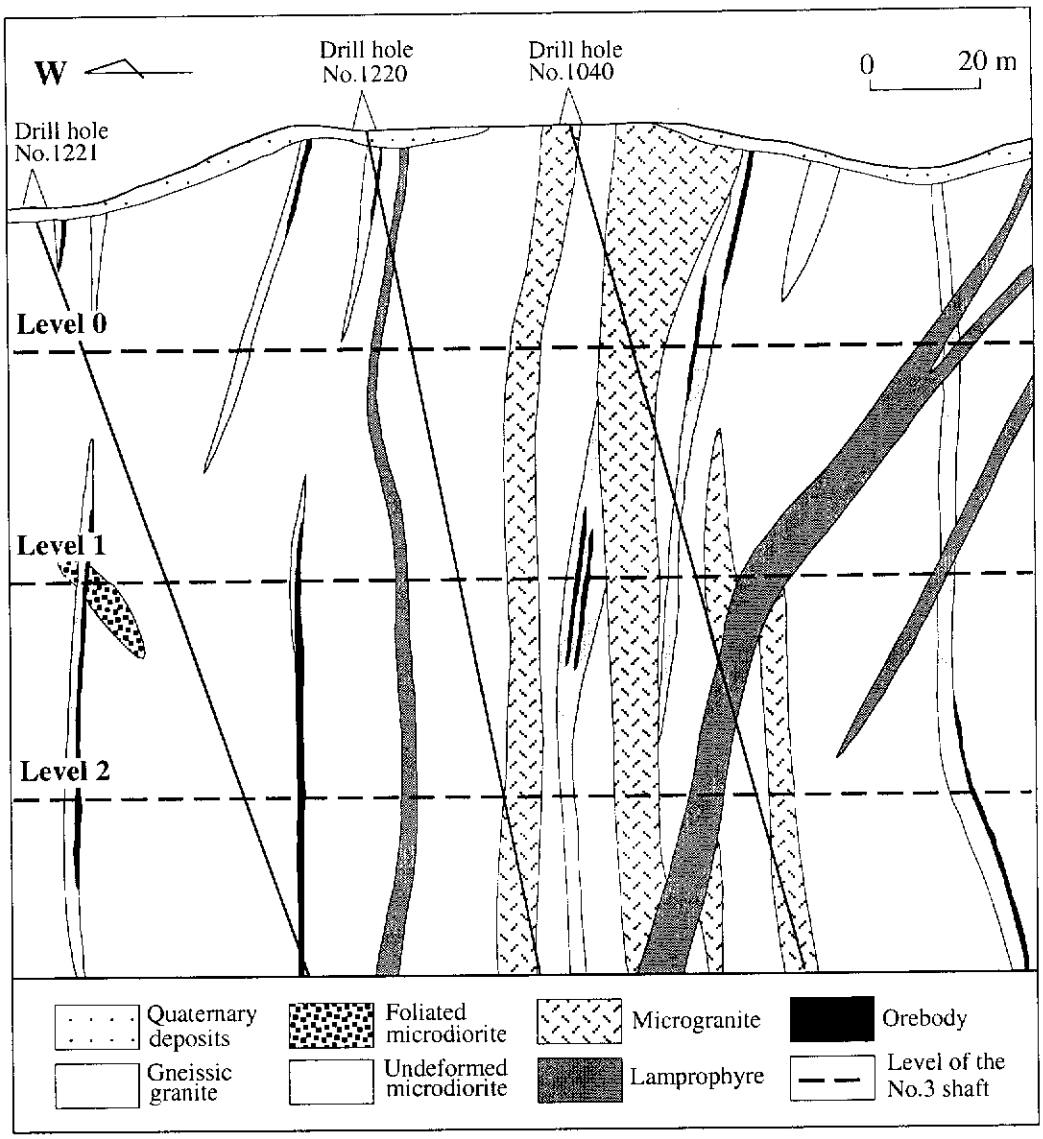

Fig. 6.4: Part of vertical section along the No. 508 exploration line at the Wulong Gold Deposit, showing the spatial relationship between dykes and orebodies (modified from unpublished maps of Wulong Gold Mine, 1996).

Fig. 6.5: Photograph showing that fragments (dark parts) of the earliest dykes are included in auriferous quartz vein (light) at the Wulong Gold Deposit. A pencil (14.5 cm long) at the bottom left corner of the photograph is used for scale.

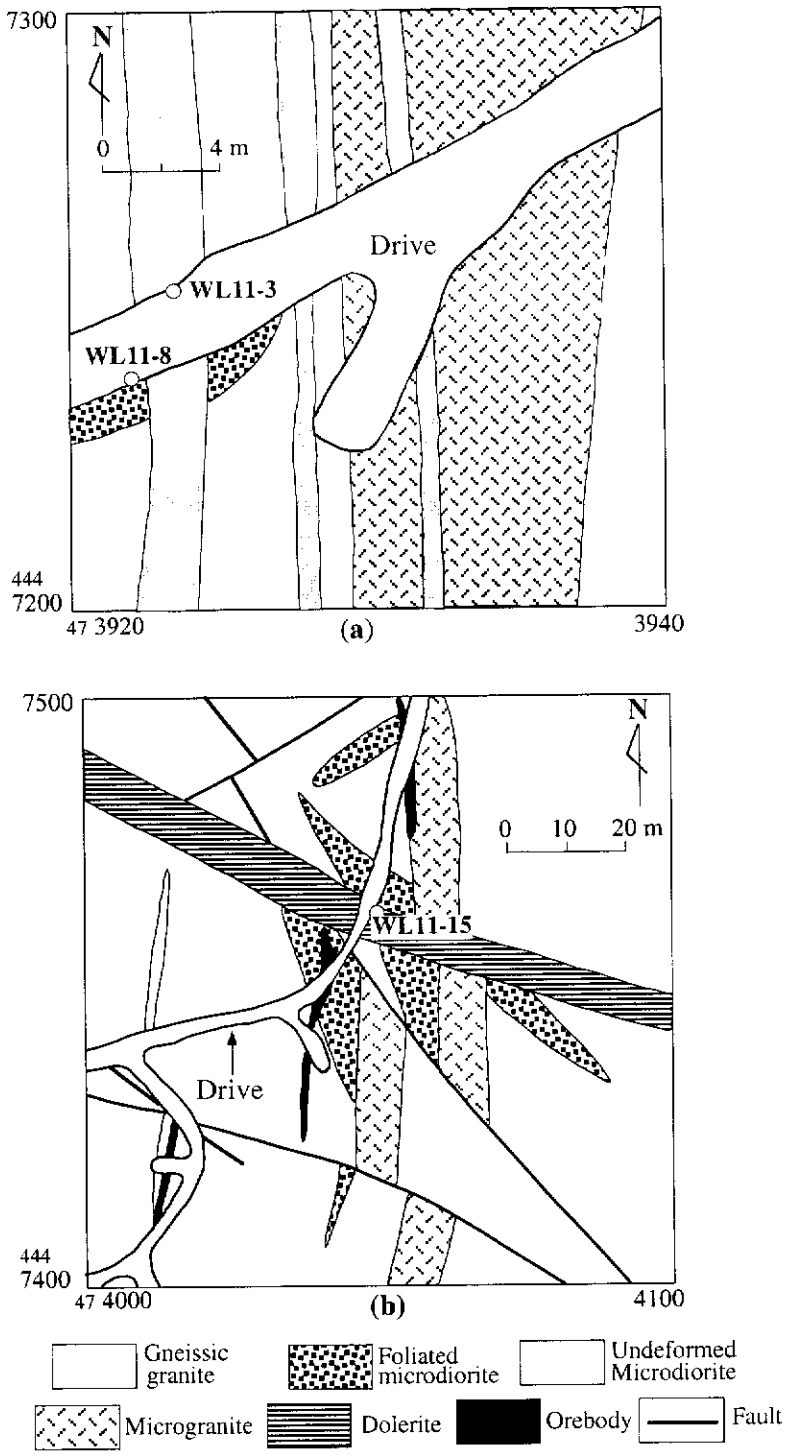

Fig. 6.6: Part of plan of Level 11 of the No.3 shaft at the Wulong Gold Deposit. The locations of geochronology samples WL11-3 and WL11-8 are shown in (a) and the site of geochronology sample WL11-15 is shown in (b).

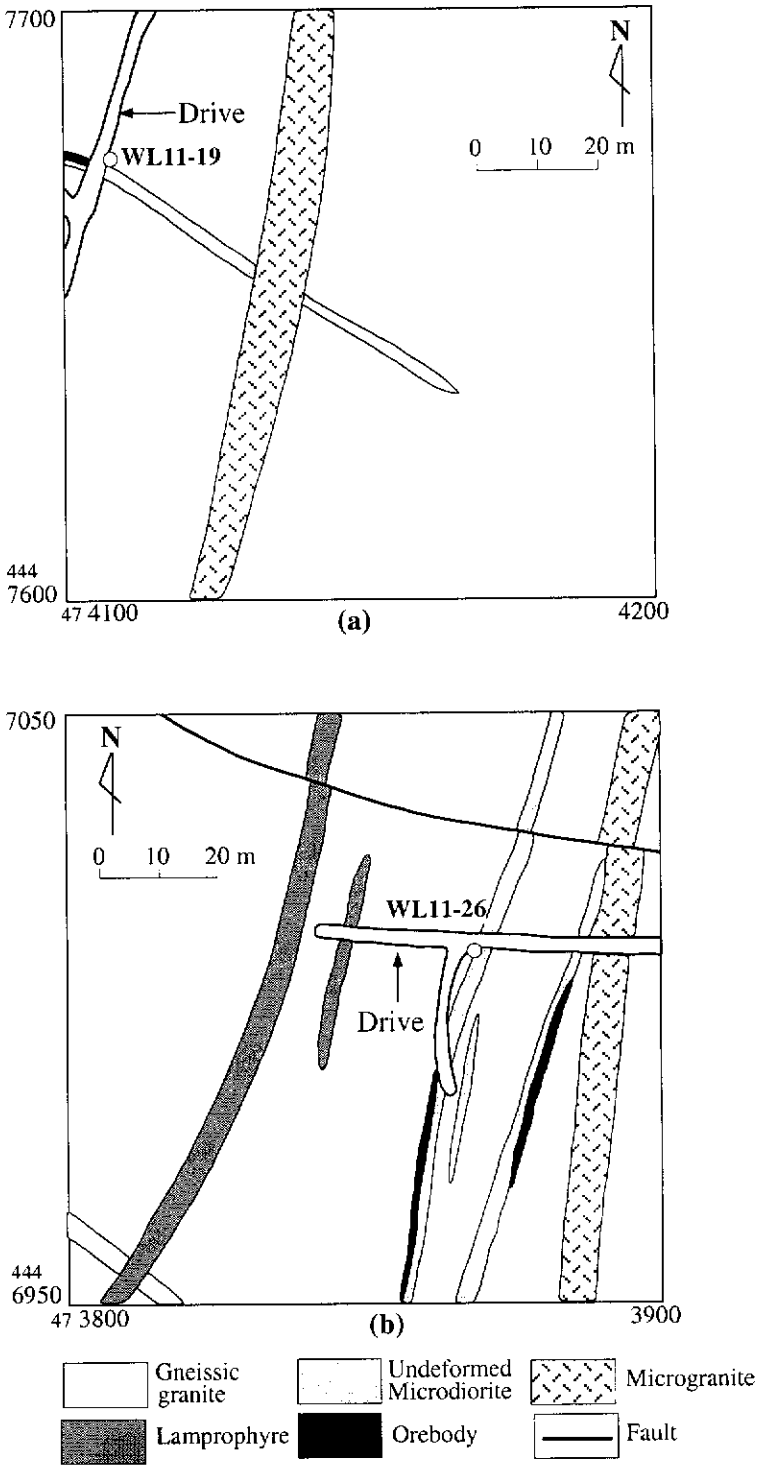

Fig. 6.7: Part of plan of Level 11 of the No.3 shaft at the Wulong Gold Deposit. (a) and (b) show the locations of geochronology samples WL11-19 and WL11-26, respectively.

a west-north-west strike (Figs. 6.3 and 6.6b), with maximum length of ca. 1000 m and a width ranging from 2 m to 4 m.

6.2.3 Ore Mineralogy and Paragenesis

Ore minerals, in order of decreasing abundance, are pyrite, pyrrhotite, chalcopyrite, sphalerite, galena, bismuthinite, scheelite, arsenopyrite and gold (Ren, 1988). Pyrite makes up 3 to 5% of the orebodies; pyrrhotite makes up 2 to 3%; other minerals such as chalcopyrite, sphalerite and galena each makes up less than 1%. Gangue minerals are dominated by quartz, which makes up more than 90% of the orebodies; other minerals include calcite, chlorite and fluorite. Four stages of mineralization have been identified (Ren, 1988). From oldest to youngest these are: Stage 1-quartz-pyrite-scheelite; Stage 2-pyrite-arsenopyrite-pyrrhotite-quartz-bismuthinite-gold; Stage 3-quartz-pyrite-bismuthinite-chalcopyrite-galena-sphalerite-chlorite-gold; Stage 4-calcite. Fluid inclusion studies of quartz suggest temperatures associated with Stages 1, 2 and 3 were 380-310°C, 300-220°C and 200-110°C, respectively (Ren, 1988).

6.2.4 Sanguliu Pluton

The Sanguliu Pluton is located ca. 5km south of the Wulong Gold Deposit (Fig. 6.1). This pluton and microdiorite and microgranite dykes of the Wulong Gold Deposit are considered to have a common origin (Ren, 1988). This can be established by their chondrite-normalized rare earth element (REE) distribution (Fig. 6.8), which shows a similar pattern decreasing regularly from steep LREE to flat HREE (Ren, 1988). The Sanguliu Pluton belongs to the Mesozoic undeformed granitoid suite within the Liaodong Peninsula (Ren, 1988) and is in the form of a stock, cropping out over 50 km^2 in area (Fig. 6.1). It is zoned, with a light grey-coloured medium- to fine-grained diorite and porphyritic granodiorite situated in its border facies, and light, grey-coloured medium- to coarse-grained syeno- and monzogranite and monzogranite distributed in its central facies.

6.2.5 Geochronological Data

In order to provide constraints on the timing of gold mineralization at the Wulong gold deposit, samples were collected from the foliated microdiorite dykes pre-dating gold mineralization (WL11-8) (Fig. 6.6a), from the undeformed microdiorite

dykes possibly synchronous with gold mineralization (WL11-3 and WL11-26) (Figs. 6.6a and 6.7b), and from the dolerite dykes post-dating gold mineralization (WL11-15) (Fig. 6.6b). However, dolerite sample WL11-15 lacked zircons, so the minimum age of the gold mineralization at this deposit cannot be constrained by this method. In addition, samples WL11-19 from the gneissic granite hosting the deposit (Fig. 6.7a), and SG-1 (monzogranite) from the central facies of the Sanguliu Pluton (Fig. 6.1), were also selected for SHRIMP U-Pb zircon analysis to precisely determine their emplacement ages in order that magmatic activity in the region could be fully documented.

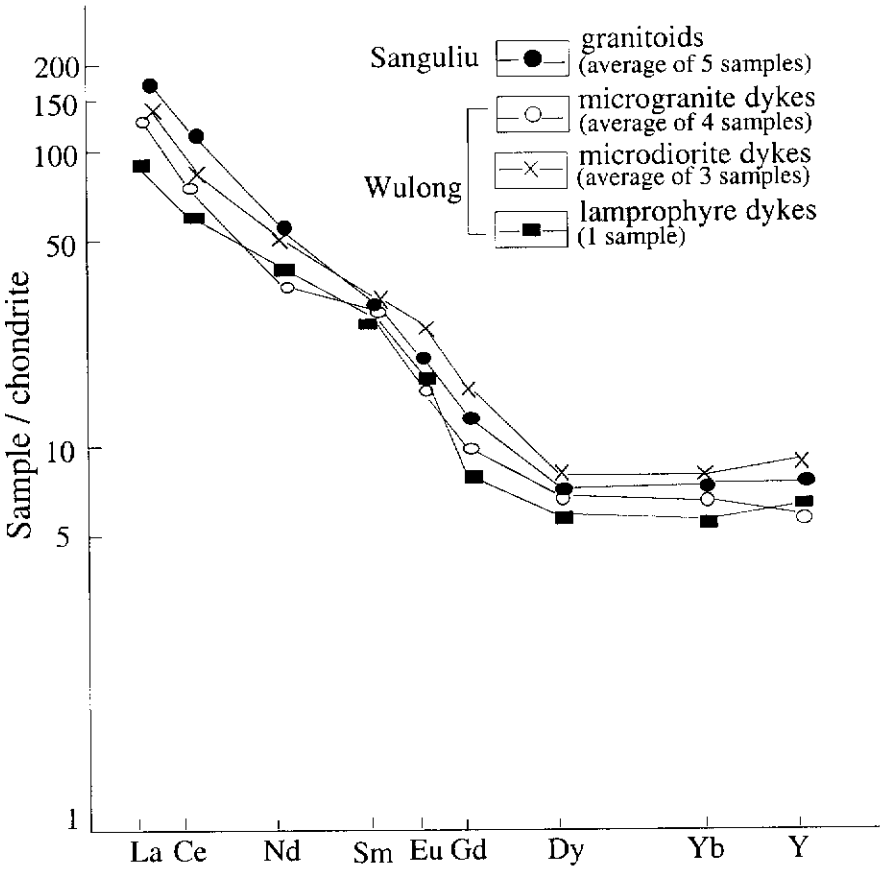

Fig. 6.8: Chondrite-normalized REE distribution patterns of samples from the Sanguliu Pluton and from dykes of the Wulong Gold Deposit (after Ren, 1988).

SHRIMP results for the samples are listed in Table 6.1 and illustrated on concordia diagrams in Figures 6.9, 6.11, 6.12, 6.14 and 6.15. All errors for individual analyses in Table 6.1 are given as 1σ. In concordia plots, group ages are quoted with 95% confidence limits (2σ), but error bars are shown as 1σ. Following are the description of the samples and the interpretation of their SHRIMP U-Pb zircon ages.

Table 6.1: SHRIMP U-Pb data for zircons from samples WL11-3, WL11-8, WL11-19 and WL11-26 from the Wulong Gold Deposit, and from sample SG-1 from the Sanguliu Pluton. Analyses are listed in order of increasing age. The following notation is used for analysed grains: 1.1=grain 1, first point analysed. Data are ^{204}Pb-corrected. Individual analyses have a 1σ error. The $^{206}Pb/^{238}U$ age is adopted for crystals with an age of less than 1.0 Ga, otherwise, the $^{207}Pb/^{206}Pb$ age is used.

spot	U (ppm)	Th (ppm)	Th/U	Total Pb (ppm)	$\frac{^{204}Pb}{^{206}Pb}$	$\frac{^{207}Pb}{^{206}Pb}$	$\frac{^{206}Pb}{^{238}U}$	$\frac{^{207}Pb}{^{235}U}$	$\frac{^{206}Pb}{^{238}U}$ Age (Ma)	$\frac{^{207}Pb}{^{206}Pb}$ Age (Ma)
WL11-8										
8.1	239	296	1.24	6	0.00049	0.049±61	0.0187±6	0.12±2	119±4	
2.1	259	312	1.20	6	0.00000	0.049±12	0.0187±6	0.13±1	120±4	
13.1	301	134	0.44	6	0.00000	0.053±12	0.0188±6	0.14±1	120±4	
17.1	281	185	0.66	6	0.00013	0.056±48	0.0188±6	0.15±1	120±4	
7.1	348	605	1.74	9	0.00051	0.045±52	0.0191±6	0.12±1	122±4	
19.1	90	101	1.11	2	0.00173	0.047±164	0.0190±7	0.12±4	122±5	
14.1	380	293	0.77	8	0.00034	0.046±38	0.0193±6	0.12±1	123±4	
5.1	378	909	2.41	12	0.00062	0.049±37	0.0196±6	0.13±1	125±4	
6.1	137	172	1.25	3	0.00000	0.059±19	0.0198±6	0.16±1	126±4	
1.1	271	289	1.07	7	0.00050	0.052±43	0.0197±6	0.14±1	126±4	
11.1	285	198	0.70	6	0.00032	0.050±54	0.0198±6	0.14±2	126±4	
18.1	272	133	0.49	6	0.00001	0.056±51	0.0198±6	0.15±2	126±4	
10.1	638	353	0.55	13	0.00018	0.047±26	0.0199±6	0.13±1	127±4	
15.1	233	132	0.56	5	0.00035	0.047±54	0.0199±6	0.13±2	127±4	
12.1	189	179	0.95	5	0.00039	0.049±73	0.0201±6	0.14±2	128±4	
16.1	181	106	0.58	4	0.00025	0.047±67	0.0201±6	0.13±2	129±4	
4.1	815	818	1.00	20	0.00015	0.048±16	0.0207±6	0.14±1	132±4	
3.1	158	65	0.41	4	0.00000	0.057±14	0.0259±8	0.20±1	165±5	
9.1	182	123	0.68	53	0.00000	0.112±6	0.2551±76	3.95±12		1837±10

Table 6.1 (continued)

spot	U (ppm)	Th (ppm)	Th/U	Total Pb (ppm)	$\frac{^{204}Pb}{^{206}Pb}$	$\frac{^{207}Pb}{^{206}Pb}$	$\frac{^{206}Pb}{^{238}U}$	$\frac{^{207}Pb}{^{235}U}$	$\frac{^{206}Pb}{^{238}U}$ Age (Ma)	$\frac{^{207}Pb}{^{206}Pb}$ Age (Ma)
WL11-3										
1.1	216	397	1.84	5	0.00065	0.058±85	0.0172±5	0.14±2	110±3	
1.2	104	166	1.60	3	0.00000	0.084±32	0.0172±5	0.20±1	110±3	
2.1	651	659	1.01	14	0.00006	0.050±25	0.0183±5	0.12±1	117±3	
8.1	792	268	0.34	15	0.00015	0.052±22	0.0187±5	0.13±1	119±3	
7.1	315	791	2.51	10	0.00000	0.057±12	0.0188±5	0.15±1	120±3	
3.1	206	250	1.21	5	0.00085	0.047±64	0.0200±5	0.13±2	127±3	
5.1	286	31	0.11	6	0.00000	0.054±11	0.0227±6	0.17±1	144±4	
12.1	488	26	0.05	12	0.00010	0.054±22	0.0257±6	0.19±1	163±4	
10.2	668	61	0.09	21	0.00010	0.052±19	0.0340±8	0.24±1	215±5	
10.1	1221	193	0.16	42	0.00016	0.050±10	0.0359±9	0.25±1	227±5	
9.1	401	46	0.11	54	0.00000	0.111±6	0.1332±32	2.03±5	806±18	
6.1	401	75	0.19	87	0.00000	0.103±5	0.2188±53	3.10±8		1673±9
13.1	946	112	0.12	333	0.00000	0.111±2	0.3576±86	5.48±13		1818±4
11.1	534	114	0.21	203	0.00001	0.123±4	0.3735±90	6.31±16		1994±5
4.1	447	400	0.89	228	0.00001	0.159±4	0.4173±101	9.15±22		2446±4
WL11-26										
8.1	106	79	0.74	2	0.00089	0.062±129	0.0179±5	0.15±3	115±3	
6.1	779	1247	1.60	20	0.00012	0.049±23	0.0188±3	0.13±1	120±2	
5.1	189	442	2.34	6	0.00000	0.053±19	0.0188±4	0.14±1	120±3	
10.1	354	470	1.33	9	0.00181	0.056±66	0.0189±4	0.15±2	121±2	
7.1	121	128	1.06	4	0.00826	0.059±222	0.0194±6	0.16±6	124±4	
9.1	119	111	0.94	3	0.00000	0.056±25	0.0203±5	0.16±1	129±3	
1.1	222	41	0.18	15	0.00017	0.106±23	0.0678±13	0.99±3	423±8	
4.1	379	142	0.37	127	0.00003	0.119±7	0.3158±56	5.16±10		1935±11

Table 6.1 (continued)

spot	U (ppm)	Th (ppm)	Th/U	Total Pb (ppm)	$\frac{^{204}Pb}{^{206}Pb}$	$\frac{^{207}Pb}{^{206}Pb}$	$\frac{^{206}Pb}{^{238}U}$	$\frac{^{207}Pb}{^{235}U}$	$\frac{^{206}Pb}{^{238}U}$ Age (Ma)	$\frac{^{207}Pb}{^{206}Pb}$ Age (Ma)
12.1	193	55	0.28	71	0.00001	0.128±8	0.3509±63	6.18±12		2067±12
11.1	292	138	0.47	118	0.00001	0.130±6	0.3697±65	6.61±13		2093±9
3.1	257	151	0.59	116	0.00001	0.137±7	0.3982±71	7.54±14		2193±8
2.1	105	59	0.56	107	0.00002	0.352±13	0.7919±146	38.47±74		3717±5
WL11-19										
1.1	364	89	0.25	9	0.00146	0.046±54	0.0239±10	0.15±2	153±6	
12.2	4636	308	0.07	139	0.00428	0.051±23	0.0250±10	0.17±1	159±6	
15.1	622	102	0.16	15	0.00000	0.050±8	0.0249±10	0.17±1	159±6	
12.1	186	104	0.56	6	0.00260	0.048±100	0.0253±11	0.17±4	161±7	
9.1	160	114	0.71	5	0.00422	0.037±133	0.0259±11	0.13±5	165±7	
11.1	100	46	0.46	4	0.00695	0.037±202	0.0260±12	0.13±7	165±8	
8.1	216	193	0.89	8	0.00290	0.049±92	0.0275±12	0.19±4	175±7	
4.1	87	75	0.87	4	0.00752	0.096±230	0.0281±14	0.37±9	179±9	
14.2	807	101	0.13	27	0.00050	0.049±16	0.0353±14	0.24±1	224±9	
14.1	1107	297	0.27	40	0.00013	0.051±9	0.0363±14	0.26±1	230±9	
6.1	308	402	1.30	16	0.00229	0.047±53	0.0381±16	0.25±3	241±10	
2.1	339	67	0.20	21	0.00037	0.107±23	0.0564±23	0.83±4	354±14	
10.1	3668	802	0.22	1266	0.00003	0.113±1	0.3418±136	5.31±21		1842±2
3.1	180	98	0.55	83	0.00021	0.134±9	0.4119±165	7.62±32		2152±11
16.1	704	813	1.15	361	0.00002	0.134±3	0.4087±162	7.56±30		2154±4
13.1	434	199	0.46	178	0.00006	0.139±5	0.3753±150	7.18±29		2212±6
7.1	638	47	0.07	248	0.00005	0.156±5	0.3831±152	8.23±33		2410±5
5.1	211	90	0.43	114	0.00022	0.158±8	0.4880±195	10.63±44		2434±9

Table 6.1 (continued)

spot	U (ppm)	Th (ppm)	Th/U	Total Pb (ppm)	$\frac{204Pb}{206Pb}$	$\frac{207Pb}{206Pb}$	$\frac{206Pb}{238U}$	$\frac{207Pb}{235U}$	$\frac{206Pb}{238U}$ Age (Ma)	$\frac{207Pb}{206Pb}$ Age (Ma)
SG-1										
2.1	63	115	1.81	3	0.01358	0.041±16	0.0191±8	0.11±4	122±5	
9.1	60	108	1.81	3	0.01129	0.033±17	0.0191±8	0.09±5	122±5	
3.1	110	252	2.30	4	0.00514	0.036±13	0.0193±7	0.10±3	123±5	
6.1	68	156	2.31	2	0.00717	0.041±16	0.0193±8	0.11±4	123±5	
10.1	46	56	1.21	2	0.01475	0.059±20	0.0193±8	0.16±5	123±5	
4.1	50	47	0.93	2	0.01451	0.025±16	0.0195±8	0.07±4	124±5	
1.1	37	51	1.39	2	0.01883	0.028±23	0.0195±9	0.07±6	125±6	
7.1	73	152	2.08	3	0.01008	0.049±16	0.0198±8	0.13±4	126±5	
8.1	53	110	2.07	2	0.01030	0.024±21	0.0197±8	0.07±6	126±5	
5.1	58	108	1.85	2	0.00658	0.038±16	0.0203±8	0.11±5	129±5	
11.1	67	126	1.89	3	0.01202	0.064±15	0.0205±8	0.18±4	131±5	

Sample WL11-8

Sample WL11-8 was taken from a foliated melanocratic, porphyritic microdiorite dyke (Fig.6.6a). Its phenocryst phase mainly comprises hornblende, some of which is partly replaced by Mg-biotite. The groundmass includes hornblende, Mg-biotite, plagioclase, K-feldspar, quartz and opaque minerals. Zircons are colourless and clear. Zircons selected for analysis range in size from +132 μm to -74 μm and most are euhedral, with good prism and pyramid faces. The average elongation ratio is about 2:1, with a maximum of 4:1.

Nineteen analyses were made on 19 zircon grains (Fig. 6.9), which display a range of ages from 1837 ± 10 Ma to 119 ± 4 Ma (Table 6.1).

Two analytical spots (9.1 and 3.1) from the centres of two separate zircon grains (9 and 3) do not yield concordant ^{207}Pb / ^{206}Pb or ^{206}Pb / ^{238}U ages (Fig. 6.9a and b), but have values of 1837 ± 10 Ma and 165 ± 5 Ma (1σ), respectively. These two zircons are euhedral and optically homogeneous, and are indistinguishable from the main magmatic zircon population in terms of morphology. The inherited zircon with an age of 1837 ± 10 Ma may indicate a Palaeoproterozoic basement in this area. The highly disconcordant 165 ± 5Ma age of another inherited zircon probably was no geological meaning.

Seventeen analyses of 17 grains form a coherent group (Fig. 6.9b) with a weighted mean $^{206}Pb/^{238}U$ age of 124 ± 3 Ma and a chi-square value of 0.86. The U and Th contents of these 17 spots range from 90 ppm to 815 ppm and 101 ppm to 909 ppm, respectively. The Th/U ratios vary from 0.44 to 2.41. Cathodoluminescence images of these crystals indicate all grains have well developed oscillatory zoning throughout the crystals (Fig. 6.10a). This growth pattern is indicative of crystallization from a melt (Vavra, 1990) and the age of 124 ± 3 Ma is taken as the time of igneous crystallization of the foliated microdiorite dyke. Field relations demonstrate that the dykes are truncated by the orebodies and other dykes including microgranite, lamprophyre and dolerite, therefore, this age is also considered as the maximum age of gold mineralization.

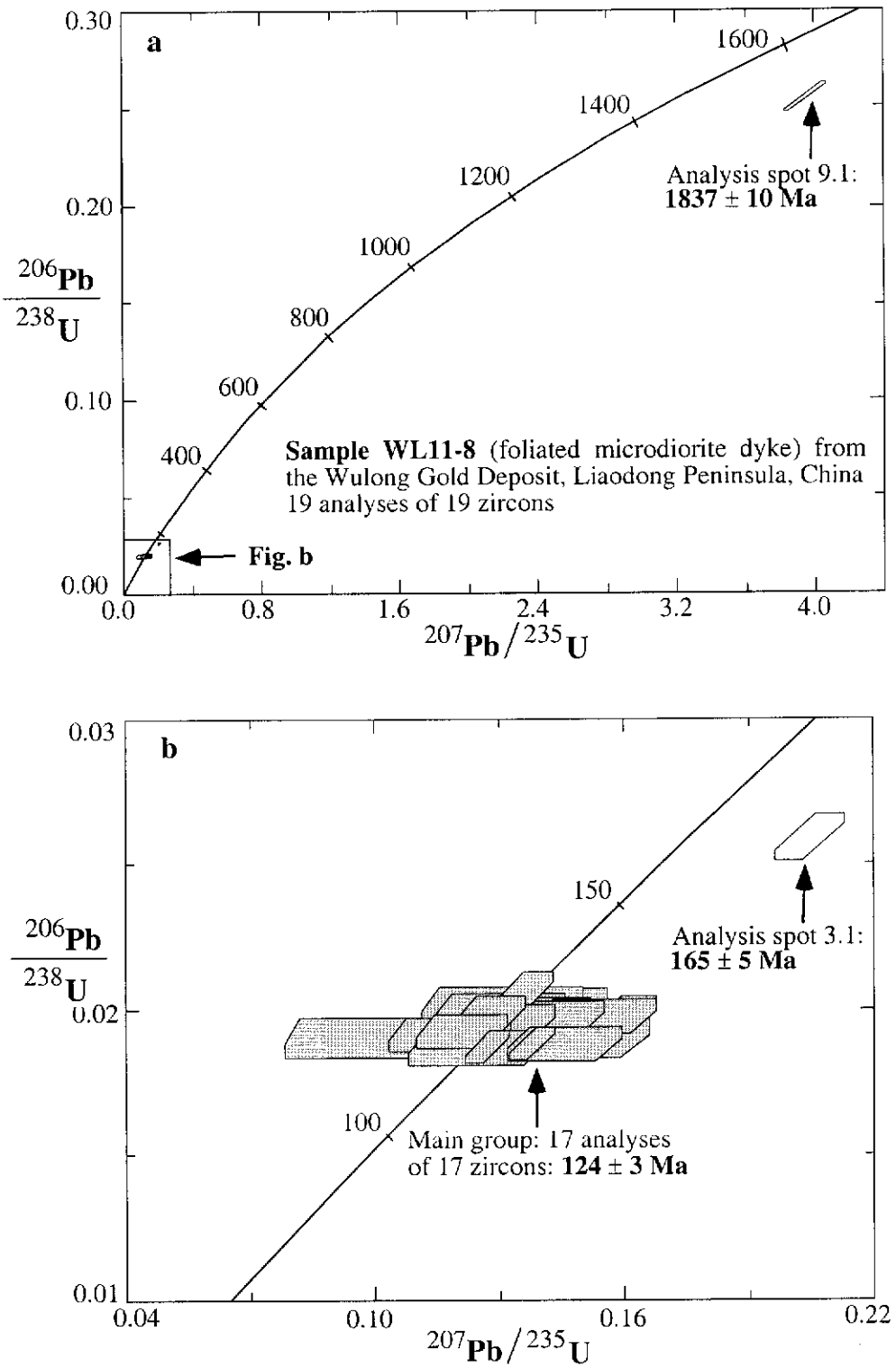

Fig. 6.9: U-Pb concordia diagrams showing (a) total SHRIMP data for Sample WL11-8 from the Wulong Gold Deposit and (b) enlargement showing the youngest zircon population.

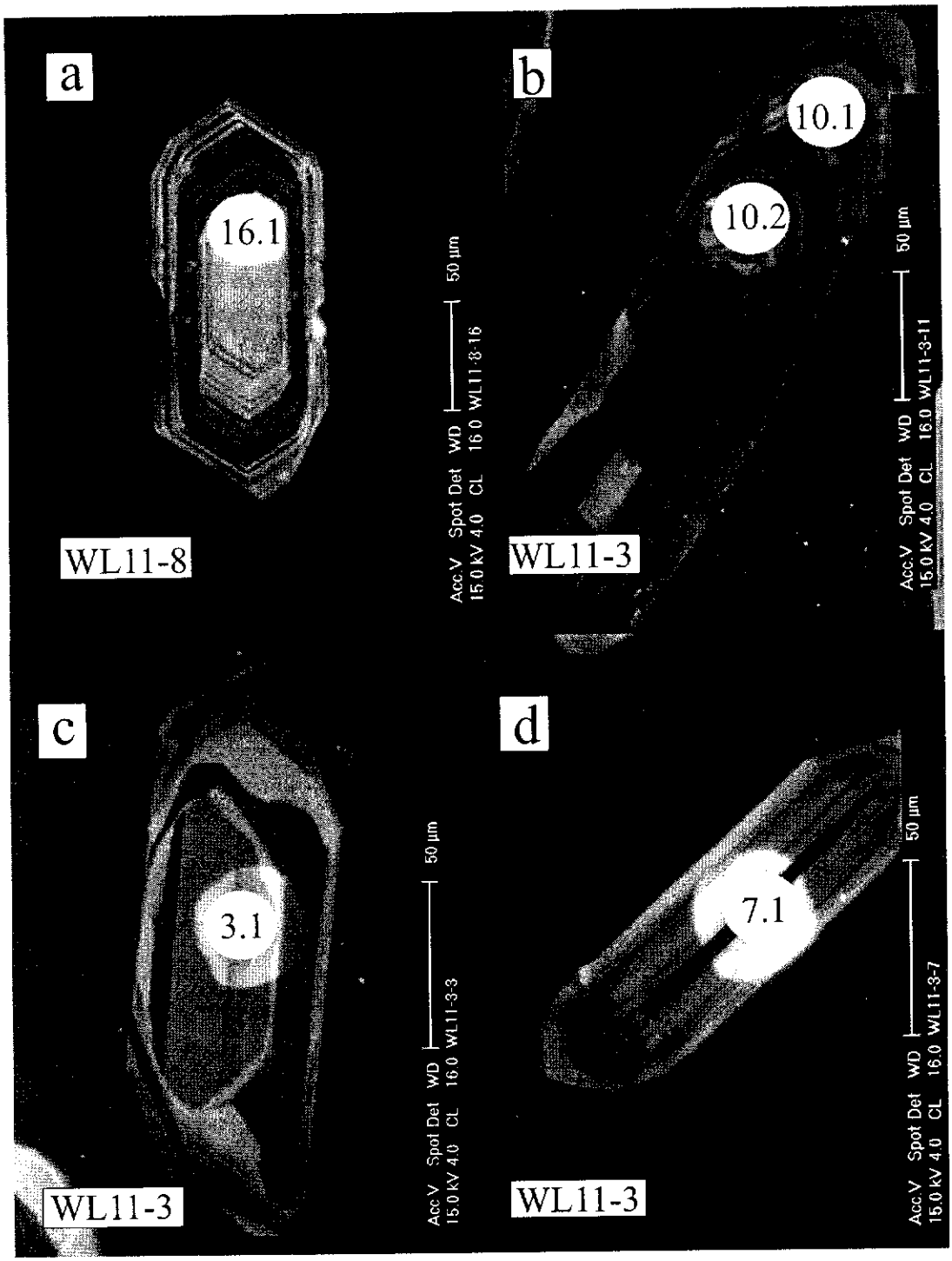

Fig. 6.10: A selection of cathodoluminescence (CL) images of zircons extracted from Samples WL11-8 and WL11-3 from the Wulong Gold Deposit. The white circles are the SHRIMP ion-probe analysis spots. (a) Zircon grain 16 from Sample WL11-8, showing very distinct magmatic oscillatory zonation throughout the crystal. The $^{206}Pb/^{238}U$ age of spot 16.1 is 129 ± 4 Ma. (b) Zircon grain 10 of Sample WL11-3, showing oscillatory zones. The weighted mean $^{206}Pb/^{238}U$ age of spots 10.1 and 10.2 is 221 ± 6 Ma. (c) Zircon grain 3 of Sample WL11-3, showing igneous oscillatory growth zones, was inherited from the oldest dyke suite. The $^{206}Pb/^{238}U$ age of spot 3.1 is 127 ± 3 Ma. (d) Zircon grain 7 of Sample WL11-3, showing oscillatory zonation. The $^{206}Pb/^{238}U$ age of spot 7.1 is 120 ± 3 Ma.

Samples WL11-3

Sample WL11-3 was obtained from an undeformed microdiorite dyke (Fig.6.6a). The rock is mesocratic and has a porphyritic texture. Its phenocryst phase is dominantly plagioclase, which is partly or wholly pseudomorphed by sericite. Rare hornblende phenocrysts are altered to chlorite. The groundmass is composed mainly of plagioclase, K-feldspar, chlorite, sericite, quartz and opaque minerals. Sericitization and chloritization are strong throughout this sample. Zircons are nearly colourless and transparent. Zircons selected for analysis range in size from +132 μm to -74 μm. Some grains are rounded, whilst others have good prism and pyramid faces, with elongation ratio varying from 2:1 to 5:1.

A total of 15 analyses were carried out on 13 zircon grains (Fig. 6.11), with ages ranging from 2446 ± 4 Ma to 110 ± 3 Ma (Table 6.1).

Analysis spots 4.1, 11.1, 13.1, 6.1 and 9.1 yield disconcordant $^{207}Pb/^{206}Pb$ or $^{206}Pb/^{238}U$ ages of 2446 ± 4 Ma, 1994 ± 5 Ma, 1818 ± 4 Ma, 1673 ± 9 Ma and 806 ± 18 Ma (1σ), respectively (Fig. 6.11a), which may indicate they were inherited from a Proterozoic source. Such inherited zircons are common in the Mesozoic igneous intrusions in the North China Craton (Wang et al., 1998). Two analyses of grain 10 yield a weighted mean concordant age of 221 ± 6 Ma (2σ) (Fig. 6.11b). Cathodoluminescence imaging indicates that grain 10 is characterised by well-defined oscillatory zones (Fig. 6.10b) and this inherited zircon was therefore formed during an earlier magmatic event. The youngest inherited zircon is grain 3 with a concordant age of 127 ± 3 Ma (1σ) (Fig. 6.11b). The CL image shows that grain 3 has oscillatory zoning indicative of an igneous origin (Fig. 6.10c). The age of 127 ± 3 Ma is within error of the age of sample WL11-8 from the early deformed microdiorite dykes at the deposit and may be inherited from this suite.

The main population consists of 3 analyses of 3 grains which form a group (Fig. 6.11b) having a weighted mean $^{206}Pb/^{238}U$ age of 119 ± 6 Ma with a chi-square value of 0.27. The U and Th contents of these 3 spots vary from 315 ppm to 792 ppm and 268 ppm to 791 ppm, respectively. The Th/U ratios range from 0.34 to 2.51. Cathodoluminescence images shows these crystals have oscillatory zonation patterns (Fig. 6.10d), which suggests that they are magmatic in origin; the age of 119 ± 6 Ma is therefore interpreted as the crystallization age of this dyke. The dyke occupies the same structure as an orebody and experienced gold-related hydrothermal alteration.

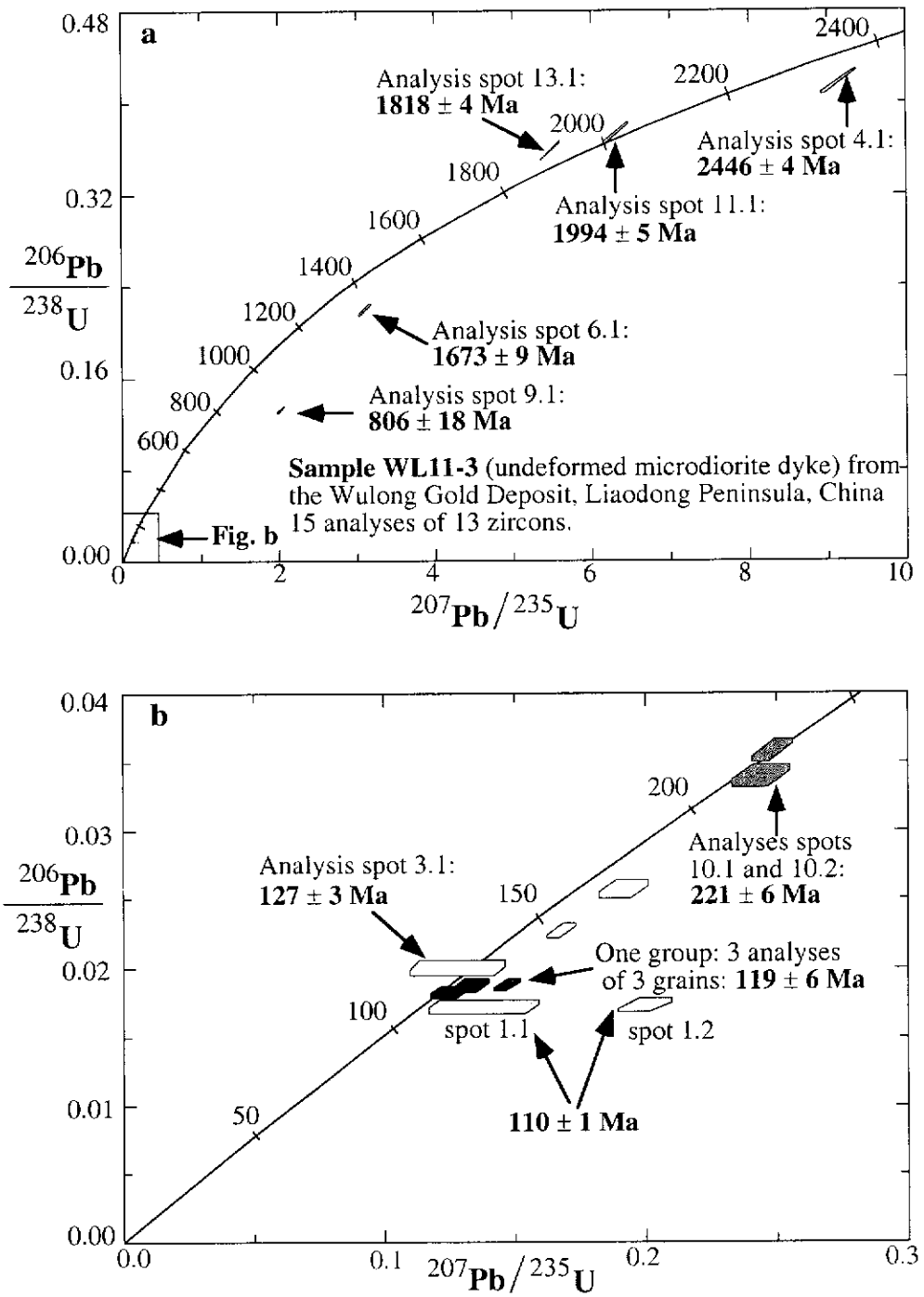

Fig. 6.11: U-Pb concordia diagrams showing (a) total SHRIMP data for Sample WL11-3 from the Wulong Gold Deposit and (b) enlargement of data with Mesozoic ages.

Therefore, they are broadly synchronous with gold mineralization and the age of 119 ± 6 Ma may possibly be regarded as the age of the ore formation event. The youngest $^{206}Pb/^{238}U$ age of 110 ± 1 Ma (Fig. 6.11b) was obtained from two analysis spots on the rim of grain 1. The U and Th contents of the two spots range from 104 ppm to 216 ppm and 166 ppm to 397 ppm, respectively. The data are discordant (Fig. 6.11b) and Th age of 110 ± 1 Ma is interpreted to represent disturbance of the earlier zircon population.

Sample WL11-26

Sample WL11-26 was collected from another undeformed microdiorite dyke (Fig. 6.7b). The rock is mesocratic and has a porphyritic texture. It contains a few deformed and altered microgranite inclusions. Its phenocryst phase is dominated by plagioclase, which is partly or wholly altered to sericite. The matrix is mainly composed of plagioclase, chlorite, sericite quartz and opaque minerals. The alteration includes sericitization, chloritization and carbonatization and is intense in this sample. Zircons are transluscent and range in colour from colourless to pale brown. Their size is mostly less than 74 μm, and their shapes vary from rounded to euhedral with an average elongation ratio is about 2:1.

Twelve analyses were completed on 12 grains (Fig. 6.12), and ages vary from 3717 ± 5 Ma to 115 ± 3 Ma (Table 6.1).

One analysis from grain 2 yields the oldest inherited concordant $^{207}Pb/^{206}Pb$ age of 3717 ± 5 Ma (1σ) (Fig. 6.12a). Cathodoluminescence imaging shows that grain 2 has oscillatory zoning (Fig. 6.13a), so the age of 3717 ± 5 Ma may represent the age of the earliest magmatic event in the region and this grain was therefore inherited from the ca. 3800 Ma basement in the Liaodong Peninsula (Liu et al., 1992). Analyses spots 3.1, 11.1, 12.1 and 4.1 yield concordant or near-concordant $^{207}Pb/^{206}Pb$ ages of 2193 ± 8 Ma, 2093 ± 9 Ma, 2067 ± 12 Ma and 1935 ± 11 Ma (1σ), respectively (Fig. 6.12a), which indicate these grains are similar to inherited grain 11 in sample WL11-3 and originated from Palaeoproterozoic rocks in the source region. Among the inherited zircons, analyses of grains 7 and 9 yields a coherent group (Group 1 in Fig. 6.12b) with a weighted mean $^{206}Pb/^{238}U$ age of 127 ± 3 Ma and a chi-square value of 0.94. The CL images of Group 1 crystals show oscillatory zonation patterns (Fig. 6.13b), which suggests these crystals have an igneous origin. Based on the fact that the age of 127 ± 3 Ma coincides within error with the age of the early dykes (sample WL11-8), these grains are most likely inherited from these.

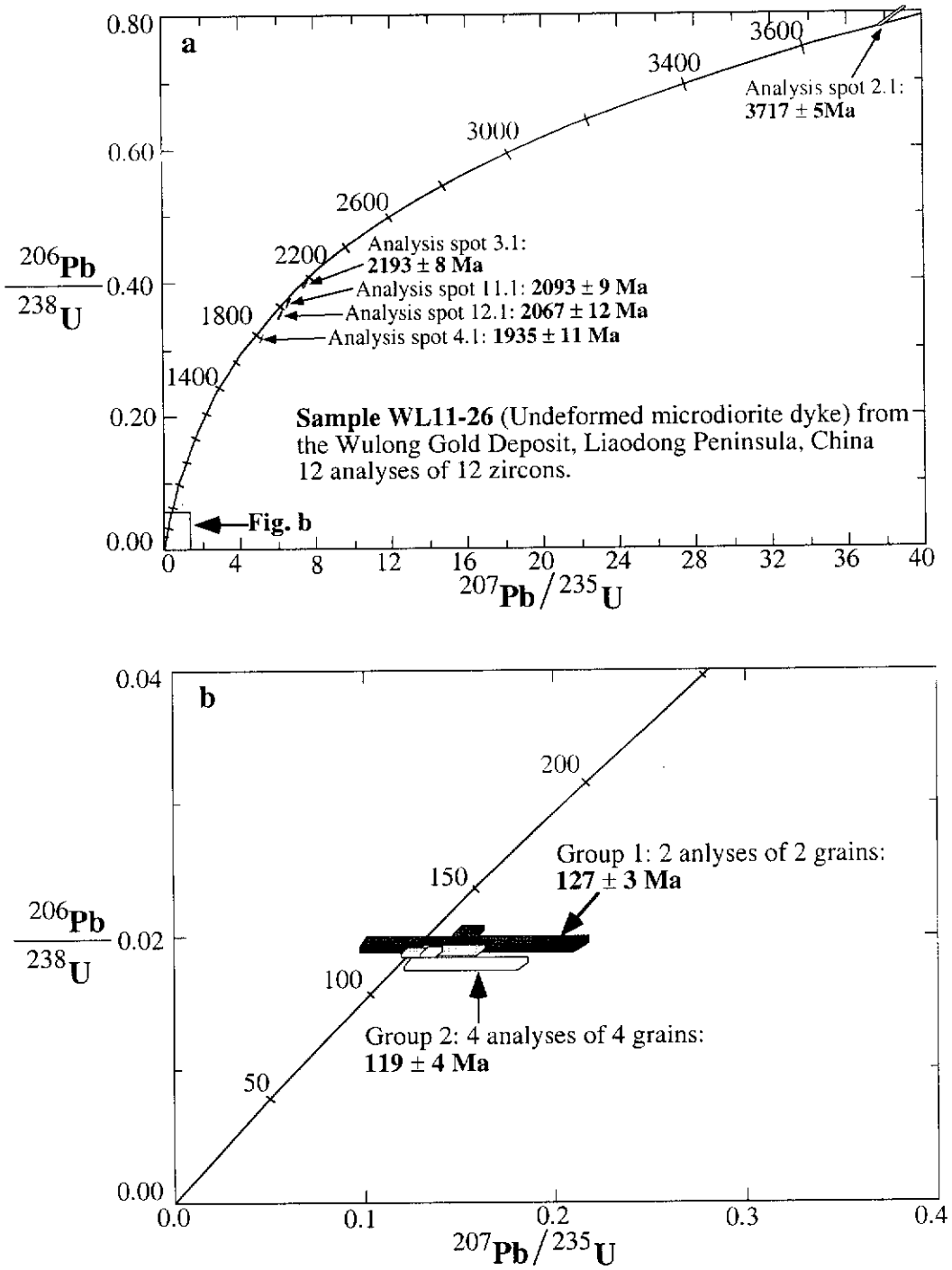

Fig. 6.12: U-Pb concordia diagrams showing (a) total SHRIMP data for Sample WL11-26 from the Wulong Gold Deposit and (b) enlargement showing younger zircon populations.

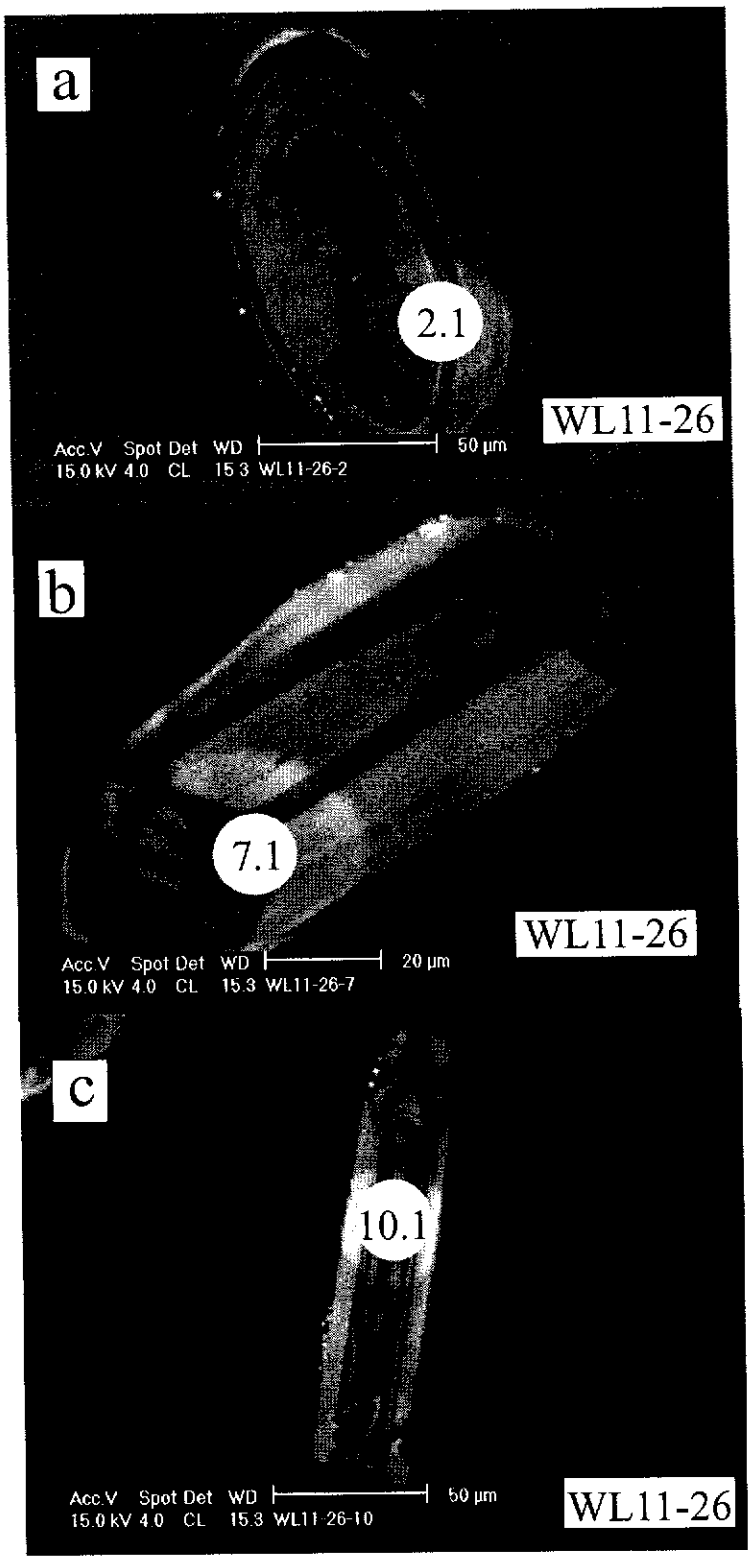

Fig. 6.13: (a) Zircon grain 2 of Sample WL11-26, showing magmatic growth zoning. This is the oldest inherited crystal with a $^{207}Pb/^{206}Pb$ age for spot 2.1 of 3717 ± 5 Ma. (b) Zircon grain 7 of Sample WL11-26, showing oscillatory zonation patterns, was inherited from the oldest dykes. The $^{206}Pb/^{238}U$ age of spot 7.1 is 124 ± 4 Ma. (c) Zircon grain 10 of Sample WL11-26, showing oscillatory growth zones. The $^{206}Pb/^{238}U$ age of spot 10.1 is 121 ± 2 Ma.

The youngest population consists of 4 analyses of 4 grains, which form a coherent group (Group 2 in Fig. 6.12b) having a weighted mean $^{206}Pb/^{238}U$ age of 119 ± 4 Ma with a chi-square value of 0.84. The Th content of spot 6.1 is very high (1247 ppm), whilst the Th contents of the other 3 spots range from 79 ppm to 470 ppm. The U contents of the 4 spots vary from 106 ppm to 779 ppm, with Th/U ratios of 0.74 to 2.34. Cathodoluminescence images show oscillatory zoning (Fig. 6.13c), which suggests that these grains have a magmatic origin and that 119 ± 4 Ma is the crystallization age of the later dykes. Just like WL11-3, this sample is also from the dykes closely related to gold mineralization in both time and space, and its age of 119 ± 4 Ma is within error of the age of sample WL11-3 (119 ± 6 Ma).

Sample WL11-19

Sample WL11-19 was collected from the host rock of the Wulong deposit and is a leucocratic medium-grained gneissic syenogranite (Fig. 6.7a). It comprises microcline (50%), quartz (30%), plagioclase (15%), muscovite (3%), biotite (mostly replaced by muscovite, 2%), and minor titanite, apatite and zircon. The rock experienced weak sericite alteration. The selected zircons are colourless and range in transparency from clear to cloudy. Their size is mainly between 105 μm and 74 μm. and their shapes are mostly euhedral with good prism and pyramid faces. The elongation ratio is between 2:1 and 3:1.

Eighteen analyses were carried out on 16 grains (Fig. 6.14), and they show a range in age from 2434 ± 9 Ma to 153 ± 6 Ma (Table 6.1).

The oldest near-concordant $^{207}Pb/^{206}Pb$ age of 2434 ± 9 Ma (1σ) was obtained from the inherited core of grain 5 (Fig. 6.14a). This grain is similar to inherited grain 4 in WL11-3, which yields a $^{207}Pb/^{206}Pb$ age of 2446 ± 4 Ma (1σ), and originated from Palaeoproterozoic rocks in the basement. Inherited zircons with ages between 1840 Ma and 2200 Ma are also present, but no statistically coherent population could be defined (Fig. 6.14a). Among them, analysis spot 10.1 of grain 10 yields a concordant $^{207}Pb/^{206}Pb$ age of 1842 ± 2 Ma (1σ). Three analyses of 2 zircons form a concordant homogeneous group (Group 1 in Fig. 6.14b). The group age is 231 ± 25 Ma with a chi-square value of 0.67. These crystals have good prism and pyramid shapes, and cannot be distinguished morphologically from the youngest grains. Therefore, these inherited zircons are thought to be formed during an earlier magmatic event and incorporated during emplacement of the granite. The presence of zircons of this age and 221 ± 6 Ma in dyke sample WL11-3, indicate the widespread nature of magmatic rocks of this age in the region.

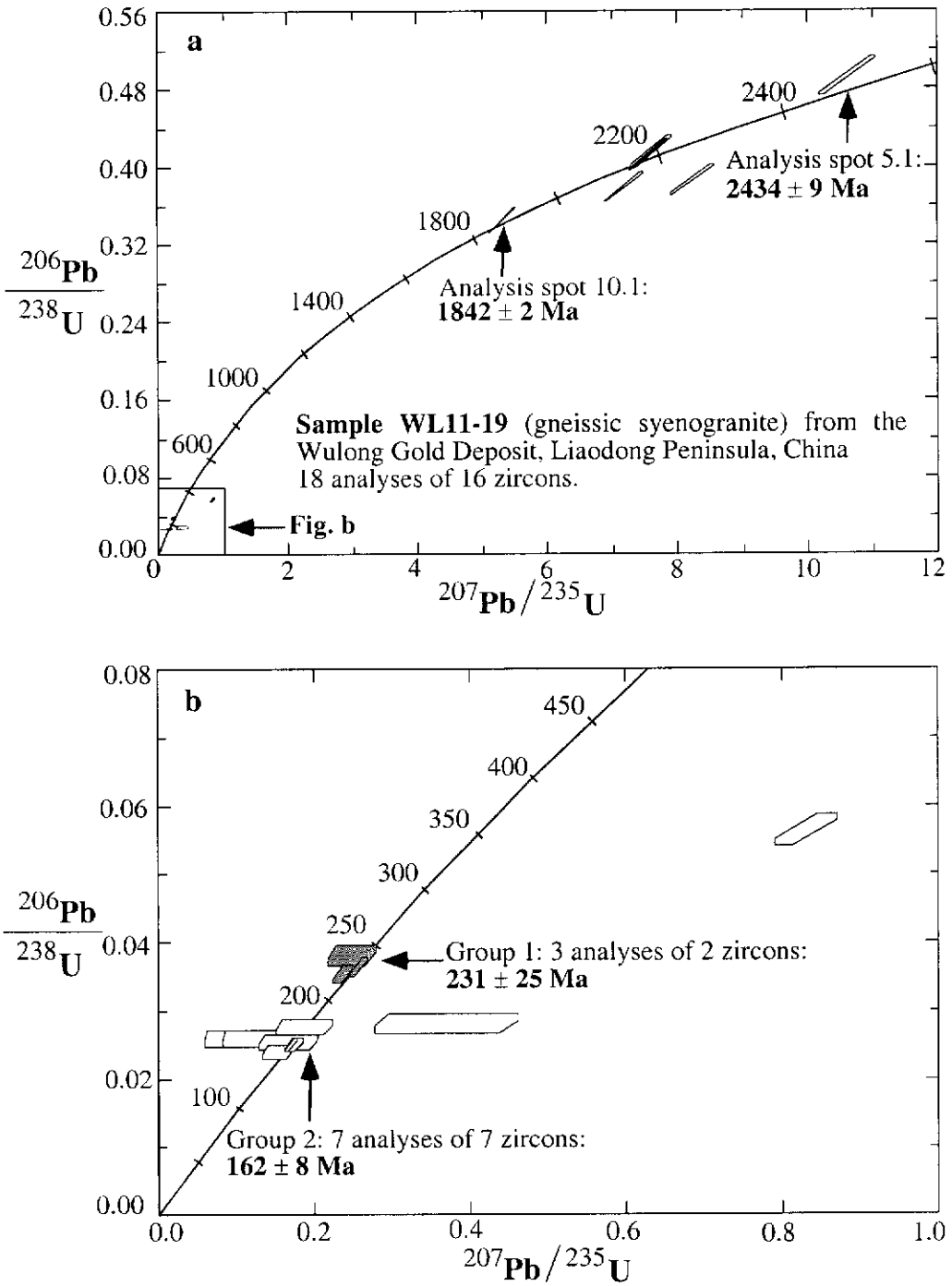

Fig. 6.14: U-Pb concordia diagrams showing (a) total SHRIMP data for Sample WL11-19 from the Wulong Gold Deposit and (b) enlargement of younger zircon populations.

Seven analyses of the youngest 7 grains from the sample form a coherent group (Group 2 in Fig. 6.14b) with a weighted mean $^{206}Pb/^{238}U$ age of 162 ± 8 Ma and a chi-square value of 0.96. The U content of spot 12.2 is extremely high (4636 ppm), whereas the U contents of the other 6 spots range from 100 ppm to 622 ppm. The Th contents of the 7 spots vary from 46 ppm to 308 ppm, with Th/U ratios of 0.07 to 0.89. These grains have euhedral morphology and growth zoning observed in transmitted light, which suggests they crystallized from a magma, and the age of 162 ± 8 Ma is interpreted to be the age of emplacement of the gneissic granite.

Sample SG-1

Sample SG-1, from the central part of the Sanguliu Pluton (Fig. 6.1), is a leucocratic coarse-grained monzogranite with a hypidiomorphic equigranular texture. The rock contains some centimetre-sized enclaves of dark, medium-grained, equigranular diorite. The monzogranite consists of 40 percent plagioclase (oligoclase to andesine), 30 percent K-feldspar (microcline perthite), 20 percent quartz, 6 percent biotite and 4 percent hornblende. Accessory minerals include chlorite, titanite, apatite, zircon and magnetite. Zircons are clear and range in colour from colourless to pale pink. The zircon grains selected for analysis range in size from +132 μm to -74 μm and most are euhedral, with pyramidal terminations. The elongation ratio is between 2:1 and 4:1.

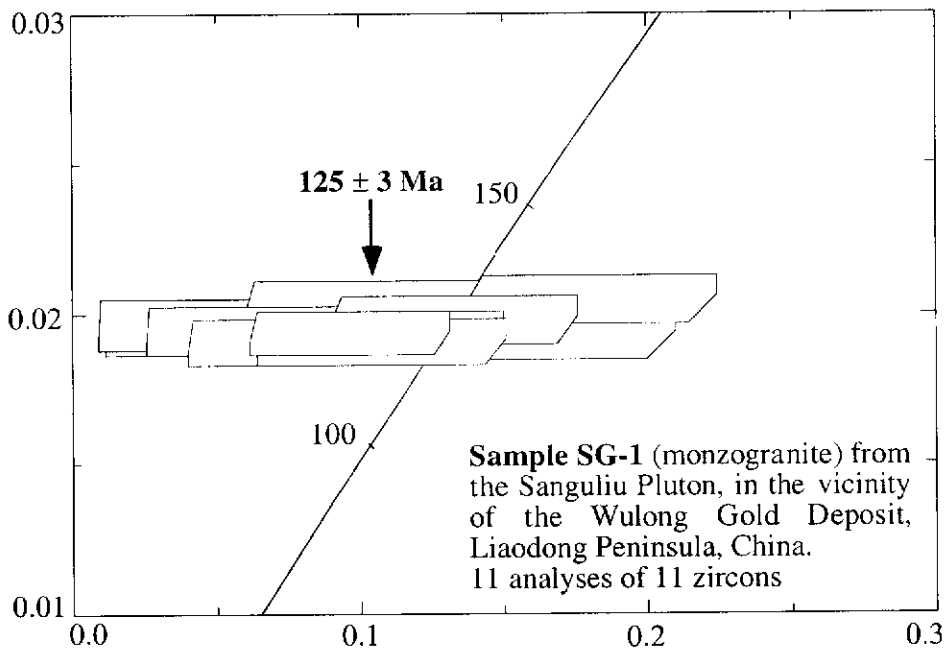

Fig. 6.15: U-Pb concordia diagram showing total SHRIMP data for Sample SG-1 from the Sanguliu Pluton.

Eleven analyses were made on 11 grains (Fig. 6.15), with ages ranging from 131 ± 5 Ma to 122 ± 5 Ma (Table 6.1). The 11 analyses form a coherent group (Fig. 6.15) with a weighted mean $^{206}Pb/^{238}U$ age of 125 ± 3 Ma and a chi-squared value of 0.3. The U and Th contents of these 11 spots vary from 37 ppm to 110 ppm and 47 ppm to 252 ppm, respectively. The Th/U ratios range from 0.93 to 2.31. The zircons formed during a single magmatic event and the age of 125 ± 3 Ma is considered to represent the intrusion age of the Sanguliu Pluton.

6.2.6 Summary

Lode gold deposits throughout the world are associated with, or proximal to, first-order transcrustal structures. However, they are rarely located within these first-order structures, but instead are hosted in second or high-order splays off the regional structures (Wyman and Kerrich, 1988; Groves and Foster, 1991). This conclusion is true of the Wulong Gold Deposit where it is proximal to the Yalujiang Fault, which is considered to be a major transcrustal lineament in the region, and gold mineralization at Wulong is controlled by the third-order structures with respect to the Yalujiang Fault (Yang, 1997). These third-order structures comprise two sets of brittle-ductile shears. One set, with sinistral shearing, strikes nearly north and dips 60°-80°W and steps to the left in an en-echelon manner; another set, with dextral shearing, trends northwest and dips 50°-70°SW and behaves as en-echelon arrays to the right. The orebodies within sinistral shears occur as left-handed en-echelon sets, whilst the orebodies in dextral shears are arranged as right-handed en-echelon sets.

At Wulong, the host to gold mineralization is a Mesozoic gneissic granitoid (WL11-19) with an emplacement age of 162 ± 8 Ma, obtained from magmatic zircon grains (Fig. 6.14). Yao et al. (1988) inferred that this kind of granitoid was formed during the Indosinian Orogeny (i.e. Late Triassic), however, this study indicates that the granitoid, similar to the Linglong and Kunyushan granitoids (with ages between 165 Ma and 150 Ma) in the Jiaodong Peninsula (Chapters 3 and 5 in this thesis), was intruded at the early stage of the Yanshanian tectono-magmatic event (160 -70 Ma). There are also three generations of inherited zircons in this granitoid with Late Archaean (ca. 2500 Ma), Palaeoproterozoic (1840-2200 Ma) and Early Mesozoic (ca. 230 Ma) ages. The inherited zircons of Precambrian age indicate that the Liaodong Peninsula is underlain by Precambrian basement. The inherited zircons with an Early Mesozoic age most likely represent a response to the collision of the North China Craton and Yangtze Craton involving crustal melting. During this collisional event, the

Precambrian basement was reworked to produce a suite of granitoids (Ames et al., 1993; Yin and Nie, 1993).

Swarms of felsic and mafic dykes, comprising microdiorite, microgranite, lamprophyre and dolerite, are widely distributed in the vicinity of the Wulong Gold Deposit. Based on field relationships, they predate, are coeval with, or post-date gold mineralization. The recognition that certain dykes are temporally associated with gold mineralization is significant in that it suggests the possibility of directly dating, or indirectly bracketing, the gold mineralization at the deposit.

The foliated microdiorite dykes are crosscut by all other dykes and by the orebodies, and fragments of these are contained within gold-bearing quartz veins, indicating that they predate gold mineralization and are the earliest dykes at the deposit. An age of 124 ± 3 Ma (Fig. 6.9) was obtained from zircons from one of these foliated microdiorite dykes. The CL images reveal that these zircons characteristically have well-developed oscillatory zones of igneous origin, thus 124 ± 3 Ma is interpreted as the emplacement age of these dykes and provides a maximum age for gold mineralization.

The undeformed microdiorite dykes are possibly synchronous with gold mineralization since they occupy the same two sets of third-order structures as the orebodies and underwent pervasively gold-related alteration. Ages of 119 ± 6 Ma and 119 ± 4 Ma were obtained from zircons from two undeformed microdiorite dykes (Figs. 6.11 and 6.12). Cathodoluminescence images of these zircons show oscillatory zonation indicative of an igneous origin and the age (ca. 119 Ma) is considered to represent the timing of emplacement of the undeformed microdiorite dykes. Due to the close temporal relationship between the dykes and gold mineralization, this age is also taken to be close to the time of gold mineralization at the Wulong Gold Deposit. Inherited zircons are abundant in the undeformed microdiorite dykes and their ages have a wide age range. The age of the youngest inherited zircons with oscillatory zonation is 127 ± 3 Ma, which coincides within error with the age of the earliest dyke suite (124 ± 3 Ma). The oldest inherited zircon with an age of 3717 ± 5 Ma provides evidence for the oldest basement of ca. 3800 Ma in the Liaodong Peninsula (Liu et al., 1992). Some inherited zircons have concordant Palaeoproterozoic ages, and some showing oscillatory zones under CL have concordant Early Mesozoic ages (ca. 220 Ma) which may suggest that these zircons were formed during an earlier magmatic event, not otherwise detected in the region.

The Sanguliu Pluton is a stock situated in the vicinity of the Wulong Gold Deposit. The age of 125 ± 3 Ma obtained from euhedral magmatic zircons represents the timing of emplacement of the pluton. This kind of pluton is similar to the last major phase of plutonic activity in the Jiaodong Peninsula, marked by the emplacement of the Guojialing granitoid suite between ca. 130 and 126 Ma (Wang et al., 1998). Based on rare earth element analysis (Fig. 6.8), the pluton and the dykes of the Wulong Gold Deposit originated from the same source.

In summary, the Wulong Gold Deposit is characterised by vein-type gold mineralization, and the orebodies dominantly occur as auriferous quartz veins, having distinct boundaries with the wall rock. After emplacement of the host gneissic granitoid at ca. 162 Ma, three episodes of dyke formation occurred at this deposit. The first episode was manifested by foliated microdiorite at ca. 124 Ma, which predates gold mineralization and approximately coincides with the emplacement of the Sanguliu Pluton (ca. 125 Ma); the second episode indicated by dykes synchronous with gold mineralization is at ca. 119 Ma; the third episode is represented by dykes post-dating gold mineralization but their age has not been determined so far.

6.3 Sidaogou Gold Deposit

The Sidaogou Gold Deposit (N40°05', E124°19') is situated near Dandong City (Fig. 2.4), and has mineable reserves of 13.5 tonnes at an average grade of 7.0 g/t. Structurally the deposit lies on the hanging wall of the Yalujiang Fault and is hosted in Proterozoic metasedimentary rocks (Fig. 6.16).

6.3.1 Lithological Units

The host of the Sidaogou Gold Deposit is dominantly rocks of the Palaeoproterozoic Liaohe Group. These include metasandstone, quartz-mica schist and graphite-bearing schist, all metamorphosed to greenschist facies. A swarm of felsic to mafic dykes, including microgranite, diorite and lamprophyre, are present in the area (Fig. 6.16) (Ren, 1988; Yao et al., 1988).

6.3.2 Yalujiang Fault

The Yalujiang Fault (Fig. 2.4) strikes 050° - 060° and dips ca. 70° NW, and is considered to be a first-order structure (Yao et al., 1988). A set of second-order faults strike in a NNE to NE direction and dip 60°-75°SE, and are subparallel to the Yalujiang

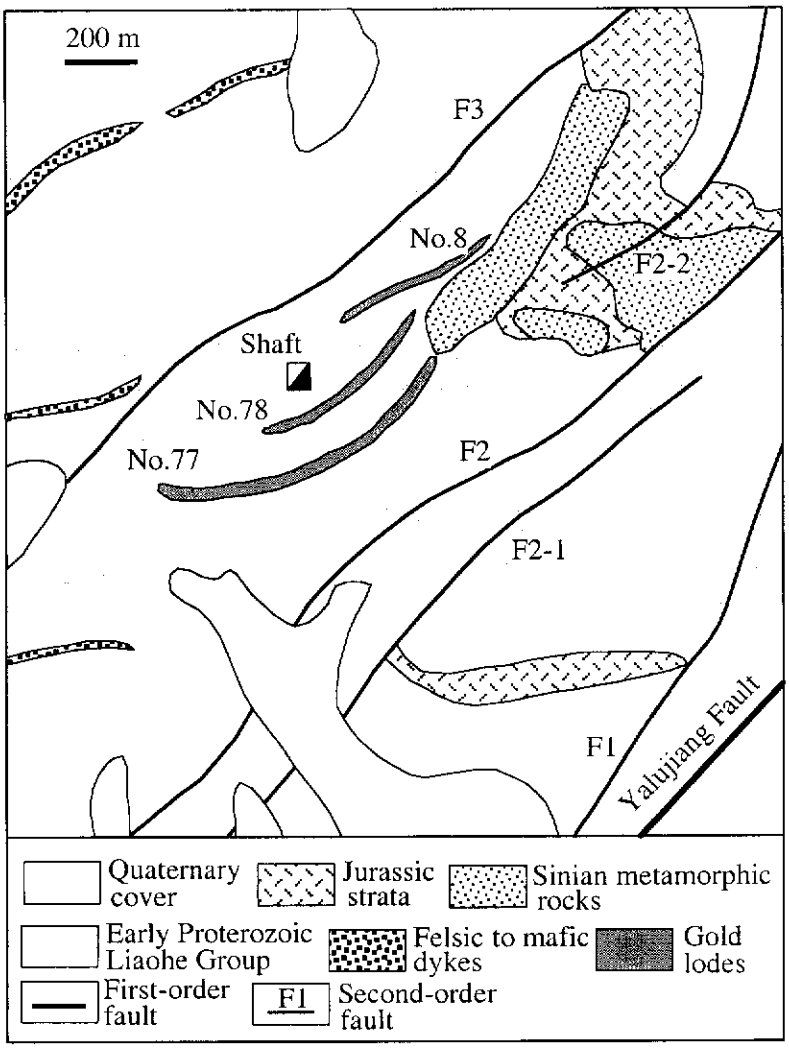

Fig. 6.16: Geological map of the Sidaogou Gold Deposit (modified from Yao et al., 1988).

Fault. The gold lodes of the Sidaogou Deposit (Fig. 6.16) are believed to be controlled by third-order faults (Yao et al., 1988), and also trend in a NE direction.

6.3.3 Alteration

At the Sidaogou Deposit, the alteration styles are dominantly silicification, sericitization, pyritization, K-feldspar alteration, carbonation and chloritization. Alteration haloes occur along both sides of the orebodies, and mainly consist of altered metasedimentary rocks and altered cataclastic rocks derived from the metasedimentary rocks. The intensity of wallrock alteration increases/decreases towards/away from the orebodies (Ren, 1988; Yao et al., 1988).

6.3.4 Lodes

The deposit mainly consists of the No.8, No.77 and No.78 lodes (Fig. 6.16). The No.77 lode is the largest. It is ca.1000 m in length and ranges from 10 m to 80 m in width, and extends for a depth of 500 m down-dip to the SE. This lode includes 8 orebodies. The second largest is the No.78 lode; it is ca. 600 m in length and varies from 25 m to 40 m in width, and has been explored to a depth of 450 m down-dip to the SE. This lode includes 10 orebodies. The No.8 lode is ca. 500 m in length and varies from 15 m to 35 m in width, and extends for a depth of 110 m down-dip in a SE direction; it consists of only 2 orebodies.

6.3.5 Ore Mineralogy and Paragenesis

Ore minerals include mainly pyrite, pyrrhotite, chalcopyrite, sphalerite, galena, bismuthinite, chalcocite and arsenopyrite, with pyrite the most abundant, making up 90% of the ore minerals and carrying about 94% of the gold. Gangue minerals mainly comprise quartz, feldspar, calcite and sericite. Gold minerals are dominantly electrum with trace amounts of native gold. The ore can be divided into 3 types. Type 1 consists of pyrite (85-94%) and quartz (5-15%), with grades of 50-200 g/t. Type 2 also comprises pyrite and quartz, but the contents of the two minerals are approximately equal. The ore grade of type 2 varies from 15 g/t to 50 g/t. Type 3 consists of altered metamorphic rocks with pyrite occurring in disseminated and veinlet forms. This type of ore contains 5-20% pyrite, with a grade of 3-15 g/t (The Sidaogou Gold Mine, 1988). Three stages of hydrothermal mineral formation have been identified (Yao et al., 1988). These stages are, from the oldest to the youngest: stage 1- gold-quartz-pyrite, with the mineral assemblage consisting mainly of subhedral, white quartz and

euhedral to subhedral pyrite; stage 2- gold-quartz-multiple metal sulphides, with the mineral paragenesis composed chiefly of fine-grained quartz, pyrite and other metallic minerals such as pyrrhotite and chalcopyrite; stage 3- quartz-carbonate, where the mineral assemblage consists mainly of quartz and calcite. Stages 1 and 2 are closely related to gold mineralization (Yao et al., 1988).

6.3.6 Geochronological Data

Zircon is highly stable in most environments, however, zirconium mobility has been observed in some hydrothermal environments where hydrothermal zircons can be formed (Rubin et al., 1989, 1993; Claoué-long et al., 1990; Kerrich and King, 1993; Nesbitt et al., 1999). Claoué-long et al. (1990) dated hydrothermal zircons from auriferous veins in the Abitibi greenstone belt to directly constrain the timing of gold mineralization. Based on the possibility that hydrothermal zircons may be present in the ore, sample SD4-7 (Fig. 6.17a) was selected for SHRIMP zircon dating. In addition, indirect constraints on the timing of gold mineralization at the Sidaogou Deposit may be provided by sample SD4-1 from the host rock and sample SD5-3 from a post-mineralization lamprophyre dyke (Fig. 6.17b and c, respectively). Since sample SD4-1 is a metasandstone, only its maximum depositional age may be defined. The zircons extracted from sample SD5-3 were insufficient for analysis, and most were rounded which may mean that they were not formed from the dyke magma. Therefore, the crystallization age of this dyke cannot be determined.

SHRIMP results for samples SD4-1 and SD4-7 are listed in Table 6.2 and illustrated on concordia diagrams in Figures 6.18 and 6.19. All errors for individual analyses in Table 6.2 and on the concordia diagrams are given as 1σ. Group ages in concordia plots are quoted with 95% confidence error limits (2σ). Following are the description of the samples and the interpretation of their SHRIMP U-Pb zircon ages.

Sample SD4-1

Sample SD4-1 is a dark green fine-grained metasandstone and mainly comprises a mosaic of quartz, biotite, sericite and minor feldspar grains. Zircons are pale pink in colour and most grains are rounded. Only a few suitable zircons were available for analysis, and these range in size from 105 μm to 74 μm. The zircons separated from the non-mineralized metasandstone did not form during the low-grade greenschist facies metamorphic event or by hydrothermal alteration, therefore, they are

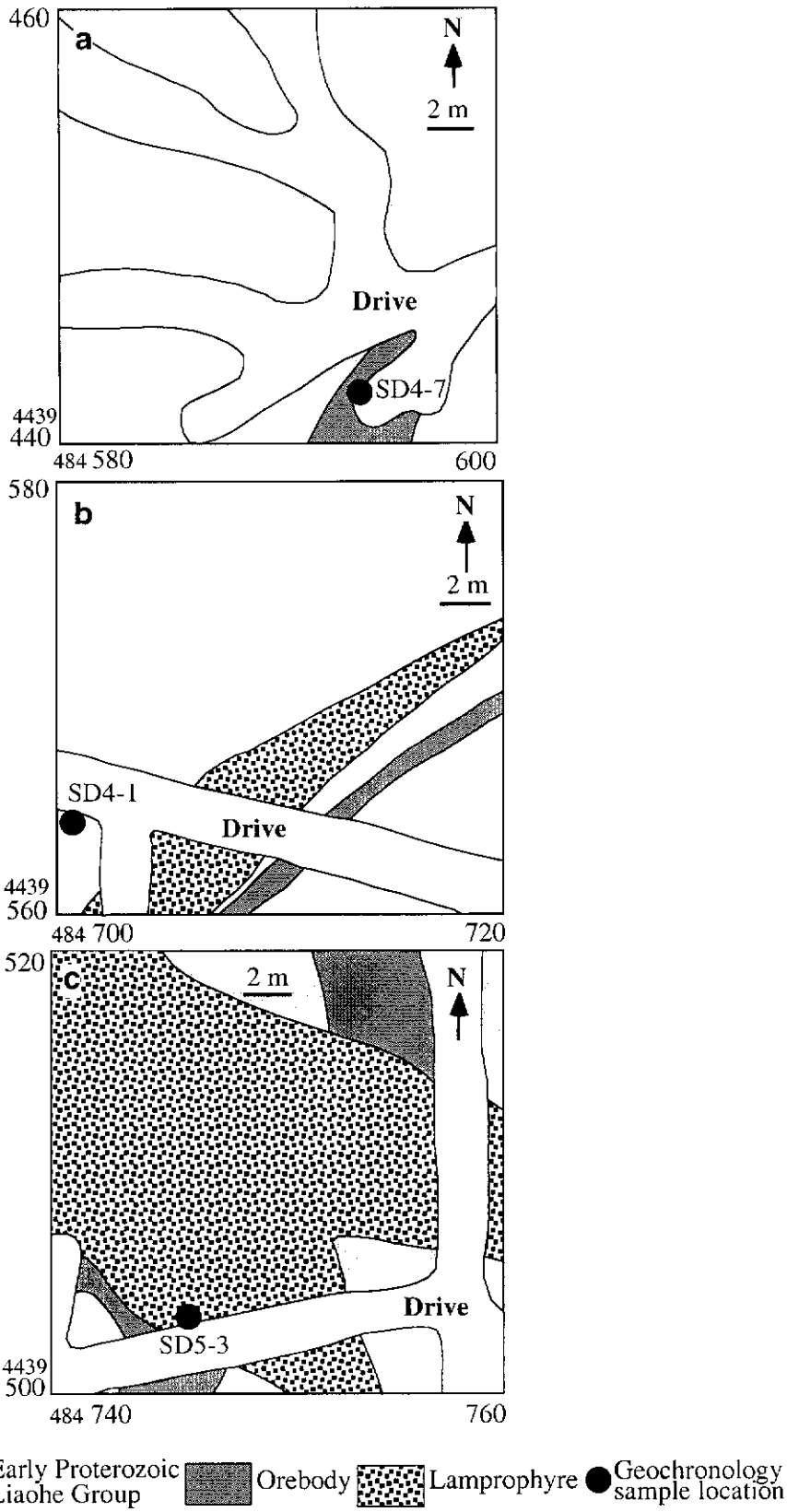

Fig. 6.17: Maps showing the location of geochronology samples from the Sidaogou Gold Deposit. (a) and (b) Parts of plan of level 4; (c) Part of plan of level 5.

Table 6.2: SHRIMP U-Pb data for zircons from the samples SD4-1 and SD4-7 from the Sidaogou Gold Deposit. Analyses are listed in order of increasing age. The following notation is used for analysed grains: 1.1=grain 1, first point analysed. Data are ^{204}Pb-corrected. Individual analyses are quoted at 1σ error. The $^{207}Pb/^{206}Pb$ age is adopted for zircons with an age of more than 1.0 Ga.

spot	U (ppm)	Th (ppm)	Th/U	Total Pb (ppm)	$\frac{^{204}Pb}{^{206}Pb}$	f206 (%)	$\frac{^{207}Pb}{^{206}Pb}$	$\frac{^{206}Pb}{^{238}U}$	$\frac{^{207}Pb}{^{235}U}$	$\frac{^{207}Pb}{^{206}Pb}$ Age (Ma)
Sample SD4-1										
6.1	255	12	0.05	97	0.00127	0.02	0.115±1	0.3627±101	5.77±18	1886±16
7.1	1969	303	0.15	727	0.00014	0.002	0.119±0	0.3646±101	5.96±17	1935±3
1.1	562	166	0.3	227	0.00001	0	0.122±0	0.3881±108	6.54±18	1989±4
2.1	1141	505	0.44	453	0	0	0.126±0	0.3629±101	6.31±18	2044±3
3.1	316	185	0.59	146	0.00001	0	0.136±0	0.4124±115	7.73±22	2175±5
8.1	282	59	0.21	124	0.00003	0	0.137±0	0.4269±119	8.06±23	2189±5
5.1	147	66	0.44	68	0.00144	0.023	0.137±1	0.3905±110	7.38±23	2190±18
4.1	502	270	0.54	229	0.00002	0	0.138±0	0.4103±114	7.82±22	2206±4
Sample SD4-7										
4.1	469	496	1.06	216	0.00004	0.001	0.129±0	0.3727±104	6.64±19	2087±5
12.1	310	163	0.52	139	0.00002	0	0.138±0	0.4045±113	7.7±22	2202±5
21.1	92	70	0.76	49	0.00008	0.001	0.153±1	0.4542±129	9.58±28	2380±10
1.1	182	160	0.88	105	0.00002	0	0.163±1	0.4749±133	10.65±31	2483±6
14.1	136	59	0.44	74	0.00001	0	0.164±1	0.4887±138	11.02±32	2492±7
11.1	250	105	0.42	131	0.00003	0.001	0.164±0	0.4729±132	10.68±30	2495±5
8.1	496	246	0.5	280	0.00003	0	0.164±0	0.5043±141	11.41±32	2498±4
3.1	68	6	0.08	31	0.00017	0.003	0.164±1	0.4384±126	9.92±31	2499±14
15.1	323	130	0.4	168	0.00001	0	0.165±0	0.4725±132	10.72±30	2503±4
13.1	403	211	0.52	220	0.00002	0	0.165±0	0.4844±135	11.03±31	2509±4
20.1	251	242	0.96	148	0.00001	0	0.165±0	0.4763±133	10.87±31	2512±5
9.1	511	469	0.92	295	0	0	0.166±0	0.471±131	10.76±30	2514±3
7.1	309	128	0.41	165	0.00002	0	0.167±0	0.485±135	11.17±32	2528±4
16.1	81	43	0.54	42	0.00001	0	0.168±1	0.4529±129	10.49±31	2537±9
2.1	44	28	0.64	26	0.00027	0.004	0.168±2	0.5008±147	11.62±38	2541±18
19.1	159	165	1.04	98	0.0001	0.002	0.172±1	0.4871±137	11.56±33	2578±6
18.1	361	7	0.02	182	0.00003	0.001	0.173±0	0.4985±139	11.87±33	2584±4
5.1	241	81	0.34	135	0.00006	0.001	0.181±1	0.5109±143	12.79±36	2667±5
5.2	325	151	0.46	182	0.00003	0.001	0.184±0	0.4932±138	12.49±35	2687±4
6.1	364	187	0.51	217	0.00003	0	0.185±0	0.5196±145	13.24±37	2697±4
17.1	122	53	0.43	73	0.00003	0.001	0.186±1	0.5311±150	13.64±39	2710±6
10.2	178	73	0.41	145	0.00002	0	0.279±1	0.685±192	26.32±75	3355±4
10.1	117	48	0.41	95	0.00006	0.001	0.279±1	0.6742±190	25.93±74	3357±4

considered to be detrital. The grain shapes suggests that they were transported considerable distances prior to their incorporation in the sandstone host rock.

Eight analyses were made on 8 zircon grains (Fig. 6.18), and ages range from 2206 ± 4 Ma to 1886 ± 16 Ma (Table 6.2).

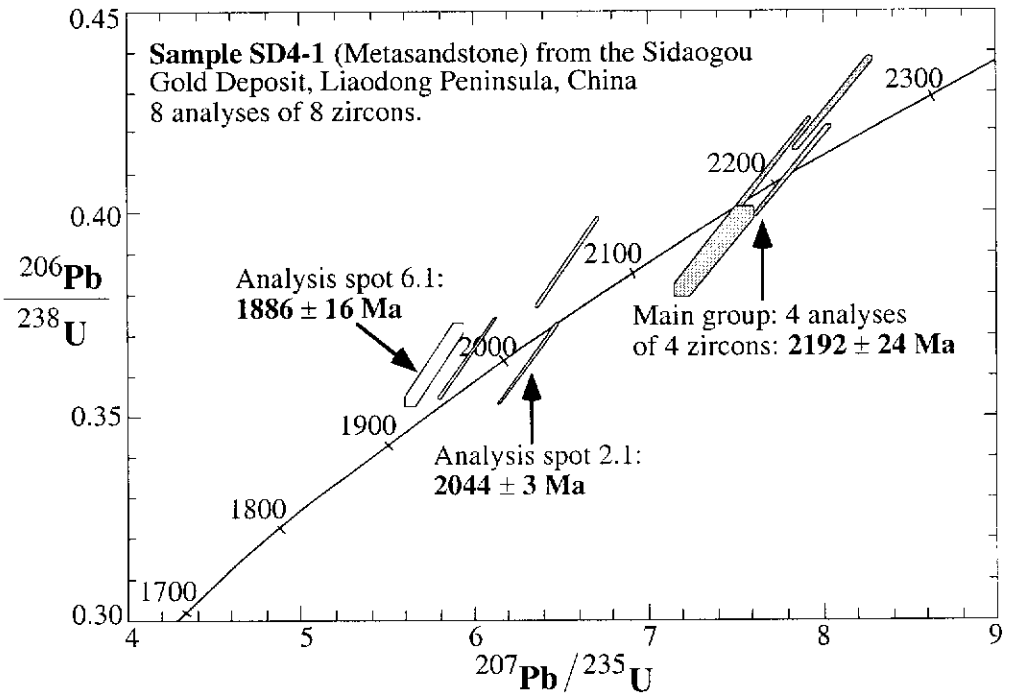

Fig. 6.18: U-Pb concordia plot showing SHRIMP zircon analytical data for sample SD4-1.

Four analyses of 4 grains form a coherent group (Fig. 6.18) with a weighted mean $^{207}Pb/^{206}Pb$ age of 2192 ± 24 Ma (2σ). The U and Th contents of these 4 spots range from 147 ppm to 502 ppm and 59 ppm to 270 ppm, respectively. The Th/U ratios vary from 0.21 to 0.59, which is within the suggested range for zircons in felsic igneous rocks (Williams and Claesson, 1987; Heaman et al., 1990). Therefore, the age of 2192 ± 24 Ma is interpreted to represent the timing of an igneous event which was responsible for the growth of these zircons which were then eroded and became incorporated in the sandstone.

A concordant $^{207}Pb/^{206}Pb$ age of 2044 ± 3 Ma (1σ) (Fig. 6.18) was obtained from spot 2.1 of grain 2. On the basis of its U-Th chemistry (Table 6.2), this age is considered to represent another igneous event. The anlysis spot 6.1 of the youngest detrital zircon grain 6 yields a $^{207}Pb/^{206}Pb$ age of 1886 ± 16 Ma (1σ) (Fig. 6.18), which defines a maximum depositional age for the sandstone.

Sample SD4-7

Sample SD4-7 is a light coloured fine-grained mineralized metasandstone, which consists of quartz, sericite, and minor feldspar, pyrite and calcite. It was collected from a disseminated orebody. Zircons are pink in colour and some grains are rounded, whereas others have rounded bipyramid terminations with an average elongation ratio of about 2:1. Zircons selected for analysis range in size from 105 μm to 74 μm.

A total of 23 analyses were carried out on 21 zircon grains (Fig. 6.19), with ages ranging from 3357 ± 4 Ma to 2087 ± 5 Ma (Table 6.2). These zircons are also of detrital in origin. Therefore, no hydrothermal zircons were present in this ore sample.

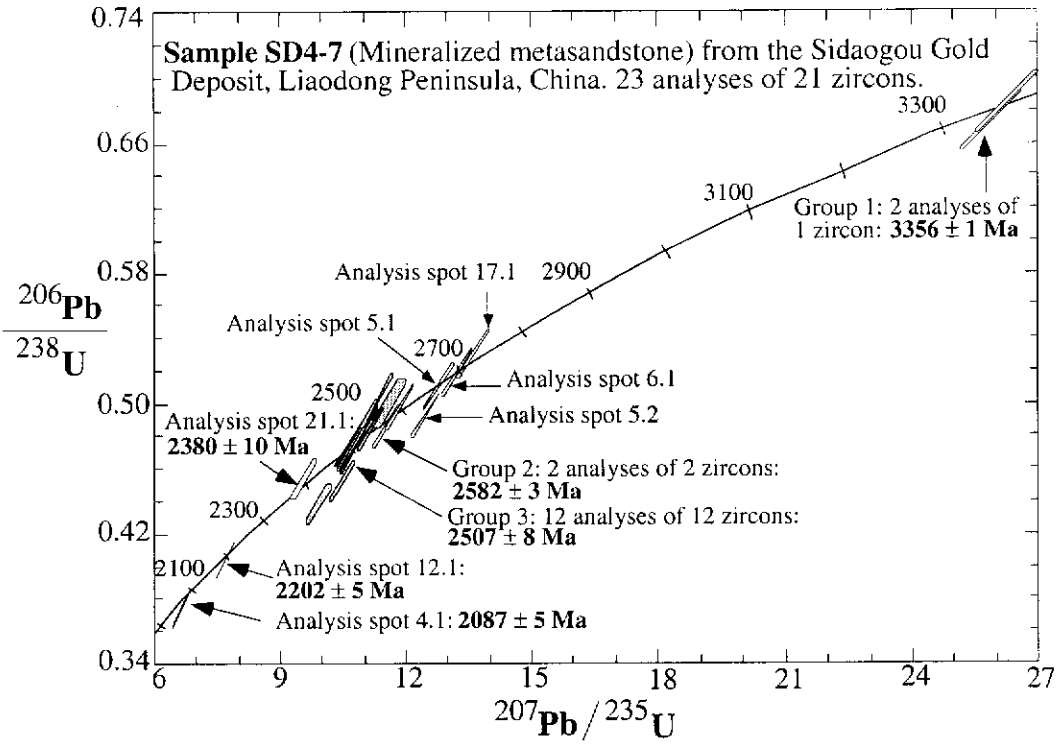

Fig. 6.19: U-Pb concordia plot showing SHRIMP zircon analytical data for sample SD4-7.

Two analyses, 10.1 and 10.2, of grain 10 define a coherent group (Group 1 in Fig. 6.19), yielding the oldest concordant $^{207}Pb/^{206}Pb$ age of 3356 ± 1 Ma (2σ). The U and Th contents of the two analysis spots vary from 117 ppm to 178 ppm and 48 ppm to 73 ppm, respectively. Their Th/U ratios are both 0.41. Grain 10 is a fragment of an euhedral crystal, hence the age of 3356 ± 1 Ma is considered to represent the oldest crystallization age of igneous source rocks which contributed to the metasedimentary rocks in this area. This age coincides with a $^{207}Pb/^{206}Pb$ age of 3362

± 5 Ma (2σ) obtained from a supracrustal rock within Anshan area (Fig. 2.4), which is interpreted as the protolith age of the supracrustals (Song et al., 1996).

Analyses spots 5.1, 5.2, 6.1 and 17.1 yield $^{207}Pb/^{206}Pb$ ages of 2667 ± 5 Ma, 2687 ± 4 Ma, 2697 ± 4 Ma and 2710 ± 6 Ma (1σ) (Table 6.2), respectively, but no statistical group could be defined. The U and Th contents of these 4 spots range from 122 ppm to 364 ppm and 53 ppm to 187 ppm, respectively. The Th/U ratios vary from 0.34 to 0.51.

Group 2 comprises 2 analyses of 2 grains, which give a weighted mean $^{207}Pb/^{206}Pb$ age of 2582 ± 3 Ma (2σ) (Fig. 6.19). The U and Th contents of spot 18.1 from grain 18 are 361 ppm and 7 ppm, with a Th/U ratio of 0.02, while the U and Th contents of spot 19.1 from grain 19 are 159 ppm and 165 ppm, with a Th/U ratio of 1.04. The age of 2582 ± 3 Ma is comparable with 2575 Ma (no errors given) which is interpreted as the timing of a magmatic event in the Chifeng area, along the north margin of the North China Craton (Cui et al., 1991).

The main population consists of 12 analyses of 12 zircons, which define a coherent group (Group 3 in Fig. 6.19) having a weighted mean $^{207}Pb/^{206}Pb$ age of 2507 ± 8 Ma (2σ). The U and Th contents of these 12 spots range from 44 ppm to 511 ppm and 6 ppm to 469 ppm, respectively. The Th/U ratios vary from 0.4 to 0.96, except for 0.08 for spot 3.1. This age coincides with the age of a magmatic event which widely occurred at around 2500 Ma in the Anshan area as well as throughout the North China Cration (Liu et al., 1992; Song et al., 1996; Kröner et al., 1998).

Analyses spots 21.1, 12.1 and 4.1 (Fig. 6.19) yield concordant $^{207}Pb/^{206}Pb$ ages of 2380 ± 10 Ma (1σ), 2202 ± 5 Ma (1σ) and 2087 ± 5 Ma (1σ) (Fig. 6.19), respectively. Based on their U-Th chemistry (Table 6.2), these ages are considered to represent three igneous events. Among them, 2202 ± 5 Ma, within the error, coincides with 2192 ± 24 Ma obtained from sample SD4-1, but the ages of 2380 ± 10 Ma and 2087 ± 5 Ma have not been previously reported in this or neighbouring areas.

Based on the above interpretation, detrital zircons from sample SD4-7 originated from several different source rocks, which formed during up to six geological events.

6.3.7 Summary

The Sidaogou Gold Deposit is hosted by rocks of the Palaeoproterozoic Liaohe Group which consist of metasandstone, quartz-mica schist and graphite-bearing schist in the mining area. Gold lodes of this deposit are believed to be controlled by third-order structures of the Yalujiang Fault. The alteration types include silicification, sericitization, pyritization, K-feldspar alteration, carbonation and chloritization.

Using SHRIMP U-Pb zircon techniques, the maximum depositional age for the metamorphic sandstone within this deposit was obtained at ca. 1886 Ma; the oldest igneous event in the source was dated at ca. 3356 Ma which coincides with the protolith age of supracrustal rocks within the Anshan area. In addition, six other igneous events were dated at ca. 2582 Ma, ca. 2500 Ma, ca. 2380 Ma, ca. 2202 Ma, ca. 2087 Ma and 2044 Ma, respectively, and contributed to the sandstone. Since no hydrothermal zircons were found in the ore (sample SD4-7), the timing of gold mineralization in this deposit cannot be obtained by dating such zircons. However, both the Sidaogou and Wulong Gold Deposits are structurally controlled by the Yalujiang Fault, therefore, they may have formed during the same gold mineralization event which was dated at ca. 119 Ma at the Wulong Deposit.

6.4 Baiyun Gold Deposit

The Baiyun Gold Deposit (N40°50', E123°36') is located ca. 50 km north-west of the city of Fengcheng (Fig. 2.4). It was discovered in 1978 by the No.107 Team of the Geology Exploration Company of the MIBLP (Metallurgical Industrial Bureau of Liaoning Province), based on regional reconnaissance. From 1978 to 1981, further detailed exploration work, including 1:10,000 and 1:2,000 scale mapping, interpretation of geophysical and geochemical data, trenching and drilling, was carried out and the known reserves were estimated at 4.18 tonnes in 1981. The orebodies are hosted in schists of the Liaohe Group, commonly with alteration haloes (Fig. 6.20). Liu and Ai (1999) considered that the orebodies and their alteration haloes were controlled by an EW-trending fault, developed at the contact between schist and marble of the Liaohe Group.

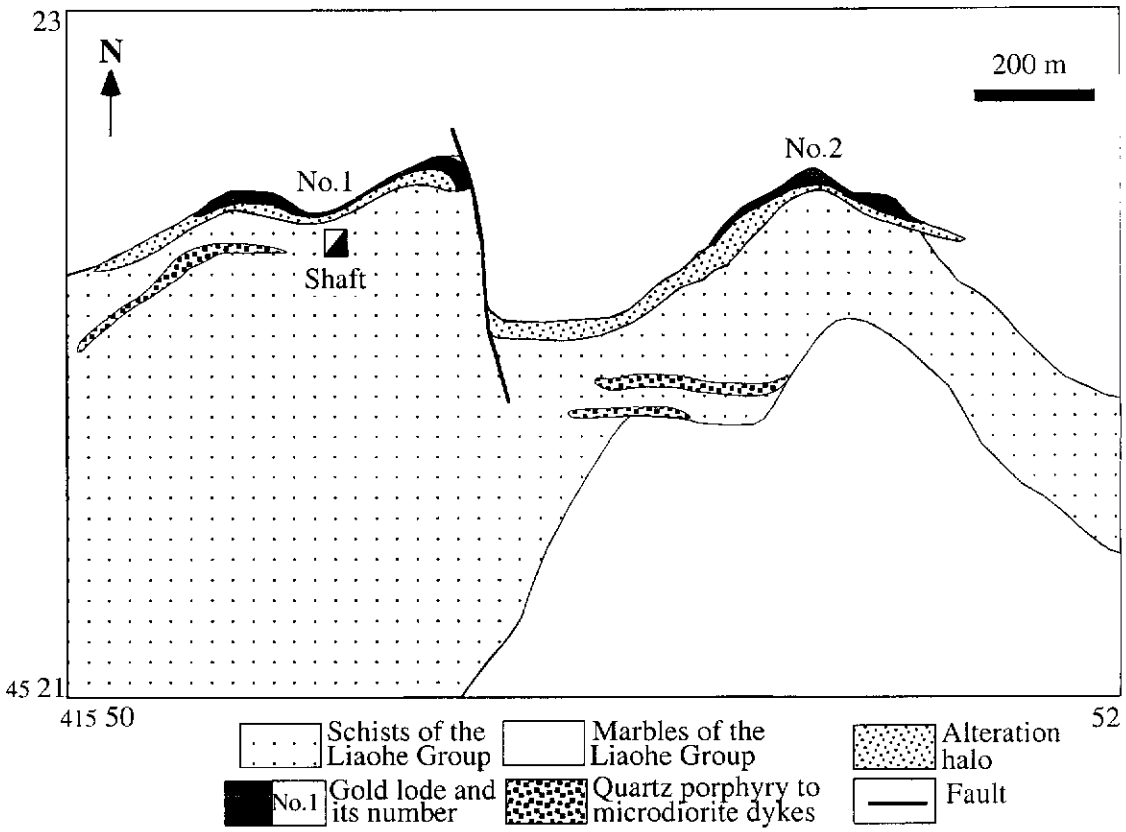

Fig. 6.20: Geological map of the Baiyun Gold Deposit (modified from Liu and Ai, 1999).

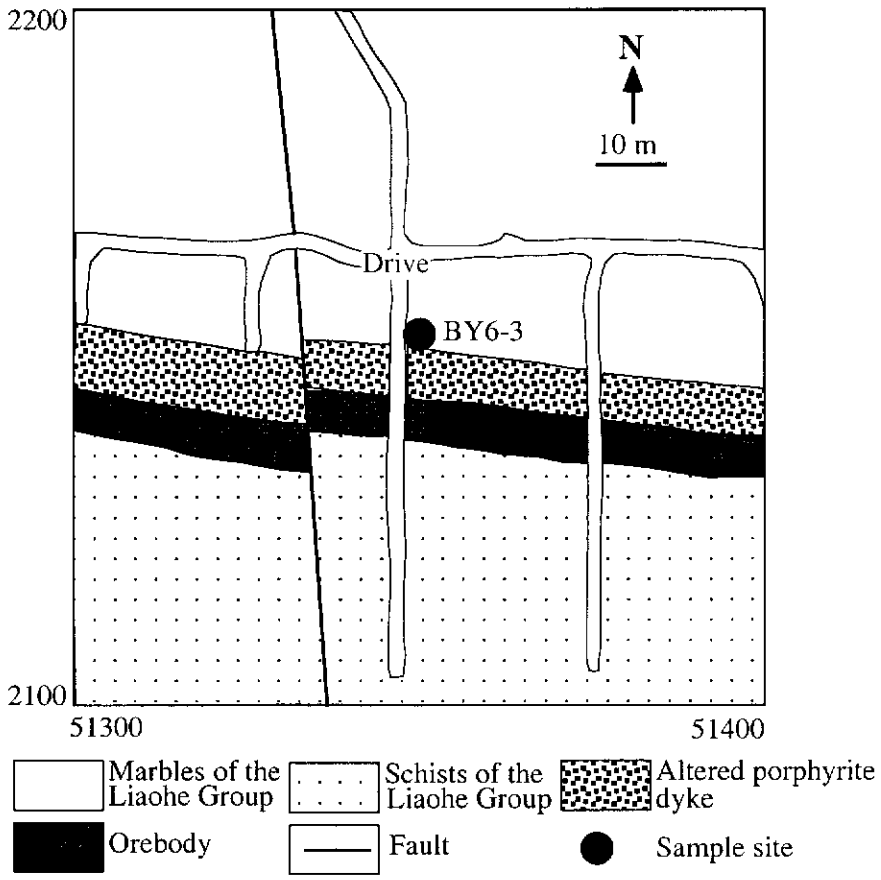

Fig. 6.21: Part of plan of 600 m level at the Baiyun Gold Deposit, showing the location of geochronology sample BY6-3.

6.4.1 Lithological Units

The deposit is hosted in the Liaohe Group (Fig. 6.20), considered to be Palaeoproterozoic in age and mainly consisting of sillimanite-biotite schist and thinly-bedded marbles. Metamorphic grade is regional amphibolite facies. A swarm of felsic to mafic dykes, including quartz porphyry, microdiorite and lamprophyre, are present in the area (The No.107 Team of the Geology Exploration Company, MIBLP, 1982; Liu and Ai, 1999).

6.4.2 Alteration

At the Baiyun Deposit, the alteration types are dominantly silicification, K-feldspar alteration, sericitization, pyritization, carbonation and chloritization. The alteration halo is ca. 1500 m in length (Fig. 6.20) and ranges from 1 m to 40 m in width. It strikes in an EW direction (Liu and Ai, 1999) and has been cut off by a NNW-trending fault (Fig. 6.20). The intensity of wallrock alteration increases/decreases towards/away from the orebodies. The alteration halo mainly comprises altered schists and cataclastic rocks derived from the schists (The No.107 Team of the Geology and Exploration Company, MIBLP, 1982).

6.4.3 Lodes

The deposit is mainly composed of the No.1 and No.2 gold lodes (Fig. 6.20), which include 5 and 8 orebodies, respectively. These orebodies strike in a nearly EW direction, dip 30°-50°S and pitch 35°-70°W. They range from 100 m to 150 m in length and from 1 m to 7 m in thickness, and extend to a depth of 250 m down-dip. In general, their gold grades vary from 1 g/t to 64.17 g/t, but locally reach a maximum of 110 g/t (The No.107 Team of the Geology and Exploration Company, MIBLP, 1982).

6.4.4 Ore Mineralogy and Paragenesis

Ore minerals include pyrite, chalcopyrite, galena, sphalerite, pyrrhotite, bornite and magnetite, with pyrite the most abundant, making up about 6% of the ore and carrying most of the gold within the deposit. Gangue minerals comprise quartz, sericite, feldspar, carbonate, and chlorite, with quartz the most abundant. Gold occurs dominantly as electrum and trace amounts of native gold (the No.107 Team of the Geology and Exploration Company, MIBLP, 1982). The ore consists of quartz, pyrite, sericite, and small amounts of other metal sulphides, including chalcopyrite,

pyrrhotite, sphalerite and galena. Three stages of hydrothermal mineral formation have been identified (The No.107 Team of the Geology and Exploration Company, MIBLP, 1982). These stages are, from the oldest to the youngest: stage 1- gold-pyrite-quartz; stage 2- gold-quartz-base metal sulphides; stage 3- quartz-carbonate.

6.4.5 Geochronological Data

Since some dykes are altered and occupy the same structure as the orebodies (Fig. 6.21), they have been considered to be temporally associated with the gold mineralization event (Yao et al., 1990). An approximate timing of gold mineralization may be obtained by dating these dykes. On the basis of this, sample BY6-3 was selected for SHRIMP analysis and the results listed in Table 6.3 and shown on a concordia plot in Figure 6.22. Following are the description of sample BY6-3 and the interpretation of its SHRIMP zircon U-Pb age.

Sample BY6-3

Sample BY6-3 was collected from an altered mesocratic porphyrite dyke. Some phenocrysts of plagioclase and amphibole are pseudomorphed by sericite and chlorite, respectively. Zircons selected for analysis range in size from 132 μm to 74 μm and are pale brown in colour. Most grains are euhedral, with well-formed pyramidal terminations, and their elongation ratios vary from 2:1 to 3:1.

Fourteen analyses were made on 13 euhedral zircon grains (Fig. 6.22), and ages range from 1771 ± 11 Ma to 158 ± 4 Ma (Table 6.3).

Thirteen analyses of 12 grains form a coherent population (Fig. 6.22b) with a weighted mean $^{206}Pb/^{238}U$ age of 168 ± 4 Ma (2σ) and a chi-square value of 1.83. The U and Th contents of the 12 spots range from 152 ppm to 977 ppm and 16 ppm to 869 ppm, respectively. The Th/U ratios vary from 0.11 to 1.18. Since these euhedral grains with good pyramid terminations are of igneous origin, the group age of 168 ± 4 Ma is considered to represent the intrusive age of the porphyrite dyke, which coincides, within error, with the emplacement age (162 ± 8 Ma) of the granite host at the Wulong Gold Deposit.

Table 6.3: SHRIMP U-Pb data for zircons from the sample BY6-3 from the Baiyun Gold Deposit. Analyses are listed in order of increasing age. The following notation is used for analysed grains: 1.1=grain 1, first point analysed. Data are ^{204}Pb-corrected. Individual analyses are quoted at 1σ error. The $^{206}Pb/^{238}U$ age is adopted for zircons with an age of less than 1.0 Ga, otherwise, the $^{207}Pb/^{206}Pb$ age is used.

spot	U (ppm)	Th (ppm)	Th/U	Total Pb (ppm)	$\frac{^{204}Pb}{^{206}Pb}$	f206 (%)	$\frac{^{207}Pb}{^{206}Pb}$	$\frac{^{206}Pb}{^{238}U}$	$\frac{^{207}Pb}{^{235}U}$	$\frac{^{206}Pb}{^{238}U}$ Age	$\frac{^{207}Pb}{^{206}Pb}$ Age
Sample BY6-3											
5.1	214	226	1.05	7	0.00346	0.055	0.036±10	0.0249±6	0.12±4	158±4	
2.1	585	375	0.64	17	0.00106	0.017	0.056±4	0.0251±6	0.19±2	160±4	
1.1	560	471	0.84	17	0.0012	0.019	0.047±4	0.0259±6	0.17±1	165±4	
9.1	360	197	0.55	11	0.0033	0.053	0.042±7	0.026±6	0.15±3	165±4	
12.1	300	354	1.18	11	0.00244	0.039	0.045±7	0.0262±6	0.16±3	167±4	
7.1	906	869	0.96	28	0.00056	0.009	0.05±2	0.0264±6	0.18±1	168±4	
4.1	747	400	0.54	22	0.00087	0.014	0.051±3	0.0266±6	0.19±1	169±4	
8.1	569	120	0.21	16	0.00143	0.023	0.049±4	0.0266±6	0.18±2	169±4	
4.2	977	784	0.8	31	0.00095	0.015	0.048±2	0.0267±6	0.18±1	170±4	
11.1	152	16	0.11	5	0.0023	0.037	0.063±10	0.0267±7	0.23±4	170±4	
10.1	561	392	0.7	17	0.001	0.016	0.052±3	0.0268±6	0.19±1	171±4	
6.1	541	214	0.4	16	0.00076	0.012	0.053±3	0.0275±6	0.2±1	175±4	
3.1	596	106	0.18	16	0.00018	0.003	0.052±2	0.028±6	0.2±1	178±4	
13.1	558	17	0.03	117	0.00016	0.003	0.108±1	0.2167±48	3.24±8		1771±11

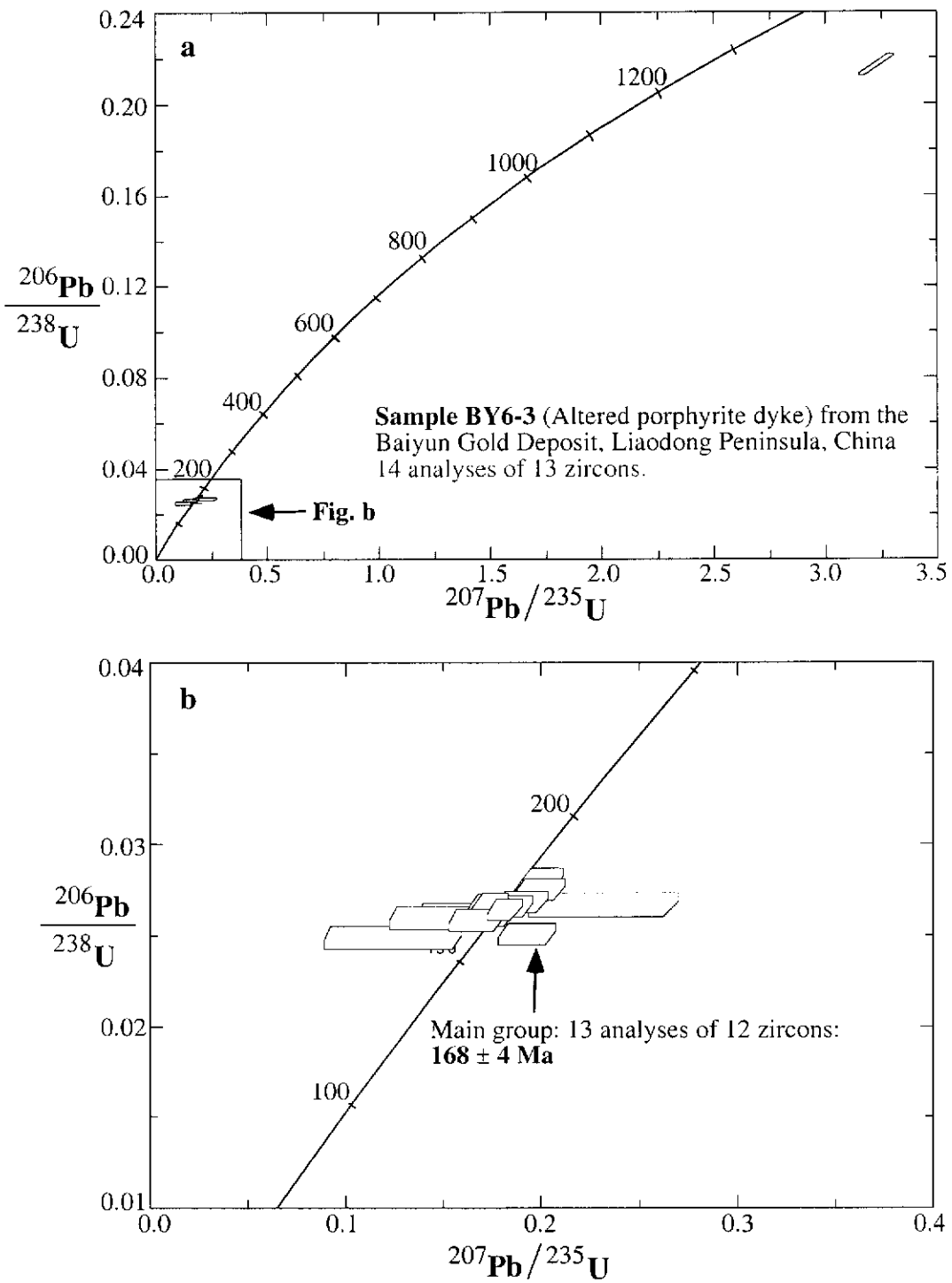

Fig. 6.22: U-Pb concordia plots showing (a) total SHRIMP zircon analytical data from sample BY6-3 and (b) enlargement detailing the main magmatic zircon population.

6.4.6 Summary

The Baiyun Gold Deposit is hosted by rocks of the Palaeoproterozoic Liaohe Group which consist of sillimanite-biotite schist and thinly-bedded marble in the mining area. The contact between the schist and marble is marked by an EW-trending fault which controlled the orebodies and their alteration haloes. The alteration types include silicification, K-feldspar alteration, sericitization, pyritization, carbonation and chloritization.

Using SHRIMP U-Pb zircon methods, one porphyrite dyke, which is altered and occupies the same structure as the orebodies, was dated at 168 ± 4 Ma. This age is considered to represent the intrusive age of the dyke, which coincides with the emplacement age (162 ± 8 Ma) of the granite host at the Wulong Gold Deposit, as well as the age of the Linglong and Kunyushan granitoids (150-165 Ma) within the Jiaodong Peninsula. Although the trends of these dykes and the mineralized fractures are similar, these data indicate that some of the dykes are much older than gold mineralization which was dated at ca. 119 Ma at the nearby Wulong Gold Deposit. It therefore appears that the fractures which controlled both dyke emplacement and mineralization were formed as early as 168 Ma and re-activated at ca. 119 Ma during regional gold mineralization.

6.5 Conclusion

Gold deposits of the Liaodong Peninsula are hosted by Mesozoic granitoids and the Palaeoproterozoic Liaohe Group. These deposits are of the Linglong-style (vein-filling type) of gold occurrences which are spatially associated with fault zones. such as the Yalujiang Fault.

Using SHRIMP U-Pb zircon techniques, the granitoids hosting gold deposits were dated at ca. 162 Ma which coincides well with the emplacement age (150-165 Ma) of the Linglong and Kunyushan granitoids within the Jiaodong Peninsula. This indicates that these granitoids were intruded at an early stage of the Yanshanian tectono-magmatic event (70-160 Ma). The Sanguliu Pluton yields an age of ca. 125 Ma, which is consistent with the emplacement age of the Guojialing granitoids (126-130 Ma) within the Jiaodong Peninsula. Therefore, another igneous event (126-130 Ma), represented by the Guojialing and Sanguliu granitoids, occurred widely throughout the Jiaodong and Liaodong Peninsulas.

As within the three gold belts (Zhao-Ye, Qi-Peng and Mu-Ru Gold Belts, which were described in Chapters 3, 4 and 5) of the Jiaodong Peninsula, dykes, including felsic, intermediate and mafic types, are also widely distributed within the gold deposits of the Liaodong Peninsula. These dykes formed during four episodes. The earliest dyke episode was dated at ca. 168 Ma, which indicates that some dykes may have formed during the igneous event that occurred between 150 and 165 Ma; the second dyke episode was dated at ca. 124 Ma, which indicates that these dykes may have formed during the major igneous event that occurred between 126 and 130 Ma; the third episode is represented by dykes synchronous with gold mineralization at ca. 119 Ma; the last episode is represented by dykes which post-date gold mineralization, but whose age has so far not been determined.

Based on the dating results presented in this thesis, it is concluded that gold deposits of the Liaodong Peninsula and those of the three gold belts of the Jiaodong Peninsula were formed during the same mineralization event (100-120 Ma).

CHAPTER 7: DISCUSSION AND CONCLUSION

China's gold resources are largely distributed along the margins of the North China Craton (Fig. 1.1). The Jiaodong and Liaodong Peninsulas, which are the major sites of both gold production and gold reserves within China (and constitute the focus of this study) are situated along the southeast margin of the North China Craton (Fig. 1.1; Nie, 1997a; Yang, 1996). Significant gold deposits also occur along the northern and southern margins of the North China Craton (Fig. 1.1; Miller et al., 1998; Jiang et al., 1999). Why is so vast an amount of gold concentrated along the marginal areas of the North China Craton? Why do so many gold deposits of over 900 tonnes gold production and ore reserves occur in the Jiaobei Terrane of the Jiaodong Peninsula, an area with length of ca. 180 km in an east-west direction and a width ranging from 20 km to 80 km in north-south direction (Zhou and Lü, 2000)? What are the controls on gold mineralization in the Jiaodong and Liaodong Peninsulas? Did there exist a single gold mineralization event in the Jiaodong and Liaodong Peninsulas? If gold mineralization was essentially a single event then when did it occur? What is a viable genetic model for the Jiaodong and Liaodong gold deposits? Based on a synthesis of research results in this thesis and an evaluation of data from the Chinese literature, the above questions will be discussed and a conclusion presented.

7.1 Favourable Tectonic Setting for Gold Mineralization

In contrast to many Archaean cratonic blocks which underwent gold mineralization in the Late Archaean (Kerrich and Cassidy, 1994; Groves et al., 1998), the North China Craton shows major mineralization confined to the Phanerozoic, in association with widespread orogenesis and magmatism. During the Carboniferous, in a major orogenic event which in the Chinese literature is referred to as the Variscan Orogeny, the Mongolian Fold Belt was amalgamated to the North China Craton by subduction beneath its present northern margin along the Junggar-Hegen suture. This was followed by the amalgamated North China Craton colliding with the Siberian Craton by closure the Mongolo-Okhotsk ocean (Davis et al., 1998). During the Indosinian Orogeny (Triassic), the Yangtze Craton is considered to have been subducted northward under the southern margin of the North China Craton along the diamond- and coesite-bearing, Kunlun-Qinling-Dabie-Su-Lu ultra-high pressure metamorphic belt (Li et al., 1993; Miller et al., 1998). During the Yanshanian orogenic event (Jurassic to Cretaceous), the Pacific plate was obliquely subducted westward

beneath the North China and Yangtze cratons as well as the whole Eurasia continent (Zhu, 1998). The present plate tectonic setting is shown in Fig. 7.1.

During the Variscan or Indosinian collisional events, lithospheric roots would likely have formed along the northern and southern margins of the North China Craton. Subsequent delamination of these roots would cause rapid uplift of the overlying crust due to the isostatic response of removing relatively dense (cold) lithosphere and replacing it with less dense (hot) asthenosphere. This leads to plutonism, extensional collapse and ultimately crustal thinning (e.g. Nelson, 1992). There are two important consequences of crustal thinning. One is that the deep ductile shears were correspondingly uplifted into the shallow part of the crust and overprinted by brittle components. Another is that the fluid from deep-seated sources in the lower crust and/or upper mantle can relatively easily migrate upwards. The environment related to both these consequences would be favourable for formation of gold deposits originating from deep-seated sources. Some Variscan-aged gold deposits occur along the northern margin of the North China Craton (Miller et al., 1998). During the Yanshanian orogenic event (especially the Early Cretaceous), intensive interaction between the Pacific Plate and the Eurasian Continent resulted in a major tectono-magmatic pulse in east China, including the North China Craton. A consequence of this event was the development of major NNE-trending, intracratonic transcurrent fault zones generated on the inner side of the Eurasia continental margin (Xu and Zhu, 1994). Among them, the Tan-Lu Fault Zone extends from the Yangtze Craton into southeastern Russia and is spatially associated with gold occurrences and deposits along much of its length. These include deposits of the Jiaodong and Liaodong Peninsulas and the Sikhote-Alin Fold Belt of the Russian Far East (Miller et al., 1998). Additionally, many pre-existing E-W trending deep fault systems at the margins of the North China Craton, such as the Junggar-Hegen Fault Zone along its northern border, were rejuvenated during this period (Miller et al., 1998). Therefore, it is assumed, based on the favourable tectonic setting along the borders of the North China Craton caused by Variscan or Indosinian Orogenies, that the Yanshanian Orogeny further contributed to establishing a more favourable tectonic niche where numerous Yanshanian gold deposits were generated, possibly involving superimposition and reconcentration of metallic elements from pre-existing proto-ores. Most gold deposits distributed along the borders of the North China Craton formed during the Yanshanian orogenic event (Zhai and Deng, 1996).

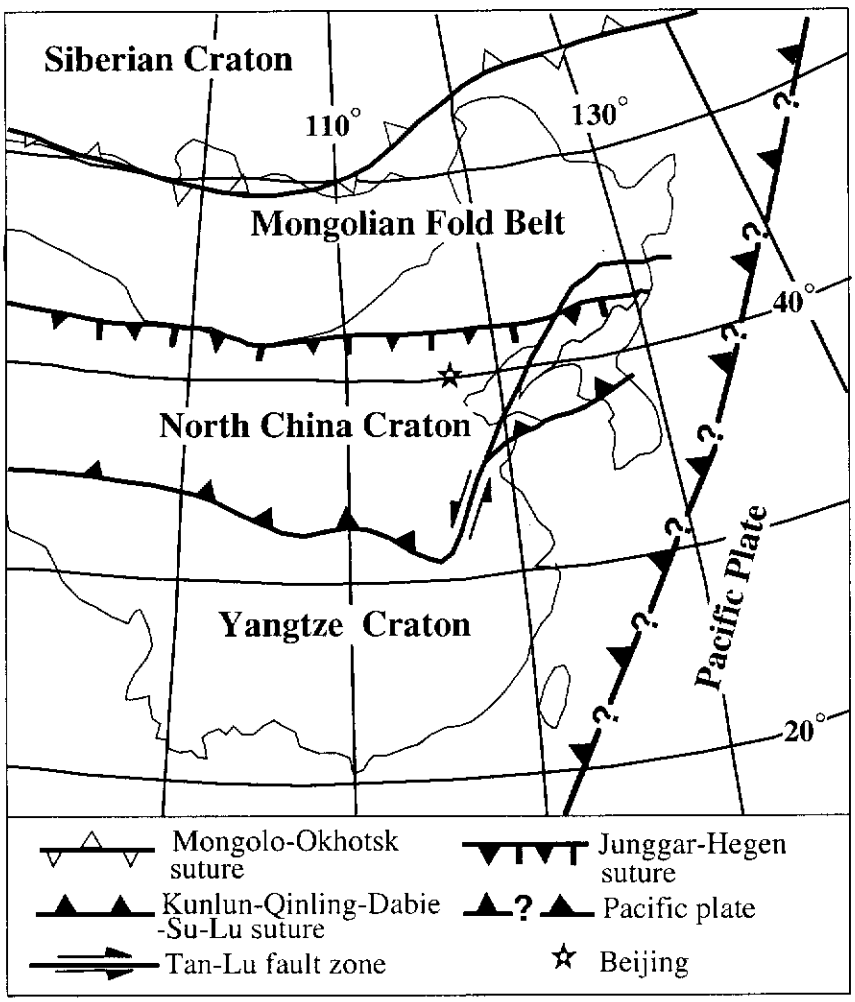

Fig. 7.1: Sketch map of present plate tectonics of China (modified from Davis et al. 1998).

Miller et al. (1998) pointed out that multiple orogenic events and associated magmatic activity, along with crustal scale structures at terrane and craton sutures, provide a metallogenic scenario for gold deposits along the margins of the North China Craton. For example, Jiaobei Terrane of the Jiaodong Peninsula, which is located along the southeast border of the North China Craton, was subjected to both the Indosinian and Yanshanian Orogenies during the Phanerozoic. Its unique tectonic setting may explain why large gold deposits are formed in this area. Miller et al. (1998) considered that the whole of the north China Phaneozoic gold deposits best fit into the orogenic or "mesothermal" type (as defined by Groves et al., 1998).

7.2 Structural Controls on Gold Mineralization

All hydrothermal ore deposits, including gold deposits, require the transport of large quantities of relatively insoluble metals in solution as complexes from a source region to the site of deposition. Therefore, fault zones are the most likely conduits for this transport and are the principal controls on mineralization. Lode gold deposits are associated with, or proximal to, first-order transcrustal, generally terrane-bounding structures. However, they are rarely situated within these first-order structures, instead are hosted in second- or higher-order splays off the main faults (Wyman and Kerrich, 1988; Kerrich and Wyman, 1990; Groves and Foster. 1991; McCuaig and Kerrich, 1998). Keays and Skinner (1988) considered that the first-order structures might have served as conduits for gold-bearing fluids derived from the lower crust and upper mantle.

The Tan-Lu Fault Zone is a major lithospheric fracture that extends for about 5000 km through the eastern part of China and into Russia (Xu et al., 1987). This first-order fault zone has been proposed as a major fluid pathway for gold mineralization (Cai, 1993; Ren et al., 1997). Regional NNE- to NE-trending fault zones, including the San-Cang, Huang-Ye, Zhao-Ping, Majiayao and Jinniushan Fault Zones within the Jiaodong Peninsula and the Yalujiang Fault Zone within the Liaodong Peninsula, are well-developed. The development of these fault zones is intimately related to the tectonic evolution of the region and they may represent deep ductile shear zones superimposed by later brittle components during crustal uplift, caused by collision and accretion along the margins of the Eurasian and Pacific Plates during the Mesozoic. These fault zones are considered to be subsidiary structures of the Tan-Lu Fault Zone (Fig. 2.1) (Xu et al., 1987; Cai, 1993; Ren et al., 1997) and spatially control the distribution of gold deposits within both the Jiaodong and Liaodong Peninsulas.

7.3 Two Types of Gold Mineralization

The Jiaojia-style (disseminated-and-veinlet type) and Linglong-style (vein-filling type) gold deposits are widely recognized in the border areas of the North China Craton. The Jiaojia-style deposits are controlled by regional fault zones, and commonly develop at lithologic contacts along the fault zones rather than within single rock units (Chapter 3). This deposit style forms where auriferous fluid disseminates within host rock and, more importantly, fills the microfractures of wall rock forming quartz or sulphide veinlets (Chapter 3). The orebodies are generally parallel to the regional fault zones and are located 0-50 m below the main fault planes (e.g. the Cangshang and Sanshandao gold deposits). The orebodies are tabular in shape with a length of more than 1000 m, and locally branch or merge along the strike and/or dip direction. The orebodies lack sharp boundaries with the host rock and they are only distinguished by cut-off grades. The gold reserves of the Jiaojia-style deposits are classified as large, ranging from ten to more than one hundred tonnes, and with grades of 4-5 grams per tonne (e.g. Zhang and Wen, 1983).

The Linglong-style deposits are controlled by the second- or higher-order faults of the regional fault zones, and form where auriferous fluids filled large fractures developed in competent host rock (Chapter 3). The orebodies of the Linglong-style are delimited by the faults. The boundary between orebodies and host rock is distinct and can be easily identified in the field. The preferred sites of these orebodies include: (a) flexures of faults along strike (refer to Fig. 3.17); (b) positions where the dip angle changes (refer to Fig. 3.18); (c) fault intersections (refer to Fig. 3.33); and (d) tension gashes created by fault movement (refer to Fig. 6.2). The Linglong-style tends to produce small gold deposits of only a few tonnes, but with an average grade of more than 10 grams per tonne (e.g. Lü and Kong, 1993).

7.4 The SHRIMP zircon U-Pb ages of the host rocks

Typical late Archaean orogenic lode-gold deposits mostly occur in greenstone belts (Groves et al., 1998), whereas Phanerozoic synorogenic gold lodes of the Pacific Rim are predominantly hosted by oceanic sedimentary rocks (Goldfarb et al., 1998). The gold deposits in the Jiaodong and Liaodong Peninsulas are mainly hosted by Mesozoic granitoids, but also in other lithologies including late Archaean metamorphic rocks, early Proterozoic metasedimentary rocks and Mesozoic sedimentary rocks (Qiu et al., 2002 ; Ren, 1988; Yang and Lü, 1996, Yang, 1997). However, it is structural

setting, and not lithology, that is the important controlling factor. Precise dating of the host

Table 7.1: The SHRIMP U-Pb zircon ages of the host rocks of investigated gold deposits

Location	Rock Types	Age (Ma)	Sample No.
Footwall of the Cangshang Gold Deposit, the Zhao-Ye Gold Belt, Jiaodong Peninsula	Granodiorite	166 ± 4	C1
Hanging wall of the Cangshang Gold Deposit, the Zhao-Ye Gold Belt, Jiaodong Peninsula	Amphibolite	1852 ± 37	C4
Wallrock of the Sanshandao Gold Deposit, the Zhao-Ye Gold Belt, Jiaodong Peninsula	Granodiorite	128 ± 2	*SSD-15
Footwall of the Wangershan Gold Deposit, the Zhao-Ye Gold Belt, Jiaodong Peninsula	Monzogranite	156 ± 3	W1
Hanging wall of the Wangershan Gold Deposit, the Zhao-Ye Gold Belt, Jiaodong Peninsula	Cataclastic granite	156 ± 7	W4
Host rock of the Linglong Goldfield, the Zhao-Ye Gold Belt, Jiaodong Peninsula	Porphyritic granodiorite	153 ± 4	*LD-20
Host rock of the Linglong Goldfield, the Zhao-Ye Gold Belt, Jiaodong Peninsula	Medium-grained granite	158 ± 4	*LX-13
Host rock of the Daliuhang Gold Deposit, the Qi-Peng Gold Belt, Jiaodong Peninsula	Granodiorite	128 ± 3	DL4
Host rock of the Denggezhuang Gold Deposit, the Mu-Ru Gold Belt, Jiaodong Peninsula	Monzogranite	154 ± 5	DG5-1
Host rock of the Jinqingding Gold Deposit, the Mu-Ru Gold Belt, Jiaodong Peninsula	Monzogranite	157 ± 4	JQ6
Host rock of the Wulong Gold Deposit, Liaodong Peninsula	Syenogranite	162 ± 8	WL11-19
Host rock of the Sidaogou Gold Deposit, Liaodong Peninsula	Metasandstone	1886 ± 16	SD4-1

(*: means the samples were analyzed by Wang et al., 1998)

rocks is important, because it can provide reliable indirect age constraints on the gold mineralization. The SHRIMP U-Pb zircon ages of the host rocks of the investigated deposits are listed in Table 7.1 and shown in Fig. 7.2, and range in age from 1852 ± 37 Ma to 128 ± 3 Ma in the Jiadong Peninsula, and from 1886 ± 16 Ma to 162 ± 8 Ma in the Liaodong Peninsula.

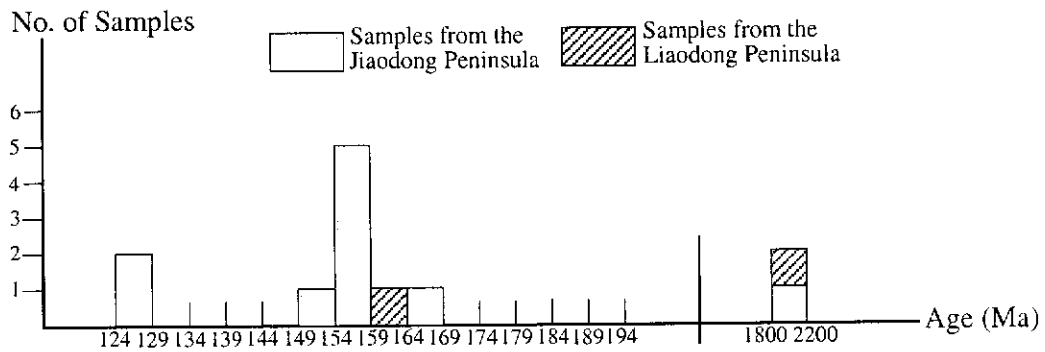

Fig. 7.2: Histogram of ages of the host rocks in this study.

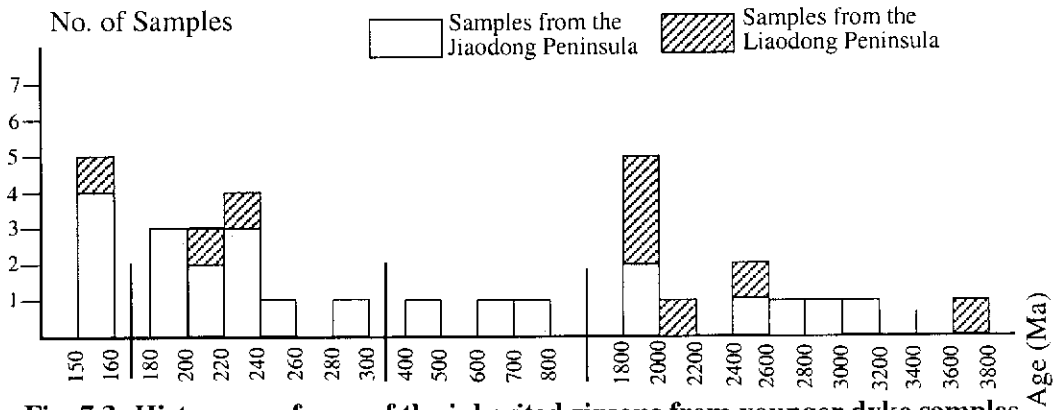

Fig. 7.3: Histogram of ages of the inherited zircons from younger dyke samples (ca. 120Ma) in this study.

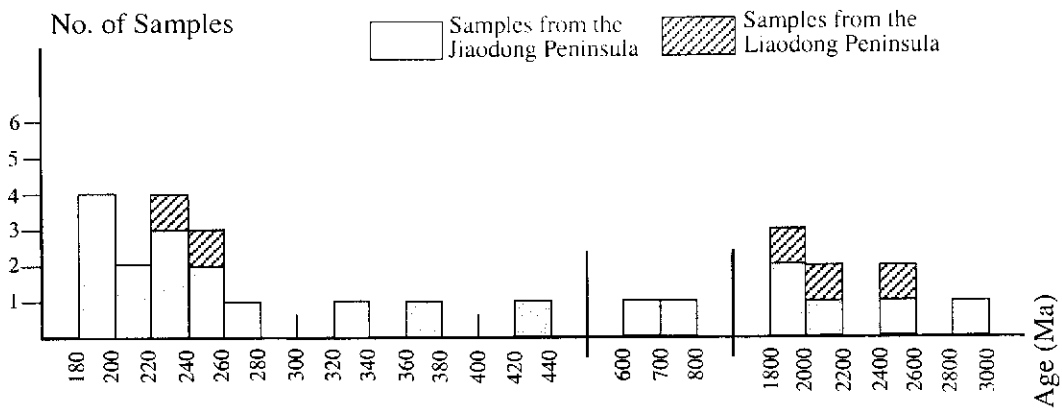

Fig. 7.4: Histogram of ages of the inherited zircons from granitoid samples (150-165 Ma) in this study.

The youngest host rocks within the Zhao-Ye and Qi-Peng Gold Belts of the Jiaodong Peninsula are granodiorite, with an age of ca. 128 Ma (Samples SSD-15 and DL4) (Table 7.1 and Fig. 7.2). The youngest host rocks in the Mu-Ru Gold Belt of the Jiaodong Peninsula are Cretaceous (ca. 130 Ma) Laiyang Formation (Penjiakuang Gold Deposit, Chapter 5 of this thesis). In the Liaodong Peninsula, no such young host rocks of gold deposits have been found so far. The most common host rocks of the gold deposits within the Jiaodong and Liaodong Peninsulas are granitoids, with ages ranging from 150 to 165 Ma (such as Samples C1, W1, LX-13, DG5-1, JQ6 and WL11-19) (Table 7.1), which are indicated in Fig. 7.2. In this thesis, the oldest dated host rocks of gold deposits in the Jiaodong Peninsula is amphibolite (Sample C4) with a metamorphic zircon age of 1852 ± 37 Ma (Table 7.1); in the Liaodong Peninsula, the oldest host rock is metasandstone (Sample SD4-1) with a youngest detrital zircon age of 1886 ± 16 Ma (Table 7.1).

7.5 The Crustal History and Tectonic Evolution of the Jiaodong and Liaodong Peninsulas

Based on SHRIMP U-Pb zircon dating, the Jiaodong and Liaodong Peninsulas have a similar crustal history and tectonic evolution. In this study, the oldest inherited zircons in the Liaodong Peninsula yield an age of 3717 ± 5 Ma (Figs. 6.12 and 7.3). Wang et al.(1998) reported that the oldest inherited zircons in the Jiaodong Peninsula give an age of 3446 ± 2 Ma. These results indicate that the Jiaodong and Liaodong Peninsulas are underlain by Precambrian basement with components up to ca. 3700 Ma old. This coincides with some earlier SHRIMP zircon U-Pb ages which suggests that remnant sialic crust up to ca. 3800 Ma old forms the basement to parts of the North China Craton (e.g. Liu et al., 1992). In the two peninsulas, there are three main generations of inherited zircons, which yield Late Archaean (ca. 2500 Ma), Palaeoproterozoic (1800-2200 Ma) and Early Mesozoic (ca. 200-250 Ma) ages (Table 7.2; Figs. 3 and 4). The Late Archaean zircons are euhedral grains of igneous origin, indicating Late Archaean magmatism in the basement rocks of the two peninsulas, an event which has been widely recognized within the North China Craton (i.e. Wutai Orogeny-see, Zhao, 2000). The Palaeoproterozoic zircons occur either as metamorphic zircon overgrowths surrounding inherited Late Archaean igneous cores, or as individual metamorphic or igneous zircons. Their ages are broadly consistent with the Lüliang Orogeny, which is a craton-wide tectono-thermal event at ca. 1800 Ma within the North China Craton (e.g. Wang and Mo, 1995). The Early Mesozoic zircons occur in three forms, which are inherited igneous cores surrounded by younger zircon rims; zircon overgrowths surrounding inherited cores with Precambrian ages; and individual

Table 7.2: Main group ages of all analyzed samples in this study

Samples from the Gold Deposits within the Jiaodong Peninsula		Samples from the Gold Deposits within the Liaodong Peninsula	
Sample Name (No.)	**Main Group Ages (Ma)**	**Sample No. (Name)**	**Main Group Ages (Ma)**
Linglong granodiorite (C1)	Group 1: 166 ± 4; Group 2: 244 ± 11	Microdiorite dyke (WL11-3)	A main group: 119 ± 6
Ore (C3)	A main group: 154 ± 5		
Amphibolite (C4)	Group 1: 1852 ± 37 Group 2: 2530 ± 17	Foliated microdiorite dyke (WL11-8)	A main group: 124 ± 3
Guojialing granodiorite (*SSD-15)	A main group: 128 ± 2		
Basaltic dyke (JJ1)	A main group: 156 ± 6		
Linglong monzogranite (W1)	A main group: 156 ± 3	Wulong syenogranite (WL11-19)	Group 1: 231 ± 25 Group 2: 162 ± 8
Ore (W2)	Group 1: 158 ± 4 Group 2: 191 ± 7		
Granitic cataclasite (W4)	Group 1: 156 ± 7 Group 2: 224 ± 12	Microdiorite dyke (WL11-26)	Group 1: 127 ± 3 Group 2: 119 ± 4
Mafic dyke (XS1)	Group 1: 119 ± 5 Group 2: 142 ± 16		
Intermediate dyke (YLB1)	No group ages, scattered from 111 ± 2 to 1852 ± 13	Sanguliu monzogranite (SG-1)	A main group: 125 ± 3 :
Porphyry (*LX-53)	A main group: 120 ± 2		
Linglong porphyritic granodiorite (*LD-20)	A main group: 153 ± 4	Metasandstone (SD4-1)	A main group: 2192 ± 24
Linglong medium-grained granite (*LX-13)	A main group: 158 ± 4	Mineralized metasandstone (SD4-7)	Group 1: 3356 ± 1 Group 2: 2582 ± 3 Group 3: 2507 ± 8
Vogesite dyke (MJ1)	Group 1: 222 ± 16 Group 2: 162 ± 10		
Guojialing granodiorite (DL4)	A main group: 128 ± 3	Porphyrite dyke (BY6-3)	A main group 168 ± 4
Microdiorite dyke (DL5)	A main group: 121 ± 4		
Altered dyke (PJ1)	A main group: 1858 ± 13		
Kunyushan monzogranite (DG5-1)	A main group: 154 ± 5		
Intermediate dyke (DG5-3)	Group 1: 184 ± 10 Group 2: 150 ± 9 Group 3: 134 ± 5		
Kunyushan monzogranite (JQ6)	A main group: 157 ± 4		

(*:samples analyzed by Wang et al., 1998)

euhedral zircons. These inherited zircons (ca. 200-250 Ma) most likely formed during a magmatic event, which was in response to the collision of the North China and Yangtze Cratons (i.e. Indosinian Orogeny). During this collisional event, the Precambrian basement was reworked by high grade metamorphism and partial melting (Wang et al., 1998) to produce an earlier suite of granitoids (ca. 200-250 Ma), as recorded in the Jiaodong and Liaodong Peninsulas (Xu et al., 1989; F. Y. Wu, personal communication, 1999).

Besides these inherited zircons, rocks with igneous crystallization ages range from 165-119 Ma in age which corresponds to the Yanshanian Orogeny. One main zircon population of an igneous origin, was dated at ca. 165-150 Ma (Table 7.2 and Fig. 7.5). This age represents another major phase of crustal reworking in the Jiaodong and Liaodong Peninsulas. The granitoids, with an age of ca. 165-150 Ma, include the Linglong, Kunyushan and Wulong granitoids. They were derived from Early Mesozoic basement (Wang et al., 1998), indicated by the presence of inherited zircons with ages of ca. 200-250 Ma. The emplacement of these granitoids probably marked the final stage of the collision involving the North China and Yangtze Cratons (e.g. Wang et al., 1998; Zhou and Lü, 2000).

Another major igneous zircon population was dated at ca. 130-119 Ma (Table 7.2 and Fig. 7.5). This age represents the last phase of magmatic activity in the Jiaodong and Liaodong Peninsulas, which is marked by the emplacement of the Guojialing and Sanguliu granitoids and younger dykes. This magmatic activity is attributed to the distal influence of subduction of the Palaeo-Pacific Plate underneath the Eurasian Continent, which belongs to the Yanshanian Orogeny (Zhou and Lü, 2000).

7.6 The Age of Gold Mineralization in the Jiaodong and Liaodong Peninsulas

The timing of gold mineralization in the Jiaodong Peninsula is highly controversial and has been inferred to be Proterozoic (e.g. Yang and Lü, 1996), Mesozoic (e.g. Luo and Wu, 1987; Wang et al., 1998; Zhai et al., 1998) and Cenozoic (e.g. Zhang et al., 1994) by different workers. Similarly, the timing of gold mineralization in the Liaodong Peninsula has variously been inferred to be Archaean (e.g. Yang, 1997), Proterozoic (e.g. Ni and Xu, 1993) or Mesozoic (e.g. Ren, 1988) in age. Constraining the age of mineralization in these two areas has been the key objective of this thesis. This has been achieved primarily by SHRIMP U-Pb zircon dating, along with limited Ar-Ar dating of sericite associated with mineralization.

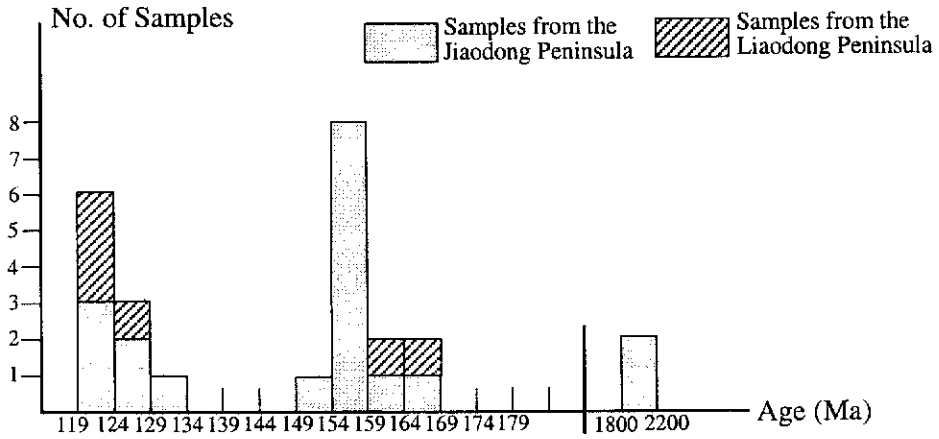

Fig. 7.5: Histogram showing emplacement ages of all analyzed samples in this study. A metamorphic age of ca. 1800 Ma (sample C4) is included.

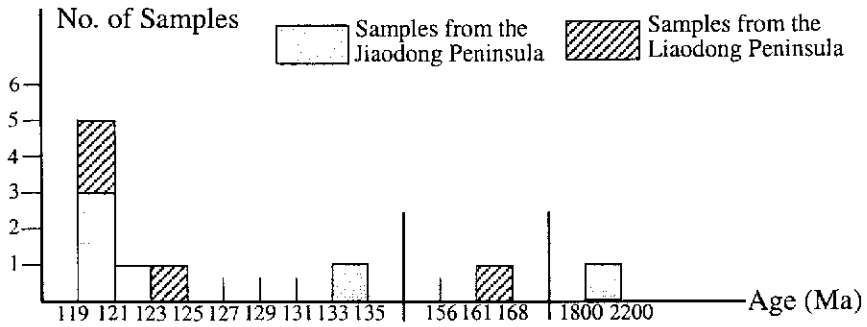

Fig. 7.6: Histogram of ages of the dykes in this study.

Reliable geochronological data have been obtained from thirteen investigated gold deposits within the Jiaodong and Liaodong Peninsulas.

7.6.1 The SHRIMP zircon U-Pb age of dykes associated with gold deposits

In a number of goldfields around the world from Archaean to Tertiary in age, coeval and cospatial associations between lamprophyres and mesothermal gold deposits have been noted (Rock and Groves, 1988; Rock et al., 1989; Wyman and Kerrich, 1989; Kerrich and Wyman, 1994; Taylor et al, 1994). Lamprophyres and other mafic dykes, such as dolerite, may coexist in a swarm (Yao et al., 1990; Mikhalsky and Skeraton, 1993) probably derived from the same (or a very similar) enriched lithospheric mantle source region, with any compositional variations due to different degrees of partial melting (Mikhalsky and Skeraton, 1993). Lamprophyre may also represent parent magmas to some of acidic dykes in the same dyke swarm which ranges from mafic end-members through intermediate to acidic porphyries (Macdonald et al., 1986; Rock et al., 1988; Perring et al., 1989; Rock et al., 1989).

A common characteristic of the Jiaodong and Liaodong gold deposits is that these deposits are all closely associated with dykes. For example, the Linglong Goldfield of the Jiaodong Peninsula has an average density of ten dykes per square kilometre (Yao et al., 1990) and a swarm of dykes is well exposed both on the surface and in underground workings of the Wulong Gold Deposit in the Liaodong Peninsula. The close spatial and temporal relationships between dykes and gold mineralization has recently been recognized in China (Yao et al., 1990; Trumbull et al., 1996; Wang et al., 1998).

Based on the cross-cutting relationship between dykes and gold lodes (and the alteration style of dykes), three types of dykes are recognized in the study area of this thesis: pre-, syn- and post-mineralization dykes. 1) Pre-mineralization dykes are commonly either cut by gold lodes and/or altered by the mineralization (e.g. sample WL11-8 in the Wulong Gold Deposit), although some occupy the same structure as later gold lodes. 2) Syn-mineralization dykes cut the gold lodes but are also altered during mineralization, such as sample XS1 in the Linglong Goldfield. Alternatively, the dyke occupies the same structure as the gold lode and is altered, such as sample YLB1 in the Linglong Goldfield and samples WL11-3 and WL11-26 in the Wulong Gold Deposit. 3) Post-mineralization dykes, in which the dyke cuts gold lodes and is unaltered or unmineralized, such as sample LX-53 in the Linglong Goldfield.

Table 7.3: The SHRIMP U-Pb zircon ages of dykes distributed within some of the investigated gold deposits

Dyke types and Locations	Rock Types	Age (Ma)	Sample No.
Pre-mineralization dyke, cutted by other dykes and orebodies in the Wulong Gold Deposit, Liaodong Peninsula	Foliated microdiorite dyke	124 ± 3	WL11-8
Syn-mineralization dyke, cutting one orebody in the Linglong Goldfield, the Zhao-Ye Gold Belt, Jiaodong Peninsula	Altered lamprophyre dyke	119 ± 5	XS1
Syn-mineralization dyke, occupying the same structure as one orebody in the Wulong Gold Deposit, Liaodong Peninsula	Undeformed microdiorite dyke	119 ± 6	WL11-3
Syn-mineralization dyke, occupying the same structure as one orebody in the Wulong Gold Deposit, Liaodong Peninsula	Undeformed microdiorite dyke	119 ± 4	WL11-26
Syn-mineralization dyke, cutting the No. 2 orebody in the Jiaojia Gold Deposit, the Zhao-Ye Gold Belt, Jiaodong Peninsula	altered basaltic dyke	156 ± 6 (not a real dyke age)	JJ1
Dyke, occupying the same structure as one orebody in the Pengjiakuang Gold Deposit, the Mu-Ru Gold Belt of the Jiaodong Peninsula	Altered dyke	1858 ± 13	PJ1
Dyke, occupying the same structure as one orebody in the Baiyun Gold Deposit, the Liaodong Peninsula	Altered porphyrite dyke	168 ± 4	BY6-3
Syn-mineralization dyke, occupying the same structure as the No.108 lode in the Linglong Goldfield, the Zhao-Ye Gold Belt, Jiaodong Peninsula	Microdiorite dyke	122 ± 2	YLB1
Dyke, occupying the same structure as one orebody in the Denggezhuang Gold Deposit, the Mu-Ru Gold Belt, Jiaodong Peninsula	Altered dyke	134 ± 5	DG5-3
Post or syn-mineralization dyke, cutting the No. VI lode in the Daliuhang Gold Deposit, the Qi-Peng Gold Belt, Jiaodong Peninsula	Microdiorite dyke	121 ± 4	DL5
Post-mineralization dyke, cutting the No.1 orebody in the Majiayao Gold Deposit, the Qi-Peng Gold Belt, Jiaodong Peninsula	Vogesite dyke	162 ± 10 (not a real dyke age)	MJ1
Post-mineralization dyke, cutting one orebody in the Linglong Goldfield, the Zhao-Ye Gold Belt, Jiaodong Peninsula	Feldspar porphyry dyke	120 ± 2	*LX-53

(*:samples analyzed by Wang et al., 1998)

This study attempts to constrain the age of gold mineralization by SHRIMP dating of such dykes. Lots of dyke samples associated with gold mineralization were collected in the field, but only a few samples have found to contain enough zircons for SHRIMP U-Pb dating. For example, samples CD19-1 (Cangshang Gold Deposit), JQ1 (Jingqingding Gold Deposit), WL11-15 (Wulong Gold Deposit) and SD5-3 (Sidaogou Gold Deposit) contained insufficient zircons for SHRIMP analysis. The dyke ages obtained using SHRIMP are listed in Table 7.3 and shown in Fig. 7.6.

Only one pre-mineralization dyke (sample WL11-8 in the Wulong Gold Deposit) was identified and dated by SHRIMP. It yields an age of 124 ± 3 Ma (Table 7.3), which coincides with the age of the Sanguliu Pluton (125 ± 3 Ma) adjacent to the Wulong Gold Deposit (see Chapter 6 of the thesis). Therefore, the age of ca. 124 Ma represents a magmatic event pre-dating the gold mineralization.

Generally speaking, the dykes synchronous with gold mineralization (such as samples XS1 and YLB1 in the Linglong Goldfield, WL11-3 and WL11-26 in the Wulong Gold Deposit) yield an age of ca. 122-119 Ma (Table 7.3), which can be interpreted to be the time of gold mineralization. However, some syn-mineralization dyke samples do not yield reasonable ages for the time of gold mineralization. This is because no euhedral zircons crystallized during dyke intrusion and instead all zircons are inherited. For example, sample JJ1 in the Jiaojia Gold Deposit, with an age of 156 ± 6 Ma (Table 7.3) (see interpretation in Chapter 3 of the thesis). Some dykes occupied the same structure as gold lodes and were themselves altered, but they cannot be identified as syn-mineralization dykes based on their SHRIMP U-Pb zircon ages. For example, sample PJ1 in the Pengjiakuang Gold Deposit yields an age of 1858 ± 13 Ma (Table 7.3), which is much older than the age of the hanging wall sequence (Cretaceous Laiyang Formation) in this deposit, hence, it cannot indicate the timing of gold mineralization, but represents a Palaeoproterozoic dyke event. The fractures intruded by the old dyke were most likely reactivated during later gold mineralization and so occupied by gold lodes. Other examples are samples DG5-3 and BY6-3, yielding ages of 134 ± 5 Ma and 168 ± 4 Ma, respectively (Table 7.3) (see interpretation in Chapters 5 and 6 of the thesis).

The SHRIMP zircon U-Pb ages of post-mineralization dykes were difficult to obtain. Since no fresh dyke samples were available, a strongly weathered sample (DL5) from the Daliuhang Gold Deposit was selected, but it cannot be exactly identified as post- or syn-mineralization. It yields an age of 121 ± 4 Ma (Table 7.3), which coincides with the age of gold mineralization (ca. 119 Ma) determined from the

syn-mineralization dykes (samples XS1, WL11-3 and WL11-26). Some post-mineralization dyke samples do not yield reasonable ages for providing the minimum constraint on the timing of gold mineralization, since no zircons crystallized during dyke intrusion, such as sample MJ1 in the Majiayao Gold Deposit, with an age 162 ± 10 Ma (Table 7.3) (see interpretation in Chapter 3 of the thesis). Sample LX-53 collected and SHRIMP dated by Wang et al. (1998) is taken to be a post-mineralization dyke sample with an age of 120 ± 2 Ma (Table 7.3). This age is also coincident with the age of gold mineralization (ca. 122-119 Ma), but there is no detailed description of the sample location, so it is unsure whether this is a syn- or post-mineralization dyke. Further work is needed for dating the dykes which post-date the gold mineralization in the Jiaodong and Liaodong Peninsulas.

7.6.2 The SHRIMP dating of zircons extracted from gold ores

Zircon is highly stable in most environments. however, zirconium mobility has been observed in environments where hydrothermal zircons can be formed (e.g. Kerrich and King, 1993; Nesbitt et al., 1999). Yeats et al. (1996), and Nesbitt et al. (1999) reported that hydrothermal zircons which were generated during the alteration process have been separated from some ore zones. The hydrothermal zircons from auriferous veins in the Abitibi greenstone belt was dated by SHRIMP (Claoué-long et al., 1990) to directly constrain the timing of gold mineralization. Also, Yeats et al. (1996) dated hydrothermal zircons from ore zones in Yilgarn greenstone belts using SHRIMP. Based on the possibility that hydrothermal zircons may be present in the ore, samples C3 (Cangshang Gold Deposit), W2 (Wangershan Gold Deposit) and SD4-7 (Sidaogou Gold Deposit) were selected for SHRIMP zircon dating. Their ages are listed in Table 7.4.

Table 7.4: The SHRIMP U-Pb dating of zircons extracted from ore zones of some investigated gold deposits

Location	Rock Types	Age (Ma)	Sample No.
the No. 1 orebody in the Cangshang Gold Deposit, the Zhao-Ye Gold Belt, Jiaodong Peninsula	Altered granitic cataclasite	154 ± 5	C3
the No.1 orebody in the Wangershan Gold Deposit, the Zhao-Ye Gold Belt, Jiaodong Peninsula	Sericite-quartz rock	158 ± 4	W2
One disseminated orebody in the Sidaogou Gold Deposit, Liaoning Peninsula	Mineralised metasandstone	2507 ± 8	SD4-7

Unfortunately, no true hydrothermal zircons were extracted from these ores. Zircons separated from sample C3 show oscillatory zonation patterns under cathodoluminescence, which suggests the age of 154 ± 5 Ma may represent a dyke emplaced along the No.1 ore zone after intrusion of the footwall granodiorite at 166 ± 4 Ma. Zircons separated from sample W2 are euhedral grains of an igneous origin, and the age of 158 ± 4 Ma coincides, within error, with the age of 156 ± 3 Ma obtained from the host monzogranite. Zircon grains extracted from sample SD4-7 are detrital in origin. Their ages range from 3357 ± 4 Ma to 2087 ± 5 Ma (Table 6.2). The main group age is 2507 ± 8 Ma, coincident with the age of a magmatic event (ca. 2500 Ma) widely recognized throughout the North China Craton (e.g. Song et al., 1996). The attempt to separate hydrothermal zircons from the ores was therefore unsuccessful, which indicates that either hydrothermal zircons do not exist in these ores or that further detailed work is needed.

7.6.3 The Ar-Ar dating of sericites associated with gold mineralization

White mica is a common hydrothermal mineral in gold deposits. Therefore, ^{40}Ar-^{39}Ar dating of this mica is a useful technique for determining the timing of gold mineralization. In order to precisely constrain the age of gold mineralization at the Cangshang Gold Deposit, hydrothermal white micas from sample CD8-2 from the No.1 orebody of this deposit were analysed by the ^{40}Ar-^{39}Ar technique, which yields a well-defined ^{40}Ar-^{39}Ar age of 121.3 ± 0.2 Ma. This age is interpreted as the time of gold mineralization at the Cangshang Deposit. To the author's knowledge, this is the first time that ^{40}Ar-^{39}Ar dating of muscovite has been used to determine the timing of gold mineralization in the Jiaodong Peninsula, as well as in China. Also, this ^{40}Ar-^{39}Ar age is consistent with the SHRIMP U-Pb age (ca. 122-119 Ma) of zircons from syn-mineralization dykes within the Jiaodong and Liaodong Peninsulas.

7.6.4 Summary of the Timing of Gold Mineralization in the Jiaodong and Liaodong Peninsulas

Based on the above SHRIMP U-Pb zircon ages and the ^{40}Ar-^{39}Ar dating of sericites, if there was a single gold mineralization event, then it occurred at ca. 122-119 Ma in the Jiaodong and Liaodong Peninsulas. In a recent study, Yang and Zhou (2001) using the Rb-Sr method on pyrite in gold-bearing quartz veins, directly dated the age of formation of the Linglong gold deposit in the northwestern Jiaodong Peninsula as 123-122 Ma. In addition, the ages of the host rocks and a post-mineralization porphyry dyke in the Linglong goldfield, determined by the SHRIMP

zircon U-Pb technique, constrained the age of gold mineralization at between 126 Ma and 120 Ma (Wang et al. 1998; Qiu et al. in press). Therefore, the age of gold mineralization determined in this thesis is consistent with these results. Yang et al. (2000) summarized the known Rb-Sr isochron ages and K-Ar ages of gold mineralization in the Zhao-Ye Gold Belt, Jiaodong Peninsula, and concluded that the gold mineralization event occurred at ca. 100-117 Ma; Zhang et al. (1993) determined the age of gold mineralization in Qi-Peng Gold Belt, Jiaodong Peninsula as ca. 106 Ma employing the Rb-Sr isochron method; Based on dating of sericite by K-Ar method and dating altered whole-rocks and sericite by Rb-Sr isochron method, Sun et al. (1995) and Zhai et al. (1996) obtained the timing of gold mineralization of Mu-Ru Gold Belt, Jiaodong Peninsula as ca. 101-105 Ma. If combined these Rb-Sr dating results and K-Ar ages, the gold mineralization event can extended to ca. 100 Ma. However, this has yet to be established and the balance of evidence favours gold mineralization as a single event at ca. 121 Ma.

7.7 Genesis for the Jiaodong and Liaodong Gold Deposits

7.7.1 Previous views

There is no consensus as to the genesis of the Jiaodong and Liaodong deposits in the Chinese literature. Traditionally, many genetic models have involved partial melting of the Archaean rocks (i.e. the source rock) to generate the Mesozoic granitoids, and subsequent derivation of gold mineralizing fluids from these granitoids (Zhang and Wen, 1983; Ren, 1988; Yao et al., 1988; Lü and Kong, 1993). Xu et al. (1989) highlighted that although the Guojialing granitoid suite in the Jiaodong Peninsula is closely related to the gold mineralization in time and space, they have no genetic relationship and the suite merely acts as the heat source for enhancing hydrothermal circulation. Peng et al. (1988) and Yang and Lü (1996) proposed that metamorphic fluids from as early as the late Archaean may have contributed to the formation of the Mesozoic Jiaodong and Liaodong deposits. Qiu et al. (2002) suggest that the Pb-isotope compositions of sulphides from gold deposits correlate with those of their host rocks, but the overlap of Pb-isotope compositions between hosting granitoids and ore does not necessarily indicate a genetic relationship between the two. Ni and Xu (1993) suggested that the genesis of Liaodong gold deposits was related to the subduction of the Palaeo-Pacific Plate beneath the Eurasian Plate. This view was shared by Lu et al. (1995) when they studied the genesis of the Jiaodong gold deposits. Wang et al. (1998) proposed that the gold deposits of the Jiaodong Peninsula

were possibly directly related to increased magmatism, further spreading, and increased compressional to transpressional tectonics as a result of Early Cretaceous plume activity occurring in the Palaeo-Pacific ocean.

The view that both the dykes and gold deposits in the Jiaodong and Liaodong Peninsulas originated from the same deep source has been proposed by some Chinese workers (Yao et al., 1990; Liu et al., 1991; Zhang et al., 1996), based on cospatial and coeval relationships between the dykes, especially the intermediate to mafic dykes (including lamprophyre), and gold lodes, as well as on common isotopic and REE features shared by these dykes and the gold ores. Wang et al. (1998) showed that the geological and isotopic characteristics of the gold deposits in the Jiaodong region are consistent with derivation of an ore fluid from deep-seated sources in the lower crust and/or mantle. Sun et al. (2000) suggested that under the Jiaodong Peninsula there is an enormous thermal domal structure related to a mantle plume, and this structure transfered gold-bearing materials from deep sources. This mantle plume model for the genesis of gold deposits has also been advocated by some other Chinese workers (Sun et al., 1995; Wang et al., 1998; Wang et al., 1999; Qü et al., 1999).

7.7.2 New Model

Based on this study, multiple orogenic events created a favourable tectonic environment for the Jiaodong and Liaodong gold deposits. During Phanerozoic orogenic events, the lithospheric root may easily delaminate (O'Reilly et al., 2001). After delaminating, the resulting "space" is replaced by hot upwelling asthenosphere. This provides a large input of heat into the crust (Schott and Schmeling, 1998). Qiu and Groves (1999) proposed that a widespread thermal anomaly associated with lithospheric delamination drove the giant crustal fluid circulation systems to produce the widespread gold mineralization in the Southwest Yilgarn Craton. The crustal thinning resulting from delamination also provides a favourable mineralization environment. Yang et al. (2002) suggested that the gold deposits along the margins of the North China Craton (NCC) were formed during large-scale delamination of NCC lithosphere. This tectonic-thermal event took place in the Late Jurassic to Early Cretaceous (160-110 Ma), although its mechanism is still not well understood (Menzies and Xu, 1998; Griffin et al., 1998; Gao et al., 2002; Wu et al., 2002). This model (Fig. 7.7) is supported by studies of granitoids with the characteristics of high Sr and low Y and the large-scale distribution of granitoids and volcanic rocks during the Late Jurassic to Early Cretaceous (160-120 Ma) in the NCC (Yang et al., 2002).

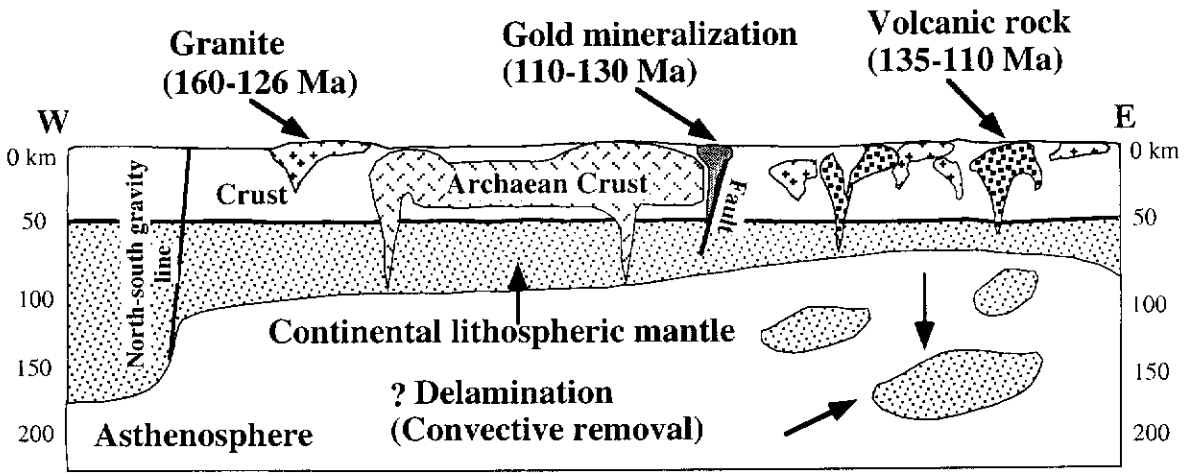

Fig. 7.7: The delamination model for gold mineralization in North China Craton (modified from Yang et al. 2002).

As the result of removal of lithospheric mantle and the resulting asthenospheric upwelling, mantle- and crust-related magmas were generated due to the increase of temperature. In addition, deep-seated fluids would be directed along major faults or suture zones and this activity may be accompanied by mineralization and subsequent uplift. It is suggested that delamination related to orogenic events probably occurred beneath the Jiaodong and Liaodong Peninsulas. The substantial heat and fluid transfer caused by delamination allowed auriferous fluids to be channelled along deep faults to favourable structures within the crust. This probably explains why the voluminous granitoid batholiths, lamprophyre and intermediate and/or mafic dykes are closely associated with gold lodes in both time and space.

REFERENCES

Ames. L., Tilton, G. R., and Zhou, G. Z., 1993. Timing of collision of the Sino-Korean and Yangtze cratons: U-Pb zircon dating of coesite-bearing eclogites. Geology, v. 21, p. 339-342.

Ames. L., Zhou, G. Z., and Xiong, B. C., 1996. Geochronology and isotopic character of ultrahigh-pressure metamorphism with implications for collision of the Sino-Korean and Yangtze cratons, central China. Tectonics, v. 15, p. 472-489.

An, J. T., Yu, D. B., Shen, K., Zhao, Z. G. and Zhang, Q. C., 1988. Study on the ore-controlling conditions of gold deposits in Muping-Rushan areas. Shandong Province. Regional Ore-forming Factors of Main Types of Gold Deposits in China. Vol. 5 Jiaodong region. p.1-45 (in Chinese with English abstract).

An, Y. H., 1990. Division of Metamorphic Stratigraphy in Jiaodong Region: Introducing Jiaodong and Jingshan Groups. Geology of Shandong Province, v.6, no.1, p.97-102 (in Chinese).

Bai, G. R., 1993. The characteristics of Jiaojia-type gold deposits and the classification of gold deposits within the Northwestern Jiaodong Peninsula. Gold, v. 14, no. 12, p. 7-10 (in Chinese with English Abstract).

Bai, J., 1993. Precambrian geology and Pb-Zn mineralization in the northern margin of the northern China platform. Beijing, Geological Publishing House, 132p (in Chinese with English abstract).

Barley, M. E., Eisenlohr, B. N., Grove, D. I., Perring, C. S. and Vearncombe, J. R., 1989. Late Archaean convergent margin tectonics and gold mineralization: A new look at the Norseman-Wiluna belt. Western Australia. Geology, v. 17, p. 826-829.

Bureau of Geology and Mineral Resources of Shadong Province, 1987. The reports of 1: 200,000 maps of No. J-50-(30) and J-51-(25) (in Chinese).

Bureau of Geology and Mineral Resources of Shandong Province, 1988. The report of 1: 50,000 map of No. J-51-98-B (in Chinese).

Bureau of Geology and Mineral Resources of Shandong Province. 1989. Summary of Mineral Resources of Shandong Province. pp.130. unpublished (in Chinese).

Bureau of Geology and Mineral Resources of Liaoning Province. 1989. Regional Geology of Liaoning Province. Beijing, Geological Publishing House, 560p. (in Chinese with English abstract).

Bureau of Geology and Mineral Resources of Shandong Province, 1991. Regional Geology of Shandong Province, China. Beijing, Geological Publishing House, 595p. (in Chinese with English abstract).

Bureau of Geology and Mineral Resources of Shandong Province, 1992. Geological outline of gold deposits in the Shandong Province. 154 p (in Chinese) unpublished.

Cai, X. P., 1993. Significance of the Tanlu fault zone on forming the concentrated area of gold deposits in the Jiaodong region. Geology of Shandong 9(2): 93-101 (in Chinese with English abstract).

Cao, G. Q., Wang, Z. B. and Zhang, C. J., 1990. Jiaonan terrane in Shandong province and the tectonic significance of the Wulian-Rongcheng fracture. Geology of Shandong, v.6, no.1, p.1-15 (in Chinese with English abstract).

Chang, N. H., 1996. The features of Jiaojia-type gold deposits: in Bureau of Geology and Mineral Resources of Shandong Province, ed., Research on geology and mineral resources of the Shandong Province, pp. 117-128 (in Chinese with English abstract).

Chappell, B. W., and White, A. J. R., 1974. Two contrasting granite types. Pacific Geology, v. 8, p. 173-174.

Chen, Y. S. and Li, D. X., 1989. Geology of Luoshan gold deposit. In: Gong, R. T. and Wang, Y. W. (Eds), Geology of gold deposits within Zhaoyuan region, p.83-103. Press of Industrial University of Jilin Province, Changchun City (in Chinese).

Claoué-Long, J. C., King, R. W. and Kerrich, R., 1990. Archaean hydrothermal zircon in the Abitibi greenstone belt: constraints on the timing of gold mineralization. Earth and Planetary Science Letters, v. 98, p. 109-128.

Compston, W., Williams, I. S. and Meyer, C., 1984. U-Pb geochronology of zircons from lunar breccia 73217 using a sensitive high-resolution ion microprobe. Journal of Geophysical Research, 89, B525-534.

Compston, W., Williams, I. S., Kirschivik, J. L., Zhang, Z. and Ma, G., 1992. Zircon U-Pb ages for the Early Cambrian time scale. Journal Geological Society of London, v. 149, p. 171-184.

Cui, W. Y., Wang, C. Q., Sun, C. Z. and Zhang, Y. Y., 1991. The zircon U-Pb ages of Archaean metamorphic rocks in western Liaoning Province-Chifeng area. Acta Scientiarum Naturalium Universitatis Pekinensis, v. 27, p. 229-239 (in Chinese with English abstract).

Cun, G., Yie, S. Y. and Wei, W. S., 1995. Brief introduction to gold resources in China. In: Gold Deposits in China: Advances and Consideration. edited by Zhang, Y. X. et al. Geological Publishing House, Beijing, 205p. (in Chinese with English summary).

Davis, G. A., Wang, C., Zheng, Y. D., Zhang, J. J., Zhang, C. H. and Gehrels, G. E., 1998. The enigmatic Yinshan fold-and-thrust belt of north China: New views on its intraplate contractional styles. Geology, v. 26, no. 1, p. 43-46.

Dunlap, W. J., Teyssier, C., McDougall, I. and Baldwin, S., 1991. Ages of deformation from K/Ar and $^{40}Ar/^{39}Ar$ dating of white micas. Geology, v. 19, p. 1213-1216.

Fu, D., 1989. Grade distribution and metallogeny of Jinqingqing gold deposit in Rushan region, Shandong Province. Review of Geology and Exploration, v. 4, no. 3, p. 87-95 (in Chinese with English abstract).

Gao, S., Rundnick, R. L., Carlson, R. W., McDonough, W. F. and Liu, Y. S., 2002. Re-Os evidence for replacement of ancient mantle lithosphere beneath the North China Craton. Earth Planet. Sci. Lett. v. 198, p. 307-322.

Gao, T. Z., Wei, G. Q., Wu, X. Y. and Yang, Y. G., 1998. An experimental study on metallogenetic tectono-geochemisrty of the quartz vein type gold deposits in Muping-Rushan gold metallogenic belt. Review of Geology and Exploration, v. 13, no. 1, p. 13-23 (in Chinese with English abstract).

Gong, R. T., 1989. Outline of gold deposits within Zhaoyuan region. In: Gong, R. T. and Wang, Y. W. (Eds), Geology of gold deposits within Zhaoyuan region, p.1-47. Press of Industrial University of Jilin Province, Changchun City (in Chinese).

Griffin, W. L., Zhang, A., O'Reilly, S. Y. and Ruan, C. G., 1998. Phanerozoic evolution of the lithosphere beneath the Sino-Korean Craton. In: Flower, M. F. J., Chung, S.-L., Lo, C.-H., Lee, T.-Y., eds. Mantle Dynamics and Plate Interactions in East Asia. American Geophysical Union Washington D. C., Geodynamics Series, v. 27, p. 107-126.

Groves, D. I. and Foster, R. P., 1991. Archaean lode gold deposits. In: Foster, R. P. (Ed.), Gold Metallogeny and Exploration. Blackie, pp. 63-103.

Groves, D. I., Goldfarb, R. J., Gebre-Mariam, M., Hagemann, S. G. and Robert, F., 1998. Orogenic gold deposits: A proposed classification in the context of their crustal distribution and relationship to other gold deposit types. Ore Geology Reviews, v. 13, p. 7-27.

Guo, W. K., 1987. Guide to the metallogenic map of endogenic ore deposits of China (1:4,000,000). Cartographic Publishing House, Beijing, 144p. (in Chinese and English summary).

Guo, Z. Y., Song, X. Z., He, X. P. and Zhai, Y. L., 1989. The ore-controlling structures, geochemical characteristics and exploration prospective in Jiaodong region. unpublished research report (in Chinese) in the Institute of Geology of Shandong Province, p. 238.

Han, Z. Z., Yuan, Q. L., Zhao, G. T. and Sheng, Q. T., 1993. Jiaodong — Lunan paired metamorphic belts and their geological significance. Geology of Shandong Province, v. 9, no.1, p. 18-30 (in Chinese with English abstract).

Heaman, L. M., Bowins, R. and Crocket, J., 1990. The Chemical composition of igneous zircon suites: Implications for geochemical tracer studies. Geochimica et Cosmochimica Acta, v. 54, p. 1597-1607.

Heaman, L. and Parrish, R., 1991. U-Pb Geochronology of Accessory Minerals. In: Heaman L., Ludden, J. N. (eds) M.A.C. Short course on "Applications of Radiogenic Isotope Systems to Problems in Geology". Mineralogical Association of Canada, Short Course Handbook, 19: 59-102.

Hodges, K. V., Hames, W. E. and Bowring, S. A., 1994. $^{40}Ar/^{39}Ar$ gradients in micas from high temperature-low-pressure metamorphic terrain: evidence for very slow cooling and implications for the interpretation of age spectra. Geology, v. 22, p. 55-58.

Hodgson, C. J., 1989. The structure of shear-related, vein-type gold deposits: a review. Ore Geology Review, v. 4, p. 231-273.

Hu, S., Wang, S. and Sang, H., 1987. Isotopic ages of the Linglong and Guojialing granitoid plutons and their geological implications. Journal of Petrology, no. 3, p. 83-89 (in Chinese with English abstract).

Ishihara, S., 1984. Granitoids series and Mo/W-Sn mineralization in East Asia: Report, Geological Survey of Japan, v. 263, p. 173-208.

Jia, W. C., 1995. Ore characteristics and genesis of Sanshandao Gold Deposit. Gold of Shandong Province, no.3-4, p. 21-23 (in Chinese).

Jiang, N., Xu, J. H. and Song, M. X., 1999. Fluid inclusion characteristics of mesothermal gold deposits in the Xiaoqinling district, Shanxi and Henan Provinces, People's Republic of China. Mineralium Deposita, v. 34, p. 150-162.

Ji, Z. Y., 1993. The new isotopic ages of Proterozoic metamorphic rocks in Jiaobei area and its geological implications. Geology of Shandong Province, v.9. No.1, p.43-51 (in Chinese).

Keays, R. R. and Skinner, B. J., 1989. Introduction. In: Keays, R. R., Ramsay, W. R. H. and Groves, D. I. (Eds), The geology of gold deposits: The perspective in 1988. Economic Geology Monograph, 6, p. 1-8.

Kennedy, A. K. and de Laeter J. R., 1994. The performance characteristics of the WA SHRIMP II ion microprobe. In: 8th International Conference on Geochronology, Cosmochronology and Isotope Geology. Berkeley. US Geological Survey Circular 1107, Abstracts, p.166.

Kent, A. J. R. and Hagemann, S. G., 1996. Constraints on the timing of lode-gold mineralisation in the Wiluna greenstone belt, Yilgarn Craton. Western Australia. Australian Journal of Earth Sciences, v. 43, p. 573-588.

Kent, A. J. R. and McDougall, I., 1995. $^{40}Ar/^{39}Ar$ and U-Pb Age constraints on the timing of gold mineralization in the Kalgoorlie Gold Field. Western Australia. Economic Geology, v. 50, p. 845-859.

Kerrich, R. and Wyman, D., 1990. Geodynamic setting of mesothermal gold deposits: An association with accretionary tectonic regimes. Geology, 18, p. 882-885.

Kerrich, R. and King. R., 1993. Hydrothermal zircon and beddeleyite in Val-d'Or Archaean mesothermal gold deposits: characteristics, composition and fluid inclusion properties with implications for timing of primary gold mineralization. Canadian Journal of Earth Science, v. 30, p. 2334-2351.

Kerrich, R. and Cassidy, K. F., 1994. Temporal relationships of lode-gold mineralization to accretion, magmatism, metamorphism and deformation, Archaean to present: A review. Ore Geology Reviews, v. 9, p. 263-310.

Kerrich, R. and Wyman, D. A., 1994. The mesothermal gold-lamprophyre association: significance for an accretionary geodynamic setting, supercontinent cycles, and metallogenic processes. Mineralogy and Petrology, v. 51, p. 147-172.

Kong, Q. C., 1989. Geology of Linglong goldfield. In: Gong, R. T. and Wang, Y. W. (Eds), Geology of gold deposits within Zhaoyuan region, p.48-82. Press of Industrial University of Jilin Province, Changchun City (in Chinese).

Kong, Q. C., Deng, Y. G., Hong, Y. and Song, Y. G., 1991. Structural controls on Linglong goldfield. In: State Bureau of Gold Resources (Ed), Research on geology of gold deposits within the Jiaodong Peninsula, p.152-159 (in Chinese).

Kröner, A., Cui, W. Y., Wang, S. Q., Wang, C. Q. and Nemchin, A. A., 1998. Single zircon ages from high-grade rocks of the Jianping Complex, Liaoning Province, NE China. Journal of Asian Earth Sciences. v. 16, nos. 5-6, p. 519-532.

Laizhou Gold Company, 1996. Geology map of gold deposits in Laizhou region. unpublished.

Lanyon, R., Black, L. P. and Seitz, H-M.,1993. U-Pb zircon dating of mafic dykes and its application to the Proterozoic geological history of the Vestfold Hills. East Antarctica. Contributions to Mineralogy and Petrology, v. 115, p. 184-203.

Li, J. Y., 1996. Geology and orebody characteristics of Sanshandao Gold Deposit. Gold of Shandong Province, no. 1, p. 1-5 (in Chinese).

Li, P. H., 2000. Geological characteristics and prospects of gold deposits within Northern Qixia-South Penglai area. Contributions to Geology and Mineral Resources Research, v. 15, no. 1, p. 46-50 (in Chinese with Eanglish Abstract).

Li, S. G., Xiao, Y. L., Liou, D. L., Chen, Y. Z., Ge, N. J., Zhang, Z. Q., Sun, S. S., Cong, B. L., Zhang, R. Y., Hart, S. R. and Wang, S. S., 1993. Collision of the North China and Yangtze Blocks and formation of coesite-bearing eclogites: Timing and processes. Chemical Geology, v. 109, p. 89-111.

Li, S. G., Wang, S. S., Chen, Y. Z., Liu, D. L., Qiu, J., Zhou, H. X. and Zhang, Z. M., 1994. Excess argon in phengite from eclogite: Evidence from dating of eclogite minerals by Sm-Nd, Rb-Sr and $^{40}Ar/^{39}Ar$ methods. Chemical Geology, v. 112, p. 343-350.

Li, Z. L., Xu, W. D., Tai, M. Q. and Pang, W. Z., 1987. Geological characteristics and ore genesis of Wulong gold deposits, Liaoning Province. Geology and Prospecting, v.2, no. 3, p. 31-39 (in Chinese with English Abstract).

Li, Z. L., 1993. Metamorphic P-T-t path of the Archaean rocks in the Jiaodong region and its implications. Geology of Shandong Province, v.9, No.1, p.31-42 (in Chinese).

Li, Z. L. and Yāng, M. Z., 1993. The geology and geochemistry of gold deposits in Jiaodong region. Tianjin Science and Technology Press, 300 pp. (in Chinese).

Li, Z. P., 1992. The genesis of the Rushan Gold Deposit within Shandong Province. Mineral Deposits, v. 11, no. 2, p. 165-178 (in Chinese with English abstract).

Liu, G. P. and Ai, Y. F., 1999. A discussion on some major problems of the Baiyun gold deposit, Eastern Liaoning. Mineral Deposits, v. 18, no. 3, p. 199-225 (in Chinese with English abstract).

Liu, D. Y., Nutman, A. P., Compston, W., Wu, J. S. and Shen, Q. H., 1992. Remnants of ≥3800 Ma crust in the Chinese part of the Sino-Korean craton. Geology, v. 20, p. 339-342.

Liu, F. C., Lu, Z. X., Fan, Y. X., Kong, Q. C. and Gong, R. T., 1991. Preliminary discuss on the relationship between intermediate to mafic dykes and gold mineralization. In: State Bureau of Gold Resources (Ed), Research on geology of gold deposits within the Jiaodong Peninsula, p.198-203 (in Chinese).

Liu, L. D., Yao, F. L., Kong, Q. C. and Gong, R. T., 1984. The significance about the vein in studying the genesis of hydrothermal ore deposits. v. 14, no. 4, p. 13-28 (in Chinese with English Abstract).

Liu, L. D., 1987. Genesis of the most important lode-gold deposits in China. Journal of Changchun College of Geology, v. 17, no. 4, p. 373-382 (in Chinese with English Abstract).

Liu, R. F., 1997. Features of ore-controlling structures and types of gold deposits in north-west Jiaodong region. Gold, v.18, 13-15 (in Chinese).

Lu, B., Hu, S. X., Zhou, S. Z., Zhao, Y. Y., Xü, B. and Ji, H. Z., 1995. Terrane tectonics and tectonic setting of gold deposits in the Shandong Peninsula. Geological Review, v. 41, no. 1, p. 7-13 (in Chinese with English).

Lü, G. X. and Kong, Q. C., 1993. The geology of Linglong- and Jiaojia-type gold deposits within Jiaodong region. 253p., Science Press, Beijing (in Chinese with English abstract).

Lu, Z. X., Hu, J. J. and Fan, Y. X. et al., 1988. Ore-controlling structures and mineralization of Jiaojia Goldfield, Jiaodong Peninsula. Regional ore-forming factors of main types of gold deposits in China. In Shenyang Institute of Geology and Mineral Resources, ed, Contribution to the project of regional metallogenic conditions of main gold deposit types in China 5: Jiaodong region. Beijing, Geological Publishing House, 132p. (in Chinese with English summary). p.85-119 (in Chinese with English abstract).

Luo, W. C. and Wu, Q. S, 1987. Timing of gold mineralisation in the Jiaodong Region: constraints from isotopic dating on alteration minerals. Bulletin of Chinese Science, v.32, no. 16, 1245-1248 (in Chinese).

Luo, Z. K., Miao, L. C., Guan, K. and Huang, J. Z., 1996. WA-China Collaborative Research Project Report. Tianjin Geological Academy, Ministry of Metallurgical Industry. 247pp. (in Chinese), unpublished.

McCuaig, T. C. and Kerrich, R., 1998. P-T-t-deformation-fluid characteristics of lode gold deposits: evidence from alteration systematics. Ore Geology Reviews, v. 12, p. 381-453.

Macdonald, R., Rock, N. M. S., Rundle, C. C. and Russell, O. J., 1986. Relations between Caledonian lamprophyric, syenitic and granitic magmas in a differentiated dike, SW Scotland. Mineralogical Magazine, v. 50, p. 547-557.

McDougall, I. and Harrison, T. M., 1988. Geochronology and thermochronology by the $^{40}Ar/^{39}Ar$ method: Oxford, Oxford University Press, 212p.

Menzies, M. A. and Xu, Y., 1998. Geodynamics of the North China Craton. In: Flower, M. F. J., Chung, S.-L., Lo, C.-H., Lee, T.-Y., eds. Mantle Dynamics and Plate Interactions in East Asia. American Geophysical Union Washington D. C., Geodynamics Series, v. 27. p. 155-163.

Mikhalsky, E. V. and Sheraton, J. W., 1993. Association of dolerite and lamprophyre dykes, Jetty Peninsula (Prince Charles Mountains, Eastern Antarctica). Antarctic Science, v. 5, no. 3, p. 297-307.

Miller, L. D., Goldfarb, R. J., Nie, F. J., Hart, C. J. R., Miller, M. L, Yang, Y. Q., Liu, Y. Q., 1998. North China Gold: a product of multiple orogens. Society of Economic Geologists Newsletter. 33 (1), 6-12.

Nelson, D. R., 1997. Compilation of SHRIMP U-Pb zircon geochronological data, 1996. Geological Survey of Western Australia, Record 1997/2, p. 189.

Nelson, K. D., 1992. Are crustal thickness variations in old mountain belts like the Appalachians a consequence of lithospheric delamination? Geology, v. 20, p. 498-502.

Nesbitt, R. W., Pascual, E., Fanning, C. M., Toscano, M., Sáez, R. and Almodóvar, G. R., 1999. U-Pb dating of stockwork zircons from the eastern Iberian Pyrite Belt. Journal of the Geological Society, London, v. 156, p. 7-10.

Ni, P. and Xu, K. Q., 1997. Geological evolution of Liaodong Peninsula and genesis of gold deposits. Mineral Deposits, v. 12, no. 3, p. 231-243 (in Chinese with English abstract).

Nie, F. J., 1997a. An overview of the gold resources of China. International Geology Review, v. 39, p. 55-81.

Nie, F. J., 1997b. Type and distribution of gold deposits along the northern margin of the North China Craton, People's Republic of China. International Geology Review, v. 39, p. 151-180.

Niu, B. X., Liu, S. C. and Liu, H. S., 1996. The age of the Penglai Group in Qixia region: the Sinian Period. Geology of the Shandong Province, v.12, no.1. p.63-68 (in Chinese with English abstract).

Okay, A. I., Xu, S. T. and Sengör, A. M. C., 1989. Coesite from the Dabie Shan eclogites, central China. European Journal of Mineralogy, v. 1, p. 595-598.

Okay, A. I. and Sengör, A. M. C., 1992. Evidence for continental thrust-related exhumation of the ultra-high-pressure rocks in China. Geology, v.20, p.411-414.

Okay, A. I., Sengör, A. M. C. and Satir, M., 1993. Tectonics of an ultrahigh-pressure metamorphic terrane: the Dabie Shan/Tongbai Shan Orogen, China. Tectonics, v. 12, p. 1320-1334.

O'Reilly, S. Y., Griffin, W. L., Djomani, Y. H. P. and Morgan, P., 2001. Are lithospheres forever? tracking changes in subcontinental lithospheric mantle through time. GSA Today, v. 11, no. 4, p. 4-10.

Page, R. W. and Sweet, I. P., 1998. Geochronology of basin phases in the western Mt Isa Inlier, and correlation with the McArthur Basin. Australian Journal of Earth Sciences, v. 45, no. 2, p. 219-232.

Peng, J. Q., Qi, C. S., Luo, S. W. and Han, Y. C., 1988. The controlling of magmatic rocks and regional structures over gold deposits in the southern Liaoning Province, in Shenyang Institute of Geology and Mineral Resources, ed. Contribution to the project of regional metallogenic conditions of main gold deposit types in China 4: South Liaoning Province: Beijing, Geological Publishing House, 132p. (in Chinese with English summary).

Perkins, C. and Kennedy. A. K., 1998. Permo-Carboniferous gold epoch of northeast Queensland. Australian Journal of Earth Sciences, v. 45, no. 2, p. 185-200.

Perring, C. S., Barley, M. E., Cassidy, K. F., Groves, D. I., McNaughton, N. J., Rock, N. M. S., Bettenay, L. F., Golding, S. D. and Hallberg, J. A., 1989. The association of linear orogenic belts, mantle-crustal magmatic, and Archaean gold mineralization in the Eastern Yilgarn Block of Western Australia. In: Keays, R. R., Ramsay, W. R. H. and Groves, D. I. (Eds), The geology of gold deposits: The perspective in 1988. Economic Geology Monograph, 6, p. 571-584.

Pidgeon, R. T., Furfaro, D., Kennedy, A. K., Nemchin, A. A., and van Bronswjk, W., 1994. Calibration of zircon standards for the Curtin SHRIMP II. In: 8th International Conference on Geochronology, Cosmochronology and Isotope Geology. Berkeley. US Geological Survey Circular 1107, Abstracts, p.251.

Pidgeon, R. T., Fūrfaro, D., Bosch, D. and Bruguier, O., 1996. Petrogenetic implications of inherited zircon and titanite in Archaean Katrine syenite, Southwestern Yilgarn Craton, Western Australia. Earth and Planetary Science Letters, v. 141, p. 187-198.

Pirajno, F., Bagas, L., Hichman, A. H. and Gold Research Team, 1997. Gold mineralization of the Chencai—Suichang Uplift and tectonic evolution of Zhejiang Province, southeast China. Ore Geology Reviews, v.12, p.35-55.

Pitcher, W. S., 1993. The nature and origin of granite. Black Academic and Professional.

Qiu, Y. M. and Groves, D. I., 1999. Late Archaean collision and delamination in the Southwest Yilgarn Craton; the driving force for Archaean orogenic lode gold mineralization? Economic Geology, v. 94, no. 1, p. 115-122.

Qiu, Y. M., Groves, D. I., McNaughton, N. J., Wang, L. and Zhou, T., 2002. Nature, age and tectonic setting of orogenic lode-gold mineralisation in the Jiaodong Peninsula of North China Craton, China, v. 37, p. 283-305.

Qü, Y. B., Xü, H. Q and Sun, Z. S., 1999. Preliminary studies on the gold origin of large-super large gold deposits. Shandong Geology, v. 15, no. 2, p. 15-23 (in Chinese with English abstract).

Ren, H. M., 1988. Gold deposits hosted by remobilized Precambrian Complex, in Zhang, Q. S., ed, Early crust and mineral deposits of the Liaodong Peninsula: Beijing, Geological Publishing House, p. 455-508 (in Chinese with English summary).

Ren, Y. S., Lin, G., Peng, X. L., 1997. Control of the Tanlu fault system on gold deposits in the western Jiaodong region. Gold, v. 18, no. 2, p. 3-7 (in Chinese with English abstract).

Rock, N. M. S. and Groves, D. I.. 1988. Can lamprophyres resolve the genetic controversy over mesothermal gold deposits? Geology, v. 16, p. 538-541.

Rock, N. M. S., Gaskarth, J. W., Henney, P. J. and Shand, P., 1988. Late Caledonian dike-swarms of northern Britain. Canadian Mineralogist, v. 28, p. 3-22.

Rock, N. M. S., Groves, D. I., Perring, C. S. and Golding, S. D., 1989. Gold lamprophyres, and porphyries: what does their association mean? In: Keays, R. R., Ramsay, W. R. H. and Groves, D. I. (Eds), The geology of gold deposits: The perspective in 1988. Economic Geology Monograph, 6, p. 609-625.

Rubin, J. N., Henry, C. D. and Price, J. G., 1989. Hydrothermal zircons and zircon overgrowths, Sierra Blanca Peaks, Texas. American Mineralogist, v. 72, p. 865-869.

Rubin, J. N., Henry, C. D. and Price, J. G., 1993. The mobility of zirconium and other "immobile" elements during hydrothermal alteration. Chemical Geology, v. 110, 29-47.

Sengör, A. M. C., Cin, A., Bowley, D. B. and Nie, S. Y., 1993. Space-time patterns of magmatism along the Tethysides: A preliminary study. Journal of Geology, v. 101, p. 51-84.

Schott, B. and Schmeling, H., 1998. Delamination and detachment of a lithospheric root. Tectonophysics, v. 296, no. 3-4, p. 225-247.

Shaw, C. A., Snee, L. W., Selverstone, J. and Reed, Jr., J. C., 1999. $^{40}Ar/^{39}Ar$ thermochronology of Mesoproterozoic metamorphism in the Colorado Front Range. Journal of Geology, v. 107, no. 1, p. 49-67.

Sheng, Y. C., Xie, H. Y., Li., G. M., Liu, T. B., Sun, X. Y. and Wang, Y. J., 1998. Geology and prospecting of the Pengjiakuang gold deposit, Shandong Province. Geology and Prospecting, v. 34, no. 5, p. 3-7 (in Chinese with English abstract).

Song, B., Nutman, A. P., Liu, D. Y. and Wu, J. S., 1996. 3800 to 2500 Ma crustal evolution in Anshan area of Liaoning Province, Northeastern China. Precambrian Research, v.78, p. 79-94.

Song, M. C., Wang, L. M., Zhang, J. X., Li, Y. Y. and Song, J. J., 1996. Jiaonan — Wenwei orogen and its evolution: in Bureau of Geology and Mineral Resources of Shandong Province, ed., Research on geology and mineral resources of the Shandong Province, pp. 51-61 (in Chinese with English abstract).

Sun, F. Y., Shi, Z. L. and Feng, B. Z., 1995. Gold ore geology, lithogenesis and metallogenesis related to the differentiation of mantle-derived C-H-O within the Jiaodong Peninsula. pp.170. Jilin People's Press, Changchun City (in Chinese with English abstract).

Sun, J. G., Hu, S. X., Zhao, Y. Y. and Yao. F. L., 2000. Preliminary discussion on the metallogenic model of gold deposits in Jiaodong region. Mineral Deposits, v. 19. no. 1, p. 26-36 (in Chinese with English abstract).

Sun, M., Armstrong, R. L., Lambert, R. S. J., Jiang, C. C and Wu, J. H., 1993. Petrochemistry and Sr, Pb and Nd isotopic geochemistry of the Paleoproterozoic Kuandian Complex, the eastern Liaoning Province, China. Precambrian Research, v. 62, p. 171-190.

Taylor, W. R., Rock, N. M. S., Groves, D. I., Perring, C. S. and Golding, S. D., 1994. Geochemistry of Archaean shoshonitic lamprophyres from the Yilgarn Blocks, Western Australia: Au abundance and association with gold mineralization. Applied Geochemistry, v. 9, p. 197-222.

The No. 107 Team of the Geology Exploration Company, Metallurgical Industrial Bureau of Liaoning Province, 1982. The preliminary exploration report of the Baiyun Gold Deposit, Liaoning Province. pp. 67 (in Chinese), unpublished.

The No.3 Geology and Exploration Team, Bureau of Geology and Mineral Resources of Shandong Province, 1989. The report of geology and exploration in deep area of the Jinqingding Gold Deposit, Rushan region. pp.155 (in Chinese), unpublished.

The No.3 Geology and Exploration Team, Bureau of Geology and Mineral Resources of Shandong Province, 1992. The exploration report of No. I lode of the Denggezhuang gold deposit, Muping region. pp. 90 (in Chinese), unpublished.

The No.3 Geology and Exploration Team, Bureau of Geology and Mineral Resources of Shandong Province, 1994. The report of geology and reserves of the Pengjiakuang gold deposit, Rushan region. pp.66 (in Chinese), unpublished.

The No.518 Team of the No.1 Geology Exploration Company of the Metallurgical Industrial Bureau, 1989. The preliminary exploration report of the Daliuhang gold deposit, Penglai region. pp. 130. (in Chinese), unpublished.

The No.6 Team of the Geology and Exploration, Bureau of Geology and Mineral Resources of Shadong Province, 1969. The preliminary exploration report of the Sanshandao Gold Deposit, Laizhou region. pp.13. (in Chinese), unpublished.

The No.6 Team of the Geology and Exploration, Bureau of Geology and Mineral Resources of Shandong Province, 1977. The features of Jiaojia-style gold deposits. Geological Bulletin of Shandong Province, no.3, p.1-32 (in Chinese).

The No.6 Geology and Exploration Team, Bureau of Geology and Mineral Resources of Shandong Province, 1981. The preliminary exploration report of the Majiayao gold deposit, Qixia region. pp.65. (in Chinese), unpublished.

The No.6 Team of the Geology and Exploration, Bureau of Geology and Mineral Resources of Shandong Province, 1985. The preliminary exploration report of the Wangershan Gold Deposit, Laizhou region. pp.77 (in Chinese), unpublished.

The No.6 Team of the Geology and Exploration, Bureau of Geology and Mineral Resources of Shandong Province, 1991. Geology report of the Cangshang Gold Deposit, pp. 136 (in Chinese), unpublished.

The Sidaogou Gold Mine, 1988. The report on the geology, ore-controlling factors and exploring ways of the Sidaogou Gold Deposit. pp. 12 (in Chinese), unpublished.

Trumbull, R.B., Liu, H., Lehrberger, G., Satir, M., Wimbauer, T. and Morteani, G., 1996. Granitoid-hosted gold deposits in the Anjiayingzi District of Inner Mongolia, People's Republic of China. Economic Geology, v.91, p. 875-895.

Vavra, G., 1990. On the kinematics of zircon growth and its petrogenetic significance: a cathodoluminescence study. Contributions to Mineralogy and Petrology, v. 106, p 90-99.

Wang, B. C. and Li, F. T., 1985. The Petrology and mineralogy of the Linglong granitoids. Shadong Geology, v. 1, no. 1, p. 1-24 (in Chinese with English abstract).

Wang, D. H., Lin, W. W., Yang, J. M. and Yan, S. H., 1999. Controlling effects of the mantle plume on the Jiaodong and Dian-Qian-Gui gold concentration areas. Acta Geoscientia Sinica, v. 20, no. 2, p. 1-6 (in Chinese with English abstract).

Wang, H. Z., and Mo, X. X., 1995. An outline of the tectonic evolution of China. Episodes, v. 18, no. 1&2, p. 6-16.

Wang, L. G., Qiu, Y. M., McNaughton, N. J., Groves, D. I., Luo, Z. K., Huang, J. Z., Miao, L. C., and Liu, Y. K., 1998. Constraints on crustal evolution and gold metallogeny in the Northwestern Jiaodong Peninsula, China, from SHRIMP U-Pb zircon studies of granitoids. Ore Geology Reviews. v.13, p.275-291.

Wang, L. M. and Yan, Y. M., 1992. The Archaean tonalite plutons in Qixia region, Shandong province. Geology of Shandong Province, v.8, No.1, p.80-87 (in Chinese with English abstract).

Wang, P.C., 1995. Relationship between the Jingshan Group and the Fenzishan Group in the Jiaobei area. Regional Geology of China. no.1, p.16-20 (in Chinese with English abstract).

Wang, P. C. and An, Y. H., 1996. The great research achievements and progresses on basic geology of Ludong region over last 10 years. Geology of Shandong Province. v.12, no.1, p.8-23 (in Chinese with English abstract).

Wang, Q., Ishiwatari, A., Zhao, Z., Hirajima, T., Enami, M., Zhai, M., Li, J. and Cong, B. L., 1993. Coesite-bearing granulite retrograded from eclogite in Weihai, eastern China: a preliminary study. Eur. J. Mineral., v.5, p.141-152.

Wang, X., Liou, J. G. and Maruyama, S., 1992. Coesite-bearing eclogites from the Dabie Mountains, central China. Petrogenesis, P-T paths, and implications for regional tectonics. Journal of Geology, v. 100, p. 231-250.

Wang, X. Q., Jiāng, S. K. and Song, J. K., 1989. Geology of Linglong goldfield. In: Gong, R. T. and Wang, Y. W. (Eds), Geology of Lingnan Gold Deposits, p.165-180. Press of Industrial University of Jilin Province, Changchun City (in Chinese).

Wen, Z. Z., 1985. Geochronology of the Linglong granitoids, Jiaodong Peninsula. Shandong Geology, v. 1, no. 2, p. 1-9 (in Chinese with English abstract).

Williams, I. S., Compston, W., Black, L. P., Ireland, T. R. and Foster, J. J., 1984. Unsupported radiogenic Pb in zircon: a cause of anomalously high Pb-Pb, U-Pb and Th-Pb ages. Contributions to Mineralogy and Petrology, v. 88, p. 322-327.

Williams, I. S. and Claesson, S., 1987. Isotopic evidence for the Precambrian provenance and Caledonian metamorphism of high-grade paragneisses from the Seve nappes, Scandinavian Caledonides II, Ion microprobe zircon U-Th-Pb. Contributions to Mineralogy and Petrology, v. 97, p. 205-217.

Williams, I. S., 1998. U-Th-Pb geochronology by ion microprobe. In: Applications of Microanalytical Techniques to Understanding Mineralizing Processes, eds by Mckibben, M. A., Shanks, III, W. C. and Ridley, W. in Reviews in Economic Geology, v. 7.

Wu, F. Y., Walker, R. J., Ren, X. W., Sun, D. Y. and Zhou, X. H., 2002. Osmium isotopic constraints on the age of lithospheric mantle beneath Northeastern China. Submitted to Chem. Geol.

Wyman, D. A. and Kerrich, R., 1988. Archaean lamprophyres, gold deposits and transcrustal structures: implications for greenstone belt gold metallogeny. Economic Geology, v. 83, p. 454-459.

Wyman, D. and Kerrich, R., 1989. Archaean shoshonitic lamprophyres associated with Superior Province gold deposits: distribution, tectonic setting, noble metal abundances, and significance for gold mineralization. In: Keays, R. R., Ramsay, W. R. H. and Groves, D. I. (Eds), The geology of gold deposits: The perspective in 1988. Economic Geology Monograph, 6, p. 651-667.

Xie, H. Y., Shen, Y. C., Wang, Y. J., Li, G. M., Liu, T. B., Zhang, Q. R. and Zen, Q. D., 1998. Location mechanism of quartz vein gold deposits in Rushan region, Shandong Province. Acta Geologica Sinica, v. 72, no. 1, p. 77-86.

Xie, H. Y., Shen, Y. C., Zhang, Q. R., Wang, Y. J., Li, S. Z. and Sun, X. Y., 1999. Metallogenic rule of gold deposits and its application to the prospecting in the central and eastern part of Rushan region, Shandong Province. Geology and Prospecting, v. 35, no. 1, p. 6-9 (in Chinese with English abstract).

Xu, J. and Zhu, G., 1994. Tectonic models of the Tan-Lu fault zone, eastern China. International Geology Review, v. 36, p. 771-784.

Xu, J. F., Shen, B. Y., Niu, L. Z. and Zheng, W. S., 1989. Research on the granitoids related to gold mineralization in the Jiaobei Terrane. Geology of Shandong, v.5, no. 2, p. 1-125 (in Chinese with English abstract).

Xu, J. W., Zhu, G., Tong, W. X., Cui, K. R. and Liu, Q., 1987. Formation and evolution of the Tancheng-Lujiang wrench fault system: a major shear system to the northwest of the Pacific Ocean. Tectonophysics, v.134, p.273-310.

Yang, C. F., 1997. The characteristics of the ore-bearing structures and orebody occurrences at the Wulong Gold Deposit. Gold, v. 18, no. 3, p. 3-8 (in Chinese with English abstract).

Yang, C. F., Ji, Z. J., Zhang, G. X. and Xu, X. N., 1997. Dyke constraints on the orebodies at the Wulong Gold Deposit. Geology and Prospecting, v. 33, no. 6, p. 7-11. (in Chinese with English abstract).

Yang, J. H., Zhou, X. H. and Chen, L. H., 2000. Dating of gold mineralization for super-large altered tectonite-type gold deposits in northwestern Jiaodong Peninsula and its implications for gold metallogeny. Acta Petrologica Sinica, v. 16, no. 3, p. 454-458 (in Chinese with English abstract).

Yang, J. H. and Zhou, X. H., 2001. Rb-Sr, Sm-Nd, and Pb isotope systematics of pyrite: implications for the age and genesis of lode gold deposits. Geology, v. 29, no. 8, p.711-714.

Yang, J. H., Wu, F. Y. and Wilde, S. A., 2002. Geodynamic setting of large-scale Late Mesozoic gold mineralization in the North China Craton: An association with lithospheric thinning. Submitted to Ore Geology Reviews.

Yang, J. Z., Shen, Y. C., Li, G. M., Liu, T. B. and Xie, H. Y., 1999. The variant characteristics of orebodies and prospecting of the Pengjiakuang gold deposit, Rushan region, Shandong Province. Geotectonica et Metallogenia, v. 23, no. 2, p. 160-166 (in Chinese with English abstract).

Yang, K. H., 1996. Gold deposits in China: main types and potential. International Geology Review, v. 38, p. 1006-1019.

Yang, M. Z. and Lü, G. X., 1996. Geology and Geochemistry of Gold Deposits Occurred in Jiaodong Greenstone Belt. 228p., Beijing, Geological Publishing House (in Chinese).

Yang S. W., Wang, S., Cheng, F. B. and Jia, B. L., 1984. The ore-forming geology and prospect in the Zhao-Ye Gold Belt. Research Project Report (in Chinese), the third exploring team of Shandong metallurgical company, 112 p unpublished.

Yang, S. W., Hou, J. Q. and Guo, B. C., 1993. Geology of Gold Deposits in Eastern Jiaodong Peninsula. pp. 169. Press of Qingdao Ocean University, Qingdao City (in Chinese).

Yang, Z. X., 1997. Studies on the mineralization of gold deposits in Liaoning Province. Liaoning Geology, no. 1, p. 40-54 (in Chinese with English abstract).

Yao, F. L., Zhou, Z. R., Liu, Y. L. and Ren, H. M., 1988. The relationship between evolution of Mesozoic granitoids and gold mineralization in the southern part of the Liaoning Province, in Shenyang Institute of Geology and Mineral Resources, ed, Contribution to the project of regional metallogenic conditions of main gold deposit types in China 4: South Liaoning Province: Beijing, Geological Publishing House, 132p. (in Chinese with English summary).

Yao, F. L., Liu, L. D., Kong, Q. C., Gong, R. T., 1990.- The lode-gold deposits in the Northwestern Jiaodong region. 234 p, Jilin Science and Technology Press, Changchun (in Chinese with English abstract).

Yeats, C. J., McNaughton, N. J. and Groves, D. I., 1996. SHRIMP U-Pb geochronological constraints on Archaean volcanic-hosted massive sulfide and lode gold mineralization at Mount Gibson, Yilgarn Craton, Western Australia. Economic Geology, v. 91, pp. 1354-1371.

Yin, A. and Nie, S., 1993. An indentation model for the North and South China collision and the development of the Tan-Lu and Honam fault systems, eastern Asia. Tectonics, v. 12, p..801-813.

Ying, 1994. REE and isotopes in two large gold deposits, eastern Jiaodong Peninsula, China. Scientia Geologica Sinica, v. 3, no. 4, p. 425-435.

Ying, 1996. Lamprophyre in the Denggezhuang and Jinqingding gold mining areas of Jiaodong Peninsula: its characteristics and relationship to gold mineralization. Acta Petrologica et Mineralogica, v. 15, no. 3, p. 221-227 (in Chinese with English abstract).

Yu, H. M., 1987. Study of Isotopic geochronology in northwestern Jiaodong region. Geology of Shandong Province, v. 3, no. 1, p.75-88 (in Chinese with English abstract).

Yu, J. H., 1989. The age and genesis of the Kunyushan complex within the eastern part of the Jiaodong Peninsula. Geology Review, v. 35, no. 4, p. 285-296 (in Chinese with English abstract).

Zhai, J. P., Hu, K. and Lu, J. J., 1996. Lamprophyres, ore-forming fluids and H, O, Sr isotope studies of the Rushan Gold Deposit. Mineral Deposits, v. 15, no. 4, p.358-364 (in Chinese with English abstract).

Zhai, J. P., Xu, G. P. and Hu, K., 1998. Mineral, ore-forming fluid and isotope characteristics of the Qixia gold deposit and their implications. Mineral Deposits, v. 17, no. 4, p. 1-8 (in Chinese with English abstract).

Zhai, Y. and Deng, J., 1996. Outline of the mineral resources of China and their tectonic setting. Australian Journal of Earth Sciences, v. 43, p. 673-685.

Zhang, D. Q., Xu, H. L., and Sun, G. Y., 1995. The ages of the Denggezhuang gold deposit and Kunyushan granitoids, Jiaodong Peninsula, and their implications. Geology Review, v. 41, no. 5, p. 415-425 (in Chinese with English abstract).

Zhang, Q. S., 1988. Early Proterozoic tectonic styles and associated mineral deposits of the North China Platform. Precambrian Research, v. 39, p. 1-29.

Zhang, R. Y., and Cong, B. L., 1991. Ultrahigh-pressure metamorphism and retrograde reaction of coesite-bearing quartz eclogite from Weihai, eastern China. EOS, Trans. Am. Geophys. Union 72: 559.

Zhang, R. Y., Liou, J. G. and Ernst, W. G., 1995. Ultrahigh pressure metamorphism and decompressional P-T path of eclogites and country rocks from Weihai, eastern China. The Island Arc. v.4, p. 293-309.

Zhang, S. T. and Chen, Q. Z., 1997. The hosting rule of the No.2 gold lode of Jiaojia Gold Deposit and its orebody prediction. Gold of Shandong Province, no.1, p. 6-11.

Zhang, W. P. and Wen, Z. Z., 1983. The Geology of Jiaojia-Type Gold Deposits, Shandong Province. Chinese Precious Metal Resources Monograph, v.1, pp. 68 (in Chinese).

Zhang, X. O., Lin, C. Y., Fan, Q. C., Shi, L. B., Chen, X. D. and Zhang, Z. M., 1996. Discussion on the origin of auriferous gas-liquid of Jiaodong gold mines. Abstract volume of the 30th International Geological Congress, v. 2, p. 719.

Zhang, X. O., Cawood, P. A., Wilde, S. A., Liu, R. Q., Song, H. L., Li, W. and Snee, L. W., 2002. Geology and timing of mineralization at the Cangshang Gold Deposit, Northwestern Jiaodong Peninsula, China, Mimeralium Deposita (in press).

Zhang, Z. H., Zhang, J. X. and Yie, S. Z., 1994. Isotopic ages of gold deposits in the Jiaodong region. 56 p, Seismological Press, Beijing (in Chinese).

Zhang, Z. M., G. R., Li, S. X and Huang, D. Y., 1973. The ore-controlling structures of Linglong Gold Deposit, Shandong Province. Geology Information of Shandong Province, no. 2 (in Chinese).

Zhang, Z. M., 1990. The forming condition and the distributive pattern of hydrothermal gold deposits in the Jiaobei Uplift. Geology and Exploration, no. 4. p.13-16 (in Chinese).

Zhang, Z. M., Liou, J. G. and Coleman, R. G., 1984. An outline of the plate tectonics of China. Geological Society of America Bulletin, v.95, p.295-312.

Zhang, Z. Q., Song Z. Y., Zhang, S. F. and Chi, S. X., 1994. New opinion on Precambrian strata of Ludong region, Shandong province. Geology of Shandong Province, v.10, extension, p.14-26 (in Chinese with English abstract).

Zhang, Z. Q. and Liu, M. W., 1996. Lithostratigraphy of Shandong Province. pp.325 (in Chinese). Press of Chinese University of Geology, Beijing.

Zhang, Z. W., Mao, J. W., Xu, W. Y. and Deng, J., Gold deposits in the Xiaoqinling region, China. Mineralium Deposita (in press).

Zhao, G. C., Wilde, S. A., Cawood, P. A. and Lu, L. Z., 1998. Thermal evolution of Archaean basement rocks from the eastern part of the North China Craton and its bearing on tectonic setting: International Geology Review, v. 40, p. 706-721.

Zhao, 2000. Assembly of the North China Craton: Constraints from the Tectonothermal Evolution of Metamorphic Complexes in the Trans-North China Orogen. PhD thesis, Curtin University of Technology.

Zhou, T. H., 1998. Major gold provinces and tectonics of China. Geol Soc Aust, Abstracts No. 49, p 496.

Zhou, T. H. and Lü, G. X., 2000. Tectonics, granitoids and mesozoic gold deposits in East Shandong, China. Ore Geology Reviews, v.16, p. 71-90.

Zhou, T. H., Goldfarb, R. J. and Phillips, G. N., 2002. Tectonics and distribution of gold deposits in China - an overview. Mineralium and Deposita, v. 37, p. 249-282.

Zhu, G, Evans, J. A., Fitches, W. R., Fletcher, C. J. N., Rundle, C. R. and Xü, J. W., 1994. Isotopic constraints on the Palaeozoic evolution of the Shandong Peninsula, N.E. China. Journal of southeast Asian Earth Sciences, v.9, no.3, p.241-248.

Zhu, J. C., 1998. Mesozoic granitoid types and metallogeny of the east China circum-Pacific continental margin. Resource Geology, v. 48. no. 4, p. 265-272.